



HAL
open science

Caractérisation de la protéine leading YfjB et étude de son importance pour l'établissement du plasmide F chez *Escherichia coli* lors de la conjugaison bactérienne

Chloé Virolle

► **To cite this version:**

Chloé Virolle. Caractérisation de la protéine leading YfjB et étude de son importance pour l'établissement du plasmide F chez *Escherichia coli* lors de la conjugaison bactérienne. Microbiologie et Parasitologie. Université Claude Bernard - Lyon I, 2023. Français. NNT : 2023LYO10045 . tel-04522787

HAL Id: tel-04522787

<https://theses.hal.science/tel-04522787>

Submitted on 27 Mar 2024

HAL is a multi-disciplinary open access archive for the deposit and dissemination of scientific research documents, whether they are published or not. The documents may come from teaching and research institutions in France or abroad, or from public or private research centers.

L'archive ouverte pluridisciplinaire **HAL**, est destinée au dépôt et à la diffusion de documents scientifiques de niveau recherche, publiés ou non, émanant des établissements d'enseignement et de recherche français ou étrangers, des laboratoires publics ou privés.



THESE de DOCTORAT DE L'UNIVERSITE CLAUDE BERNARD LYON 1

École Doctorale N° ED341
Évolution Écosystèmes Microbiologie Modélisation

Discipline : Microbiologie

Soutenue publiquement le 30/03/2023, par :
Chloé Virolle

Caractérisation de la protéine *leading* YfjB et étude de son importance pour l'établissement du plasmide F chez *Escherichia coli* lors de la conjugaison bactérienne

Devant le jury composé de :

Hallet Bernard	Professeur	Université catholique du Louvain	Rapporteur
Laloux Géraldine	Assistant professeur	Université catholique du Louvain	Rapporteuse
Charpentier Xavier	Directeur de recherches	CIRI-Lyon1, Lyon	Président
Possoz Christophe	Chargé de recherches	I2BC-Paris-Saclay, Paris	Examineur
Vianney Anne	Maitre de conférences	CIRI-Lyon1, Lyon	Examinatrice
Lesterlin Christian	Directeur de recherches	MMSB-Lyon1, Lyon	Directeur de thèse
Johnston Calum	Chargé de recherches	LMGM-CBI, Toulouse	Invité

Université Claude Bernard – Lyon 1

Président de l'Université	Frédéric FLEURY
Président du Conseil Académique	Hamda BEN HADID
Vice-Président du Conseil d'Administration	Didier REVEL
Vice-Président de la Commission de la Formation et de la Vie Universitaire	Céline BROCHIER
Directeur Général des Services	Pierre ROLLAND

COMPOSANTES SANTE

Département de Formation et Centre de Recherche en Biologie Humaine	Laetitia BIGNON
Faculté d'Odontologie	Jean-Christophe MAURIN
Faculté de Médecine et Maïeutique Lyon Sud – Charles Mérieux	Philippe PAPAREL
Faculté de Médecine Lyon-Est	Gilles RODE
Institut des Sciences et Techniques de la Réadaptation (ISTR)	Jacques LUAUTE
Institut des Sciences Pharmaceutiques et Biologiques (ISBP)	Claude DUSSART

COMPOSANTES SECTEUR SCIENCES & TECHNOLOGIES

Département Génie Électrique et des Procédés (GEP)	Rosaria FERRIGNO
Département Informatique	Saida BOUAKAZ BRONDEL
Département Mécanique	Marc BUFFAT
École Supérieure de Chimie, Physique, Électronique (CPE Lyon)	Gérard PIGNAULT
Institut de Science Financière et d'Assurance (ISFA)	Nicolas LEBOISNE
Institut National du Professorat et de l'Éducation (INSPé)	Pierre CHAREYRON
Institut Universitaire de Technologie de Lyon 1	Michel MASSENZIO
Observatoire de Lyon	Bruno GUIDERDONI
Polytechnique Lyon	Emmanuel PERRIN
UFR Biosciences	Kathrin GIESELER
UFR des Sciences et Techniques des Activités Physiques et Sportives (STAPS)	Guillaume BODET
UFR Faculté des Sciences	Bruno ANDRIOLETTI

Remerciements

Je souhaite remercier dans un premier temps les membres de mon jury de thèse Bernard Hallet, Géraldine Laloux, Xavier Charpentier, Christophe Possoz, Calum Johnston et Anne Vianney pour avoir accepté de donner de leur temps afin de juger mes travaux de thèses, certains d'entre eux ayant voyagé de grandes distances depuis Toulouse, Paris ou encore la Belgique.

J'aimerais également remercier les membres de mon comité de suivi de thèse Xavier Charpentier, Yoshiharu Yamaichi, Sophie Nolivos et Calum Johnston pour leurs conseils et les discussions toujours très intéressantes autour de mes travaux de thèse.

Je remercie Jean-Michel Jault et Christophe Grangeasse qui se sont succédés à la direction du MMSB ces dernières années et qui m'ont permis de réaliser ma thèse dans l'équipe TacC. Je remercie évidemment nos gestionnaires Dorothée Bernard, Souad Boukoum et plus récemment Clara Ecuivillon, toujours disponibles pour répondre à la moindre question et ce toujours dans la bienveillance. Également je remercie toutes les personnes que j'ai pu croiser quotidiennement lors de mes différentes visites des étages du bâtiment, avec qui j'ai pu échanger de simples bonjour, quelques mots ou encore quelques verres. Vous avez tous contribué à illuminer un peu plus mes journées et rendre ces années à l'IBCP agréables.

Je tiens aussi à remercier Chantal Tessa, qui s'occupe entre autres de la préparation de milieux et réactifs pour l'unité. Je te remercie plus particulièrement pour toutes les fois où tu as confirmé ou corrigé mes calculs de concentration, de molarité et j'en passe. Il m'arrivait de venir te voir plusieurs fois à la suite pour poser les mêmes questions, et je te remercie de ta patience ! Désormais je peux fièrement dire que je sais exactement combien je dois mettre de réactif dans mes différentes préparations, et c'est en partie grâce à toi (il était temps, après toutes ces années d'études supérieures !). J'ai également apprécié ta franchise et ton énergie, ainsi que nos discussions neige ou Doc Martens.

Je souhaiterais désormais passer plus de temps à remercier les personnes de l'équipe TacC. Tout d'abord je souhaite remercier chaudement les deux étudiantes que j'ai encadré au cours de leurs stages : Lucie Achard et Sybille Ferrarin. Vous encadrer m'a énormément apporté à la fois scientifiquement et socialement parlant. Ces quelques mois ont été pour moi une expérience très intéressante et m'ont donné goût à l'encadrement. Ça m'a également appris à lâcher prise, moi qui

ai un problème à toujours tout vouloir contrôler à ma façon... Je vous souhaite tout le meilleur pour la suite de vos études et de vos carrières respectives !

Comment ne pas remercier Julien Cayron après cela... J'ai été pendant mon premier stage de laboratoire la padawan du padawan de Christian, et je te remercie beaucoup pour tout. Je sais que je ne suis pas arrivée au meilleur moment de ta thèse, mais tu as quand même pris le temps nécessaire pour m'apprendre la majeure partie de ce que je sais faire désormais au laboratoire. Ton humour a égayé chaque journée, même quand les manips ne marchaient pas forcément et que les résultats n'étaient pas au rendez-vous. J'ai parfois eu l'impression de répéter un peu ton histoire, en cherchant la fonction d'une protéine dont on ne connaît pas grand-chose. Et bien sûr, je n'oublierais jamais cette fameuse soupe aux corbeaux...

Je remercie également Annick Dedieu, notre Lab Manager, toujours là pour nous et qui sait toujours où sont rangées les choses au laboratoire. Grâce à ton côté écureuil et tes réserves aux quatre coins du labo, nous avons pu tenir la cadence malgré les diminutions rapides et soudaines des consommables. Merci d'avoir toujours été disponible pour la moindre question. Ta bonne humeur, tes nombreuses anecdotes et tes expressions Stéphanoises (parfois assez singulières) rendent chaque journée un peu différente de la précédente ! Ne t'inquiète pas, je continuerais de mettre ma blouse !

Bien évidemment, un énorme merci à Kelly Goldlust, Sarah Djermoun et Audrey Reuter. Nous avons passé la (presque) totalité de nos thèses ensemble et c'est une formidable amitié qui demeure après ces quelques années, qui auraient été complètement différentes sans vous. Comme vous vous en doutez j'écris ces lignes les larmes aux yeux. Merci à vous trois pour ce soutien mutuel et les nombreux fous rires de ces dernières années. Ma chère Audrey, nous avons commencé ensemble dans l'équipe TacC, toi pendant ton stage de M2 et moi mon stage de M1. J'ai toujours admiré tes histoires avec chute incroyable, ton tact légendaire ainsi que ton second degré toujours pertinent. Heureusement que tu étais là pendant ces années, avec qui d'autre j'aurais pu échanger des références Kaamelott, youtube et jeux vidéos ? J'admire la personne franche et forte que tu es, et merci beaucoup pour les nombreux rires que tu as apporté quotidiennement au labo. Kelly, je sais que tu as bien rigolé en m'imaginant pleurer en écrivant tout ça, alors que nous savons toi et moi que ton côté poisson te rend sensible actuellement. On a commencé nos thèses plus ou moins en même temps, et ce n'était pas donné au début. Tout ça à cause d'un livre mal posé... Tu as toujours trouvé une façon de nous faire rire et d'apporter un peu de bonne humeur quand ça n'allait pas fort, avec tes musiques ou tes vidéos improvisées. Conserve bien toutes ces photos et vidéos que tu as de nous, je pense qu'il y a de quoi rire très longtemps ! Même si on ne le devine pas forcément de

premier abord, une fois que tu as mangé le midi tu laisses place à une personne au grand cœur. Merci pour tout bro. Enfin Sarah, ça va beaucoup me manquer de ne plus te voir littéralement pleurer de rire. Camarade de cheveux, de sport, de nourriture... Qui va pouvoir gueuler pour nous maintenant, quand on part UNE SEMAINE en formation ? Merci beaucoup pour toutes ces discussions et ces rires, que ça soit au laboratoire ou quand on se retrouvaient toutes ensemble à l'extérieur. Je ne suis pas vraiment désolée de t'avoir fait te remettre à world of warcraft, comme ça on est deux à partager cette addiction ! Vous comptez toutes les trois beaucoup pour moi, et je suis fière d'être devenue votre amie pendant ces années passées. Nous avons partagé énormément de fous rires qui nous ont fortement soudé, et je compte bien continuer à rire avec vous pendant encore longtemps !

Elisabeth, on n'aura pas partagé très longtemps le bureau mais j'ai quand même beaucoup aimé ces moments d'échanges sur les jeux vidéos ou animés. Je te souhaite une bonne continuation dans ton projet de thèse et j'espère que tu vas te plaire à poursuivre dans ton équipe « plantes » au LEM ! Bon courage avec l'administratif également, toi qui apparemment entame ta 3^e année après seulement 6 mois de thèse... Tu as fait fort ! Je remercie également Rania pour ces moments partagés à discuter paillettes, couleur de cheveux et chaussures. A l'image de tes changements capillaires, tu as participé à mettre un peu de couleur au labo. Et qui sait, peut-être qu'un jour j'accepterais un câlin à titre très exceptionnel ! Agathe, tu as toujours été au labo en même temps que moi, d'abord par intermittence entre stage et CDD, et maintenant pendant ta thèse. Discuter audiobook, séries et maté pendant que je fais ma 100000^e strie va quand même me manquer un peu ! Également un grand merci à Sarah, aka la reine mère du labo, pour tes conseils et toutes les discussions que nous avons eu, qu'elles soient scientifiques ou tournées sur les vernis à ongle. C'était un réel plaisir de partager ma paillasse avec la tienne, et de t'observer construire des murs de boîtes vides qui disparaissaient mystérieusement quelques jours plus tard (spoiler : c'était moi qui te les rangeais !).

Enfin, merci beaucoup à Christian, pour m'avoir accueillie dans ton équipe il y a de ça déjà 5 ans. Merci de m'avoir encadré ces dernières années et de m'avoir fait confiance pour ma thèse. Tu m'as toujours un peu forcé à sortir de ma zone de confort et à gagner en autonomie, et je t'en remercie. Au final, c'est aussi toi qui as fait de la « scientifique » que je suis aujourd'hui, et j'espère avoir été à la hauteur de tes attentes. Merci pour tes conseils, et pour m'avoir donné l'opportunité de tester pleins de nouvelles techniques que personne ne pratiquait dans l'équipe. Toujours partant pour boire un verre, j'ai apprécié les nombreuses discussions décontractées que nous avons pu tous avoir avec toi ainsi qu'échanger autour de passions communes autour du Japon et de la cuisine. Je

garde toujours ce fichier compilant toute l'histoire de la musique reggae, et promis un jour je l'écouterai entièrement !

Merci à vous tous pour tous ces moments passés, pour ces labmeeting accompagnés de leur viennoiseries, parfois un peu trop longs mais toujours intéressants. Très proches, on a constitué un genre de « famille scientifique » toujours prête à se retrouver autour d'un barbecue ou d'un repas de Noël, avec le fameux secret santa dont personne ne connaît les règles après toutes ces années. C'est avec grand plaisir que je reviendrais vous voir de temps en temps.

Merci beaucoup à Agathe (« MA Agathe » !), mon amie depuis mon arrivée à Lyon en L3 et ma colocataire ces dernières années. On a très bien pu comprendre les joies et galères de thèse de l'autre en discutant le soir autour d'un verre de vin pailleté. Merci pour les nombreux petits mots laissés sur mon bureau, et pour tous les gâteaux que tu amenais au passage. Eux aussi ont fait du bien au moral ! Ça va me manquer de ne plus monter les étages pour venir partager une petite pause thé... Merci beaucoup pour ces derniers mois également, à faire les courses, le ménage et souvent cuisiner pour moi. Je suis très fière de voir chaque jour la grande scientifique tu deviens. Je te souhaite évidemment le plus de réussite et de bonheur possible, tu le mérites amplement ! Merci pour tout, chat !

Merci également aux g@merz, Robin, Margot, Bubusch, Agathe, Vic, Claudia, Nico et Typoir. Je suis vraiment heureuse qu'on se soit tous retrouvés (ou rencontrés pour certains) autour des jeux vidéos presque tous les soirs pendant cette période post-confinement. Ces nombreux rires partagés ont fait énormément de bien et je vous remercie pour tout ça. Une véritable amitié s'est créée grâce aux jeux vidéos, et pour moi qui suis une geek dans l'âme, que rêver de mieux ? Grâce à vous j'ai pu visiter des villes où je ne pensais jamais aller (Romo, Throyes ou encore Gaujac). Même si on s'éparpille de plus en plus aux quatre coins de la France (et peut être même du monde ?) je sais qu'on continuera de se voir parfois. Let's go !

Enfin même s'il est de plus en plus difficile de tous se retrouver en même temps, je remercie également à Agathe, Célia, Rémi, Quentin et Valer (et mention à la petite Hortense qui nous a rejoint récemment) pour continuer de former ce petit groupe d'amis depuis si longtemps déjà !

Je remercie évidemment mes parents et mon frère, pour leur soutien inconditionnel. Merci papa et maman de toujours m'avoir poussé aux études, c'est grâce à vous que j'ai pu m'accrocher

quand c'était difficile et qu'il était plus simple d'arrêter. Merci de toujours avoir été là pour moi, d'avoir fait les allers retours à Lyon, et d'avoir toujours cuisiné des bons petits plats quand je rentrais les week-end. Vous m'avez appris que l'important c'est de faire ce qu'on aime, et c'est grâce à vous que j'ai réussi à arriver jusque-là. Merci Hugo pour toutes ces soirées passées ensemble à geeker ou à regarder des animés. Je suis vraiment heureuse d'être ta sœur et de te voir grandir en la merveilleuse personne que tu es maintenant (Live, Laugh, Love). Je ne m'excuse pas de t'harceler avec mes messages parfois, après tout tu es mon frère tu es là pour ça. Même s'il ne peut pas lire, merci à mon petit nono pour tous ces câlins qui ont fait chaud au cœur. Merci au reste de ma famille, tata Isabelle, tata Agnès, Sylvie, mémé, pour prendre de mes nouvelles et me soutenir de loin pendant ces années durant. Merci aux cousins et cousines pour me demander quand est-ce que je vais « finir mes études et commencer à travailler ».

Enfin, merci beaucoup à toi Nicolas, pour m'avoir beaucoup soutenue cette dernière année et d'avoir été très compréhensif. Merci d'avoir été là quand ça n'allait pas et que le stress prenait le dessus, tout ça a été plus simple grâce à toi. Merci d'avoir été aux petits soins avec moi pendant ma rédaction, et de t'être presque entièrement occupé de la cuisine et du ménage. Je suis très heureuse de t'avoir à mes côtés. Je t'aime.

Table des matières

Résumé	10
Abstract	12
Liste des figures	14
Liste des abréviations.....	15
Objectifs et contenu de la thèse.....	16
Partie I : Introduction bibliographique	19
Chapitre I : Transfert horizontal de gènes par conjugaison.....	19
I. Évolution du génome bactérien et importance du transfert horizontal.....	19
II. Découverte et importance de la conjugaison bactérienne	21
1. Découverte.....	21
2. Importance	23
A. Symbioses	24
B. Virulence.....	24
C. Résistances aux métaux lourds	25
D. Résistances aux antibiotiques	26
3. Mécanisme général de la conjugaison	27
Chapitre II : Mécanismes moléculaires de la conjugaison bactérienne	28
1. Contexte	28
2. Contenu	28
3. Ma contribution	29
Chapitre III : Plasmide F : un paradigme pour l'étude de la conjugaison.....	30
I. Spécificités du plasmide F et classification	30
II. Région <i>leading</i>	32
1. Expression zygotique et <i>ssi</i>	32
2. <i>PsiB</i> et réponse <i>SOS</i>	33
3. <i>Ssb^F</i> , un homologue de la protéine chromosomique <i>Ssb</i>	34
Résultats	36
Partie II : Dynamique de la conjugaison : production séquentielle des facteurs plasmidiques pour l'établissement dans la cellule hôte	36
1. Contexte	36
2. Contenu	36
3. Ma contribution	37
4. Discussion	38

Partie III : Caractérisation de la protéine <i>leading</i> YfjB et son rôle lors du transfert du plasmide F par conjugaison bactérienne.....	39
1. <i>Contexte</i>	39
2. <i>Contenu</i>	39
3. <i>Ma contribution</i>	40
4. <i>Discussion</i>	42
Partie IV : Dynamique et mécanistique de l'acquisition de résistance antibiotique par conjugaison	43
1. <i>Contexte</i>	43
2. <i>Contenu</i>	43
3. <i>Ma contribution</i>	44
4. <i>Discussion</i>	45
Partie V : Discussion générale	46
Bibliographie.....	52

Résumé

L'incroyable capacité d'adaptation des bactéries face à leur environnement leur permet de coloniser diverses niches écologiques, allant des sols et eaux jusqu'aux tissus vivants et surfaces inertes. Il est désormais acquis que le transfert horizontal de gènes joue un rôle prépondérant dans la plasticité des génomes bactériens, permettant un bond évolutif associé à la dissémination rapide et efficace de nouveaux traits phénotypiques. La conjugaison bactérienne est ainsi un mécanisme de transfert horizontal de gènes d'intérêt majeur puisque responsable de 80% des disséminations de résistances aux antibiotiques acquises chez les bactéries. Étant le sujet de nombreuses recherches depuis la découverte du mécanisme en 1946, le plasmide F est désormais considéré comme un modèle pour l'étude de la conjugaison bactérienne. Parmi les différentes régions génétiques le composant, la région *leading* est définie comme étant la première à être transférée dans les cellules receveuses. Retrouvée conservée chez certains plasmides conjugatifs appartenant à divers groupes d'incompatibilité, il a été montré que cette région est exprimée de manière précoce lors de l'entrée du plasmide dans la receveuse. Bien que la plupart des gènes qui la composent soient de fonctions inconnues, il est proposé que la région *leading* joue un rôle majeur dans les étapes initiales d'établissement du plasmide dans la nouvelle cellule hôte.

L'objectif principal de cette thèse est d'étudier le rôle de la région *leading* au cours de la conjugaison du plasmide F chez *Escherichia coli*, et plus précisément de caractériser le gène *yfjB*. La protéine YfjB partage une homologie avec les protéines de la famille ParB, notamment par la conservation d'un domaine de liaison à l'ADN. Afin de caractériser cette protéine *leading*, j'ai eu recours à une approche multidisciplinaire combinant la microbiologie classique, la microscopie à fluorescence en cellules vivantes, la génétique, les analyses omic ou encore la biochimie structurale. Les résultats obtenus permettent de mieux comprendre la dynamique de la protéine YfjB au niveau cellulaire, son activité moléculaire et son rôle dans l'établissement du plasmide F chez la bactérie receveuse. Mes travaux nous amènent alors à proposer un rôle de la protéine YfjB pour le bon déroulement des premières étapes de transfert du plasmide via une reprogrammation globale du profil d'expression génétique de la bactérie hôte. Cela irait dans le sens d'une stratégie développée par le plasmide F visant à limiter l'impact négatif de son acquisition sur la physiologie de la cellule receveuse, appuyant l'hypothèse d'une importance de la région *leading* pour l'établissement du plasmide.

Par ailleurs, j'ai pu participer à différents projets du laboratoire portant sur la dynamique intracellulaire de la conjugaison et son impact sur les populations bactériennes. Par utilisation de la microscopie à fluorescence en cellules vivantes, nous avons révélé une organisation spatio-temporelle précise des étapes clés de la conjugaison ainsi que la rapidité et l'efficacité de cette séquence d'évènements. En décrivant le profil et le timing d'expression des gènes plasmidiques dans la nouvelle cellule hôte, nous avons entre autres démontré l'importance de deux séquences de la région *leading* agissant comme promoteurs simples brins pour l'expression précoce et transitoire des gènes associés lors de l'entrée du plasmide dans la cellule receveuse. La conversion subséquente du plasmide en ADN double-brin abolit alors l'expression de la région *leading* et permet l'activation des promoteurs conventionnels qui contrôlent l'expression des autres gènes portés par le plasmide. Cette chronologie d'expression programmée des gènes plasmidiques permet la production des facteurs *leading* lors des premières étapes de transfert, puis des gènes impliqués dans le maintien du plasmide et finalement des machineries de conjugaison. L'utilisation de la microscopie à fluorescence nous a également permis d'analyser la dynamique de la mise en place de la résistance à la tétracycline conférée par un transposon Tn10 porté par le plasmide F. Nous avons ainsi pu corrélérer la production de la pompe à efflux TetA avec la concentration intracellulaire de tétracycline en temps réel et en cellules vivantes. Notre étude démontre la mise en place d'une balance entre entrée et efflux de tétracycline dépendante de la concentration initiale de pompes à efflux spécifiques et généralistes codées par le chromosome et le plasmide, mais dépendant également de la concentration en tétracycline dans le milieu.

Bien que le transfert de gènes par conjugaison ait été extensivement étudié au cours des dernières décennies, les différents projets de recherche auxquels j'ai pu participer au cours de ma thèse apportent de nouvelles connaissances par diverses approches innovantes. En couvrant l'ensemble du mécanisme de conjugaison, nous proposons alors de nouveaux modèles intégrant les différents mécanismes moléculaires régissant la conjugaison dans le contexte de la cellule vivante.

Abstract

The incredible adaptation capacity of bacteria to their environment allow them to colonise diverse ecological niches, from soils and waters to alive tissues and inert surfaces. It is now acquired that horizontal gene transfer plays a preponderant role for bacterial genome plasticity, allowing an evolutionary leap associated with rapid and efficient dissemination of new phenotypic traits amongst bacterial populations. Conjugation is therefore a horizontal gene transfer mechanism of major interest since it is responsible of 80% of acquired antibiotic resistances dissemination in bacteria. Being the subject of extensive researches since the first description of the mechanism in 1946, the F plasmid is now considered as a model for bacterial conjugation study. Amongst the multiple genetic regions composing it, the *leading* region is defined as the first to be transferred inside recipient cells. Conserved in various plasmids belonging to different incompatibility groups, it was shown that this region is early expressed during the plasmid entry inside the recipient. Even if the genes composing it are mainly unknown, it is suggested that the *leading* region play a key role for the early steps of plasmid establishment within the new host cell.

The main objective of this thesis is to study the role of the *leading* region during F plasmid conjugation in *Escherichia coli*, and more precisely to characterise the *yfjB* gene. The YfjB protein shares a homology with proteins from the ParB family especially by conservation of a DNA binding domain. In order to characterise this *leading* protein, I had recourse to a multidisciplinary approach combining classical microbiology, fluorescence microscopy in live cells, genetic, omics analysis or structural biochemistry. The data obtained allow to better understand the YfjB protein dynamics at the cellular scale, its molecular activity and its role for the F plasmid establishment inside the recipient bacteria. My work leads us to suggest a role of the YfjB protein for the first steps of plasmid transfer via global reprogramming of the host genetic expression profile. This would be in coherence with a strategy developed by the F plasmid aiming to limit the negative impact of its own acquisition on bacterial host physiology, supporting the hypothesis of the probable importance of the *leading* region for plasmid establishment.

Moreover, I also participated to various projects of the laboratory studying the intracellular dynamic of the conjugation and its impact on bacterial populations. By using fluorescent microscopy on alive cells, we revealed a precise spatiotemporal organisation for each key step of the conjugation as well as the rapidity and effectiveness of these sequential events. By describing the profile and expression timing of the plasmidic genes inside the new host cell, we demonstrate the importance

of two *leading* region sequences behaving like single-stranded promoters for the early and transitory expression of the corresponding genes during the first steps of DNA transfer. The plasmid conversion to double-stranded DNA abolishes the *leading* region expression, subsequently allowing the activation of conventional promoters for the expression of other genes carried by the plasmid. This chronology of programmed expression of the plasmidic genes allow the production of *leading* factors during the first step of the transfer, then those of the genes involved in plasmid maintenance and finally the conjugation machineries. The use of fluorescence microscopy also allowed us to analyse the dynamics of tetracycline resistance establishment conferred by a Tn10 transposon carried by the F plasmid. We thus correlate the TetA efflux pump production and tetracycline intracellular concentration in real time and in alive cells. Our study demonstrated the set-up of a balance between tetracycline entry and efflux depending on the initial concentration of specific and generalist efflux pumps encoded by the chromosome and the plasmid, but also dependant of the tetracycline concentration in the medium.

Although gene transfer by conjugation was extensively studied during the last decades, the multiple research projects to which I had the opportunity to participate during my thesis bring new knowledge by innovative approaches. By covering the conjugation mechanism in its entirety, we suggest new models integrating the various molecular mechanisms governing the conjugation in an alive cell context.

Liste des figures

Figure 1 : Représentation schématique de trois types principaux types de transfert horizontal de gènes chez les bactéries.

Figure 2 : Mécanisme de transfert conjugatif du plasmide F d'une bactérie donneuse à une bactérie receveuse.

Figure 3 : Carte génétique simplifiée du plasmide F.

Figure 4 : Carte génétique de la région *leading* sous forme d'ADN double-brin.

Figure 5 : Réponse SOS chez *Escherichia coli*.

Figure 6 : Régulation de la régulation du système TetA/TetR porté par le plasmide FTn10.

Figure 7 : Système toxine-antitoxine Hok/Sok.

Figure 8 : Schématisation des régulations transcriptionnelles et traductionnelles lors de la transition de phase exponentielle à stationnaire.

Liste des abréviations

ADN : Acide désoxyribonucléique

ADNdb : ADN double-brin

ADNsb : ADN simple-brin

ARN : Acide ribonucléique

ARNm : Acide ribonucléique messenger

Atc : Anhydrotétracycline

ChiP : Immunoprécipitation de chromatine

Cas : CRISPR-associated endonuclease

CRISPR : Clustered Regularly Interspaced Short Palindromic Repeats

GFP : Green fluorescent protein

Inc : Incompatibilité

MOB : Mobilisation

nt : Nucléotides

oriT : Origine de transfert

pb : Paires de bases

PsiB : Plasmid SOS Inhibition

sfGFP : Superfolder green fluorescent protein

Ssb : Single-stranded binding protein

ssi : Single-stranded initiation sequence

Système TA : Toxine-Antitoxine

T4CP : Type IV coupling protein – protéine de couplage

T4SS : Système de sécrétion de type IV

TAPs : Targeted Antibacterial Plasmids

Tc : Tétracycline

Objectifs et contenu de la thèse

L'axe de recherche principalement développé au laboratoire consiste en l'étude de l'organisation intracellulaire du mécanisme de transfert horizontal de gènes par conjugaison chez les bactéries. Depuis sa découverte en 1946 par Lederberg et Tatum, de multiples approches de génétique et biochimie structurale ont permis la compréhension des mécanismes moléculaires et facteurs impliqués dans la conjugaison. Toutefois, l'organisation du transfert conjugatif reste encore peu décrite au niveau cellulaire. Différents outils génétiques et expérimentaux sont ainsi développés au laboratoire, nous permettant l'étude de la dynamique du transfert conjugatif en cellules vivantes par l'utilisation de la microscopie à fluorescence couplée à la microfluidique. Dans ce contexte, l'objectif initial des travaux de thèse présentés dans ce manuscrit est d'à la fois caractériser les facteurs moléculaires impliqués dans le transfert du plasmide F chez *Escherichia coli* ainsi que de mesurer leur importance pour la pérennité du plasmide conjugatif.

La **première partie** de ce manuscrit consiste en une introduction bibliographique articulée autour de trois chapitres. **Le premier chapitre** présente le transfert horizontal de gènes de façon général ainsi que son importance pour la plasticité et l'adaptabilité des bactéries à leur niche écologique, tout en appuyant l'importance de la conjugaison. Ce type de transfert génétique permet l'acquisition rapide de nouvelles fonctions métaboliques par les bactéries, jouant un rôle critique dans la dissémination de gènes de symbiose, de virulence ou de résistances aux antibiotiques et métaux lourds au sein des populations bactériennes. **Le deuxième chapitre** de cette introduction bibliographique présente une revue sur la conjugaison chez les bactéries gram-négatives, publiée dans le journal *Genes* en 2020 et pour laquelle je partage la place de co-premier auteur avec les doctorantes Kelly Goldlust et Sarah Djermoun. En faisant le choix d'un angle centré sur le plasmide F, nous faisons un état de l'art des savoirs accumulés sur la conjugaison bactérienne tout en regroupant connaissances, hypothèses et questionnements dans une seule et même revue. Enfin, le plasmide F étant le modèle d'étude utilisé au cours de cette thèse, le **troisième et dernier chapitre** traite de façon plus précise de son importance et de ses spécificités. J'introduis alors la notion « d'expression zygotique » caractéristique des gènes composant la région *leading*, première région génétique à être transférée et exprimée dans la bactérie receveuse au cours de la conjugaison.

Les articles publiés et résultats obtenus au cours de cette thèse sont présentés dans les trois parties suivantes de ce manuscrit. Par suivi de l'ADN plasmidique simple-brin (ADNsb) au cours du transfert et en utilisant des rapporteurs de sa conversion en ADN double-brin (ADNdb), notre

approche de visualisation directe nous a permis de publier un article dans le journal *Nature communication* en 2023 présenté en **deuxième partie** du manuscrit et pour lequel j'ai participé en tant que deuxième auteur. Notre étude nous a permis de mettre en avant l'organisation et la chronologie des différentes étapes impliquées dans le transfert conjugatif à l'échelle cellulaire. Par analyse quantitative d'images de microscopie en temps réel, nous révélons une dynamique séquentielle de l'expression des gènes plasmidiques en fonction de leur position génétique sur le plasmide F, laquelle est régulée par la transition du plasmide de la forme simple-brin à double-brin. Nous apportons plus de précisions quant au rôle longtemps questionné dans la littérature de la protéine plasmidique Ssb^F pour le transfert et établissement du plasmide conjugatif, et nous confirmons également *in vivo* la présence de deux promoteurs simple-brin pour l'expression précoce et transitoire des gènes *leading*. Ensembles, les résultats présentés dans cette partie appuient l'importance de la région *leading* pour le bon déroulement des premières étapes du transfert conjugatif.

La **troisième partie** de ce manuscrit vise à caractériser le rôle du gène inconnu *yjfB*, porté par la région *leading*. C'est là mon sujet principal de thèse, s'inscrivant dans la continuité des observations réalisées au cours de ces dernières années au laboratoire et publié précédemment. Les résultats obtenus sont présentés sous la forme d'un article en préparation que je signe en tant que premier auteur. Une approche multidisciplinaire alliant à la fois la microscopie à fluorescence en cellule vivantes, les techniques classiques de génétique et microbiologie, les analyses omics mais également la biochimie structurale confirme une fonction de liaison à l'ADN de la protéine YjfB, comme le laisse suggérer son homologie avec les protéines ParB. Par ailleurs, j'ai montré que la protéine plasmidique YjfB induit un changement global du profil d'expression génétique de la bactérie hôte, affectant ainsi sa physiologie. Bien que la fonction d'YjfB ne soit pas encore complètement élucidée, mes travaux ont permis d'élaborer un modèle décrivant le rôle de cette protéine « ParB-like » dans le contexte de la conjugaison. Nous proposons que l'activité d'YjfB fasse partie d'une stratégie mise en place par le plasmide F pour moduler temporairement la physiologie de la nouvelle cellule hôte, vraisemblablement dans le but d'éviter un impact négatif trop important de l'acquisition du plasmide, tout en permettant l'établissement rapide et efficace du plasmide F pour l'expression plus tardive des autres facteurs plasmidiques.

Enfin, la **quatrième partie** de ce manuscrit présente un article de recherche publié dans le journal *FEMS Microbiology Reviews* en 2020 pour lequel j'ai eu l'opportunité de signer en tant que co-premier auteur avec Audrey Reuter et Kelly Goldlust. Faisant suite aux travaux menés par le Dr.

Nolivos Sophie et publiés par le laboratoire en 2019 dans le journal *Science*, notre article présente l'étude de la dynamique d'acquisition et de mise en place d'une résistance à la tétracycline par conjugaison chez *Escherichia coli*. Nous avons pour cela une nouvelle fois adopté une approche de quantification par microscopie à fluorescence en cellules vivantes en prenant avantage de la propriété d'auto-fluorescence de la molécule de tétracycline et en décrivant la localisation cellulaire de la protéine TetA fusionnée à un marqueur fluorescent. Nos résultats révèlent alors une balance entre entrée et efflux de la tétracycline dépendant de la concentration basale en pompe à efflux chromosomiques et plasmidiques, mais également dépendante de la concentration en antibiotique utilisé.

La **cinquième et dernière partie** de ce manuscrit constitue la discussion finale des différents résultats présentés et permet d'y développer en détails les différentes conclusions et hypothèses qui en émanent. En résumé, les travaux de recherche qui constituent ce manuscrit de thèse illustrent une étude sur plusieurs échelles cellulaires, portant à la fois sur i) la dynamique de mécanismes cellulaires impliqués dans le transfert de l'ADN simple-brin au cours de la conjugaison et de sa conversion en ADN double-brin, ii) la caractérisation de la protéine plasmidique YfjB et son impact sur la physiologie de la bactérie receveuse et iii) la caractérisation de la mise en place d'une résistance antibiotique portée par un plasmide conjugatif. Bien que diverses approches techniques aient permis la réalisation de ces travaux, la microscopie à fluorescence en cellules vivantes constitue l'outil d'analyse central de ces travaux. Cette approche technique est en constant développement, apportant un nouvel angle d'étude pour confirmer ou infirmer des hypothèses pour lesquelles il n'était pas encore possible de répondre avec les moyens techniques précédant, tout en permettant de nouvelles découvertes qui ouvrent à leur tour de nouvelles questions.

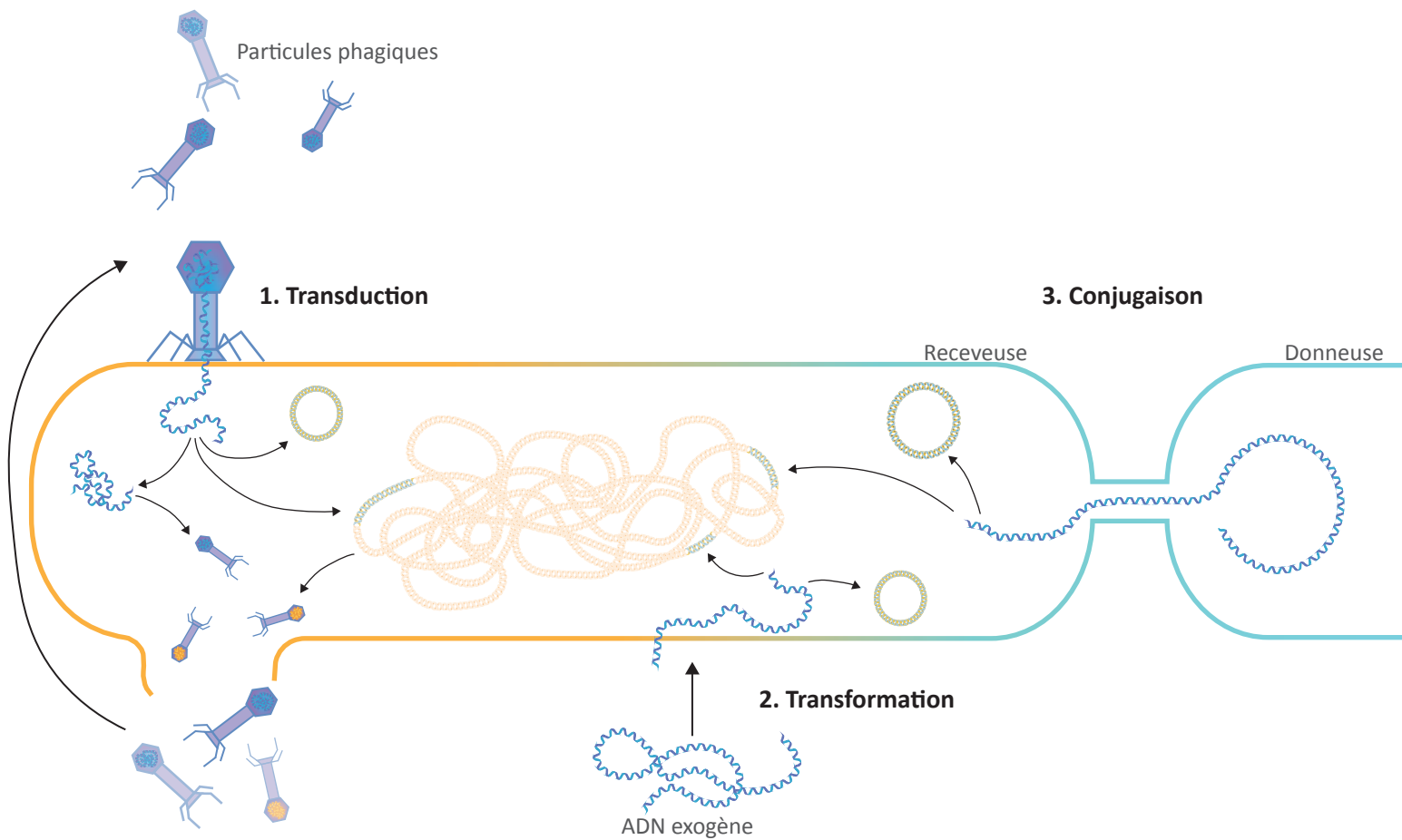


Figure 1. Représentation schématique de trois types principaux de transfert horizontal de gènes chez les bactéries.

1. Transduction médiée par les bactériophages. Après injection du matériel phagique dans la bactérie, celui-ci peut s'intégrer au génome hôte, devenir un élément extra-chromosomique indépendant ou contourner les machineries cellulaires pour la production de particules virales ensuite relarguées par lyse de la bactérie. De l'ADN chromosomique bactérien peut se retrouver encapsidé dans les nouvelles particules produites et être transféré à d'autres bactéries.
2. Transformation naturelle. Après entrée de matériel génétique exogène dans la bactérie naturellement compétente, celui-ci peut soit s'intégrer au génome hôte soit se répliquer de façon autonome. L'ADN exogène peut provenir de la lyse d'autres bactéries dans l'environnement.
3. Conjugaison bactérienne. De l'information génétique est transférée par la bactérie donneuse après contact avec une bactérie receveuse, pouvant ensuite se répliquer en un plasmide extra-chromosomique ou bien s'intégrer au génome hôte.

Partie I : Introduction bibliographique

Chapitre I : Transfert horizontal de gènes par conjugaison

I. Évolution du génome bactérien et importance du transfert horizontal

Les bactéries possèdent une grande capacité d'adaptation à leur environnement, leur permettant de coloniser la plupart des écosystèmes. Cette capacité d'adaptation peut provenir d'évènements de mutations spontanées, lesquelles seront sélectionnées et transmises à la descendance si elles confèrent un avantage à la bactérie suivant les principes Darwinien de l'évolution des espèces par sélection naturelle. Cependant, l'adaptation rapide des bactéries repose également sur leur capacité à acquérir de l'information génétique exogène, c'est-à-dire provenant du milieu extérieur ou d'autres bactéries, via le transfert horizontal de gènes (Frost et al. 2005; Daubin and Szöllösi 2016). Les trois principaux mécanismes de transfert horizontal de gènes chez les bactéries sont la transduction, la transformation et la conjugaison bactérienne (Figure 1).

La transduction est un processus indirect de transfert entre bactéries médié par les bactériophages, particules virales principalement composées d'acide nucléique contenu dans une capsule protéique et infectant spécifiquement les bactéries via un cycle de multiplication lytique ou lysogénique. Lors de l'infection bactérienne, les bactériophages lytiques vont détourner la machinerie cellulaire afin de produire un grand nombre de particules virales, lesquelles seront ensuite libérées par la lyse de la bactérie hôte infectée. Dans le cas de figure d'un cycle lysogénique, le matériel génétique injecté par le phage peut se répliquer en un plasmide autonome ou bien s'intégrer au chromosome bactérien et être répliqué au cours des divisions bactériennes (Chiang, Penadés, and Chen 2019). Bien que dans la majorité des cas les particules nouvellement produites contiennent de l'information génétique virale, il arrive que de l'ADN hôte soit encapsidé à la place. Cet ADN bactérien peut alors être transmis à une nouvelle bactérie lors d'un nouveau cycle d'infection. Cette acquisition de nouveaux gènes va alors modifier le profil génétique de l'hôte et potentiellement permettre l'acquisition de nouvelles propriétés métaboliques (Menouni et al. 2015).

La transformation bactérienne consiste en un processus impliquant une bactérie receveuse et de l'ADN exogène présent dans son environnement. Cette transformation dite « naturelle » repose sur la capacité de la bactérie receveuse à coder et produire les machineries protéiques nécessaires à l'internalisation et l'intégration de l'ADN étranger dans son génome par recombinaison homologue

(Johnston, Martin, et al. 2014). Découvert en 1928 chez la bactérie Gram-positive *Streptococcus pneumoniae*, le transfert de gènes par transformation a depuis été identifié chez près de 80 espèces bactériennes différentes, à la fois chez les bactéries Gram-positives telles que *Bacillus subtilis* ou *Streptococcus pneumoniae* et chez les Gram-négatives telles qu'*Acinetobacter baylyi*, *Vibrio cholerae* ou encore *Neisseria gonorrhoeae* (Griffith 1928; Johnston, Martin, et al. 2014; Averhoff et al. 2021).

Enfin, la conjugaison bactérienne est un transfert actif d'information génétique dépendant d'un contact entre une bactérie donneuse et une bactérie receveuse, laquelle devient une nouvelle bactérie appelée « transconjugante » présentant un mélange des propriétés génétiques des deux souches parentales. Considérée comme un type de reproduction sexuée chez la bactérie, la conjugaison bactérienne est ainsi un processus ubiquitaire permettant le transfert d'une variété d'éléments conjugatifs allant de plasmides de tailles variées, de transposons ou encore de chromosomes.

Le développement des techniques de séquençage au cours de ces dernières décennies a permis d'établir que le transfert horizontal de gènes est un acteur majeur de la plasticité des génomes bactériens. De grands fragments d'ADN peuvent ainsi être transférés en un seul événement, provoquant un bond évolutif et une adaptation abrupte des bactéries face à un environnement changeant et leur permettant de coloniser de nouvelles niches écologiques auparavant inaccessibles. Cette rapide modification génétique serait difficilement réalisable par simple mutation spontanée ou par réorganisation du génome (Eberhard 1989; Lawrence and Ochman 1998; Daubin and Szöllösi 2016; Pang and Lercher 2019; Lee et al. 2022). Ainsi, 18% du chromosome d'*Escherichia coli* et 2 à 6% du génome du groupe *Pseudomonas fluorescens* proviennent d'évènements de transferts horizontaux (Lawrence and Ochman 1998). Il a été établi par de nombreuses études de méta-génomique et pan-génomique que l'ADN phagique issu des évènements de transduction constitue une part non-négligeable des génomes procaryotes, allant de 5% chez *Salmonella* et jusqu'à 15% chez *Escherichia coli* (Feschotte and Gilbert 2012; Bobay, Rocha, and Touchon 2013). L'ADN phagique peut ainsi avoir des implications physiologiques importantes chez la bactérie, comme c'est le cas du phage CTX ϕ codant une choléra-toxine bactérienne responsable de la virulence chez *Vibrio cholerae* (Boyd 2012) ou encore des phages-*stx* codant pour les shiga-toxines STX chez les bactéries *Escherichia coli* entéropathogènes (Tozzoli et al. 2014). La transformation bactérienne permet aux bactéries d'acquérir et intégrer au sein de leur génome de nouveaux gènes provenant de transposons, intégrons ou encore d'ADN issu de la lyse de bactéries présentes dans la niche écologique (Carvalho et al. 2020). C'est notamment le cas pour *Streptococcus pneumoniae*, un pathogène humain

possédant une forte capacité de recombinaison par transformation de gènes xénologues (gènes homologues issus d'évènements de transfert horizontal) pouvant conduire à un changement des composés de sa capsule, augmentant sa virulence tout en diminuant l'efficacité des vaccins (Johnston, Campo, et al. 2014; Sabharwal et al. 2014). Un autre exemple concerne *Bacillus subtilis* qui possède une pléthore de gènes accessoires majoritairement acquis par transformation et permettant à la bactérie de coloniser diverses niches écologiques, allant des sols aux animaux et plantes (Brito et al. 2018). Enfin, la conjugaison bactérienne permet le transfert de plasmides conjugatifs pouvant porter des gènes conférant divers avantages biologiques à la bactérie hôte.

II. Découverte et importance de la conjugaison bactérienne

1. Découverte

Découverte pour la première fois en 1946 par Joshua Lederberg et Edward Tatum, la conjugaison bactérienne est un processus ubiquitaire de transfert de matériel génétique entre bactéries (Lederberg and Tatum 1946). Les premières études chez *Escherichia coli* font alors référence à un mécanisme de transfert sexué porté par le facteur de fertilité F, qualifié plus tard de « plasmide F ». Le terme générique « plasmide » n'est proposé qu'en 1952 pour qualifier « tout élément héréditaire extra-chromosomique » (Lederberg 1952). Un plasmide est une structure génétique codant ses propres machineries de réplication et de partition, typiquement retrouvée sous forme d'ADN circulaire bien que certains plasmides puissent être composés d'ADN linéaire (Meinhardt, Schaffrath, and Larsen 1997; Hawkey et al. 2022). Après contact bactérien et transfert horizontal du plasmide par conjugaison, la bactérie receveuse ayant acquis le plasmide est alors appelée « bactérie transconjugante » et peut devenir une nouvelle donneuse capable à son tour de transfert conjugatif.

De nombreux plasmides ont été identifiés au cours des six dernières décennies et isolés chez de multiples micro-organismes, avec une taille pouvant aller de 744 pb à 2.58 Mb pour une moyenne de 80 kb (Shintani, Sanchez, and Kimbara 2015). Une analyse de la base de données *NCBI Plasmid Genome database* réalisée en 2015 démontre que 96% des séquences complètes plasmidiques séquencées sont retrouvées chez les bactéries (Shintani, Sanchez, and Kimbara 2015). De multiples classifications ont ainsi été établies face à la diversité et nombre important de plasmides étudiés. L'incompatibilité (Inc) reflète l'inhabilité des plasmides à être maintenus dans la même cellule hôte s'ils possèdent des systèmes de réplication ou de partition similaires. Établis dans les années 1970, les groupes Inc sont alors classifiés en fonction des trois genres *Enterobacteriaceae* (27 groupes Inc),

Pseudomonas (12 groupes Inc) et *Staphylococcus* (18 groupes Inc). Une autre classification basée sur la séquence en acides aminés de la relaxase des plasmides est également établie en six groupes de mobilisation (MOB) dans la *GenBank Database* (María Pilar Garcillán-Barcia, Francia, and de la Cruz 2009; Maria Pilar Garcillán-Barcia, Alvarado, and de la Cruz 2011; Shintani, Sanchez, and Kimbara 2015). Une relaxase est une protéine multifonctionnelle essentielle à la conjugaison, capable de cliver une molécule ADN au niveau de l'origine de transfert *oriT* du plasmide par activité de transestérification, entraînant l'initiation du transfert conjugatif. Elle possède également une activité hélicase qui permet de séparer les brins du plasmide conjugatif, dont l'un sera transféré à la cellule receveuse et ainsi appelé « *T-strand* » (brin transféré). Cependant seul un quart des plasmides décrits jusque-là sont prédits comme étant conjugatifs, c'est-à-dire possédant la particularité de porter additionally des gènes codant pour une machinerie permettant leur transfert autonome par conjugaison (Smillie et al. 2010; Coluzzi et al. 2022). D'autres éléments conjugatifs intégratifs (ICE), aussi appelés transposons conjugatifs, peuvent être impliqués dans les événements de conjugaison au sein de populations Gram négatives et Gram positives (Grohmann, Muth, and Espinosa 2003; de la Cruz et al. 2010).

Hautement conservée chez les bactéries Gram-négatives, la machinerie permettant le transfert autonome des plasmides conjugatifs est composée de trois éléments essentiels : un complexe protéique appelé « relaxosome » qui permet la prise en charge et la préparation de l'ADN plasmidique pour le transfert vers la bactérie receveuse; une protéine de couplage T4CP (*Type 4 Coupling Protein*) faisant le lien entre le complexe nucléoprotéique et le pore conjugatif; et un système de sécrétion de type IV (T4SS) permettant le transfert de matériel génétique à travers les membranes cellulaires (de la Cruz et al. 2010; Arutyunov and Frost 2013; Grohmann et al. 2018; Kohler, Keller, and Grohmann 2019; Virolle et al. 2020). Bien que la machinerie de transfert d'ADN simple-brin (ADNsb) soit fortement conservée parmi les bactéries Gram-négatives, des événements de transfert d'ADN double-brin (ADNdb) sont également observés chez les bactéries Gram-positives. C'est le cas des bactéries du genre *Streptomyces*, pour qui les plasmides conjugatifs codent un système de transfert ADN unique médié par une seule protéine plasmidique TraB homologue à la protéine FtsK. TraB va ainsi permettre la translocation de l'ADNdb en fonctionnant de manière similaire à la ségrégation de l'ADN chromosomique lors de la division cellulaire et de la sporulation. Des adhésines sont également impliquées dans le contact entre cellules (Goessweiner-Mohr et al. 2013; Shintani, Sanchez, and Kimbara 2015; Thoma and Muth 2016). De façon plus rare, des

évènements de transfert inter-espèces peuvent également être observés, l'exemple le plus connu concernant *Agrobacterium tumefaciens*. Cette bactérie phyto-pathogène est capable de transférer aux cellules végétales des gènes oncogéniques via son plasmide Ti (Tumor inducing), à l'origine de la maladie de la « gale du collet » chez la plante (Gordon and Christie 2014). La conjugaison est également observée entre bactéries et archées, comme c'est le cas pour le plasmide à large spectre d'hôte RP4 capable d'être transféré d'une souche *Escherichia coli* vers *Methanococcus maripaludis* (Dodsworth et al. 2010). Enfin, bien qu'expérimentale, une approche *in vitro* a permis de réaliser un transfert conjugatif entre *Escherichia coli* et des cellules mitochondriales, démontrant la versatilité du mécanisme de conjugaison (Yoon and Koob 2005).

2. Importance

La présence d'un plasmide dans une bactérie, qu'il soit conjugatif ou non, va être associé à un coût métabolique global allant de 1% à 28% en conséquence de la répllication de l'information génétique plasmidique ainsi que de la production des protéines correspondantes (Carroll and Wong 2018). Afin d'être maintenus au sein des populations bactériennes, les plasmides conjugatifs portent alors des cargos de gènes impliqués dans de nombreuses fonctions biologiques. Ils constituent ainsi un réservoir génétique pouvant aider à l'adaptation à une niche écologique changeante, faisant de la conjugaison un pilier central pour l'évolution des génomes bactériens. De façon remarquable les plasmides sont maintenus dans les populations bactériennes et ce même en absence de pression de sélection : c'est ce qu'on appelle le « paradoxe plasmidique » (Harrison and Brockhurst 2012). Une coévolution plasmide-hôte, un fort taux de transfert, des mécanismes de partition efficaces ou encore des mutations adaptatives peuvent contribuer à ce phénomène (Carroll and Wong 2018). Considéré comme un important mode de communication et de transfert d'informations génétiques entre bactéries, le transfert de plasmides par conjugaison peut conduire à l'établissement de symbioses mais également participer à la virulence des bactéries, en passant par la dissémination de résistances aux métaux lourds et antibiotiques (Aminov 2011). Ces plasmides conjugatifs peuvent également influencer la composition-même de la niche écologique de l'hôte en permettant la dégradation d'enzymes produites par les bactéries voisines ou en sécrétant des molécules de défense telles que les bacitracines ou antibiotiques (Livermore 1995; Riley et Wertz 2002; Rankin, Rocha, et Brown 2011). Certains exemples illustrant la variété des fonctions biologiques conférées par les plasmides conjugatifs sont décrits ci-après.

A. Symbioses

Les plasmides conjugatifs peuvent jouer un rôle dans l'établissement de symbioses, définies par une relation mutuellement bénéfique entre deux organismes vivants. C'est ainsi le cas des plasmides pSym portés par les bactéries Gram-négatives du genre *Rhizobium*, qui codent des gènes *nod* et *nif* contrôlant la nodulation et fixation du nitrogène par les racines des plantes légumineuses (Ibáñez, Reinoso, and Fabra 2010). Les nodules sont des structures spécialisées au niveau du système racinaire des plantes dont la formation est uniquement associée à un établissement symbiotique avec une bactérie. Via la production de facteurs de nodulation à partir du plasmide conjugatif, la bactérie va favoriser la formation de ces structures ; en retour la plante fournit divers nutriments carbonés pour la multiplication bactérienne. L'expression des gènes *nif* va ensuite permettre la production de nitrogénases réduisant le nitrogène atmosphérique N_2 en ammonium NH_3 utilisé par la plante pour sa croissance (Chen et al. 2003). Des études montrent que *Rhizobium etli* est capable de transférer son plasmide conjugatif pSym à d'autres bactéries endophytes ; cela renforce l'idée que les nodules constituent un environnement propice à l'échange d'information génétique entre bactéries en plus de leur fonction structurale pour la fixation et assimilation de nitrogène par la plante. Ce processus symbiotique peut être ainsi considéré comme un sujet d'étude important afin de développer de nouvelles techniques de cultures pour un meilleur rendement agricole (Lindström and Mousavi 2020).

B. Virulence

La pathogénicité de certaines bactéries va dépendre de fonctions de virulence variées incluant l'adhésion aux cellules hôtes, la cytotoxicité, l'invasion cellulaire et la résistance face aux systèmes de défense hôte. Certains plasmides conjugatifs vont ainsi porter différentes enzymes ou protéines cytotoxiques conférant un phénotype virulent à la bactérie hôte en facilitant la colonisation et l'avancée de l'infection ou bien augmentant la virulence d'une souche déjà pathogène (Bukowski et al. 2019). C'est le cas du pathogène humain *Salmonella enterica* serovar Typhimurium dont le plasmide conjugatif pSLT peut médier sa virulence. Ce dernier code pour des effecteurs transloqués dans les cellules eucaryotes via un système de sécrétion de type III et qui interfèrent avec le cytosquelette d'actine, conduisant à la mort par apoptose des cellules infectées (Guiney and Fierer 2011). On peut également citer la bactérie Gram-positif *Clostridium perfringens*, considérée comme pathogène majeur pour l'Homme et le bétail et qui possède un large éventail de toxines associées à un caractère virulent important. Certaines de ces toxines se retrouvent alors codées par le plasmide

conjugatif pCW3, qui porte additionnellement d'autres facteurs impliqués dans la virulence et les résistances aux antimicrobiens (Mehdizadeh Gohari et al. 2021).

C. Résistances aux métaux lourds

Les métaux lourds sont naturellement présents dans l'environnements et peuvent être retrouvés dans les eaux et sols par processus naturel de corrosion mais également par l'activité humaine issue des productions industrielles ou pesticides agricoles (Palm et al. 2022). Bien que certains métaux tels que le cuivre, le fer ou le nickel soient essentiels chez les bactéries pour certaines réactions biochimiques ou pour l'intégrité membranaire, d'autres métaux lourds comme le mercure et l'argent sont quant à eux toxiques. Ces composés vont générer des dérivés réactifs de l'oxygène (ROS) pouvant endommager les protéines et l'ADN bactérien, déstabiliser l'intégrité des membranes lipidiques par peroxydation ou encore interférer avec la fonction de diverse enzymes essentielles aux bactéries (Bruins, Kapil, and Oehme 2000). Le zinc, l'arsenic ou encore le cuivre réduisent même de 2 à 100 fois l'efficacité des transferts conjugatifs de plasmides IncF chez *Escherichia coli* (Palm et al. 2022). De par l'accumulation de ces contaminants dans les sols et sédiments ainsi que leur utilisation comme désinfectants et produits antimicrobiens, il est naturel que les bactéries aient développé des résistances à ces métaux lourds par la mise en place de mécanismes d'efflux ou systèmes de réduction d'ions métalliques, dont certains sont retrouvées codées par les plasmides (Hobman and Crossman 2015). C'est le cas des plasmides conjugatifs pRJ1004 et pUPI199 retrouvés chez les bactéries *Escherichia coli* et *Acinetobacter baumannii* portant respectivement des gènes de résistance au cuivre et l'argent (Tetaz and Luke 1983; Deshpande and Chopade 1994). Une co-occurrence de résistance aux métaux lourds et antibiotiques peut également être observé, comme c'est le cas du plasmide pSTM6-2765 de *Salmonella enterica*. Ce dernier porte de multiples gènes de résistance aux antibiotiques ampicilline, streptomycine, chloramphénicol ou encore tétracycline, mais porte également un transposon *Tn7* codant pour une résistance à l'argent et au cuivre (Li, Xia, and Zhang 2017; Billman-Jacobe et al. 2018). La résistance associée au transposon est portée par les systèmes *Sil* et *Pco*, protéines de liaison aux ions métalliques et transporteurs. Des associations similaires de résistances aux antibiotiques et métaux lourds ont ainsi été détectés chez d'autres plasmides IncHI2 portés par des bactéries associées aux animaux (Fang et al. 2016). Cet exemple illustre la capacité des plasmides conjugatifs à évoluer et agréger des systèmes de gènes conférant des avantages sélectifs multiples dans certains environnements.

D. Résistances aux antibiotiques

L'analyse génomique de souches commensales, environnementales et pathogènes retrouvées dans des isolats cliniques révèle l'importance des plasmides conjugatifs dans la dissémination de résistances à la quasi-totalité des classes antibiotiques utilisées en clinique. Considérées comme un problème majeur de santé mondial par l'Organisation Mondiale de la Santé (OMS), les résistances aux antibiotiques causent actuellement près de 700 000 morts par an ; ce constat pourrait atteindre les 10 millions d'ici 2050, dépassant alors largement le nombre de décès liés au cancer (O'Neill 2014; OMS 2020). Il a été établi que près de 80% des résistances aux antibiotiques acquises chez les bactéries proviennent d'évènements de conjugaison (Hall-Stoodley, Costerton, and Stoodley 2004; Barlow 2009). C'est le cas notamment des gènes ESBL (β -Lactamases à spectre étendu) conférant une résistance aux antibiotiques β -lactames et carbapénèmes tels que la pénicilline, les carbapénèmes ou encore les céphalosporines (Paterson and Bonomo 2005). Ces gènes peuvent alors être disséminés par conjugaison intra- et inter- espèces chez les *Enterobacteriaceae*, *Pseudomonas* et *Acinetobacter* (Mathers et al. 2011; Huang et al. 2015; Weingarten et al. 2018; Lermينياux and Cameron 2019). Un exemple le plus notable concerne le gène *bla_{OXA-48}* généralement porté par le plasmide conjugatif pOXA-48 et codant pour une carbapénémase pouvant dégrader la molécule antibiotique par hydrolyse. Découvert pour la première fois en 2001 chez *Klebsiella pneumoniae*, ce gène de résistance plasmidique est désormais très répandu dans les environnements hospitaliers et représente un problème majeur pour le traitement des infections (Poirel et al. 2005; Nordmann, Naas, and Poirel 2011; Hamprecht et al. 2019). Il est tout à fait possible que certains plasmides conjugatifs accumulent plusieurs gènes de résistance conférant à la bactérie hôte une résistance simultanée à plusieurs classes d'antibiotiques (Nikaido 2009). Ces plasmides MDR (*MultiDrug Resistant*) limitent alors d'autant plus les possibilités de traitement, et sont de ce fait considérés comme vecteurs importants pour la dissémination de ces clusters de gènes.

La variété de fonctions biologiques conférées par les plasmides conjugatifs reflète l'importance du transfert de gènes par conjugaison pour l'adaptabilité phénotypique des bactéries à leur niche écologique, soulignant ainsi la nécessité de développer de nouvelles approches pour limiter leur dissémination. Différentes études proposent une approche par combinaison de molécules induisant la perte plasmidique avec des inhibiteurs de conjugaison (Cabezón, de la Cruz, and Arechaga 2017; Lopatkin et al. 2017). D'autres stratégies sont également étudiées pour utiliser le transfert d'ADN par conjugaison contre les bactéries elles-mêmes. C'est le cas d'une étude du laboratoire qui a permis

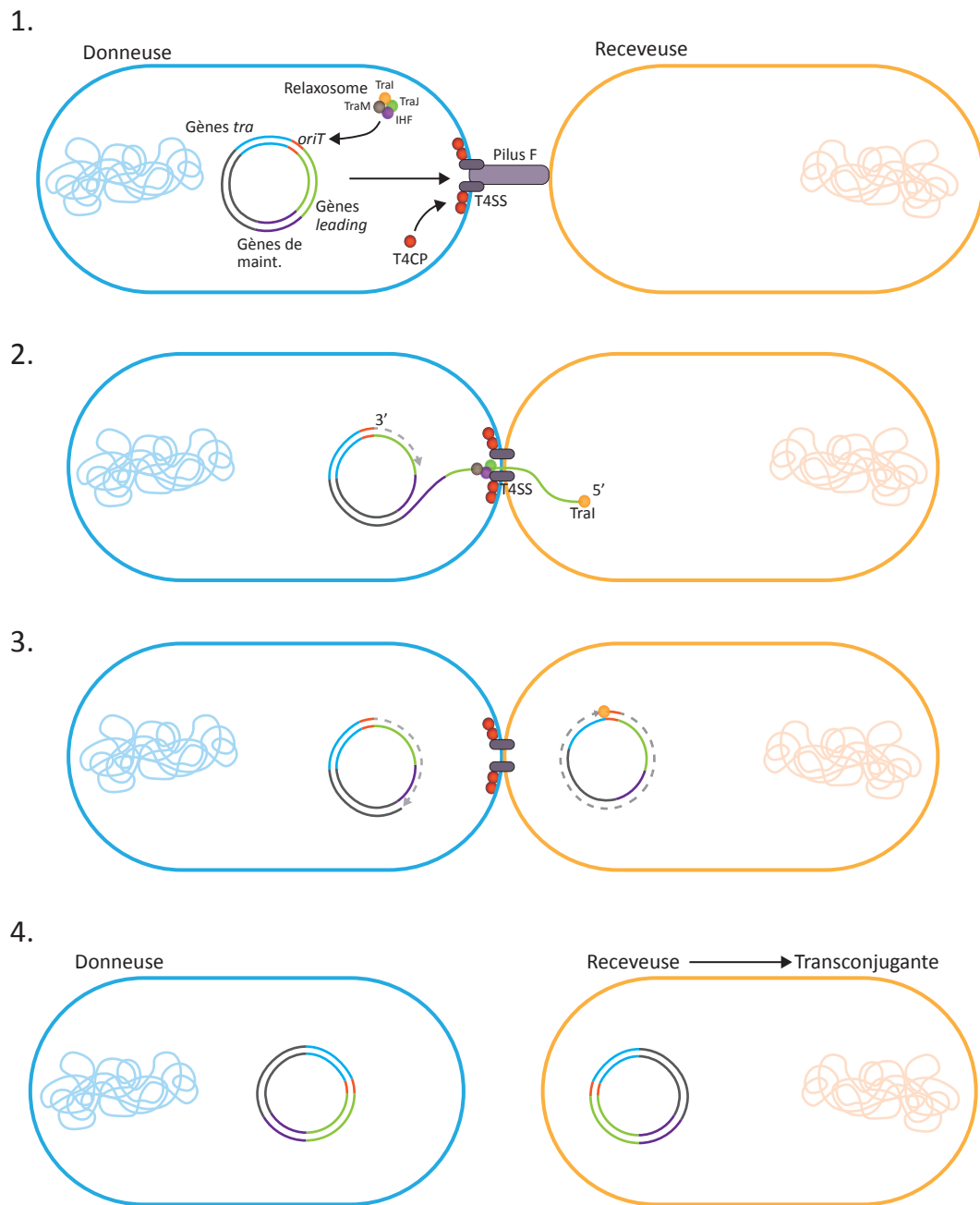


Figure 2. Mécanisme de transfert conjugatif du plasmide F d'une bactérie donneuse à une bactérie receveuse.

Le plasmide F est composé des gènes *leading* (vert), gènes de maitien (violet), gènes *tra* (bleu) et gènes accessoires (gris).

1. La relaxase *Tral*, les protéines *TraJ* et *TraM* ainsi que la protéine hôte *IHF* forment le relaxosome et lient l'*oriT* du plasmide F. En parallèle, l'attachement du pilus F à la receveuse forme la paire d'accouplement tandis que la protéine *T4CP* est recrutée au niveau du *T4SS*.
2. La relaxase *Tral* clive l'ADN plasmidique au niveau de l'*oriT* et reste liée de façon covalente au brin transféré. Le plasmide est transféré sous forme d'ADNsb dans le sens 5'-3' vers la bactérie receveuse.
3. L'ADNsb est simultanément circularisé et converti en ADNdb dans les bactéries donneuse et receveuse.
4. Après conversion en ADNdb et expression des gènes plasmidiques, les protéines associées induisent un changement phénotypique de la bactérie receveuse qui devient alors une transconjugante, c'est-à-dire une nouvelle bactérie donneuse.

de développer des plasmides TAPs (*Targeted Antibacterial Plasmids*) portant un système CRISPR-Cas et capables d'être transférés par conjugaison, permettant de cibler et tuer une souche donnée au sein de populations multi-microbiennes (Reuter et al. 2021). Il est ainsi essentiel d'approfondir nos connaissances fondamentales des mécanismes et des facteurs impliqués dans le processus conjugatif afin d'identifier de nouvelles cibles thérapeutiques et développer des approches innovantes pour limiter la dissémination des plasmides par conjugaison.

3. Mécanisme général de la conjugaison

Bien que le fonctionnement du transfert conjugatif puisse être versatile et varier d'un plasmide à l'autre, un mécanisme général commun de conjugaison peut être dégagé des nombreuses études sur le sujet. Le mécanisme de transfert du plasmide F sert ainsi de paradigme pour l'étude des étapes de la conjugaison, lesquelles sont brièvement décrites ci-après (Figure 2). Le pilus aussi appelé pilus F, va établir un contact entre la bactérie donneuse et une bactérie receveuse et ainsi former la paire d'accouplement (Anthony et al. 1994; Goldlust et al. 2022). La protéine plasmidique TraN exposée à la surface de la cellule donneuse va alors lier la protéine OmpA au niveau de la surface de la cellule receveuse et stabiliser le contact entre les bactéries (Figure 2A) (Manoil and Rosenbusch 1982; Anthony et al. 1994; Virolle et al. 2020; Goldlust et al. 2022; Low et al. 2022). En parallèle, trois protéines plasmidiques TraJ, TraM et TraI s'associent dans la donneuse avec la protéine hôte IHF au niveau de l'*oriT* du plasmide afin de former le relaxosome. La protéine de couplage TraD (T4CP) permet quant à elle de recruter le complexe nucléoprotéique au niveau du T4SS. L'activité relaxase et hélicase de TraI permettent d'induire une coupure spécifique en un site *nic* et initier le transfert unidirectionnel du plasmide dans le sens 5' vers 3' à travers le pore conjugatif (Figure 2B). Le couplage de la réplication plasmidique avec le transfert d'ADNsb permet la génération du brin complémentaire dans les deux bactéries, tandis que la circularisation du brin d'ADN dans la bactérie receveuse ne peut s'effectuer qu'une fois les deux extrémités transférées (Figure 2C) (Lanka and Wilkins 1995; Ilangovan et al. 2017; Dostál and Schildbach 2010). Finalement, l'expression des gènes plasmidiques confère de nouvelles propriétés métaboliques à la cellule transconjugante, faisant d'elle une nouvelle donneuse capable de transférer le plasmide conjugatif (Figure 2D).

Chapitre II : Mécanismes moléculaires de la conjugaison bactérienne

Plasmid Transfer by Conjugation in Gram-Negative Bacteria: From the Cellular to the community Level

Chloé Virolle, Kelly Goldlust, Sarah Djermoun, Sarah Bigot & Christian Lesterlin

Revue publiée dans *Genes* (2020)

1. Contexte

Ma thèse a commencé en septembre 2019, seulement quelques mois avant la crise sanitaire mondiale liée à l'épidémie Covid19 ; dans ce contexte d'abord de confinement puis de retour progressif au laboratoire, l'accès à ma paillasse a été limité voire impossible pendant plusieurs mois, impactant fortement l'avancée de mes travaux expérimentaux. Au laboratoire, nous avons toutefois mis à profit cette période de confinement pour se consacrer à l'écriture d'une revue sur la conjugaison bactérienne publiée dans le journal *Genes* en 2020. Avec deux autres doctorantes également en première année de thèse, Kelly Goldlust et Sarah Djermoun, nous avons réalisé un travail de recherche bibliographique qui, au-delà de l'écriture de la revue, aura été bénéfique pour approfondir nos connaissances sur la conjugaison en ce début de thèse. Cette revue que nous signons toutes trois en co-1^{er} auteur fut l'occasion de faire un état de l'art du processus de conjugaison, à la fois sur le détail de la mécanistique des différentes étapes mais aussi sur son importance au sein des communautés bactériennes. Au vu du niveau de détails de l'étude, cette revue constitue une partie fondamentale de l'introduction de ce manuscrit de thèse.

2. Contenu

Pour l'écriture de cette revue, nous avons fait le choix de décrire le mécanisme de conjugaison bactérienne d'un point de vue plasmide-centré et principalement focalisé sur le plasmide F. Étant le plus décrit dans la littérature et répandu chez les *Enterobacteriaceae*, le plasmide F est considéré comme un paradigme pour l'étude de la conjugaison. C'est donc naturellement que nous avons décidé de nous concentrer uniquement sur ce dernier comme modèle de description, tout en appuyant les différences les plus importantes observées chez d'autres plasmides. Le but de cette revue est de récapituler dans un seul papier des décennies de recherches et publications sur la conjugaison, et de décrire les mécanismes moléculaires régissant la conjugaison du plasmide F de façon chronologique,


allant de la préparation du plasmide dans la cellule donneuse à son transfert et établissement dans la cellule receveuse, son maintien au sein des populations bactériennes et enfin à son rôle au sein des communautés tels que les biofilms. Cette publication nous a également permis d'appuyer les points encore débattus ou questionnés dans la littérature au moment de l'écriture. Elle s'articule ainsi en trois parties : la première section traite des événements se déroulant dans la bactérie donneuse en décrivant la régulation et fonction des gènes *tra* requis pour la conjugaison ; la deuxième section se concentre quant à elle sur la dynamique des facteurs plasmidiques lors de l'établissement et maintien dans la bactérie receveuse, permettant plus tard sa conversion phénotypique en transconjugante ; enfin la troisième et dernière section fait la revue des connaissances actuelles sur l'étendue et l'impact de la conjugaison dans les biofilms, un habitat bactérien pertinent à la fois d'un point de vue environnemental et clinique.

3. Ma contribution

Le travail de recherche bibliographiques a été partagé entre Kelly Goldlust, Sarah Djermoun et moi-même. Mes travaux de recherche se concentrant sur le rôle d'une protéine plasmidique au sein de la nouvelle cellule hôte, j'ai principalement contribué à la partie relative aux étapes de la conjugaison se déroulant dans la bactérie receveuse. Comme dit précédemment, les systèmes de sécrétion de type IV des plasmides conjugatifs sont très conservés chez les bactéries Gram-négatives. Il est donc logique de retrouver de nombreux homologues des différentes protéines qui les composent parmi les plasmides conjugatifs et espèces bactériennes étudiées. Afin de faciliter la lecture et la compréhension de cette revue, Kelly Goldlust et moi-même avons établi une table listant les gènes *tra* du plasmides F et les homologues correspondant à la nomenclature générale.

Review

Plasmid Transfer by Conjugation in Gram-Negative Bacteria: From the Cellular to the Community Level

Chloé Virolle [†], Kelly Goldlust [†], Sarah Djermoun [†], Sarah Bigot and Christian Lesterlin ^{*†} 

Microbiologie Moléculaire et Biochimie Structurale (MMSB), Université Lyon 1, CNRS, Inserm, UMR5086, 69007 Lyon, France; chloe.virolle@ibcp.fr (C.V.); kelly.goldlust@ibcp.fr (K.G.); sarah.djermoun@ibcp.fr (S.D.); sarah.bigot@ibcp.fr (S.B.)

* Correspondence: Christian.lesterlin@ibcp.fr

[†] These authors contributed equally to this work.

Received: 16 September 2020; Accepted: 20 October 2020; Published: 22 October 2020



Abstract: Bacterial conjugation, also referred to as bacterial sex, is a major horizontal gene transfer mechanism through which DNA is transferred from a donor to a recipient bacterium by direct contact. Conjugation is universally conserved among bacteria and occurs in a wide range of environments (soil, plant surfaces, water, sewage, biofilms, and host-associated bacterial communities). Within these habitats, conjugation drives the rapid evolution and adaptation of bacterial strains by mediating the propagation of various metabolic properties, including symbiotic lifestyle, virulence, biofilm formation, resistance to heavy metals, and, most importantly, resistance to antibiotics. These properties make conjugation a fundamentally important process, and it is thus the focus of extensive study. Here, we review the key steps of plasmid transfer by conjugation in Gram-negative bacteria, by following the life cycle of the F factor during its transfer from the donor to the recipient cell. We also discuss our current knowledge of the extent and impact of conjugation within an environmentally and clinically relevant bacterial habitat, bacterial biofilms.

Keywords: horizontal gene transfer; conjugation in Gram-negative bacteria; phenotypic conversion; drug-resistance dissemination; bacterial biofilms; mobile plasmids; F plasmid

1. Introduction

Conjugation was first discovered in 1946 by Edward Tatum and Joshua Lederberg, who showed that bacteria could exchange genetic information through the unidirectional transfer of DNA, mediated by a so-called F (Fertility) factor [1]. It was later realized that the F factor is a replicative extra-chromosomal genetic element, for which they later coined the term plasmid, that can be transferred across the cell membranes of the parental strains. Since this seminal discovery, the identification of a plethora of conjugative elements, including plasmids, conjugative transposons, and integrative conjugative elements (ICEs), has revealed that conjugation is a universally conserved DNA transfer mechanism among Gram-negative and Gram-positive bacteria [2,3]. Conjugation was also shown to be a ubiquitous process that occurs in bacterial communities present in environments such as the soil, on plant surfaces, and in water and sewage, as well as in biofilms and bacterial communities associated with plant or animal hosts [4]. Within these niches, conjugation facilitates the adaptation of bacterial strains by mediating the propagation of advantageous metabolic properties, such as symbiotic lifestyle, virulence, or resistance to heavy metals and antimicrobials. Conjugation is therefore a major driver of the rapid evolution of bacterial genomes [5,6]. This fundamental importance has made conjugation the focus of extensive study over the last decades. Experimental approaches have provided a detailed understanding of the molecular mechanism of conjugational DNA transfer, while systematic sequencing has uncovered the extent of conjugation at the ecological scale.

Conjugative plasmids generally carry all the genes required for their maintenance during the vertical transfer from the mother to the daughter cells, as well as the genes necessary for horizontal transfer during conjugation from the donor to the recipient cell. These functions are encoded by different regions or modules that compose what is generally referred to as the plasmid backbone. Isolation and sequence analysis of an increasing number of conjugative plasmids has revealed considerable diversity in terms of genetic properties and organization. This diversity also indicates that different plasmids might use various regulations, molecular reactions, and strategies to achieve productive conjugational transfer and maintenance.

In this article, we review the key steps of conjugation by following the life cycle of the plasmid during its transfer from the donor to the recipient cell (Figure 1). We focus on the first discovered and extensively described F plasmid, which we use as a paradigm to discuss other conjugative systems in Gram-negative bacteria. The first section describes events occurring within the donor cell, i.e., the expression regulation of the plasmid *tra* genes required for conjugation, the processing of the plasmid by the relaxosome prior to transfer, the composition and function of the conjugative pilus in the mating pair formation process, the central role of type IV coupling proteins (T4CPs), and transfer by the type IV secretion system (T4SS). The second section focuses on the dynamics of the newly acquired plasmid within the recipient cell, i.e., plasmid establishment, which includes protection against host systems dedicated to foreign DNA elimination, early expression of leading genes, and the conversion of the ssDNA plasmid into dsDNA; plasmid maintenance, which includes plasmid replication and segregation; and the eventual phenotypic conversion of the transconjugant into a new donor cell with novel metabolic properties. In the third section, we review our current knowledge of the extent and impact of conjugation within an environmentally and clinically relevant bacterial habitat, bacterial biofilms.

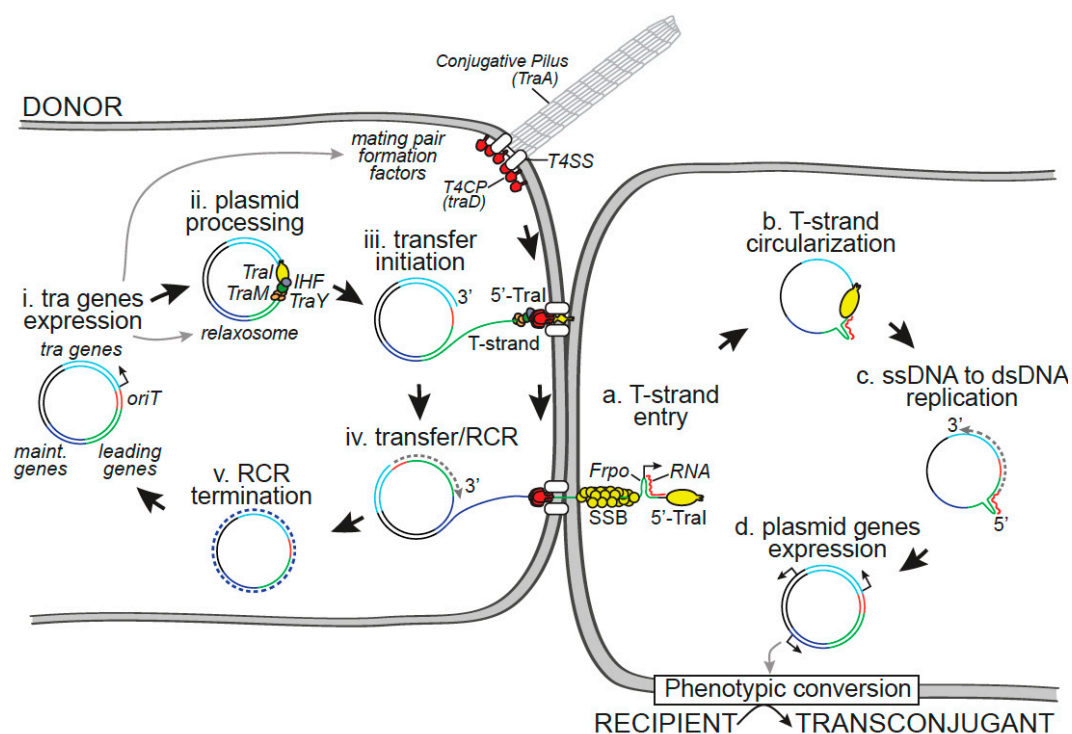


Figure 1. Schematic diagram of the life cycle of the F plasmid during conjugational transfer from the donor to the recipient cell. This F plasmid backbone is composed of the *tra* regions encoding all genes involved in conjugational transfer (light blue); the origin of transfer *oriT* (red); the leading region (green), which is the first to be transferred into the recipient cell; and the maintenance region (dark blue) involved in plasmid replication and partition. (i) The initiation of conjugation requires the expression

of the *tra* genes. Some of the produced Tra proteins form the T4SS and the conjugative pilus that will recruit the recipient cell and mediate mating pair stabilization. (ii) Other Tra proteins constitute the relaxosome (TraI, TraM, and TraY), which, in combination with the integration host factor (IHF), bind to the *oriT* and prepare the plasmid for transfer by inducing the nicking reaction by the TraI relaxase. (iii) Interaction between the relaxosome and the Type IV Coupling Protein (T4CP) initiates the transfer of the T-strand by the T4SS. (iv, v) Transfer of the TraI-bound T-strand in the recipient is concomitant with the conversion of the ssDNA into dsDNA by Rolling Circle Replication (RCR) in the donor. (a) Upon entry into the recipient, the ssDNA T-strand is coated by the host chromosomal SSB, and the single-stranded promoter FrpO adopts a stem-loop structure recognized by the host RNA polymerase to initiate the synthesis of RNA primers. (b) TraI performs the circularization of the fully internalized T-strand. (c) The RNA–DNA duplex is recognized by the host DNA polymerase to initiate the complementary strand synthesis reaction. (d) Once the conversion of the ssDNA plasmid into dsDNA is completed, plasmid gene expression results in the phenotypic conversion of the recipient cell into a transconjugant cell.

2. Within the Donor Cell

2.1. Transfer Gene Expression

2.1.1. Regulation of *tra* Gene Expression

The ability of the donor strain to perform conjugation requires the expression of the transfer genes clustered in the *tra* region of the plasmid. The transfer genes encode all the protein factors involved in the elaboration of the conjugative pilus and the T4SS required for the formation of the mating pair, as well as the relaxosome components needed for the processing of the plasmid prior to transfer (Figure 1, step i). The expression of *tra* genes is regulated by several factors, including plasmid and host proteins, cell cycle progression, and environmental conditions. Most *tra* genes are gathered in one operon under the control of the P_Y promoter, while *traJ* and *traM* genes are located upstream and controlled by independent promoters (Figure 2) [7]. Transfer gene expression follows a specific regulation cascade that starts with the production of the TraJ protein (Figure 2, Step 1), which activates the P_Y promoter and the transcription of the *tra* operon (Figure 2, Step 2). The first gene to be transcribed, *traY*, encodes the TraY regulator protein that activates the P_M promoter, resulting in the production of the relaxosome accessory protein TraM (Figure 2, Step 3) [8]. Therefore, this regulation cascade results in the expression of all genes involved in the elaboration of the conjugative pilus, the T4SS, and the relaxosome, which is composed of TraY, TraM, and TraI. It is observed that *tra* genes are normally repressed, presumably to avoid the fitness cost that would be associated with their constitutive expression [9]. It is important to remark that most regulation systems act by modulating the cellular levels or activity of the primary activator TraJ. In most F-like plasmids (R100, R1, R6-5, and ColB2-K77), the expression of *traJ*, and therefore that of other transfer genes, is repressed at the post-transcriptional level by the fertility inhibition system FinOP (Figure 2) [10,11]. FinP is an antisense RNA that is complementary to the stem-loop structures of *traJ* mRNA. FinP binding hides the ribosome binding site and prevents TraJ translation [12,13]. FinO is an RNA chaperon that protects FinP from degradation by RNase E and stabilizes the formation of the FinP–*traJ* mRNA duplex [14–16]. Moreover, *tra* gene expression is also regulated by chromosomal-encoded host factors [17]. One such regulation involves the silencing of P_Y, P_M, and P_J promoters by the chromosome-encoded histone-like nucleoid structuring protein (H-NS) [18,19]. The H-NS copy number per cell varies during growth [20], thus rendering the F plasmid transfer rate growth phase-dependent, i.e., maximum in the exponential phase, reduced in the mid-exponential phase, and mostly abolished in the stationary phase [21,22]. However, during the exponential phase, H-NS repression activity is itself counteracted by the cooperative binding of TraJ and the host protein ArcA (aerobic respiration control of anoxic redox control) to the P_Y promoter [23]. In the case of the virulence plasmid pSLT of *Salmonella enterica*, H-NS repression activity also reportedly depends on Dam (DNA adenine methylase) methylation of the DNA [24]. Other examples of host factor-mediated regulation of *tra* gene expression include repression by the RNA binding protein Hfq,

which destabilizes both *traJ* and *traM* transcripts [18], and by GroEL chaperone proteins that directly activate proteolysis of plasmid R1 TraJ during the cellular heat shock response [25].

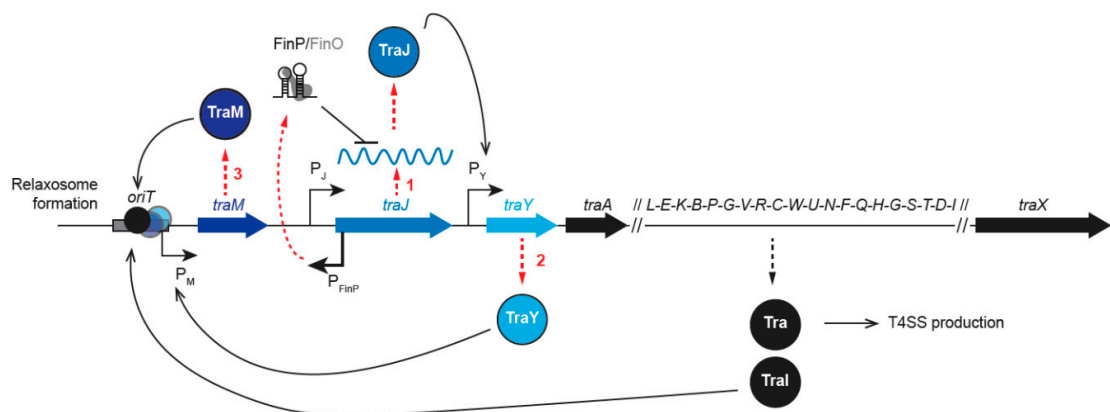


Figure 2. Activation cascade of *tra* gene expression. The P_J promoter first drives *traJ* expression (1). Translated TraJ protein binds to the P_Y promoter to notably produce TraY, which activates the P_M promoter (2), other Tra proteins constituting the T4SS, and the relaxase TraI. Once produced (3), TraM autoregulates its own expression through the P_M promoter and, in combination with TraY and TraI, forms the relaxosome bound to *oriT*. The activation of TraJ at the post-cascade is modulated by the FinP/FinO complex, which represses the translation of TraJ at the post-transcriptional level. Dotted red arrows illustrate the transcription–translation process.

For some other Gram-negative conjugation systems, *tra* gene expression is regulated by quorum-sensing (QS) mechanisms. This is the case for the conjugative tumor-inducing plasmid (pTi), which allows *Agrobacterium* to infect and disseminate within plant hosts. At high cellular density, *Agrobacterium* produces agrocinopine molecules that activate different operons, including the *arc* operon that encodes TraR (unrelated to the F TraR protein), a LuxR-like protein. The binding of TraR to the QS molecule 3-oxo-octanoylhomoserine lactone (OOHL) triggers the transcription of the *trb* and *tra* operons, resulting in the production of the T4SS and relaxosome proteins. The QS lactonase BlcC is also produced, resulting in the degradation of OOHL molecules in the stationary phase or during the carbon and nitrogen starvation associated with host plant death. This regulation provides coordination between the pTi conjugation proficiency and the host state or to the bacterial density within plant tissues during infection [26]. *Pseudomonas aeruginosa* uses QS as a defense mechanism against interspecies conjugation through the production of the QS molecule N-acyl homoserine lactone (AHL), which is involved in the regulation of mechanisms such as virulence, biofilm formation, and metabolism in the *P. aeruginosa* population [27]. AHL produced by *P. aeruginosa* can bind to the *E. coli* LuxR-like transcriptional factor SdiA, which then represses *traI* gene expression and prevents the conjugation of the RP4 broad host range plasmid that is integrated into the chromosome of *E. coli* donors.

Regulating the expression of transfer genes is the chief strategy used to modulate the transfer efficiency of conjugative plasmids. The above examples illustrate that *tra* gene expression is controlled by complex regulatory circuits, which involve the combined activities of plasmids and chromosomal host factors. This tight regulation allows for the control of the transfer efficiency in connection with the plasmid life cycle and the host physiology in response to environmental conditions and populational interactions.

2.1.2. Superspreader Mutations

Over the years, several studies have revealed genetic modifications, so-called superspreader mutations, that dramatically enhanced the conjugation efficiency of conjugative plasmids belonging to diverse incompatibility groups. The first superspreader mutation was characterized in the F

plasmid, which carries an IS3 insertion sequence into the *finO* gene. FinO inactivation destabilizes the FinP-*traJ* mRNA duplex, thus resulting in the upregulation of *traJ* and the constitutive expression of *tra* genes [28]. This naturally occurring mutation accounts for the enhanced transfer efficiency of the F plasmid compared with the related IncF plasmids R100, R6-5, and R1, in which the FinOP regulatory system is still active [29]. More recently, genetically induced superspreader mutations of several resistance plasmids have been isolated in laboratory settings. In the IncI plasmid pESBL, which is associated with extended-spectrum β -lactamase production in *Enterobacteria*, inactivation of the Hft locus triggered the overexpression of conjugative pili and 20-fold enhancement of the transfer efficiency [30,31]. In the *Citrobacter freundii* IncM group plasmid pCTX-M3 that carries the *bla*_{CTX-M-3} gene, the deletion of two genes (*orf35* and *orf36*) resulted in the enhanced expression of *tra* genes and increased plasmid transfer [32]. Another example was reported in the Gram-positive broad host range (Inc18) plasmid pIP501, which is involved in the propagation of vancomycin resistance from *Enterococci* to methicillin-resistant strains of *Staphylococcus aureus*. In this case, the deletion of the *traN* gene encoding the small cytosolic protein TraN (unrelated to the F TraN protein) resulted in the upregulation of transfer factors and the enhancement of the transfer efficiency [33].

Inducing the overexpression of plasmid transfer genes might not be the only way through which *superspreader* mutations increase the transfer efficiency of conjugative plasmids. It was shown that insertion of the Tn1999 transposon into the *tir* (transfer inhibition of RP4) gene of the IncL/M-type plasmid pOXA-48a, responsible for the dissemination of specific extended-spectrum β -lactamase genes in *Enterobacteriaceae*, increases the transfer efficiency by 50–100-fold without affecting *traM* expression levels [34]. The mechanism by which the inactivation of the Tir protein enhances transfer efficiency remains to be elucidated. These studies show that superspreader mutations can emerge by various mechanisms in different conjugative plasmids and have the potential to aggravate the spread of drug resistance plasmids among bacterial organisms.

2.2. Conjugative Pilus, Mating Pair Formation, and Stabilization

2.2.1. F-Pilus Structure and Biosynthesis

Bacterial conjugation is a contact-dependent horizontal gene transfer mechanism that involves a conjugative pilus associated with a T4SS. Electron microscopy imaging was instrumental in analyzing the morphology of numerous conjugation pili encoded by plasmids belonging to different incompatibility groups [35–38]. These studies revealed that pili fall into two main morphological categories—thin flexible and thick rigid, which influence the ability to support conjugation in liquid or on a solid surface. F encodes a thin flexible pilus, which has a tubular structure $\sim 8 \mu\text{m}$ in diameter and up to $\sim 20 \mu\text{m}$ in length and which is constituted by a helicoidal arrangement of a unique protein subunit, the F pilin or TraA [39–44] (Figure 1, step i). The *traA* gene encodes a 121 amino acid pro-pilin peptide that subsequently processed into a 70 amino acid F Pilin [45,46]. The maturation process involves TraQ and TraX proteins [47]. The TraQ chaperone-like protein binds transiently to the TraA pro-pilin precursor, thus allowing its accumulation in the inner membrane by an ATP-dependent pathway [48] and imparting it with the right conformation for a signal peptide cleavage. The processing of pro-pilin into mature pilin requires both cleavage by the host leader peptidase B (LepB) and N-terminal acetylation by TraX [49,50]. This maturation process ensures the availability of pilin subunits in the inner membrane before the assembly of the pilus by TraE, TraK, TraB, TraV, TraC, TraW, TraG, TraF, TraH, TraL, and TrbC encoded by the transfer region [51–53]. Mutational experiments have shown that this set of proteins can separate into different functions. Briefly, TraE, K, C, G, and L are responsible for the assembly of the tip, while TraB, V, W, F, and H are important for the pilus extension, and TrbI is required for pilus retraction [52,53]. The pathway of F-pilus biosynthesis has been extensively reviewed [52,54] and is not detailed here (Table 1).

Table 1. Description of Tra proteins. Proteins are presented following the order of the corresponding *tra* genes in the *tra* region of the F plasmid. The proposed function, the description of their biological activity, the subcellular localization (IM: Inner membrane; OM: Outer membrane; C: Cytoplasm; P: Periplasm), and the homologs in RP4, pTi, or R388 plasmids are shown.

Protein	Proposed Function	Description	Localization	Homolog	Reference
TraM	Relaxosome	<i>oriT</i> binding, TraI stimulation, Interaction with TraD	C		[17,52,55,56]
TraJ	Regulation	Transcription factor (anti-silencer/activator of P _Y)	C		[17,55,57]
TraY	Relaxosome Regulation	<i>oriT</i> binding, Transcription factor (activator of P _M)	C		[17,52,55,57]
TraA	Pilin	Major subunit of the pilus	IM	VirB2 (pTi) TrbC (RP4)	[52,55,56]
TraL	Pilus assembly	Pilus assembly	OM	VirB3 (pTi) TrbD (RP4)	[52,53,55,57,58]
TraE	Pilus assembly	Pilus assembly	IM/P	VirB5 (pTi)	[52,53,55]
TraK	Pilus assembly	Cell envelope-spanning channel	IM/P	VirB9 (pTi)	[52,53,55,56]
TraB	Pilus extension	Cell envelope-spanning channel	IM	VirB10 (pTi) TrbI (RP4)	[52,53,55,56,58]
TraP	Pilus extension	Extended pilus stabilization	IM		[55,57]
TraG	Pilus assembly	Pilus tip assembly	IM	VirB6/VirB8 (pTi)	[52,53,55,57,59]
	Mating pair stabilization	Stabilization via C-terminal Interaction with TraN,			
	Exclusion	Interaction with TraS			
TraV	Pilus extension	Lipoprotein	OM/P	VirB7 (pTi)	[52,53,55,56]
TraR	Regulation	Transcription regulator by binding to RNA polymerase	C		[58,60]
TraC	Pilus assembly	NTPase	IM	VirB4 (pTi) TrbE (RP4)	[52,53,55,56]
TraW	Pilus extension	Pilus synthesis	P		[52,53,56,57,61]
TraU	DNA transfer	DNA transfer	P		[52,55,56]
TraN	Mating pair stabilization	Stabilization of OmpA and Lps binding	OM		[52,55,56]
	Exclusion system	Interaction with TraG			
TraF	Pilus extension	Disulfide bonds for T4SS assembly	P		[52,53,55,56]
TraQ	Pilin maturation	Chaperone-like	IM		[55–57]
TraH	Pilus extension	Interaction with TraF and TraU	P		[52,55]
TraG	Pilus assembly	Pilus tip assembly	IM	VirB6/VirB8 (pTi)	[52,55,57,59]
	Mating pair stabilization	Stabilization via C-terminal Interaction with TraN,			
	Exclusion	Interaction with TraS			
TraS	Entry Exclusion (Eex)	Interaction with TraG	IM		[55,56]
TraT	Surface exclusion (Sfx)	Disaggregation of mating pair after DNA transfer, Interferes with TraN–OmpA interaction	OM		[55,56,62,63]

Table 1. Cont.

Protein	Proposed Function	Description	Localization	Homolog	Reference
TraD	T4CP	Coupling protein/DNA dependent ATPase Interaction with TraM	IM	VirD4 (pTi) TraG (RP4) TrwB (R388)	[55–57,64]
TraI	Relaxosome	Relaxase, transesterase and helicase	C	VirD2 (pTi) TrwC (R388)	[55,57,65,66]
TraX	Pilin maturation	N-terminal acetylase	IM	TrbP (RP4)	[55–57](1)(3)(8)

2.2.2. Pilus Biological Function

The role of the F-pilus in conjugation has been actively debated. It was first proposed that the F-pilus extends to contact the recipient cell and then retracts to bring together the donor and recipient cells and form the mating pair [41,67,68]. This idea was convincingly supported by the direct visualization of the F-pilus dynamics in live cells, using a fluorescently labeled R17 bacteriophage that specifically binds along the pilus sides [69]. This work showed that donor cells produce flexible pili that continuously undergo cycles of extension and retracting, thereby probing the surroundings, regardless of the absence or presence of recipient cells. However, when contact is established with a recipient, pilus retraction draws the cells together, resulting in the formation of a mating pair [69]. In liquid culture, the pili mediate the formation of larger mating aggregates that contain donor and recipient cells in tight wall-to-wall contact [70,71].

Allowing the formation of wall-to-wall contact between mating partners might not be the only role of the F-pilus, which was also proposed to serve as a channel through which single-stranded DNA is transferred during conjugation between distant donor and recipient cells [72]. Undeniably, the pilus axial hole has a diameter (30 Å) that is large enough to accommodate the DNA molecule [41,44]. However, only a few reports provide evidence for conjugational DNA transfer between mating partners that are spatially separated from each other. It was shown that DNA transfer could occur between a donor and recipient that are separated by a 6 micron membrane with pores 0.01–0.1 micron in diameter [73]. Furthermore, microscopy imaging provided some evidence that DNA can be acquired by recipient cells that are not in direct contact with a donor cell [74]. Nevertheless, the F-pilus' ability to transport DNA is still questioned and awaits the clear visualization of DNA transfer between distant donor and recipient cells that are only connected by a pilus.

2.2.3. Factors Involved in the Specificity of Donor–Recipient Interactions

The ability of the pilus to establish contact between donor and recipient cells can be considered the first rate-limiting step in the conjugation process and a key determinant of plasmid host range specificity. In the 1970s, numerous studies attempted to identify the specific recipient receptor required for F plasmid transfer [70,75–80]. The results revealed that mutations localized in the fourth external loop of the major porin *OmpA* or those that alter the inner core composition of the lipopolysaccharide (LPS) affect the transfer of the F plasmid and other IncF-like plasmids, such as R386, R538-1drd, and R1-19, but not the IncFII-type plasmid R100-1 [77,80–82]. Analysis of several *ompA* and LPS mutants revealed that they do not affect pili binding but result in defective mating pair stabilization [83]. Further investigation excluded that TraA is the donor component responsible for specific recognition of the recipient receptors [84] and uncovered the mating pair stabilization function of the outer membrane protein TraN, whose three external loops have been reported to interact with *OmpA* and LPS [85–87]. These findings indicate that *ompA* and LPS mutations do not alter the conjugation efficiency of the closely related IncFII-type plasmid R100, in which the amino acid sequence of the TraN central region is highly divergent from that of F-encoded TraN [59,77,80]. Mating pair stabilization additionally

involves the multifunctional inner membrane protein TraG, of which the N-terminal part also plays a role in piliation and surface exclusion [59,88–90].

OmpA or LPS receptor factors cannot be considered strictly essential to F conjugation since their mutation only decreases transfer efficiency by 2–3 log. Moreover, mating pair stabilization defects can be overridden by performing mating on solid media, suggesting that interactions with OmpA or LPS are needed to stabilize the mating pair formation only in liquid mating [77,81,83]. One might then ask, is the F plasmid an exception to the need for recipient factors in some conditions? A recent study in *Klebsiella pneumoniae* identified the outer membrane OmpK36 homolog of the *E. coli* outer membrane OmpC as a receptor that mediates conjugation of the IncFII plasmid pKpQIL [91]. As observed in the case of the F plasmid, TraN_{pKpQIL} determines the OmpK36-receptor specificity, while complementing a traN_{pKpQIL} mutant with TraN_{R100} abolished this dependence, demonstrating that recipient receptors might be highly specific to the transferred plasmid. In addition to the IncF-type, the conjugation process of IncI-type plasmids was also shown to be sensitive to LPS mutations, and interestingly, some LPS mutations that affect IncI plasmid transfer do not impact the entry of the F plasmid, while others affect both types of plasmid [76,92]. Recently, the PilV adhesin encoded by the IncI1-type plasmid R64 was identified as the donor factor that binds to LPS in the recipient cell [93]. This adhesin is thought to localize to the tip of the thin type IV pilus that is required only in liquid mating conditions, rendering the interaction between PilV and LPS important only under these conditions, as observed for TraN and OmpA or LPS interactions in the case of the F plasmid. In contrast, no such recipient receptors could be identified for the broad host range plasmids RP4 and R388. Indeed, the *ompA* and LPS recipient mutants, which drastically decrease the efficiency of F conjugation, do not affect RP4 conjugation efficiency [94]. Large-scale mutant screening using the *E. coli* Keio collection or random *E. coli* insertion mutant library failed to identify recipient mutants that affect the transfer of the plasmids RP4 [95] or R388 [96].

Remarkably, some broad host range IncP-like plasmids can also be transferred in archaea [97] and eukaryotes such as yeast [98] and mammalian cells [99]. Although the efficiency of conjugation varies among types of recipient cells, these findings strongly suggest that plasmid transfer does not require any specific factors or active mechanisms on the recipient side. Alternatively, a “shoot and pump” conjugation model envisages that the type IV secretion apparatus could act like a syringe that is able to inject DNA into any kind of membrane, using the pilus as a needle [100]. Perforation of the cell wall bilayer of the recipient could be achieved by force or by dedicated enzymatic activity exposed at the pilus tip. The lack of a requirement for specific receptors on the surface of the target cell is not an exception to the conjugative T4SS. Indeed, although the structural components of the type VI secretion system machinery have been widely documented, no studies have yet characterized genetic factors that can act as target receptors on the prey cell surface.

2.3. Plasmid Processing by the Relaxosome

The initiation of conjugation requires the assembly and activity of a protein complex, the relaxosome, that allows the processing of the plasmid before DNA transfer (Figure 1, step ii). Plasmid processing involves a site- and strand-specific DNA cut (nick) at the *nic* site located in the origin of transfer (*oriT*) and the extrusion of the single-stranded DNA that will be transferred (T-strand) [101–103]. In the F system, these two reactions are performed by the multifunctional TraI relaxase protein, which has both a transesterase domain that catalyzes the *nic* reaction and a DNA helicase domain that unwinds the plasmid DNA [64,104–109]. Crucially, TraI recruitment and activity are governed by auxiliary proteins, including the integration host factor (IHF) and the plasmid-encoded TraY and TraM proteins, which have distinct roles in the relaxosome formation and activity at *oriT* [110–112]. The binding of IHF and TraY to their respective cognate binding sites *ihfA/ihfB* and *sbyA* located in *oriT* modulates the architecture of the DNA, thereby stimulating the loading of TraI [113–117]. The TraM protein regulates its own expression by binding to the *sbmA* and *sbmB* sites, located in the PM promoter, and stimulates the DNA relaxation reaction through direct interaction with TraI after binding to the

sbmC site located in the *oriT* region [118–122]. The TraI nicking reaction involves a catalytically active Tyr residue [65,123] and results in the relaxation of the plasmid dsDNA, where the 5'-phosphate (P) end of the nicked strand (or T-strand) remains covalently bound to TraI (Figure 1, step iii) [106,108,124–127]. After the nicking reaction, the circular ssDNA conjugative plasmid is converted into dsDNA by Rolling Circle Replication (RCR) in the donor, while the linearized T-strand DNA bound to TraI at the 5' end is transferred into the recipient cell through the conjugative pore (Figure 1, step iv).

2.4. Initiation of Rolling Circle Replication in the Donor Cell

The rolling circle replication (RCR) mechanism is employed for the vegetative replication of some bacterial plasmids and has been very well reviewed [128–130]. RCR is key to the transfer process of many Gram-negative and Gram-positive conjugative plasmids but also to the infection cycle of other mobile genetic elements, such as DNA/RNA viruses and bacteriophages [123,131]. The RCR reactions involved in vegetative replication or in plasmid transfer are very similar. The initiation and termination of RCR reactions, performed by the Rep protein during vegetative plasmid replication, are achieved by the relaxase protein during conjugation. Indeed, Rep and relaxases serve closely related functions, primarily allowing RCR initiation by nicking the double-strand DNA at the *dso* site (double-stranded origin) or the *oriT* site, respectively [132]. The nicking reaction generates a 5'-P end that remains covalently bound to Rep or TraI and a 3'OH end used as a primer for the host DNA polymerase III. While DNA polymerase III performs leading strand elongation, the parental double helix is unwound, and RCR ends with a second nicking reaction that releases the newly synthesized DNA strand (Figure 1, step v). In the case of vegetative RCR, DNA unwinding is performed by a host DNA helicase recruited by the Rep protein, while Rep itself ensures termination and the second nicking reaction. One major aspect of conjugation-associated RCR is that replication of the two ssDNA strands occurs in different cells, i.e., the leading strand is replicated in the donor, while the T-strand (lagging strand) is transferred and replicated in the recipient cell (Figure 1). Because the relaxase that initiates the nicking reaction is transferred together with the T-strand [65,133,134], a second relaxase protein is required in the donor to perform DNA unwinding as well as the second nicking reaction [3,65,123]. Consistently, biochemical assays show that two relaxase molecules bind to *oriT*: one associated with the 5' end that is in an open transesterase conformation and one associated with the 3' end that is in a closed helicase conformation [135].

2.5. T4CP Connects the Relaxosome to the T4SS

After processing by the relaxosome complex, the nucleoprotein complex, composed of the T-strand and the covalently bound TraI, needs to be recruited to the conjugative pore for transfer (Figure 1, step iii). This connection is mediated by the interaction between the relaxosome and the Type IV Coupling Protein (T4CP) located at the cell membrane [3,100]. All conjugative systems have their own T4CPs, such as TraD, TraG, and TrwB for the F, RP4, and R388 plasmids, respectively. T4CPs are not required for pilus production or DNA processing, yet they are key to substrate specificity [136]. Our understanding of the molecular interactions required for specific substrate recognition and translocation is still incomplete. A great deal of information has been provided by comparing the structure of F-like T4SS [137] to various T4SSs involved in protein or nucleoprotein transport [138–141]. It appears likely that conjugation systems are derived from ancestral protein translocation machinery that evolved to coincidentally translocate DNA. In this view, the T4CP would serve as the substrate receptor that interacts with one or several relaxosome components to recruit the T-strand to the T4SS. In the case of the F plasmid and some other plasmid systems, it is well established that TraD interacts with the TraM relaxosome protein [142–146]. Interaction between the T4CP and the relaxase has been demonstrated for RP4 [147], R1 [1] and R388 plasmids [148]. Such interaction has been speculated in the F system but remains elusive [107,149].

T4CPs are DNA-dependent ATPases anchored to the cell membrane via their N-terminal domain and have been shown to interact with the T4SS components in R27 [150] and R388 plasmid

systems [148]. T4CPs show similarities to membrane-anchored ring DNA translocases, such as SpoIIIIE and FtsK, which are involved in chromosome DNA translocation during sporulation and cell division, respectively [100,151,152]. T4CP binds non-specifically to DNA, with a higher affinity for ssDNA [147,153,154], on which it forms oligomers with enhanced ATPase activity [155,156].

Altogether, these findings led to a model in which membrane-anchored T4CPs interact directly with the relaxosome and form hexameric structures on the T-strand, which actively translocate through the conjugation pore during transfer. However, it remains unclear whether a signal is required to activate the coupling function of the T4CP in a donor cell in which the T4SS and the relaxosome are already assembled and functional [3]. It has been suggested that the stability of the TraD oligomeric complex depends on an as yet unidentified F-encoded protein, which could then be a key regulator of plasmid transfer activation [155]. It has also been suggested that the formation of the mating pair could transduce a signal to activate the T4CP and trigger the transfer of the processed T-strand [3]. Notably, it was shown that the relaxase has to be unfolded to be translocated into recipient cells [134]. In *A. tumefaciens*, as in many other Gram-negative and Gram-positive systems, the unfolding of translocated proteins is proposed to be performed by the VirB11-like ATPase, which is absent from the F plasmid system [52,140,157]. However, one can reasonably presume that TraI unfolding also requires ATPase activity that involves one of the ATPases of the F T4SS.

3. Within the Recipient Cell

3.1. Plasmid Circularization by TraI

The relaxase is transferred to the recipient, where it is refolded and able to perform several activities required for the completion of the conjugation process (Figure 1, step a) [65,133,158]. The helicase activity of the internalized relaxase is thought to perform 5' to 3' tracking of the T-strand. Pulling by the relaxase from the recipient together with pushing by the T4CP from the donor presumably facilitates the transport of the T-strand through the conjugation pore [3]. Once both extremities of the *oriT* are brought together in the recipient, the relaxase performs the joining reaction, resulting in the recircularization of the ssDNA plasmid (Figure 1, step b) [65,133,158,159]. An alternative model proposes that the nicking of the newly synthesized *oriT* occurs in the donor cell before transfer [160]. There is no evidence for the requirement of additional host or plasmid factors in the circularization of the internalized T-strand. After completion of the recircularization reaction, the recipient cell possesses a single-stranded circular copy of the conjugative plasmid.

3.2. Avoiding Host Defense Systems against Foreign DNA

The newly acquired ssDNA conjugative plasmid might be considered as foreign DNA, against which host bacteria have developed defense mechanisms, such as restriction modification, exonucleases, and recombination system or adaptive immunity, such as the CRISPR-Cas system [161]. Despite these defense mechanisms, horizontal gene transfer plays an important role in genomic evolution (5–6% of bacterial genomes and up to 20% in some organisms) [6,162,163], implying that transferrable plasmids have evolved adaptive mechanisms to counteract these host defenses.

The restriction modification system (RM) is a ubiquitous defense mechanism found in 90% of sequenced bacterial genomes and other prokaryotes and is based on restriction enzymes and methylation [164]. Restriction modification mechanisms are described as a “primitive immunity system” against exogenous DNA [165]. These systems are based on restriction enzymes that specifically target unmethylated dsDNA sequences located in the newly acquired mobile genetic elements, while the host DNA is protected by methyl groups added to specific adenine or cytosine residues [165]. Whether the RM system can target the ssDNA plasmid before the complementary strand synthesis remains unclear. However, plasmids have evolved various strategies to counteract enzymatic DNA degradation upon entry into the new host cell. IncN, IncI, and IncF plasmids encode ArdA and ArdB proteins (alleviation of restriction of DNA) that directly inhibit the REase (Restriction Endonuclease) by

mimic DNA sequences, thus competing for enzyme targets [166–168]. IncW plasmids encode the ArdC protein that protects the transferred T-strand by transiently blocking the restriction sites [169]. More recently, it was shown that an *hde* operon (host defense evasion) of IncI plasmids encodes two genes involved in anti-RM (*vcrx089* and *vcrx090*) [170]. In addition to the production of inhibitory proteins, some plasmids have completely lost these restriction sites, as in the case of the RP4 plasmid [171].

CRISPR-Cas immune systems (Clustered Regularly Interspaced Short Palindromic Repeats and the CRISPR-associated protein) represent another defense mechanism against foreign DNA. CRISPR-Cas systems, found in ~45% of bacterial and up to 84% of Archaea genomes [172,173], have been described as being protective against infection by bacteriophages and, more recently, against plasmid acquisition [174]. It was then discovered that some phages encode an anti-CRISPR Acr protein that inhibits the activity of the CRISPR-Cas system [175,176]. Importantly, anti-CRISPR Acr *loci* have been identified in conjugative elements and plasmids of *Listeria*, *Enterococcus*, *Streptococcus*, and *Staphylococcus* [177]. These *loci* encode the CRISPR-Cas inhibitors AcrIIA16–19, which prevent exogenous DNA nicking mediated by the Cas9 enzyme *in vivo*. Mahendra et al. have also shown that conjugation of a Cas9-targeted plasmid of *E. faecalis* was possible in the presence of these CRISPR-Cas inhibitors. Encoding Acr-like proteins is therefore an efficient strategy by which conjugative plasmids facilitate their dissemination by avoiding degradation by the host CRISPR-Cas immune system. Another strategy is for conjugative plasmids to encode a Bet/Exo system able to repair double-strand breaks caused by CRISPR-Cas during conjugation, as recently reported for the IncC plasmid pVCR94 [170]. Expression of these genes inside recipient bacteria after the acquisition of the *V. cholerae* pCVR94 plasmid enables survival against exogenous DNA defense mechanisms without the involvement of anti-CRISPR-Cas proteins.

3.3. Role of the Leading Region Genes and Conversion of the ssDNA Plasmid into dsDNA

3.3.1. Early Expression of the Leading Region Genes

The leading region of conjugative plasmids is the first to be transferred into the recipient cell during conjugation (Figure 1, step a) [57]. The F plasmid leading region is well conserved, with a size of 13 kb and a location that is directly adjacent to the *oriT*, and encodes for at least eight proteins [178], including a homolog to the chromosomal single-strand binding protein SSB (SSB_C), PsiB, and other proteins of unknown function. Importantly, plasmid *ssb* (*ssb_p*) and *psiB* genes are expressed early upon entry of the plasmid into the recipient bacteria but not in the donor cells [179]. Similarly, RT-PCR studies showed that the expression of the *psiB* and *ardA* genes of the IncI1 plasmid begins 5 min after transfer initiation [180]. These observations suggested that leading region genes could be expressed rapidly from the newly acquired plasmid in single-stranded form, before its conversion into dsDNA. It was later shown that the leading region contains a specific 328 bp *Frpo* region (for F plasmid RNA polymerase), which, when single-stranded, can form a stem-loop structure presenting –10 and –35 double-stranded boxes that are recognized by the host RNA polymerase, which initiates the synthesis of RNA primers *in vitro* [181]. It was therefore proposed that *Frpo* may serve as a single-stranded promoter that allows the early expression of the leading region genes (Figure 1, step a).

Frpo was also proposed to direct the single-strand to double-strand conversion of the F plasmid. *In vitro* assays showed that the RNA primers synthesized by the RNA polymerase from *Frpo* persist as an RNA–DNA duplex that is recognized by host DNA polymerase III to initiate complementary strand synthesis [181]. *Frpo*-type sequences, also termed *ssi* for single-strand initiation sequence, are found on various conjugative plasmids, including R6K, R100, Cole1, Cole2, Col1B, and RSF1010 [182–185], and are functionally comparable to *ssu* sequences (single-stranded origin) involved in the rolling circle replication mechanism [123,129,186]. These findings are consistent with the previous observation that complementary strand synthesis of the ssDNA F plasmid inside the recipient bacteria involves a cooperative mechanism between host RNA polymerase and DNA polymerase III [187].

Altogether, these findings led to a model in which *Frpo* can help to initiate early gene expression and the DNA synthesis reaction that converts the ssDNA plasmid into dsDNA duplex immediately upon entry of the T-strand into the recipient cell (Figure 1, step a–c). Whether *Frpo* performs these functions during conjugation in vivo remains to be demonstrated.

3.3.2. PsiB Inhibits the SOS Response

In the recipient cell, the presence of abnormal amounts of ssDNA, usually associated with DNA damage, results in the induction of the SOS response [188,189]. More precisely, the loading of the RecA recombination protein onto ssDNA results in the formation of the presynaptic filament, which stimulates the autocatalytic cleavage of LexA, the repressor of the SOS regulon. The SOS response triggers the induction of the division inhibitor Sula, resulting in cell filamentation and potentially the death of the transconjugant cell. SOS also induces the production of nucleases and other DNA processing factors that could provoke the degradation or mutation of the transferred ssDNA or its processing as a recombination intermediate [190]. To counteract these effects, several conjugative plasmids, including F, encode the PsiB protein (plasmid SOS inhibition), which inhibits SOS induction [191]. The depletion of *psiB* has mild effects on the efficiency of conjugation but increases the host SOS response by up to six-fold [179]. PsiB interacts directly with RecA, thereby inhibiting several activities, such as DNA binding, LexA cleavage, and the strand exchange reaction [192,193]. SOS response inhibition by PsiB is even more potent in the presence of the SSB_C protein that coats the ssDNA. PsiB is well conserved among conjugative plasmids and is considered important for the early steps of plasmid establishment in the recipient, consistent with its early production in the transconjugant cells [57,191].

3.3.3. Roles of the Host and Plasmidic SSB Proteins in Plasmid Establishment

Upon entry into the recipient cell, the transferred ssDNA plasmid is coated by the host SSB_C protein. SSB_C is a universally conserved essential protein that binds non-specifically to ssDNA. It is involved in various mechanisms, including DNA replication, repair, and recombination; SOS induction; and other DNA metabolic processes [194,195]. Upon binding, SSB protects the ssDNA against enzymatic degradation and increases the processivity of DNA polymerases II and III [196] during the replication reaction that converts the ssDNA strand into the dsDNA helix. The rapid recruitment of the host SSB_C protein to the transferred ssDNA has recently been visualized by fluorescence microscopy [197]. This work revealed that SSB_C proteins are rapidly recruited to the ssDNA that penetrates the recipient cell, presumably protecting it and facilitating its processing (Figure 1, step a). Interestingly, the F plasmid, as in many other conjugative plasmids, encodes its own SSB_P protein, which is homologous to the *E. coli* SSB_C [198]. One might then ask, what is the benefit gained by conjugative plasmids encoding their own SSB_P, and what is the specific function of SSB_P compared with the chromosomal SSB_C?

SSB_P binds ssDNA non-specifically, and SSB_P of different incompatibility groups (IncF, IncI, IncY, Inc9, IncT, and IncB/O) can partially complement conditional mutations of the *E. coli* *ssb_C* gene [197,199–201]. Although the expression of the F plasmid-encoded SSB_P protein in *trans* enables the growth of the *ssb_C* deletion mutant, complemented mutants exhibit some filamentation and growth rate reduction [202]. Moreover, a reduced affinity to ssDNA is observed for the F plasmid SSB_P in comparison with the *E. coli* SSB_C, and the F plasmid SSB_P cannot stimulate the reaction of DNA synthesis by DNA polymerase III in vitro [203]. Sequence alignment revealed that SSB_P proteins that complement the *E. coli* *ssb_C* mutant share high homology only with the N-terminal part of *E. coli* SSB_C [203]. The SSB_C N-terminal region contains the domains for ssDNA binding and monomer–monomer interactions to cooperatively maintain the binding of the tetrameric structure of SSB_C to ssDNA. This structural conservation would explain the ability of SSB_P to bind ssDNA. However, the C-terminal domains of SSB_P are much more homologous to each other than to SSB_C [203]. However, as this domain interacts with partner proteins that constitute the SSB_C interactome, one possibility would be that the interactome of SSB_P and the reaction it is involved in might be different from that of SSB_C.

Not all SSB_P proteins have been shown to complement *E. coli* *ssb_C* mutants [199]. The latter study found that the inability of SSB_P from IncP-like RK2 to complement the *E. coli* *ssb₁* mutation could be attributed to *ssb_P* gene repression by the RK2 *kor* genes and that a derepressed plasmid indeed complemented the thermosensitive growth of *E. coli* *ssb₁* mutations [204]. It is thus reasonable to consider the possibility that abundant SSB_P could also complement the *ssb_C* mutant.

To date, the function of the F plasmid SSB_P in the context of conjugation is still unclear. The SSB_P protein could contribute to the protection of the transferred ssDNA by inhibiting enzymatic degradation or the recruitment of inhibiting proteins of the host. However, its expression timing instead supports the idea that SSB_P could be involved in the complementary strand synthesis of the transferred DNA or could simply increase the pool of available single-strand binding protein, which is required for the first cycle of vegetative replication of the plasmid.

3.4. Plasmid Maintenance: Replication and Segregation

Maintenance of the newly acquired dsDNA conjugative plasmid in the recipient cell lineage depends on two main active mechanisms: plasmid replication and segregation of the plasmid copies into daughter cells over generations.

The mechanisms of plasmid DNA replication in bacteria have been extensively studied and are the focus of well-referenced reviews [123,128,205–208]. Here, we stress the role of replication in conjugation host-range specificity. The F plasmid is efficiently transferred to *E. coli* and relatively close enterobacteria, while no transconjugant can be recovered after mating with more distant bacteria, such as *Vibrio* or *Pseudomonas*. As early as 1982, host range restriction was attributed to the plasmid's inability to replicate in the recipient bacteria rather than to the inefficiency of plasmid transfer *per se* [188]. This was demonstrated by showing that mobilizable plasmids containing a cis-acting origin of transfer of the F plasmid and an origin of replication that is active in the tested recipient can then be transferred by the F conjugation machinery in *Pseudomonas* [188], *V. cholerae* [209], and yeast [98]. The same approach was employed to show that pCTX-M3, an IncI-like plasmid, was able to use its conjugation machinery to transfer a mobilizable plasmid to host recipients in which pCTX-M3 does not replicate [32]. The failure to replicate the F plasmid in *P. aeruginosa* comes in part from an inability of the plasmid replication protein RepE in the RepFIA replicon in complex with host DnaA-*oriS* to form a stable interaction with the host helicase DnaB [210]. In contrast, broad host range plasmids such as RK2 regulate their maintenance by modulating alternative strategies of replication depending on the host [211]. These findings indicate that the host range of the conjugation machinery and replication origins belonging to the same plasmid differ and can be mechanistically uncoupled. The specificity of narrow host range plasmids appears to be limited by the specificity of their replicon rather than by their transfer range.

Maintenance of the newly acquired dsDNA plasmid also requires the segregation of plasmid copies into the daughter cells during transconjugant cell division. To do so, low copy number plasmids encode active partition systems, of which the mechanism, biological functions, and conservation have been extensively reviewed [212–216]. In the context of conjugation, it is worth mentioning another maintenance strategy that involves the integration of the newly acquired conjugative DNA into the chromosome. Chromosome integration ensures the stable inheritance of the conjugative elements by vertical gene transfer over generations. The first characterized example was again the F plasmid, which uses insertion sequences (IS) and RecA-dependent homologous recombination to integrate into the *E. coli* genome [217]. The integrated plasmid can still initiate the conjugative transfer of the whole chromosome of the resulting "Hfr" strain (high frequency of recombination). This process of transfer is both progressive and oriented, and the order in which chromosomal genes are transferred depends on the position where the F plasmid was integrated. Alternatively, the integrated F plasmid can be excised out of the chromosome and recover its original autonomous form [218]. Chromosome integration is widely used by mobile DNA, such as ICE (Integrative Conjugative Elements), transposons, and phages,

in both Gram-negative and Gram-positive bacteria; all of these systems have their particularities, especially regarding the recombination systems used for their integration/excision [219,220].

3.5. Phenotypic Conversion of the Transconjugant

The expression of genes carried by the newly acquired genetic element results in the phenotypic conversion of the recipient cell into a transconjugant that exhibits additional metabolic properties (Figure 1, step d). The expression of plasmid genes involved in DNA transfer converts the transconjugant into a new donor that is able to further transfer the plasmid to the population, thus accounting for the exponential rate of conjugative plasmid dissemination (see *tra* gene expression, Section 2.1). Not all genes encoded within the *tra* region of the plasmid backbone are directly involved in the process of DNA transfer. Indeed, conjugative plasmids often carry immunity (or exclusion) gene systems that are widespread in Gram-negative and Gram-positive organisms [90,221–228]. These immunity systems limit the ability of plasmid-carrying cells to serve as a recipient for the same plasmid [42,54,62,229]. Preventing self-mating by surface exclusion is thought to avoid the metabolic cost and potential cell death associated with repeated plasmid transfer but also to be important for plasmid stability and evolution [62,229].

The F plasmid immunity system relies on two factors—TraT and TraS proteins, neither of which is required for F-pilus synthesis or DNA transfer [56,230–232]. These two exclusion factors work at different levels. TraT is an abundant outer membrane protein that is thought to span the cell surface [230,231]. TraT production inhibits the formation of stable mating aggregates, presumably by interfering with the interaction between the pilus and recipient surface receptors. Consistent with this idea, it was reported that TraT interacts with OmpA, further suggesting that it could compete with TraN, which is key to mating pair stabilization [85,86,233]. TraS is an inner membrane protein, the production of which only slightly reduced the aggregation of mating populations but reduced DNA transfer frequencies by 100–200-fold. It is thus proposed that TraS acts by preventing DNA transfer when stable mating aggregates have already formed [230,231,234]. In F-like plasmids, it is proposed that TraS interacts with TraG to achieve the entry exclusion process [89,90]. For these reasons, TraS is referred to as an entry exclusion protein (Eex), and TraT as a surface exclusion protein (Sfx). Like other *tra* genes, *traS* and *traT* expression is controlled by TraJ, implying that transconjugant cells concomitantly acquire plasmid transfer ability and immunity to self-transfer during the phenotypic conversion.

In addition to genes located on the plasmid backbone, conjugative plasmids may carry additional genes that are not directly involved in conjugation but in a variety of biological functions, such as virulence, biofilm formation, symbiotic lifestyle, membrane trafficking, resistance to heavy metals, and, most importantly, resistance to antibiotics. Acquisition of these metabolic functions potentially facilitates bacterial adaptation and survival in changing environments and makes conjugation a major driver of the evolution of bacterial genomes. The successful maintenance of conjugative elements in bacterial populations shows that this selective advantage compensates for the metabolic burden associated with the metabolism of the newly acquired genetic information (highjacking of the host replication, transcription, and translation machineries) [235]. The most prominent example is the acquisition of conjugative drug resistance plasmids, which enable bacterial proliferation in microbial communities that contain antibiotic-producing organisms or in antibiotic-polluted and clinical environments. Indeed, analysis of commensal, environmental, and clinical antibiotic-resistant pathogenic strains revealed a multitude of conjugative plasmids that carry one or more genes for resistance to most, if not all, classes of antibiotics currently used in clinical treatments. Conjugation is considered to be the most widespread intra- and interspecies resistance transfer mechanism, accounting for 80% of acquired resistance [236].

4. Conjugation in Natural Habitats: The Example of Bacterial Biofilms

Gene transfer by conjugation is known to contribute to the genetic dynamics of bacterial populations living in a variety of environments, including the soil, on plant surfaces, and in water and sewage,

as well as in bacterial communities associated with plant or animal hosts [4]. Bacteria are generally considered to be planktonic unicellular organisms, yet in natural and clinical environments, they often live in complex structures called biofilms. Biofilms shelter bacteria from external hazards but have also been proposed to offer a niche that facilitates the dissemination of drug resistance determinants by conjugation. Below, we review our current understanding of the interplay between biofilms and bacterial conjugation.

4.1. The Biofilm as a Niche Promoting Bacterial Conjugation

In natural environments, bacteria predominantly live in spatially structured communities termed biofilms, in which a self-produced extracellular matrix holds the cells together [237]. Planktonic cells that initiate biofilm formation can adhere to a living or inert surface (surface-attached biofilms) or can be present at the air–liquid interface as a free-floating community (pellicle). Bacterial biofilms are found in virtually every ecosystem on Earth, from aquatic systems (sludge, rocks, and wastewater) to terrestrial environments (rhizosphere) and human organisms (skin, intestinal, urogenital, and respiratory tracts). Furthermore, biofilms are associated with persistent and severe infections because of their ability to colonize medical devices and implants. Indeed, biofilm structures offer protection against hostile environments and, more worryingly, against antibiotic treatments. The biofilm architecture depends on the bacterial species, the surface colonized, and environmental conditions, but this lifestyle is characterized by the production of extracellular polymeric substances (EPSs) mainly composed of polysaccharides, proteins, lipids, and extracellular DNA. EPS matrix production is dynamic and continuous and mediates the formation of the biofilm architecture in which aggregates of microorganisms are trapped.

Many studies on bacterial conjugation have shown that plasmid transfer can occur in both natural and artificial biofilms, from the aquatic environment [238], phytosphere [239], animal and human hosts [240,241], or reactor-associated biofilms [242,243]. These papers studied plasmid transfer at the population level and mainly relied on limited cultivation-based assays that probably underestimate the extent of conjugation in natural biofilms. Further works have studied conjugative plasmids expressing fluorescent markers, allowing the direct in situ visualization of donors, recipients, and transconjugants at the single-cell level within several types of biofilms formed at the liquid–air surface [244], on a semisolid agar surface [245–247], on a filter [248], in flow chambers [246,249,250], or in a reactor [251].

The biofilm environment provides a high cell density and close cell-to-cell proximity that may facilitate HGT through bacterial conjugation. In line with the view that biofilm is a hot spot niche of conjugation, several studies have shown that the frequency of plasmid transfer is higher in the biofilm than in the planktonic mode of growth [252–255]. Although the biofilm appears to be a favorable environment for HGT by conjugation, many studies at the single-cell level have reported limited plasmid propagation inside a preformed established biofilm beyond the contact zone between the donors and recipients [256]. These observations are directly linked to the complex spatial structure of the biofilm, which might have a critical impact on horizontal plasmid spread within a biofilm.

4.2. Impact of the Biofilm Structure on Conjugation

The biofilm is a complex structure and sometimes composed of mixed bacterial species. The matrix shapes the spatial organization by clustering cells in microcolonies in an architecture characterized by nonuniform cell arrangements, open channels, pores, cavities, and different layers of living cells [257,258]. Such an organization determines the formation of cell clusters/aggregates and could therefore influence the efficiency of conjugative transfer [244]. This possibility can be addressed using microscopy to analyze the distribution of cells that are active in conjugation within biofilms. To date, most studies have investigated the spread of the GFP-tagged *Pseudomonas putida* TOL plasmid. Analysis of *P. putida* recipient biofilms established in flow chambers revealed that transconjugants appeared at the top surface of the biofilm but not in the deeper layers, reflecting a limited invasion of the transferred plasmid [246,250]. On an agar plate, transconjugants only appeared at the contact

zone between the TOL plasmid donors and the recipient colonies [245,246,259]. Limited transfer to the outer layers of the biofilm was also observed for IncF, IncI, and IncW plasmids in *E. coli* [247]. It has been proposed that transfer can only be efficient over a short period between metabolically active cells growing at the donor–recipient interface [246,260]. Consistently, it was shown that plasmid invasion stops in non-dividing cells [259].

Within biofilm structures, chemical gradients of oxygen, nutrients, temperature, and pH create microenvironments that influence the metabolic activity of bacterial cells [261]. This results in physiological heterogeneity between the cells that surround the border of the biofilm and those that are embedded deep inside. Furthermore, variations in the spontaneous mutation frequency within parts of the biofilm result in the emergence of variant subpopulations with genetic heterogeneity [262]. Whether and how these factors impact the spatial pattern of conjugation within biofilms remain unknown.

4.3. Impact of Conjugative Plasmids on Biofilm Formation

Several studies have investigated the implication of the presence of conjugative plasmids from diverse incompatibility groups for biofilm formation ability [263–267]. To initiate biofilm formation, planktonic cells produce cell appendages like flagella and adhesion factors such as type IV pili and type 1 and curli fimbriae [268,269]. Genes coding for these types of accessory factors that promote attachment to biotic or abiotic surfaces are often found in conjugative plasmids, resulting in increased host biofilm formation [253]. Examples include type 3 fimbriae of the IncX1 plasmid pOLA52 [270], non-conjugative type IV pili of the IncI1 plasmid pSERB1 [271], or pilus-like structure and surface adhesins of the *Enterococcus faecalis* plasmids pBEE99 and pCF10, respectively [272–274]. In 2001, Ghigo made the unexpected observation that the conjugative pilus itself of a derepressed F plasmid can promote the biofilm of *E. coli* cells that are initially unable to form such a structure and revealed that the pilin TraA is the main adhesion factor that induces biofilm formation [263]. Microscopic structure analysis of derepressed IncF plasmid R1drd19- and F-carrying *E. coli* biofilm showed the rapid formation of a dense and mature 3D mushroom-type biofilm similar to the *P. aeruginosa* biofilm architecture [275]. The formation of this peculiar architecture and the biofilm maturation generated by derepressed plasmids override the need for cell surface appendages such as flagella, type 1 fimbriae, Ag43, or curli, which are essential to *E. coli* biofilm [275]. In contrast, maturation of the 3D mushroom-type biofilm structure depends on curli production, induced in *E. coli* by the natural F plasmid, which does not constitutively express F-pili [276]. The presence of the plasmid R1drd19 also increases *E. coli* biofilm formation by decreasing the motility and increasing the level of quorum-sensing inducer AI-2 [277,278], and the IncP-9 TOL plasmid in *P. putida* increases the production of extracellular DNA known to play a role in the structure of the biofilm [279] and thus the biofilm formation capacity [280]. However, the genetic mechanism by which conjugative plasmids increase biofilm formation has not been elucidated, but the presence of repressed or natural conjugative plasmids affects the global host chromosomal gene expression [276,278].

While the role of the conjugative pili has been mainly studied in *E. coli* biofilms, one may speculate that their impact differs depending on the host. Indeed, Røder et al. observed that the conjugative pili of the IncP-1 plasmid pKJK5 reduced the surface attachment of *P. putida* by increasing cell–cell adhesion, resulting in reduced biofilm formation [281]. Further investigation will be necessary to decipher the complex interconnections between the conjugative plasmid and biofilm formation.

4.4. Influence of Antibiotic Treatment on Conjugation within Biofilms

Interactions between conjugation and biofilms have been proposed to promote both community-building and gene transfer. This synergic interaction raises serious questions about the contribution of HGT to the evolution and adaptation of biofilm-forming pathogens. Because of the increase in antibiotic-resistant infections, recent investigations have aimed to provide a new understanding of biofilm responses to antimicrobial treatments.

Subminimal inhibitory concentrations (sub-MICs) of aminoglycosides enhance the biofilm biomass of the *P. aeruginosa* strain PAO1 and clinical isolates of *E. coli* through the response regulator Arr, a predicted phosphodiesterase that alters cyclic di-guanosine monophosphate (c-di-GMP) levels [282]. Linares et al. further demonstrated that, in addition to aminoglycosides, sub-MICs of tetracycline and norfloxacin also increase the formation of *P. aeruginosa* biofilm. However, no clear causal factors were identified [283]. Interestingly, a combination of tetracycline and cephradine has a synergistic effect on the biofilm formation of a mixed culture of *E. coli* and *P. aeruginosa* [284]. Tetracycline also promotes the biofilm formation of the pathogen *Acinetobacter baumannii*, and whole-genome sequence analysis revealed an increase in the rate of mutations such as SNPs, as well as insertions and deletions, under subinhibitory drug exposition [285]. In addition to the accumulation of genotypic variation, biofilm treatment with a low level of antibiotics produces changes in the gene expression profile, some of which may be linked to increased biofilm formation [283,285,286].

Recently, Diaz-Pascual et al. investigated *Vibrio cholerae* biofilm at the community scale using a single-cell imaging system, revealing changes in biofilm dynamics and architecture in response to antibiotic treatment [287]. After tetracycline exposure, they observed modifications in biofilm architecture and cell morphology, including a 2.5-fold increase in cell volume and a 29% decrease in cell density. This cell density decrease reflected a considerable alteration of the multicellular arrangement and the breakdown of the matrix within the biofilm. Furthermore, biofilms became susceptible to the colonization of their interior by new cells, and the colonizer population increased until they invaded the resident biofilm. Clearly, a sublethal dose of antibiotics influences the biofilm lifestyle, inducing significant modifications to the entire population. The biofilm matrix forms a shield to prevent the penetration and diffusion of antimicrobials, and the increase in biofilm formation in response to antibiotics, illustrated by an enhancement of the biofilm matrix, seems to be a defense mechanism of the bacterial community.

In parallel, some antibiotics have also been recognized as signaling molecules that increase conjugative transfer [288–296]. Interestingly, when conjugation occurs in an antibiotic-free environment with a donor strain that is pretreated with subconcentrations of antibiotics, the conjugation frequency increases significantly [297,298]. The mechanisms by which antibiotics affect plasmid transfer remain unclear. In the literature, it is proposed that sub-MIC antibiotic treatment enhances the frequency of conjugation through the upregulation of *tra* gene expression in donors [291,297–299]. However, in many studies, the increase in conjugation frequency was evaluated using an antibiotic whose resistance gene is carried by the tested conjugative plasmid itself [288,290,291,293,294,299,300]. This approach makes it difficult to distinguish between the selection bias induced by the antibiotic in the mating population and the actual effect on conjugation frequencies. Two studies instead support that antibiotics primarily act through the differential selection of the donor, recipient, and transconjugant once gene transfer has occurred, rather than stimulating conjugation *per se* [197,301]. By using living cell microscopy, they were able to visualize conjugation dynamics in real time. Nolivos et al. showed that the transfer frequency of an F plasmid harboring the gene for tetracycline resistance was not increased by the presence of tetracycline. Lopatkin et al. also demonstrated that antibiotics from six major classes had no effect on the conjugation efficiency of plasmids from five different incompatibility groups. These reports suggested that the direct contribution of antibiotics to gene transfer has been overestimated and proposed that antibiotics may act only as post-transfer selection drivers, favoring the growth of transconjugants over recipients. Although a number of studies have advanced the potential stimulating effect of antibiotics on conjugation, their real impact needs to be further explored, and antibiotics with different modes of action must be tested.

Undoubtedly, antibiotics play a role that must not be overlooked in the emergence of new multi-resistant pathogenic strains. It is troubling that antibiotic treatments amplify biofilm formation, increasing the difficulty in healing biofilm-associated infections. Antibiotics not only induce biofilm formation but also improve gene transfer within the community. Furthermore, profound changes induced by antibiotics allow for the invasion of the biofilm by external microorganisms [287]. As

biofilms are suitable environments for conjugative transfer, we can easily imagine that antibiotics could potentiate the invasion by a potential donor that harbors gene resistance and that its dissemination within the biofilm could act as a synergistic factor instead of an antagonist one. Microfluidic technology represents a promising method to investigate, in real-time and without disrupting biofilm structure, the dynamics of conjugation within communities. Recent studies have used microfluidic devices combined with confocal microscopy to monitor real-time plasmid RP4 transfer in mixed *P. putida* and *E. coli* biofilms and in activated sludge [302]. They were able to show that the structure and composition of the biofilm could modulate gene transfer routes. Indeed, in *E. coli* biofilms, the explosive spread of transconjugants illustrated the significant role of plasmid transfer, while in the sludge community, vertical gene transfer was more predominant. Using these advanced techniques, it is now more necessary to understand how antibiotics can influence gene dissemination within these complex structures.

5. Conclusions

Our current knowledge of the sequence of reactions required for plasmid conjugation is well documented, especially for model plasmids such as the F factor, but also for other plasmids like RP4, R388, or pTi. The combination of genetic and biochemistry approaches has allowed the function of key Tra proteins in these reactions to be described. However, even for these systems, the mechanistic functions of most Tra proteins remain elusive. They have mainly been described in terms of their essentiality for mating pair formation or stabilization, DNA transfer, and immunity, and a further understanding of their activity at the molecular scale is lacking. Furthermore, as emphasized in this review, a number of major fundamental questions remains, such as the pilus' ability to transport DNA during distant transfer, the existence and nature of a potential signal that is triggered by mating pair formation that would activate conjugation, or the role of the leading genes in the early steps of plasmid establishment, for instance. Because of its intimate connection with the dissemination of drug resistance, conjugation has reemerged as the focus of a global research effort. Modern experimental approaches should help to gain new insights into the mechanism of conjugation at the molecular and cellular scales, as well as those regarding the extent of conjugation in natural bacterial communities and its impact on the dissemination of bacterial metabolic traits.

Author Contributions: Conceptualization, S.B. and C.L.; writing—original draft preparation, C.V., K.G., S.D. and S.B.; writing—review and editing, S.B. and C.L.; figure preparation, S.B. and C.L.; table preparation, C.V., K.G.; supervision, S.B. and C.L.; funding acquisition, C.L. All authors have read and agreed to the published version of the manuscript.

Funding: This research was funded by French National Research Agency, grant number ANR-18-CE35-0008 to C.L. and K.G. and ANR-19-ARMB-0006-01 to C.L., S.B., and S.D., and the University of Lyon through funding to C.V. C.L. also acknowledges the Schlumberger Foundation for Education and Research (FSER 2019) and the Foundation for Innovation in Infectiology FINOVI (AO-2014) for financial support.

Acknowledgments: The authors thank Yoshiharu Yamaichi, Nelly Dubarry, and Erwan Gueguen for their helpful discussions. Annick Dedieu for proof-reading of the manuscript. We are also grateful to all research groups contributing to improving our understanding of bacterial DNA conjugation, and we apologize for the potentially incomplete citation list.

Conflicts of Interest: The authors declare no conflict of interest.

References

1. Lederberg, J.; Tatum, E.L. Gene recombination in *Escherichia coli*. *Nature* **1946**, *158*, 558. [[CrossRef](#)] [[PubMed](#)]
2. Grohmann, E.; Muth, G.; Espinosa, M. Conjugative plasmid transfer in gram-positive bacteria. *Microbiol. Mol. Biol. Rev.* **2003**, *67*, 277–301. [[CrossRef](#)] [[PubMed](#)]
3. Cruz, F.D.L.; Frost, L.S.; Meyer, R.J.; Zechner, E.L. Conjugative DNA metabolism in Gram-negative bacteria. *FEMS Microbiol. Rev.* **2010**, *34*, 18–40. [[CrossRef](#)] [[PubMed](#)]
4. Davison, J. Genetic exchange between bacteria in the environment. *Plasmid* **1999**, *42*, 73–91. [[CrossRef](#)]

5. Lawrence, J.G. Gene transfer, speciation, and the evolution of bacterial genomes. *Curr. Opin. Microbiol.* **1999**, *2*, 519–523. [[CrossRef](#)]
6. Ochman, H.; Lawrence, J.G.; Groisman, E.A. Lateral gene transfer and the nature of bacterial innovation. *Nature* **2000**, *405*, 299–304. [[CrossRef](#)]
7. Ippen-Ihler, K.; Achtman, M.; Willetts, N. Deletion map of the Escherichia coli K-12 sex factor F: The order of eleven transfer cistrons. *J. Bacteriol.* **1972**, *110*, 857–863. [[CrossRef](#)]
8. Penfold, S.S.; Simon, J.; Frost, L.S. Regulation of the expression of the traM gene of the F sex factor of Escherichia coli. *Mol. Microbiol.* **1996**, *20*, 549–558. [[CrossRef](#)] [[PubMed](#)]
9. Koraimann, G.; Wagner, M.A. Social behavior and decision making in bacterial conjugation. *Front. Cell. Infect. Microbiol.* **2014**, *4*. [[CrossRef](#)]
10. Timmis, K.N.; Andrés, I.; Achtman, M. Fertility repression of F-like conjugative plasmids: Physical mapping of the R6–5 finO and finP cistrons and identification of the finO protein. *Proc. Natl. Acad. Sci. USA* **1978**, *75*, 5836–5840. [[CrossRef](#)]
11. Willetts, N. The transcriptional control of fertility in F-like plasmids. *J. Mol. Biol.* **1977**, *112*, 141–148. [[CrossRef](#)]
12. Frost, L.; Lee, S.; Yanchar, N.; Paranchych, W. finP and fisO mutations in FinP anti-sense RNA suggest a model for FinOP action in the repression of bacterial conjugation by the Flac plasmid JCFL0. *Mol. Gen. Genet.* **1989**, *218*, 152–160. [[CrossRef](#)] [[PubMed](#)]
13. Koraimann, G.; Teferle, K.; Markolin, G.; Woger, W.; Högenauer, G. The FinOP repressor system of plasmid R1: Analysis of the antisense RNA control of traJ expression and conjugative DNA transfer. *Mol. Microbiol.* **1996**, *21*, 811–821. [[CrossRef](#)] [[PubMed](#)]
14. van Biesen, T.; Frost, L.S. Differential levels of fertility inhibition among F-like plasmids are related to the cellular concentration of finO mRNA. *Mol. Microbiol.* **1992**, *6*, 771–780. [[CrossRef](#)] [[PubMed](#)]
15. van Biesen, T.; Frost, L.S. The FinO protein of IncF plasmids binds FinP antisense RNA and its target, traJ mRNA, and promotes duplex formation. *Mol. Microbiol.* **1994**, *14*, 427–436. [[CrossRef](#)]
16. Jerome, L.J.; van Biesen, T.; Frost, L.S. Degradation of FinP antisense RNA from F-like plasmids: The RNA-binding protein, FinO, protects FinP from ribonuclease E. *J. Mol. Biol.* **1999**, *285*, 1457–1473. [[CrossRef](#)] [[PubMed](#)]
17. Wong, J.J.W.; Lu, J.; Glover, J.N.M. Relaxosome function and conjugation regulation in F-like plasmids—A structural biology perspective. *Mol. Microbiol.* **2012**, *85*, 602–617. [[CrossRef](#)]
18. Will, W.R.; Frost, L.S. Characterization of the opposing roles of H-NS and TraJ in transcriptional regulation of the F-Plasmid tra Operon. *J. Bacteriol.* **2006**, *188*, 507–514. [[CrossRef](#)]
19. Will, W.R.; Lu, J.; Frost, L.S. The role of H-NS in silencing F transfer gene expression during entry into stationary phase. *Mol. Microbiol.* **2004**, *54*, 769–782. [[CrossRef](#)]
20. Ali Azam, T.; Iwata, A.; Nishimura, A.; Ueda, S.; Ishihama, A. Growth phase-dependent variation in protein composition of the Escherichia coli nucleoid. *J. Bacteriol.* **1999**, *181*, 6361–6370. [[CrossRef](#)]
21. Frost, L.S.; Manchak, J. F-phenocopies: Characterization of expression of the F transfer region in stationary phase. *Microbiology* **1998**, *144 Pt 9*, 2579–2587. [[CrossRef](#)]
22. Headd, B.; Bradford, S.A. The conjugation window in an Escherichia coli K-12 strain with an IncFII Plasmid. *Appl. Environ. Microbiol.* **2020**, *86*. [[CrossRef](#)] [[PubMed](#)]
23. Lu, J.; Peng, Y.; Wan, S.; Frost, L.S.; Raivio, T.; Glover, J.N.M. Cooperative function of TraJ and ArcA in regulating the F Plasmid tra Operon. *J. Bacteriol.* **2019**, *201*. [[CrossRef](#)] [[PubMed](#)]
24. Camacho, E.M.; Serna, A.; Madrid, C.; Marqués, S.; Fernández, R.; de la Cruz, F.; Juárez, A.; Casadesús, J. Regulation of finP transcription by DNA Adenine Methylation in the virulence Plasmid of Salmonella enterica. *J. Bacteriol.* **2005**, *187*, 5691–5699. [[CrossRef](#)] [[PubMed](#)]
25. Zahrl, D.; Wagner, A.; Tscherner, M.; Koraimann, G. GroEL plays a central role in stress-induced negative regulation of bacterial conjugation by promoting proteolytic degradation of the activator protein TraJ. *J. Bacteriol.* **2007**, *189*, 5885–5894. [[CrossRef](#)]
26. Dessaux, Y.; Faure, D. Quorum sensing and Quorum quenching in Agrobacterium: A “Go/No Go system”? *Genes* **2018**, *9*, 210. [[CrossRef](#)]
27. Lu, Y.; Zeng, J.; Wu, B.; Wang, L.; Cai, R.; Zhang, N.; Li, Y.; Huang, X.; Huang, B.; Chen, C.; et al. Quorum sensing N-acyl homoserine Lactones-SdiA suppresses Escherichia coli-Pseudomonas aeruginosa conjugation through Inhibiting traI expression. *Front. Cell. Infect. Microbiol.* **2017**, *7*. [[CrossRef](#)]

28. Cheah, K.C.; Skurray, R. The F plasmid carries an IS3 insertion within finO. *J. Gen. Microbiol.* **1986**, *132*, 3269–3275. [[CrossRef](#)]
29. Yoshioka, Y.; Ohtsubo, H.; Ohtsubo, E. Repressor gene finO in plasmids R100 and F: Constitutive transfer of plasmid F is caused by insertion of IS3 into F finO. *J. Bacteriol.* **1987**, *169*, 619–623. [[CrossRef](#)]
30. Poidevin, M.; Sato, M.; Altinoglu, I.; Delaplace, M.; Sato, C.; Yamaichi, Y. Mutation in ESBL Plasmid from *Escherichia coli* O104:H4 leads to autoagglutination and enhanced plasmid dissemination. *Front. Microbiol.* **2018**, *9*, 130. [[CrossRef](#)]
31. Yamaichi, Y.; Chao, M.C.; Sasabe, J.; Clark, L.; Davis, B.M.; Yamamoto, N.; Mori, H.; Kurokawa, K.; Waldor, M.K. High-Resolution genetic analysis of the requirements for horizontal transmission of the ESBL plasmid from *Escherichia coli* O104:H4. *Nucleic Acids Res.* **2015**, *43*, 348–360. [[CrossRef](#)]
32. Dmowski, M.; Gołębiewski, M.; Kern-Zdanowicz, I. Characteristics of the conjugative transfer system of the IncM plasmid pCTX-M3 and identification of its putative regulators. *J. Bacteriol.* **2018**, *200*. [[CrossRef](#)]
33. Kohler, V.; Goessweiner-Mohr, N.; Aufschneider, A.; Fercher, C.; Probst, I.; Pavkov-Keller, T.; Hunger, K.; Wolinski, H.; Büttner, S.; Grohmann, E.; et al. TraN: A novel repressor of an Enterococcus conjugative type IV secretion system. *Nucleic Acids Res.* **2018**, *46*, 9201–9219. [[CrossRef](#)] [[PubMed](#)]
34. Potron, A.; Poirel, L.; Nordmann, P. Derepressed transfer properties leading to the efficient spread of the plasmid encoding carbapenemase OXA-48. *Antimicrob. Agents Chemother.* **2014**, *58*, 467–471. [[CrossRef](#)] [[PubMed](#)]
35. Bradley, D.E. Derepressed plasmids of incompatibility group I1 determine two different morphological forms of pilus. *Plasmid* **1983**, *9*, 331–334. [[CrossRef](#)]
36. Bradley, D.E. Specification of the conjugative pili and surface mating systems of Pseudomonas plasmids. *J. Gen. Microbiol.* **1983**, *129*, 2545–2556. [[CrossRef](#)]
37. Bradley, D.E. Characteristics and function of thick and thin conjugative pili determined by transfer-derepressed plasmids of incompatibility groups I1, I2, I5, B, K and Z. *J. Gen. Microbiol.* **1984**, *130*, 1489–1502. [[CrossRef](#)]
38. Bradley, D.E.; Taylor, D.E.; Cohen, D.R. Specification of surface mating systems among conjugative drug resistance plasmids in *Escherichia coli* K-12. *J. Bacteriol.* **1980**, *143*, 1466–1470. [[CrossRef](#)]
39. Costa, T.R.D.; Ilangovan, A.; Ukleja, M.; Redzej, A.; Santini, J.M.; Smith, T.K.; Egelman, E.H.; Waksman, G. Structure of the bacterial sex F Pilus reveals an assembly of a stoichiometric protein-phospholipid complex. *Cell* **2016**, *166*, 1436–1444.e10. [[CrossRef](#)]
40. Date, T.; Inuzuka, M.; Tomoeda, M. Purification and characterization of F pili from *Escherichia coli*. *Biochemistry* **1977**, *16*, 5579–5585. [[CrossRef](#)]
41. Folkhard, W.; Leonard, K.R.; Malsey, S.; Marvin, D.A.; Dubochet, J.; Engel, A.; Achtman, M.; Helmuth, R. X-ray diffraction and electron microscope studies on the structure of bacterial F pili. *J. Mol. Biol.* **1979**, *130*, 145–160. [[CrossRef](#)]
42. Ippen-Ihler, K.A.; Minkley, E.G. The conjugation system of F, the fertility factor of *Escherichia coli*. *Annu. Rev. Genet.* **1986**, *20*, 593–624. [[CrossRef](#)] [[PubMed](#)]
43. Silverman, P.M.; Clarke, M.B. New insights into F-pilus structure, dynamics, and function. *Integr. Biol.* **2010**, *2*, 25–31. [[CrossRef](#)] [[PubMed](#)]
44. Wang, Y.A.; Yu, X.; Silverman, P.M.; Harris, R.L.; Egelman, E.H. The structure of F-pili. *J. Mol. Biol.* **2009**, *385*, 22–29. [[CrossRef](#)]
45. Frost, L.S.; Paranchych, W.; Willetts, N.S. DNA sequence of the F traALE region that includes the gene for F pilin. *J. Bacteriol.* **1984**, *160*, 395–401. [[CrossRef](#)]
46. Minkley, E.G.; Polen, S.; Brinton, C.C.; Ippen-Ihler, K. Identification of the structural gene for F-pilin. *J. Mol. Biol.* **1976**, *108*, 111–121. [[CrossRef](#)]
47. Maneewannakul, K.; Maneewannakul, S.; Ippen-Ihler, K. Synthesis of F pilin. *J. Bacteriol.* **1993**, *175*, 1384–1391. [[CrossRef](#)]
48. Harris, R.L.; Sholl, K.A.; Conrad, M.N.; Dresser, M.E.; Silverman, P.M. Interaction between the F plasmid TraA (F-pilin) and TraQ proteins. *Mol. Microbiol.* **1999**, *34*, 780–791. [[CrossRef](#)]
49. Majdalani, N.; Ippen-Ihler, K. Membrane insertion of the F-pilin subunit is Sec independent but requires leader peptidase B and the proton motive force. *J. Bacteriol.* **1996**, *178*, 3742–3747. [[CrossRef](#)]
50. Moore, D.; Hamilton, C.M.; Maneewannakul, K.; Mintz, Y.; Frost, L.S.; Ippen-Ihler, K. The *Escherichia coli* K-12 F plasmid gene traX is required for acetylation of F pilin. *J. Bacteriol.* **1993**, *175*, 1375–1383. [[CrossRef](#)]

51. Firth, N.; Berg, T.; Skurray, R.A. Evolution of conjugative plasmids from gram-positive bacteria. *Mol. Microbiol.* **1999**, *31*, 1598–1600. [[PubMed](#)]
52. Lawley, T.D.; Klimke, W.A.; Gubbins, M.J.; Frost, L.S. F factor conjugation is a true type IV secretion system. *FEMS Microbiol. Lett.* **2003**, *224*, 1–15. [[CrossRef](#)]
53. Manchak, J.; Anthony, K.G.; Frost, L.S. Mutational analysis of F-pilin reveals domains for pilus assembly, phage infection and DNA transfer. *Mol. Microbiol.* **2002**, *43*, 195–205. [[CrossRef](#)] [[PubMed](#)]
54. Firth, N.; Ippen-Ihler, K.; Skurray, R.A. *Gene Transfer: Conjugation Structure and Function of the F Factor and Mechanism of Conjugation*; American Society of Microbiology: Washington, DC, USA, 1999.
55. Koraimann, G. Spread and persistence of virulence and antibiotic resistance genes: A ride on the F Plasmid conjugation module. *EcoSal Plus* **2018**, *8*. [[CrossRef](#)] [[PubMed](#)]
56. Arutyunov, D.; Frost, L.S. F conjugation: Back to the beginning. *Plasmid* **2013**, *70*, 18–32. [[CrossRef](#)]
57. Frost, L.S.; Ippen-Ihler, K.; Skurray, R.A. Analysis of the sequence and gene products of the transfer region of the F sex factor. *Microbiol. Rev.* **1994**, *58*, 162–210. [[CrossRef](#)]
58. Anthony, K.G.; Kathir, P.; Moore, D.; Ippen-Ihler, K.; Frost, L.S. Analysis of the traLEKBP sequence and the TraP protein from three F-like plasmids: F, R100-1 and ColB2. *J. Bacteriol.* **1996**, *178*, 3194–3200. [[CrossRef](#)]
59. Anthony, K.G.; Klimke, W.A.; Manchak, J.; Frost, L.S. Comparison of proteins involved in Pilus synthesis and mating pair stabilization from the related Plasmids F and R100-1: Insights into the mechanism of conjugation. *J. Bacteriol.* **1999**, *181*, 5149–5159. [[CrossRef](#)]
60. Gopalkrishnan, S.; Ross, W.; Chen, A.Y.; Gourse, R.L. TraR directly regulates transcription initiation by mimicking the combined effects of the global regulators DksA and ppGpp. *Proc. Natl. Acad. Sci. USA* **2017**, *114*, E5539–E5548. [[CrossRef](#)]
61. Shala-Lawrence, A.; Bragagnolo, N.; Nowroozi-Dayeni, R.; Kheyson, S.; Audette, G.F. The interaction of TraW and TrbC is required to facilitate conjugation in F-like plasmids. *Biochem. Biophys. Res. Commun.* **2018**, *503*, 2386–2392. [[CrossRef](#)]
62. Garcillán-Barcia, M.P.; de la Cruz, F. Why is entry exclusion an essential feature of conjugative plasmids? *Plasmid* **2008**, *60*, 1–18. [[CrossRef](#)] [[PubMed](#)]
63. Achtman, M. Mating aggregates in *Escherichia coli* conjugation. *J. Bacteriol.* **1975**, *123*, 505–515. [[CrossRef](#)] [[PubMed](#)]
64. Lanka, E.; Wilkins, B.M. DNA processing reactions in bacterial conjugation. *Annu. Rev. Biochem.* **1995**, *31*. [[CrossRef](#)]
65. Dostál, L.; Shao, S.; Schildbach, J.F. Tracking F plasmid TraI relaxase processing reactions provides insight into F plasmid transfer. *Nucleic Acids Res.* **2011**, *39*, 2658–2670. [[CrossRef](#)] [[PubMed](#)]
66. Matson, S.W.; Sampson, J.K.; Byrd, D.R.N. F Plasmid conjugative DNA transfer the TraI helicase activity is essential for DNA strand transfer. *J. Biol. Chem.* **2001**, *276*, 2372–2379. [[CrossRef](#)]
67. Curtiss, R. Bacterial conjugation. *Annu. Rev. Microbiol.* **1969**, *23*, 69–136. [[CrossRef](#)]
68. Marvin, D.A.; Hohn, B. Filamentous bacterial viruses. *Bacteriol. Rev.* **1969**, *33*, 172–209. [[CrossRef](#)]
69. Clarke, M.; Maddera, L.; Harris, R.L.; Silverman, P.M. F-pili dynamics by live-cell imaging. *Proc. Natl. Acad. Sci. USA* **2008**, *105*, 17978–17981. [[CrossRef](#)]
70. Achtman, M.; Morelli, G.; Schwuchow, S. Cell-Cell interactions in conjugating *Escherichia coli*: Role of F pili and fate of mating aggregates. *J. Bacteriol.* **1978**, *135*, 1053–1061. [[CrossRef](#)]
71. Dürrenberger, M.B.; Villiger, W.; Bächli, T. Conjugational junctions: Morphology of specific contacts in conjugating *Escherichia coli* bacteria. *J. Struct. Biol.* **1991**, *107*, 146–156. [[CrossRef](#)]
72. Brinton, C.C. The structure, function, synthesis and genetic control of bacterial pili and a molecular model for DNA and RNA transport in gram negative bacteria. *Trans. N. Y. Acad. Sci.* **1965**, *27*, 1003–1054. [[CrossRef](#)] [[PubMed](#)]
73. Harrington, L.C.; Rogerson, A.C. The F pilus of *Escherichia coli* appears to support stable DNA transfer in the absence of wall-to-wall contact between cells. *J. Bacteriol.* **1990**, *172*, 7263–7264. [[CrossRef](#)] [[PubMed](#)]
74. Babić, A.; Lindner, A.B.; Vulić, M.; Stewart, E.J.; Radman, M. Direct visualization of horizontal gene transfer. *Science* **2008**, *319*, 1533–1536. [[CrossRef](#)] [[PubMed](#)]
75. Davies, J.K.; Reeves, P. Colicin tolerance and map location of conjugation-deficient mutants. *J. Bacteriol.* **1975**, *123*, 372–373. [[CrossRef](#)]
76. Falkinham, J.O.; Curtiss, R. Isolation and characterization of conjugation-deficient mutants of *Escherichia coli* K-12. *J. Bacteriol.* **1976**, *126*, 1194–1206. [[CrossRef](#)] [[PubMed](#)]

77. Havekes, L.M.; Hoekstra, W.P. Characterization of an *Escherichia coli* K-12 F-Con-mutant. *J. Bacteriol.* **1976**, *126*, 593–600. [[CrossRef](#)]
78. Manning, P.A.; Puspurs, A.; Reeves, P. Outer membrane of *Escherichia coli* K-12: Isolation of mutants with altered protein 3A by using host range mutants of bacteriophage K3. *J. Bacteriol.* **1976**, *127*, 1080–1084. [[CrossRef](#)] [[PubMed](#)]
79. Monner, D.A.; Jonsson, S.; Boman, H.G. Ampicillin-Resistant mutants of *Escherichia coli* K-12 with lipopolysaccharide alterations affecting mating ability and susceptibility to sex-specific bacteriophages. *J. Bacteriol.* **1971**, *107*, 420–432. [[CrossRef](#)]
80. Skurray, R.A.; Hancock, R.E.; Reeves, P. Con-mutants: Class of mutants in *Escherichia coli* K-12 lacking a major cell wall protein and defective in conjugation and adsorption of a bacteriophage. *J. Bacteriol.* **1974**, *119*, 726–735. [[CrossRef](#)]
81. Manoil, C.; Rosenbusch, J.P. Conjugation-deficient mutants of *Escherichia coli* distinguish classes of functions of the outer membrane OmpA protein. *Mol. Gen. Genet.* **1982**, *187*, 148–156. [[CrossRef](#)]
82. Morona, R.; Klose, M.; Henning, U. *Escherichia coli* K-12 outer membrane protein (OmpA) as a bacteriophage receptor: Analysis of mutant genes expressing altered proteins. *J. Bacteriol.* **1984**, *159*, 570–578. [[CrossRef](#)] [[PubMed](#)]
83. Achtman, M.; Schwuchow, S.; Helmuth, R.; Morelli, G.; Manning, P.A. Cell-Cell interactions in conjugating *Escherichia coli*: Con- mutants and stabilization of mating aggregates. *Mol. Gen. Genet. MGG* **1978**, *164*, 171–183. [[CrossRef](#)]
84. Anthony, K.G.; Sherburne, C.; Sherburne, R.; Frost, L.S. The role of the pilus in recipient cell recognition during bacterial conjugation mediated by F-like plasmids. *Mol. Microbiol.* **1994**, *13*, 939–953. [[CrossRef](#)] [[PubMed](#)]
85. Klimke, W.A.; Frost, L.S. Genetic analysis of the role of the transfer gene, traN, of the F and R100-1 plasmids in mating pair stabilization during conjugation. *J. Bacteriol.* **1998**, *180*, 4036–4043. [[CrossRef](#)]
86. Klimke, W.A.; Rypien, C.D.; Klinger, B.; Kennedy, R.A.; Rodriguez-Maillard, J.M.; Frost, L.S. The mating pair stabilization protein, TraN, of the F plasmid is an outer-membrane protein with two regions that are important for its function in conjugation. *Microbiology* **2005**, *151*, 3527–3540. [[CrossRef](#)] [[PubMed](#)]
87. Maneewannakul, S.; Kathir, P.; Ippen-Ihler, K. Characterization of the F plasmid mating aggregation gene traN and of a new F transfer region locus trbE. *J. Mol. Biol.* **1992**, *225*, 299–311. [[CrossRef](#)]
88. Willetts, N.; Achtman, M. Genetic analysis of transfer by the *Escherichia coli* sex factor F, using P1 transductional complementation. *J. Bacteriol.* **1972**, *110*, 843–851. [[CrossRef](#)]
89. Audette, G.F.; Manchak, J.; Beatty, P.; Klimke, W.A.; Frost, L.S. Entry exclusion in F-like plasmids requires intact TraG in the donor that recognizes its cognate TraS in the recipient. *Microbiology (Read. Engl.)* **2007**, *153*, 442–451. [[CrossRef](#)]
90. Marrero, J.; Waldor, M.K. Determinants of entry exclusion within Eex and TraG are cytoplasmic. *J. Bacteriol.* **2007**, *189*, 6469–6473. [[CrossRef](#)]
91. Low, W.W.; Wong, J.; Pena, A.; Seddon, C.; Costa, T.; Beis, K.; Frankel, G. OmpK36 and TraN facilitate conjugal transfer of the *Klebsiella pneumoniae* carbapenem resistance plasmid pKpQIL. *Microbiology* **2020**. [[CrossRef](#)]
92. Havekes, L.; Tommassen, J.; Hoekstra, W.; Lugtenberg, B. Isolation and characterization of *Escherichia coli* K-12 F- mutants defective in conjugation with an I-type donor. *J. Bacteriol.* **1977**, *129*, 1–8. [[CrossRef](#)] [[PubMed](#)]
93. Ishiwa, A.; Komano, T. PilV Adhesins of Plasmid R64 Thin Pili specifically bind to the lipopolysaccharides of recipient cells. *J. Mol. Biol.* **2004**, *343*, 615–625. [[CrossRef](#)] [[PubMed](#)]
94. Frost, L.S.; Simon, J. Studies on the pili of the promiscuous plasmid RP4. In *Molecular Mechanisms of Bacterial Virulence*; Kado, C.I., Crosa, J.H., Eds.; Developments in Plant Pathology; Springer: Dordrecht, The Netherlands, 1994; Volume 3, pp. 47–65. ISBN 978-94-010-4322-9.
95. Moriguchi, K.; Zoolkefli, F.I.R.M.; Abe, M.; Kiyokawa, K.; Yamamoto, S.; Suzuki, K. Targeting antibiotic resistance genes is a better approach to block acquisition of antibiotic resistance than blocking conjugal transfer by recipient cells: A genome-wide screening in *Escherichia coli*. *Front. Microbiol.* **2020**, *10*. [[CrossRef](#)] [[PubMed](#)]
96. Pérez-Mendoza, D.; de la Cruz, F. *Escherichia coli* genes affecting recipient ability in plasmid conjugation: Are there any? *BMC Genom.* **2009**, *10*, 71. [[CrossRef](#)]

97. Dodsworth, J.A.; Li, L.; Wei, S.; Hedlund, B.P.; Leigh, J.A.; de Figueiredo, P. Interdomain conjugal transfer of DNA from bacteria to Archaea. *Appl. Environ. Microbiol.* **2010**, *76*, 5644–5647. [[CrossRef](#)]
98. Heinemann, J.A.; Sprague, G.F. Bacterial conjugative plasmids mobilize DNA transfer between bacteria and yeast. *Nature* **1989**, *340*, 205–209. [[CrossRef](#)]
99. Waters, V.L. Conjugation between bacterial and mammalian cells. *Nat. Genet.* **2001**, *29*, 375–376. [[CrossRef](#)]
100. Llosa, M.; Gomis-Rüth, F.X.; Coll, M.; de la Cruz Fd, F. Bacterial conjugation: A two-step mechanism for DNA transport. *Mol. Microbiol.* **2002**, *45*, 1–8. [[CrossRef](#)]
101. Clewell, D.B.; Helinski, D.E. Existence of the colicinogenic factor-sex factor Coll-b-P9 as a supercoiled circular DNA-protein relaxation complex. *Biochem. Biophys. Res. Commun.* **1970**, *41*, 150–156. [[CrossRef](#)]
102. Cohen, A.; Fisher, W.D.; Curtiss, R.; Adler, H.I. DNA isolated from *Escherichia coli* minicells mated with F+ cells. *Proc. Natl. Acad. Sci. USA* **1968**, *61*, 61–68. [[CrossRef](#)]
103. Willetts, N.; Skurray, R. The conjugation system of F-like plasmids. *Annu. Rev. Genet.* **1980**, *14*, 41–76. [[CrossRef](#)] [[PubMed](#)]
104. Dostál, L.; Schildbach, J.F. Single-Stranded DNA binding by F TraI relaxase and helicase domains is coordinately regulated. *J. Bacteriol.* **2010**, *192*, 3620–3628. [[CrossRef](#)] [[PubMed](#)]
105. Everett, R.; Willetts, N. Characterisation of an In Vivo system for nicking at the origin of conjugal DNA transfer of the sex factor F. *J. Mol. Biol.* **1980**, *136*, 129–150. [[CrossRef](#)]
106. Matson, S.W.; Morton, B.S. *Escherichia coli* DNA helicase I catalyzes a site- and strand-specific nicking reaction at the F plasmid oriT. *J. Biol. Chem.* **1991**, *266*, 16232–16237.
107. Matson, S.W.; Ragonese, H. The F-plasmid TraI protein contains three functional domains required for conjugative DNA strand transfer. *J. Bacteriol.* **2005**, *187*, 697–706. [[CrossRef](#)]
108. Reygers, U.; Wessel, R.; Müller, H.; Hoffmann-Berling, H. Endonuclease activity of *Escherichia coli* DNA helicase I directed against the transfer origin of the F factor. *EMBO J.* **1991**, *10*, 2689–2694. [[CrossRef](#)]
109. Traxler, B.A.; Minkley, E.G. Evidence that DNA helicase I and oriT site-specific nicking are both functions of the F TraI protein. *J. Mol. Biol.* **1988**, *204*, 205–209. [[CrossRef](#)]
110. Howard, M.T.; Nelson, W.C.; Matson, S.W. Stepwise assembly of a relaxosome at the F plasmid origin of transfer. *J. Biol. Chem.* **1995**, *270*, 28381–28386.
111. Nelson, W.C.; Morton, B.S.; Lahue, E.E.; Matson, S.W. Characterization of the *Escherichia coli* F factor traY gene product and its binding sites. *J. Bacteriol.* **1993**, *175*, 2221–2228. [[CrossRef](#)]
112. Schildbach, J.F.; Robinson, C.R.; Sauer, R.T. Biophysical characterization of the TraY protein of *Escherichia coli* F factor. *J. Biol. Chem.* **1998**, *273*, 1329–1333. [[CrossRef](#)]
113. Luo, Y.; Gao, Q.; Deonier, R.C. Mutational and physical analysis of F plasmid traY protein binding to oriT. *Mol. Microbiol.* **1994**, *11*, 459–469. [[CrossRef](#)] [[PubMed](#)]
114. Nelson, W.C.; Howard, M.T.; Sherman, J.A.; Matson, S.W. The traY gene product and integration host factor stimulate *Escherichia coli* DNA helicase I-catalyzed nicking at the F plasmid oriT. *J. Biol. Chem.* **1995**, *270*, 28374–28380. [[PubMed](#)]
115. Rice, P.A.; Yang, S.; Mizuuchi, K.; Nash, H.A. Crystal structure of an IHF-DNA complex: A protein-induced DNA U-turn. *Cell* **1996**, *87*, 1295–1306. [[CrossRef](#)]
116. Tsai, M.M.; Fu, Y.H.; Deonier, R.C. Intrinsic bends and integration host factor binding at F plasmid oriT. *J. Bacteriol.* **1990**, *172*, 4603–4609. [[CrossRef](#)]
117. Williams, S.L.; Schildbach, J.F. TraY and integration host factor oriT binding sites and F conjugal transfer: Sequence variations, but not altered spacing, are tolerated. *J. Bacteriol.* **2007**, *189*, 3813–3823. [[CrossRef](#)]
118. Di Laurenzio, L.; Frost, L.S.; Paranchych, W. The TraM protein of the conjugative plasmid F binds to the origin of transfer of the F and ColE1 plasmids. *Mol. Microbiol.* **1992**, *6*, 2951–2959. [[CrossRef](#)]
119. Fu, Y.H.; Tsai, M.M.; Luo, Y.N.; Deonier, R.C. Deletion analysis of the F plasmid oriT locus. *J. Bacteriol.* **1991**, *173*, 1012–1020. [[CrossRef](#)]
120. Kupelwieser, G.; Schwab, M.; Högenauer, G.; Koraimann, G.; Zechner, E.L. Transfer protein TraM stimulates TraI-catalyzed cleavage of the transfer origin of plasmid R1 In Vivo. *J. Mol. Biol.* **1998**, *275*, 81–94. [[CrossRef](#)]
121. Mihajlovic, S.; Lang, S.; Sut, M.V.; Strohmaier, H.; Gruber, C.J.; Koraimann, G.; Cabezon, E.; Moncalián, G.; de la Cruz, F.; Zechner, E.L. Plasmid r1 conjugative DNA processing is regulated at the coupling protein interface. *J. Bacteriol.* **2009**, *191*, 6877–6887. [[CrossRef](#)] [[PubMed](#)]

122. Ragonese, H.; Haisch, D.; Villareal, E.; Choi, J.-H.; Matson, S.W. The F plasmid-encoded TraM protein stimulates relaxosome-mediated cleavage at oriT through an interaction with TraI. *Mol. Microbiol.* **2007**, *63*, 1173–1184. [[CrossRef](#)]
123. Wawrzyniak, P.; Płucienniczak, G.; Bartosik, D. The different faces of rolling-circle replication and its multifunctional initiator proteins. *Front. Microbiol.* **2017**, *8*, 2353. [[CrossRef](#)] [[PubMed](#)]
124. Byrd, D.R.; Matson, S.W. Nicking by transesterification: The reaction catalysed by a relaxase. *Mol. Microbiol.* **1997**, *25*, 1011–1022. [[CrossRef](#)] [[PubMed](#)]
125. Guiney, D.G.; Helinski, D.R. Relaxation complexes of poasmid DNA and protein. III. Association of protein with the 5' terminus of the broken DNA strand in the relaxed complex of plasmid ColE1. *J. Biol. Chem.* **1975**, *250*, 8796–8803.
126. Matson, S.W.; Nelson, W.C.; Morton, B.S. Characterization of the reaction product of the oriT nicking reaction catalyzed by Escherichia coli DNA helicase I. *J. Bacteriol.* **1993**, *175*, 2599–2606. [[CrossRef](#)] [[PubMed](#)]
127. Pansegrau, W.; Ziegelin, G.; Lanka, E. Covalent association of the traI gene product of plasmid RP4 with the 5'-terminal nucleotide at the relaxation nick site. *J. Biol. Chem.* **1990**, *265*, 10637–10644. [[PubMed](#)]
128. Khan, S.A. Rolling-Circle replication of bacterial plasmids. *Microbiol. Mol. Biol. Rev.* **1997**, *61*, 442–455. [[CrossRef](#)] [[PubMed](#)]
129. Khan, S.A. Plasmid rolling-circle replication: Highlights of two decades of research. *Plasmid* **2005**, *53*, 126–136. [[CrossRef](#)]
130. Ruiz-Masó, J.A.; Machón, C.; Bordanaba-Ruiseco, L.; Espinosa, M.; Coll, M.; Del Solar, G. Plasmid rolling-circle replication. *Microbiol. Spectr.* **2015**, *3*. [[CrossRef](#)]
131. Waters, V.L.; Guiney, D.G. Processes at the nick region link conjugation, T-DNA transfer and rolling circle replication. *Mol. Microbiol.* **1993**, *9*, 1123–1130. [[CrossRef](#)]
132. Lorenzo-Díaz, F.; Fernández-López, C.; Garcillán-Barcia, M.P.; Espinosa, M. Bringing them together: Plasmid pMV158 rolling circle replication and conjugation under an evolutionary perspective. *Plasmid* **2014**, *74*, 15–31. [[CrossRef](#)]
133. Draper, O.; César, C.E.; Machón, C.; de la Cruz, F.; Llosa, M. Site-Specific recombinase and integrase activities of a conjugative relaxase in recipient cells. *Proc. Natl. Acad. Sci. USA* **2005**, *102*, 16385–16390. [[CrossRef](#)] [[PubMed](#)]
134. Trokter, M.; Waksman, G. Translocation through the conjugative type IV secretion system requires unfolding of its protein substrate. *J. Bacteriol.* **2018**, *200*. [[CrossRef](#)] [[PubMed](#)]
135. Ilangovan, A.; Kay, C.W.M.; Roier, S.; El Mkami, H.; Salvadori, E.; Zechner, E.L.; Zanetti, G.; Waksman, G. Cryo-EM structure of a relaxase reveals the molecular basis of DNA unwinding during bacterial conjugation. *Cell* **2017**, *169*, 708–721.e12. [[CrossRef](#)] [[PubMed](#)]
136. Cabezón, E.; Sastre, J.I.; de la Cruz, F. Genetic evidence of a coupling role for the TraG protein family in bacterial conjugation. *Mol. Gen. Genet.* **1997**, *254*, 400–406. [[CrossRef](#)] [[PubMed](#)]
137. Cascales, E.; Christie, P.J. Definition of a bacterial type IV secretion pathway for a DNA substrate. *Science* **2004**, *304*, 1170–1173. [[CrossRef](#)] [[PubMed](#)]
138. Christie, P.J. Type IV secretion: The Agrobacterium VirB/D4 and related conjugation systems. *Biochim. Biophys. Acta* **2004**, *1694*, 219–234. [[CrossRef](#)]
139. Christie, P.J. The mosaic type IV secretion systems. *EcoSal Plus* **2016**, *7*. [[CrossRef](#)] [[PubMed](#)]
140. Christie, P.J.; Whitaker, N.; González-Rivera, C. BBA review revised mechanism and structure of the bacterial type IV secretion systems. *Biochim. Biophys. Acta* **2014**, *1843*, 1578. [[CrossRef](#)]
141. Beranek, A.; Zettl, M.; Lorenzoni, K.; Schauer, A.; Manhart, M.; Koraimann, G. Thirty-Eight C-terminal amino acids of the coupling protein TraD of the F-like conjugative resistance plasmid R1 are required and sufficient to confer binding to the substrate selector protein TraM. *J. Bacteriol.* **2004**, *186*, 6999–7006. [[CrossRef](#)]
142. Disqué-Kochem, C.; Dreiseikelmann, B. The cytoplasmic DNA-binding protein TraM binds to the inner membrane protein TraD In Vitro. *J. Bacteriol.* **1997**, *179*, 6133–6137. [[CrossRef](#)]
143. Lu, J.; Frost, L.S. Mutations in the C-terminal region of TraM provide evidence for In Vivo TraM-TraD interactions during F-plasmid conjugation. *J. Bacteriol.* **2005**, *187*, 4767–4773. [[CrossRef](#)]
144. Lu, J.; Zhao, W.; Frost, L.S. Mutational analysis of TraM correlates oligomerization and DNA binding with autoregulation and conjugative DNA transfer. *J. Biol. Chem.* **2004**, *279*, 55324–55333. [[CrossRef](#)]

145. Lu, J.; Wong, J.J.W.; Edwards, R.A.; Manchak, J.; Frost, L.S.; Glover, J.N.M. Structural basis of specific TraD-TraM recognition during F plasmid-mediated bacterial conjugation. *Mol. Microbiol.* **2008**, *70*, 89–99. [[CrossRef](#)] [[PubMed](#)]
146. Schröder, G.; Krause, S.; Zechner, E.L.; Traxler, B.; Yeo, H.-J.; Lurz, R.; Waksman, G.; Lanka, E. TraG-like proteins of DNA transfer systems and of the *Helicobacter pylori* type IV secretion system: Inner membrane gate for exported substrates? *J. Bacteriol.* **2002**, *184*, 2767–2779. [[CrossRef](#)] [[PubMed](#)]
147. Llosa, M.; Zunzunegui, S.; de la Cruz, F. Conjugative coupling proteins interact with cognate and heterologous VirB10-like proteins while exhibiting specificity for cognate relaxosomes. *Proc. Natl. Acad. Sci. USA* **2003**, *100*, 10465–10470. [[CrossRef](#)]
148. Haft, R.J.F.; Palacios, G.; Nguyen, T.; Mally, M.; Gachelet, E.G.; Zechner, E.L.; Traxler, B. General mutagenesis of F plasmid TraI reveals its role in conjugative regulation. *J. Bacteriol.* **2006**, *188*, 6346–6353. [[CrossRef](#)]
149. Gilmour, M.W.; Gunton, J.E.; Lawley, T.D.; Taylor, D.E. Interaction between the IncHI1 plasmid R27 coupling protein and type IV secretion system: TraG associates with the coiled-coil mating pair formation protein TrhB. *Mol. Microbiol.* **2003**, *49*, 105–116. [[CrossRef](#)]
150. Egelman, E.H. Structural biology. Pumping DNA. *Nature* **2001**, *409*, 573–575. [[CrossRef](#)]
151. Gomis-Rüth, F.X.; Moncalián, G.; Pérez-Luque, R.; González, A.; Cabezón, E.; de la Cruz, F.; Coll, M. The bacterial conjugation protein TrwB resembles ring helicases and F1-ATPase. *Nature* **2001**, *409*, 637–641. [[CrossRef](#)] [[PubMed](#)]
152. Moncalián, G.; Cabezón, E.; Alkorta, I.; Valle, M.; Moro, F.; Valpuesta, J.M.; Goñi, F.M.; de La Cruz, F. Characterization of ATP and DNA binding activities of TrwB, the coupling protein essential in plasmid R388 conjugation. *J. Biol. Chem.* **1999**, *274*, 36117–36124. [[CrossRef](#)]
153. Schröder, G.; Lanka, E. TraG-like proteins of type IV secretion systems: Functional dissection of the multiple activities of TraG (RP4) and TrwB (R388). *J. Bacteriol.* **2003**, *185*, 4371–4381. [[CrossRef](#)] [[PubMed](#)]
154. Haft, R.J.F.; Gachelet, E.G.; Nguyen, T.; Toussaint, L.; Chivian, D.; Traxler, B. In Vivo oligomerization of the F conjugative coupling protein TraD. *J. Bacteriol.* **2007**, *189*, 6626–6634. [[CrossRef](#)] [[PubMed](#)]
155. Tato, I.; Zunzunegui, S.; de la Cruz, F.; Cabezón, E. TrwB, the coupling protein involved in DNA transport during bacterial conjugation, is a DNA-dependent ATPase. *Proc. Natl. Acad. Sci. USA* **2005**, *102*, 8156–8161. [[CrossRef](#)] [[PubMed](#)]
156. Christie, P.J.; Atmakuri, K.; Krishnamoorthy, V.; Jakubowski, S.; Cascales, E. Biogenesis, architecture, and function of bacterial type IV secretion systems. *Annu. Rev. Microbiol.* **2005**, *59*, 451–485. [[CrossRef](#)] [[PubMed](#)]
157. Garcillán-Barcia, M.P.; Jurado, P.; González-Pérez, B.; Moncalián, G.; Fernández, L.A.; de la Cruz, F. Conjugative transfer can be inhibited by blocking relaxase activity within recipient cells with intrabodies. *Mol. Microbiol.* **2007**, *63*, 404–416. [[CrossRef](#)] [[PubMed](#)]
158. Chandler, M.; de la Cruz, F.; Dyda, F.; Hickman, A.B.; Moncalian, G.; Ton-Hoang, B. Breaking and joining single-stranded DNA: The HUH endonuclease superfamily. *Nat. Rev. Microbiol.* **2013**, *11*, 525–538. [[CrossRef](#)]
159. Becker, E.C.; Meyer, R. Origin and fate of the 3' ends of single-stranded DNA generated by conjugal transfer of plasmid R1162. *J. Bacteriol.* **2012**, *194*, 5368–5376. [[CrossRef](#)]
160. Forsberg, K.J.; Malik, H.S. Microbial genomics: The expanding universe of bacterial defense systems. *Curr. Biol.* **2018**, *28*, R361–R364. [[CrossRef](#)]
161. Casjens, S. Prophages and bacterial genomics: What have we learned so far? *Mol. Microbiol.* **2003**, *49*, 277–300. [[CrossRef](#)]
162. Narra, H.P.; Ochman, H. Of what use is sex to bacteria? *Curr. Biol.* **2006**, *16*, R705–R710. [[CrossRef](#)]
163. Johnston, C.D.; Cotton, S.L.; Rittling, S.R.; Starr, J.R.; Borisy, G.G.; Dewhirst, F.E.; Lemon, K.P. Systematic evasion of the restriction-modification barrier in bacteria. *Proc. Natl. Acad. Sci. USA* **2019**, *116*, 11454–11459. [[CrossRef](#)] [[PubMed](#)]
164. Bickle, T.A. Restricting restriction. *Mol. Microbiol.* **2004**, *51*, 3–5. [[CrossRef](#)] [[PubMed](#)]
165. Chen, K.; Reuter, M.; Sanghvi, B.; Roberts, G.A.; Cooper, L.P.; Tilling, M.; Blakely, G.W.; Dryden, D.T.F. Arda proteins from different mobile genetic elements can bind to the EcoKI Type I DNA methyltransferase of *E. coli* K12. *Biochim. Biophys. Acta* **2014**, *1844*, 505–511. [[CrossRef](#)] [[PubMed](#)]
166. McMahon, S.A.; Roberts, G.A.; Johnson, K.A.; Cooper, L.P.; Liu, H.; White, J.H.; Carter, L.G.; Sanghvi, B.; Oke, M.; Walkinshaw, M.D.; et al. Extensive DNA mimicry by the Arda anti-restriction protein and its role in the spread of antibiotic resistance. *Nucleic Acids Res.* **2009**, *37*, 4887–4897. [[CrossRef](#)]

167. Wilkins, B.M. Plasmid promiscuity: Meeting the challenge of DNA immigration control. *Environ. Microbiol.* **2002**, *4*, 495–500. [[CrossRef](#)]
168. Belogurov, A.A.; Delver, E.P.; Agafonova, O.V.; Belogurova, N.G.; Lee, L.Y.; Kado, C.I. Antirestriction protein Ard (Type C) encoded by IncW plasmid pSa has a high similarity to the “protein transport” domain of TraC1 primase of promiscuous plasmid RP4. *J. Mol. Biol.* **2000**, *296*, 969–977. [[CrossRef](#)]
169. Roy, D.; Huguette, K.T.; Grenier, F.; Burrus, V. IncC conjugative plasmids and SXT/R391 elements repair double-strand breaks caused by CRISPR-Cas during conjugation. *Nucleic Acids Res.* **2020**, 8815–8827. [[CrossRef](#)]
170. Wilkins, B.M.; Chilley, P.M.; Thomas, A.T.; Pocklington, M.J. Distribution of restriction enzyme recognition sequences on broad host range plasmid RP4: Molecular and evolutionary implications. *J. Mol. Biol.* **1996**, *258*, 447–456. [[CrossRef](#)]
171. Grissa, I.; Vergnaud, G.; Pourcel, C. The CRISPRdb database and tools to display CRISPRs and to generate dictionaries of spacers and repeats. *BMC Bioinform.* **2007**, *8*, 172. [[CrossRef](#)]
172. Makarova, K.S.; Wolf, Y.I.; Alkhnbashi, O.S.; Costa, F.; Shah, S.A.; Saunders, S.J.; Barrangou, R.; Brouns, S.J.J.; Charpentier, E.; Haft, D.H.; et al. An updated evolutionary classification of CRISPR-Cas systems. *Nat. Rev. Microbiol.* **2015**, *13*, 722–736. [[CrossRef](#)]
173. Garneau, J.E.; Dupuis, M.-È.; Villion, M.; Romero, D.A.; Barrangou, R.; Boyaval, P.; Fremaux, C.; Horvath, P.; Magadán, A.H.; Moineau, S. The CRISPR/Cas bacterial immune system cleaves bacteriophage and plasmid DNA. *Nature* **2010**, *468*, 67–71. [[CrossRef](#)] [[PubMed](#)]
174. Bondy-Denomy, J.; Pawluk, A.; Maxwell, K.L.; Davidson, A.R. Bacteriophage genes that inactivate the CRISPR/Cas bacterial immune system. *Nature* **2013**, *493*, 429–432. [[CrossRef](#)] [[PubMed](#)]
175. Bondy-Denomy, J.; Garcia, B.; Strum, S.; Du, M.; Rollins, M.F.; Hidalgo-Reyes, Y.; Wiedenheft, B.; Maxwell, K.L.; Davidson, A.R. Multiple mechanisms for CRISPR-Cas inhibition by anti-CRISPR proteins. *Nature* **2015**, *526*, 136–139. [[CrossRef](#)] [[PubMed](#)]
176. Mahendra, C.; Christie, K.A.; Osuna, B.A.; Pinilla-Redondo, R.; Kleinstiver, B.P.; Bondy-Denomy, J. Broad-Spectrum anti-CRISPR proteins facilitate horizontal gene transfer. *Nat. Microbiol.* **2020**, *5*, 620–629. [[CrossRef](#)] [[PubMed](#)]
177. Cram, D.; Ray, A.; O’Gorman, L.; Skurray, R. Transcriptional analysis of the leading region in F plasmid DNA transfer. *Plasmid* **1984**, *11*, 221–233. [[CrossRef](#)]
178. Jones, A.L.; Barth, P.T.; Wilkins, B.M. Zygotic induction of plasmid *ssb* and *psiB* genes following conjugative transfer of Inc11 plasmid Collb-P9. *Mol. Microbiol.* **1992**, *6*, 605–613. [[CrossRef](#)] [[PubMed](#)]
179. Althorpe, N.J.; Chilley, P.M.; Thomas, A.T.; Brammar, W.J.; Wilkins, B.M. Transient transcriptional activation of the Inc11 plasmid anti-restriction gene (*ardA*) and SOS inhibition gene (*psiB*) early in conjugating recipient bacteria. *Mol. Microbiol.* **1999**, *31*, 133–142. [[CrossRef](#)]
180. Masai, H.; Arai, K. Frpo: A novel single-stranded DNA promoter for transcription and for primer RNA synthesis of DNA replication. *Cell* **1997**, *89*, 897–907. [[CrossRef](#)]
181. Honda, Y.; Sakai, H.; Komano, T. Two single-strand DNA initiation signals located in the *oriV* region of plasmid RSF1010. *Gene* **1988**, *68*, 221–228. [[CrossRef](#)]
182. Masai, H.; Arai, K. Mechanisms of primer RNA synthesis and D-loop/R-loop-dependent DNA replication in *Escherichia coli*. *Biochimie* **1996**, *78*, 1109–1117. [[CrossRef](#)]
183. Nomura, N.; Low, R.L.; Ray, D.S. Selective cloning of Co1E1 DNA initiation sequences using the cloning vector M13 delta E101. *Gene* **1982**, *18*, 239–246. [[CrossRef](#)]
184. Nomura, N.; Masai, H.; Inuzuka, M.; Miyazaki, C.; Ohtsubo, E.; Itoh, T.; Sasamoto, S.; Matsui, M.; Ishizaki, R.; Arai, K. Identification of eleven single-strand initiation sequences (*ssi*) for priming of DNA replication in the F, R6K, R100 and ColE2 plasmids. *Gene* **1991**, *108*, 15–22. [[CrossRef](#)] [[PubMed](#)]
185. Díaz, A.; Lacks, S.A.; López, P. Multiple roles for DNA polymerase I in establishment and replication of the promiscuous plasmid pLS1. *Mol. Microbiol.* **1994**, *14*, 773–783. [[CrossRef](#)] [[PubMed](#)]
186. Wilkins, B.M.; Hollom, S.E. Conjugational synthesis of F *lac+* and Col I DNA in the presence of rifampicin and in *Escherichia coli* K12 mutants defective in DNA synthesis. *Mol. Gen. Genet.* **1974**, *134*, 143–156. [[CrossRef](#)]
187. Baharoglu, Z.; Mazel, D. SOS, the formidable strategy of bacteria against aggressions. *FEMS Microbiol. Rev.* **2014**, *38*, 1126–1145. [[CrossRef](#)]

188. Baharoglu, Z.; Bikard, D.; Mazel, D. Conjugative DNA transfer induces the bacterial SOS response and promotes antibiotic resistance development through Integron activation. *PLoS Genet.* **2010**, *6*, e1001165. [[CrossRef](#)]
189. Maslowska, K.H.; Makiela-Dzubska, K.; Fijalkowska, I.J. The SOS system: A complex and tightly regulated response to DNA damage. *Environ. Mol. Mutagen.* **2019**, *60*, 368–384. [[CrossRef](#)]
190. Golub, E.; Bailone, A.; Devoret, R. A gene encoding an SOS inhibitor is present in different conjugative plasmids. *J. Bacteriol.* **1988**, *170*, 4392–4394. [[CrossRef](#)]
191. Bailone, A.; Bäckman, A.; Sommer, S.; Célérier, J.; Bagdasarian, M.M.; Bagdasarian, M.; Devoret, R. PsiB polypeptide prevents activation of RecA protein in *Escherichia coli*. *Mol. Gen. Genet.* **1988**, *214*, 389–395. [[CrossRef](#)]
192. Petrova, V.; Chitteni-Pattu, S.; Drees, J.C.; Inman, R.B.; Cox, M.M. An SOS inhibitor that binds to free RecA protein: The PsiB protein. *Mol. Cell* **2009**, *36*, 121–130. [[CrossRef](#)]
193. Meyer, R.R.; Laine, P.S. The single-stranded DNA-binding protein of *Escherichia coli*. *Microbiol. Rev.* **1990**, *54*, 342–380. [[CrossRef](#)] [[PubMed](#)]
194. Shereda, R.D.; Kozlov, A.G.; Lohman, T.M.; Cox, M.M.; Keck, J.L. SSB as an organizer/mobilizer of genome maintenance complexes. *Crit. Rev. Biochem. Mol. Biol.* **2008**, *43*, 289–318. [[CrossRef](#)]
195. Sigal, N.; Delius, H.; Kornberg, T.; Gefter, M.L.; Alberts, B. A DNA-unwinding protein isolated from *Escherichia coli*: Its interaction with DNA and with DNA polymerases. *Proc. Natl. Acad. Sci. USA* **1972**, *69*, 3537–3541. [[CrossRef](#)] [[PubMed](#)]
196. Nolivos, S.; Cayron, J.; Dedieu, A.; Page, A.; Delolme, F.; Lesterlin, C. Role of AcrAB-TolC multidrug efflux pump in drug-resistance acquisition by plasmid transfer. *Science* **2019**, *364*, 778–782. [[CrossRef](#)]
197. Golub, E.I.; Low, K.B. Conjugative plasmids of enteric bacteria from many different incompatibility groups have similar genes for single-stranded DNA-binding proteins. *J. Bacteriol.* **1985**, *162*, 235–241. [[CrossRef](#)] [[PubMed](#)]
198. Kolodkin, A.L.; Capage, M.A.; Golub, E.I.; Low, K.B. F sex factor of *Escherichia coli* K-12 codes for a single-stranded DNA binding protein. *Proc. Natl. Acad. Sci. USA* **1983**, *80*, 4422–4426. [[CrossRef](#)]
199. Golub, E.I.; Low, K.B. Derepression of single-stranded DNA-binding protein genes on plasmids derepressed for conjugation, and complementation of an *E. coli* ssb-mutation by these genes. *Mol. Gen. Genet.* **1986**, *204*, 410–416. [[CrossRef](#)]
200. Howland, C.J.; Rees, C.E.; Barth, P.T.; Wilkins, B.M. The ssb gene of plasmid ColIb-P9. *J. Bacteriol.* **1989**, *171*, 2466–2473. [[CrossRef](#)]
201. Porter, R.D.; Black, S. The single-stranded-DNA-binding protein encoded by the *Escherichia coli* F factor can complement a deletion of the chromosomal ssb gene. *J. Bacteriol.* **1991**, *173*, 2720–2723. [[CrossRef](#)]
202. Ruvolo, P.P.; Keating, K.M.; Williams, K.R.; Chase, J.W. Single-Stranded DNA binding proteins (SSBs) from prokaryotic transmissible plasmids. *Proteins* **1991**, *9*, 120–134. [[CrossRef](#)]
203. Jovanovic, O.S.; Ayres, E.K.; Figurski, D.H. The replication initiator operon of promiscuous plasmid RK2 encodes a gene that complements an *Escherichia coli* mutant defective in single-stranded DNA-binding protein. *J. Bacteriol.* **1992**, *174*, 4842–4846. [[CrossRef](#)] [[PubMed](#)]
204. del Solar, G.; Giraldo, R.; Ruiz-Echevarria, M.J.; Espinosa, M.; Díaz-Orejas, R. Replication and control of circular bacterial plasmids. *Microbiol. Mol. Biol. Rev.* **1998**, *62*, 434–464. [[CrossRef](#)]
205. Pinto, U.M.; Pappas, K.M.; Winans, S.C. The ABCs of plasmid replication and segregation. *Nat. Rev. Microbiol.* **2012**, *10*, 755–765. [[CrossRef](#)] [[PubMed](#)]
206. Rakowski, S.A.; Filutowicz, M. Plasmid R6K replication control. *Plasmid* **2013**, *69*, 231–242. [[CrossRef](#)] [[PubMed](#)]
207. Nordström, K. Plasmid R1–replication and its control. *Plasmid* **2006**, *55*, 1–26. [[CrossRef](#)]
208. Guiney, D.G. Host range of conjugation and replication functions of the *Escherichia coli* sex plasmid Flac. *J. Mol. Biol.* **1982**, *162*, 699–703. [[CrossRef](#)]
209. Zhong, Z.; Helinski, D.; Toukdarian, A. Plasmid host-range: Restrictions to F replication in *Pseudomonas*. *Plasmid* **2005**, *54*, 48–56. [[CrossRef](#)]
210. Adamczyk, M.; Jagura-Burdzy, G. Spread and survival of promiscuous IncP-1 plasmids. *Acta Biochim. Pol.* **2003**, *50*, 425–453. [[CrossRef](#)]
211. Baxter, J.C.; Funnell, B.E. Plasmid partition mechanisms. *Microbiol. Spectr.* **2014**, *2*. [[CrossRef](#)]
212. Ebersbach, G.; Gerdes, K. Plasmid segregation mechanisms. *Annu. Rev. Genet.* **2005**, *39*, 453–479. [[CrossRef](#)]

213. Gerdes, K.; Howard, M.; Szardenings, F. Pushing and pulling in prokaryotic DNA segregation. *Cell* **2010**, *141*, 927–942. [[CrossRef](#)] [[PubMed](#)]
214. Møller-Jensen, J.; Jensen, R.B.; Gerdes, K. Plasmid and chromosome segregation in prokaryotes. *Trends Microbiol.* **2000**, *8*, 313–320. [[CrossRef](#)]
215. Schumacher, M.A. Bacterial plasmid partition machinery: A minimalist approach to survival. *Curr. Opin. Struct. Biol.* **2012**, *22*, 72–79. [[CrossRef](#)]
216. Deonier, R.C.; Davidson, N. The sequence organization of the integrated F plasmid in two Hfr strains of *Escherichia coli*. *J. Mol. Biol.* **1976**, *107*, 207–222. [[CrossRef](#)]
217. Deonier, R.C.; Mirels, L. Excision of F plasmid sequences by recombination at directly repeated insertion sequence 2 elements: Involvement of recA. *Proc. Natl. Acad. Sci. USA* **1977**, *74*, 3965–3969. [[CrossRef](#)] [[PubMed](#)]
218. Johnson, C.M.; Grossman, A.D. Integrative and Conjugative Elements (ICEs): What they do and how they work. *Annu. Rev. Genet.* **2015**, *49*, 577–601. [[CrossRef](#)]
219. Shao, Q.; Hawkins, A.; Zeng, L. Phage DNA dynamics in cells with different fates. *Biophys. J.* **2015**, *108*, 2048–2060. [[CrossRef](#)] [[PubMed](#)]
220. Gago-Córdoba, C.; Val-Calvo, J.; Miguel-Arribas, A.; Serrano, E.; Singh, P.K.; Abia, D.; Wu, L.J.; Meijer, W.J.J. Surface exclusion revisited: Function related to differential expression of the surface exclusion system of *Bacillus subtilis* Plasmid pLS20. *Front. Microbiol.* **2019**, *10*, 1502. [[CrossRef](#)] [[PubMed](#)]
221. Galli, D.M.; Chen, J. Entry exclusion activity on conjugative plasmid pVT745. *Plasmid* **2006**, *55*, 158–163. [[CrossRef](#)]
222. Gunton, J.E.; Ussher, J.E.R.; Rooker, M.M.; Wetsch, N.M.; Alonso, G.; Taylor, D.E. Entry exclusion in the IncHI1 plasmid R27 is mediated by EexA and EexB. *Plasmid* **2008**, *59*, 86–101. [[CrossRef](#)]
223. Haase, J.; Kalkum, M.; Lanka, E. TrbK, a small cytoplasmic membrane lipoprotein, functions in entry exclusion of the IncP α plasmid RP4. *J. Bacteriol.* **1996**, *178*, 6720–6729. [[CrossRef](#)] [[PubMed](#)]
224. Humbert, M.; Huguet, K.T.; Coulombe, F.; Burrus, V. Entry exclusion of conjugative Plasmids of the IncA, IncC, and related untyped incompatibility groups. *J. Bacteriol.* **2019**, *201*. [[CrossRef](#)]
225. Kraushaar, B.; Appel, B.; Lanka, E.; Strauch, E. Entry exclusion and oriT of a conjugative system encoded by the cryptic plasmid p29930 of *Yersinia enterocolitica*. *Plasmid* **2010**, *64*, 79–84. [[CrossRef](#)] [[PubMed](#)]
226. Pohlman, R.F.; Genetti, H.D.; Winans, S.C. Entry exclusion of the IncN plasmid pKM101 is mediated by a single hydrophilic protein containing a lipid attachment motif. *Plasmid* **1994**, *31*, 158–165. [[CrossRef](#)]
227. Possoz, C.; Gagnat, J.; Sezonov, G.; Guérineau, M.; Pernodet, J.-L. Conjugal immunity of *Streptomyces* strains carrying the integrative element pSAM2 is due to the pif gene (pSAM2 immunity factor). *Mol. Microbiol.* **2003**, *47*, 1385–1393. [[CrossRef](#)] [[PubMed](#)]
228. Thomas, C.M.; Nielsen, K.M. Mechanisms of, and barriers to, horizontal gene transfer between bacteria. *Nat. Rev. Microbiol.* **2005**, *3*, 711–721. [[CrossRef](#)] [[PubMed](#)]
229. Achtman, M.; Kennedy, N.; Skurray, R. Cell-Cell interactions in conjugating *Escherichia coli*: Role of traT protein in surface exclusion. *Proc. Natl. Acad. Sci. USA* **1977**, *74*, 5104–5108. [[CrossRef](#)]
230. Manning, P.A.; Beutin, L.; Achtman, M. Outer membrane of *Escherichia coli*: Properties of the F sex factor traT protein which is involved in surface exclusion. *J. Bacteriol.* **1980**, *142*, 285–294. [[CrossRef](#)]
231. Minkley, E.G.; Ippen-Ihler, K. Identification of a membrane protein associated with expression of the surface exclusion region of the F transfer operon. *J. Bacteriol.* **1977**, *129*, 1613–1622. [[CrossRef](#)]
232. Riede, I.; Eschbach, M.L. Evidence that TraT interacts with OmpA of *Escherichia coli*. *FEBS Lett.* **1986**, *205*, 241–245. [[CrossRef](#)]
233. Jalajakumari, M.B.; Guidolin, A.; Buhk, H.J.; Manning, P.A.; Ham, L.M.; Hodgson, A.L.; Cheah, K.C.; Skurray, R.A. Surface exclusion genes traS and traT of the F sex factor of *Escherichia coli* K-12. Determination of the nucleotide sequence and promoter and terminator activities. *J. Mol. Biol.* **1987**, *198*, 1–11. [[CrossRef](#)]
234. San Millan, A.; MacLean, R.C. Fitness costs of Plasmids: A limit to Plasmid transmission. *Microbiol. Spectr.* **2017**, *5*. [[CrossRef](#)]
235. Barlow, M. What antimicrobial resistance has taught us about horizontal gene transfer. *Methods Mol. Biol.* **2009**, *532*, 397–411. [[CrossRef](#)] [[PubMed](#)]
236. Hall-Stoodley, L.; Costerton, J.W.; Stoodley, P. Bacterial biofilms: From the natural environment to infectious diseases. *Nat. Rev. Microbiol.* **2004**, *2*, 95–108. [[CrossRef](#)] [[PubMed](#)]

237. Bale, M.J.; Fry, J.C.; Day, M.J. Plasmid transfer between strains of *Pseudomonas aeruginosa* on membrane filters attached to river stones. *J. Gen. Microbiol.* **1987**, *133*, 3099–3107. [[CrossRef](#)]
238. Lilley, A.K.; Bailey, M.J. Impact of Plasmid pQBR103 acquisition and carriage on the phytosphere fitness of *Pseudomonas fluorescens* SBW25: Burden and benefit. *Appl. Environ. Microbiol.* **1997**, *63*, 1584–1587. [[CrossRef](#)]
239. Munck, C.; Sheth, R.U.; Freedberg, D.E.; Wang, H.H. Recording mobile DNA in the gut microbiota using an *Escherichia coli* CRISPR-Cas spacer acquisition platform. *Nat. Commun.* **2020**, *11*, 95. [[CrossRef](#)]
240. Ronda, C.; Chen, S.P.; Cabral, V.; Yaung, S.J.; Wang, H.H. Metagenomic engineering of the mammalian gut microbiome in situ. *Nat. Methods* **2019**, *16*, 167–170. [[CrossRef](#)]
241. Ehlers, L.J.; Bouwer, E.J. RP4 plasmid transfer among species of pseudomonas in a biofilm reactor. *Water Sci. Technol.* **1999**, *39*, 163–171. [[CrossRef](#)]
242. Yang, D.; Wang, J.; Qiu, Z.; Jin, M.; Shen, Z.; Chen, Z.; Wang, X.; Zhang, B.; Li, J.-W. Horizontal transfer of antibiotic resistance genes in a membrane bioreactor. *J. Biotechnol.* **2013**, *167*, 441–447. [[CrossRef](#)]
243. Hausner, M.; Wuertz, S. High rates of conjugation in bacterial biofilms as determined by quantitative in situ analysis. *Appl. Environ. Microbiol.* **1999**, *65*, 3710–3713. [[CrossRef](#)] [[PubMed](#)]
244. Christensen, B.B.; Sternberg, C.; Molin, S. Bacterial plasmid conjugation on semi-solid surfaces monitored with the green fluorescent protein (GFP) from *Aequorea victoria* as a marker. *Gene* **1996**, *173*, 59–65. [[CrossRef](#)]
245. Haagensen, J.A.J.; Hansen, S.K.; Johansen, T.; Molin, S. In situ detection of horizontal transfer of mobile genetic elements. *FEMS Microbiol. Ecol.* **2002**, *42*, 261–268. [[CrossRef](#)] [[PubMed](#)]
246. Reisner, A.; Wolinski, H.; Zechner, E.L. In situ monitoring of IncF plasmid transfer on semi-solid agar surfaces reveals a limited invasion of plasmids in recipient colonies. *Plasmid* **2012**, *67*, 155–161. [[CrossRef](#)]
247. Lilley, A.K.; Bailey, M.J. The transfer dynamics of *Pseudomonas* sp. plasmid pQBR11 in biofilms. *FEMS Microbiol. Ecol.* **2002**, *42*, 243–250. [[CrossRef](#)] [[PubMed](#)]
248. Aspray, T.J.; Hansen, S.K.; Burns, R.G. A soil-based microbial biofilm exposed to 2,4-D: Bacterial community development and establishment of conjugative plasmid pJP4. *FEMS Microbiol. Ecol.* **2005**, *54*, 317–327. [[CrossRef](#)]
249. Christensen, B.B.; Sternberg, C.; Andersen, J.B.; Eberl, L.; Moller, S.; Givskov, M.; Molin, S. Establishment of new genetic traits in a microbial biofilm community. *Appl. Environ. Microbiol.* **1998**, *64*, 2247–2255. [[CrossRef](#)]
250. Nanchaiah, Y.V.; Wattiau, P.; Wuertz, S.; Bathe, S.; Mohan, S.V.; Wilderer, P.A.; Hausner, M. Dual labeling of *Pseudomonas putida* with fluorescent proteins for in situ monitoring of conjugal transfer of the TOL plasmid. *Appl. Environ. Microbiol.* **2003**, *69*, 4846–4852. [[CrossRef](#)]
251. Abe, K.; Nomura, N.; Suzuki, S. Biofilms: Hot spots of horizontal gene transfer (HGT) in aquatic environments, with a focus on a new HGT mechanism. *FEMS Microbiol. Ecol.* **2020**, *96*. [[CrossRef](#)]
252. Madsen, J.S.; Burmølle, M.; Hansen, L.H.; Sørensen, S.J. The interconnection between biofilm formation and horizontal gene transfer. *FEMS Immunol. Med. Microbiol.* **2012**, *65*, 183–195. [[CrossRef](#)]
253. Molin, S.; Tolker-Nielsen, T. Gene transfer occurs with enhanced efficiency in biofilms and induces enhanced stabilisation of the biofilm structure. *Curr. Opin. Biotechnol.* **2003**, *14*, 255–261. [[CrossRef](#)]
254. Nesse, L.L.; Simm, R. Biofilm: A hotspot for emerging bacterial genotypes. *Adv. Appl. Microbiol.* **2018**, *103*, 223–246. [[CrossRef](#)] [[PubMed](#)]
255. Stalder, T.; Top, E. Plasmid transfer in biofilms: A perspective on limitations and opportunities. *NPJ Biofilms Microbiomes* **2016**, *2*. [[CrossRef](#)] [[PubMed](#)]
256. Fuchs, F.M.; Holland, G.; Moeller, R.; Laue, M. Directed freeze-fracturing of *Bacillus subtilis* biofilms for conventional scanning electron microscopy. *J. Microbiol. Methods* **2018**, *152*, 165–172. [[CrossRef](#)] [[PubMed](#)]
257. Serra, D.O.; Richter, A.M.; Klauck, G.; Mika, F.; Hengge, R. Microanatomy at cellular resolution and spatial order of physiological differentiation in a bacterial biofilm. *mBio* **2013**, *4*, e00103–00113. [[CrossRef](#)]
258. Seoane, J.; Yankelevich, T.; Dechesne, A.; Merkey, B.; Sternberg, C.; Smets, B.F. An individual-based approach to explain plasmid invasion in bacterial populations. *FEMS Microbiol. Ecol.* **2011**, *75*, 17–27. [[CrossRef](#)]
259. Licht, T.R.; Christensen, B.B.; Krogfelt, K.A.; Molin, S. Plasmid transfer in the animal intestine and other dynamic bacterial populations: The role of community structure and environment. *Microbiology* **1999**, *145 Pt 9*, 2615–2622. [[CrossRef](#)]
260. Serra, D.O.; Hengge, R. Stress responses go three dimensional—The spatial order of physiological differentiation in bacterial macrocolony biofilms. *Environ. Microbiol.* **2014**, *16*, 1455–1471. [[CrossRef](#)]
261. Stewart, P.S.; Franklin, M.J. Physiological heterogeneity in biofilms. *Nat. Rev. Microbiol.* **2008**, *6*, 199–210. [[CrossRef](#)]

262. Ghigo, J.M. Natural conjugative plasmids induce bacterial biofilm development. *Nature* **2001**, *412*, 442–445. [[CrossRef](#)]
263. Lim, J.Y.; La, H.J.; Sheng, H.; Forney, L.J.; Hovde, C.J. Influence of plasmid pO157 on *Escherichia coli* O157:H7 Sakai biofilm formation. *Appl. Environ. Microbiol.* **2010**, *76*, 963–966. [[CrossRef](#)] [[PubMed](#)]
264. Liu, Z.; Que, F.; Liao, L.; Zhou, M.; You, L.; Zhao, Q.; Li, Y.; Niu, H.; Wu, S.; Huang, R. Study on the promotion of bacterial biofilm formation by a *Salmonella* conjugative plasmid and the underlying mechanism. *PLoS ONE* **2014**, *9*, e109808. [[CrossRef](#)] [[PubMed](#)]
265. Reisner, A.; Höller, B.M.; Molin, S.; Zechner, E.L. Synergistic effects in mixed *Escherichia coli* biofilms: Conjugative plasmid transfer drives biofilm expansion. *J. Bacteriol.* **2006**, *188*, 3582–3588. [[CrossRef](#)] [[PubMed](#)]
266. Shi, H.; Zhou, X.; Zou, W.; Wang, Y.; Lei, C.; Xiang, R.; Zhou, L.; Liu, B.; Zhang, A.; Wang, H. Co-Occurrence of biofilm formation and quinolone resistance in *Salmonella enterica* serotype typhimurium carrying an IncHI2-type oqxAB-positive plasmid. *Microb. Pathog.* **2018**, *123*, 68–73. [[CrossRef](#)]
267. Beloin, C.; Roux, A.; Ghigo, J.M. *Escherichia coli* biofilms. *Curr. Top. Microbiol. Immunol.* **2008**, *322*, 249–289. [[CrossRef](#)]
268. Craig, L.; Forest, K.T.; Maier, B. Type IV pili: Dynamics, biophysics and functional consequences. *Nat. Rev. Microbiol.* **2019**, *17*, 429–440. [[CrossRef](#)]
269. Burmølle, M.; Bahl, M.I.; Jensen, L.B.; Sørensen, S.J.; Hansen, L.H. Type 3 fimbriae, encoded by the conjugative plasmid pOLA52, enhance biofilm formation and transfer frequencies in Enterobacteriaceae strains. *Microbiology* **2008**, *154*, 187–195. [[CrossRef](#)]
270. Dudley, E.G.; Abe, C.; Ghigo, J.-M.; Latour-Lambert, P.; Hormazabal, J.C.; Nataro, J.P. An IncI1 plasmid contributes to the adherence of the atypical enteroaggregative *Escherichia coli* strain C1096 to cultured cells and abiotic surfaces. *Infect. Immun.* **2006**, *74*, 2102–2114. [[CrossRef](#)]
271. Bhatti, M.; Cruz, M.R.; Frank, K.L.; Gomez, J.A.L.; Andrade, F.; Garsin, D.A.; Dunny, G.M.; Kaplan, H.B.; Christie, P.J. *Enterococcus faecalis* pCF10-encoded surface proteins PrgA, PrgB (aggregation substance) and PrgC contribute to plasmid transfer, biofilm formation and virulence. *Mol. Microbiol.* **2015**, *95*, 660–677. [[CrossRef](#)]
272. Coburn, P.S.; Baghdayan, A.S.; Craig, N.; Burroughs, A.; Tendolkar, P.; Miller, K.; Najar, F.Z.; Roe, B.A.; Shankar, N. A novel conjugative plasmid from *Enterococcus faecalis* E99 enhances resistance to ultraviolet radiation. *Plasmid* **2010**, *64*, 18–25. [[CrossRef](#)]
273. Tendolkar, P.M.; Baghdayan, A.S.; Shankar, N. Putative surface proteins encoded within a novel transferable locus confer a high-biofilm phenotype to *Enterococcus faecalis*. *J. Bacteriol.* **2006**, *188*, 2063–2072. [[CrossRef](#)] [[PubMed](#)]
274. Reisner, A.; Haagensen, J.A.J.; Schembri, M.A.; Zechner, E.L.; Molin, S. Development and maturation of *Escherichia coli* K-12 biofilms. *Mol. Microbiol.* **2003**, *48*, 933–946. [[CrossRef](#)] [[PubMed](#)]
275. May, T.; Okabe, S. *Escherichia coli* harboring a natural IncF conjugative F plasmid develops complex mature biofilms by stimulating synthesis of colanic acid and Curli. *J. Bacteriol.* **2008**, *190*, 7479–7490. [[CrossRef](#)] [[PubMed](#)]
276. Barrios, A.F.G.; Zuo, R.; Ren, D.; Wood, T.K. Hha, YbaJ, and OmpA regulate *Escherichia coli* K12 biofilm formation and conjugation plasmids abolish motility. *Biotechnol. Bioeng.* **2006**, *93*, 188–200. [[CrossRef](#)]
277. Yang, X.; Ma, Q.; Wood, T.K. The R1 conjugative plasmid increases *Escherichia coli* biofilm formation through an envelope stress response. *Appl. Environ. Microbiol.* **2008**, *74*, 2690–2699. [[CrossRef](#)]
278. Okshevsky, M.; Meyer, R.L. The role of extracellular DNA in the establishment, maintenance and perpetuation of bacterial biofilms. *Crit. Rev. Microbiol.* **2015**, *41*, 341–352. [[CrossRef](#)]
279. D’Alvise, P.W.; Sjöholm, O.R.; Yankelevich, T.; Jin, Y.; Wuertz, S.; Smets, B.F. TOL plasmid carriage enhances biofilm formation and increases extracellular DNA content in *Pseudomonas putida* KT2440. *FEMS Microbiol. Lett.* **2010**, *312*, 84–92. [[CrossRef](#)]
280. Røder, H.L.; Hansen, L.H.; Sørensen, S.J.; Burmølle, M. The impact of the conjugative IncP-1 plasmid pJK5 on multispecies biofilm formation is dependent on the plasmid host. *FEMS Microbiol. Lett.* **2013**, *344*, 186–192. [[CrossRef](#)]
281. Hoffman, L.R.; D’Argenio, D.A.; MacCoss, M.J.; Zhang, Z.; Jones, R.A.; Miller, S.I. Aminoglycoside antibiotics induce bacterial biofilm formation. *Nature* **2005**, *436*, 1171–1175. [[CrossRef](#)]

282. Linares, J.F.; Gustafsson, I.; Baquero, F.; Martinez, J.L. Antibiotics as intermicrobial signaling agents instead of weapons. *Proc. Natl. Acad. Sci. USA* **2006**, *103*, 19484–19489. [[CrossRef](#)]
283. Salcedo, D.E.; Lee, J.H.; Ha, U.H.; Kim, S.P. The effects of antibiotics on the biofilm formation and antibiotic resistance gene transfer. *Desalin. Water Treat.* **2015**, *54*, 3582–3588. [[CrossRef](#)]
284. Penesyan, A.; Nagy, S.S.; Kjelleberg, S.; Gillings, M.R.; Paulsen, I.T. Rapid microevolution of biofilm cells in response to antibiotics. *NPJ Biofilms Microbiomes* **2019**, *5*, 34. [[CrossRef](#)]
285. Bagge, N.; Schuster, M.; Hentzer, M.; Ciofu, O.; Givskov, M.; Greenberg, E.P.; Høiby, N. *Pseudomonas aeruginosa* biofilms exposed to imipenem exhibit changes in global gene expression and β -lactamase and alginate production. *Antimicrob. Agents Chemother.* **2004**, *48*, 1175–1187. [[CrossRef](#)] [[PubMed](#)]
286. Díaz-Pascual, F.; Hartmann, R.; Lempp, M.; Vidakovic, L.; Song, B.; Jeckel, H.; Thormann, K.M.; Yildiz, F.H.; Dunkel, J.; Link, H.; et al. Breakdown of *Vibrio cholerae* biofilm architecture induced by antibiotics disrupts community barrier function. *Nat. Microbiol.* **2019**, *4*, 2136–2145. [[CrossRef](#)]
287. Al-Masaudi, S.B.; Day, M.J.; Russell, A.D. Effect of some antibiotics and biocides on plasmid transfer in *Staphylococcus aureus*. *J. Appl. Bacteriol.* **1991**, *71*, 239–243. [[CrossRef](#)]
288. Barr, V.; Barr, K.; Millar, M.R.; Lacey, R.W. β -Lactam antibiotics increase the frequency of plasmid transfer in *Staphylococcus aureus*. *J. Antimicrob. Chemother.* **1986**, *17*, 409–413. [[CrossRef](#)] [[PubMed](#)]
289. Feld, L.; Schjørring, S.; Hammer, K.; Licht, T.R.; Danielsen, M.; Krogh, K.; Wilcks, A. Selective pressure affects transfer and establishment of a *Lactobacillus plantarum* resistance plasmid in the gastrointestinal environment. *J. Antimicrob. Chemother.* **2008**, *61*, 845–852. [[CrossRef](#)] [[PubMed](#)]
290. Liu, G.; Bogaj, K.; Bortolaia, V.; Olsen, J.E.; Thomsen, L.E. Antibiotic-Induced, increased conjugative transfer is common to diverse naturally occurring ESBL Plasmids in *Escherichia coli*. *Front. Microbiol.* **2019**, *10*, 2119. [[CrossRef](#)]
291. Lu, Y.; Zeng, J.; Wang, L.; Lan, K.; Shunmei, E.; Wang, L.; Xiao, Q.; Luo, Q.; Huang, X.; Huang, B.; et al. Antibiotics promote *Escherichia coli*-*Pseudomonas aeruginosa* conjugation through inhibiting quorum sensing. *Antimicrob. Agents Chemother.* **2017**, *61*. [[CrossRef](#)] [[PubMed](#)]
292. Ma, H.; Bryers, J.D. Non-Invasive determination of conjugative transfer of plasmids bearing antibiotic-resistance genes in biofilm-bound bacteria: Effects of substrate loading and antibiotic selection. *Appl. Microbiol. Biotechnol.* **2013**, *97*, 317–328. [[CrossRef](#)] [[PubMed](#)]
293. Ohlsen, K.; Ternes, T.; Werner, G.; Wallner, U.; Löffler, D.; Ziebuhr, W.; Witte, W.; Hacker, J. Impact of antibiotics on conjugational resistance gene transfer in *Staphylococcus aureus* in sewage. *Environ. Microbiol.* **2003**, *5*, 711–716. [[CrossRef](#)]
294. Xia, Z.-J.; Wang, J.; Hu, W.; Liu, H.; Gao, X.-Z.; Wu, Z.-H.; Zhang, P.-Y.; Li, Y.-Z. Improving conjugation efficacy of *Sorangium cellulosum* by the addition of dual selection antibiotics. *J. Ind. Microbiol. Biotechnol.* **2008**, *35*, 1157–1163. [[CrossRef](#)] [[PubMed](#)]
295. Zhang, P.-Y.; Xu, P.-P.; Xia, Z.-J.; Wang, J.; Xiong, J.; Li, Y.-Z. Combined treatment with the antibiotics kanamycin and streptomycin promotes the conjugation of *Escherichia coli*. *FEMS Microbiol. Lett.* **2013**, *348*, 149–156. [[CrossRef](#)]
296. Møller, T.S.B.; Liu, G.; Boysen, A.; Thomsen, L.E.; Lüthje, F.L.; Mortensen, S.; Møller-Jensen, J.; Olsen, J.E. Treatment with Cefotaxime affects expression of conjugation associated proteins and conjugation transfer frequency of an IncI1 Plasmid in *Escherichia coli*. *Front. Microbiol.* **2017**, *8*, 2365. [[CrossRef](#)]
297. Shun-Mei, E.; Zeng, J.-M.; Yuan, H.; Lu, Y.; Cai, R.-X.; Chen, C. Sub-Inhibitory concentrations of fluoroquinolones increase conjugation frequency. *Microb. Pathog.* **2018**, *114*, 57–62. [[CrossRef](#)] [[PubMed](#)]
298. Cantas, L.; Midtlyng, P.J.; Sørum, H. Impact of antibiotic treatments on the expression of the R plasmid tra genes and on the host innate immune activity during pRAS1 bearing *Aeromonas hydrophila* infection in zebrafish (*Danio rerio*). *BMC Microbiol.* **2012**, *12*, 37. [[CrossRef](#)] [[PubMed](#)]
299. Kim, S.; Yun, Z.; Ha, U.-H.; Lee, S.; Park, H.; Kwon, E.E.; Cho, Y.; Choung, S.; Oh, J.; Medriano, C.A.; et al. Transfer of antibiotic resistance plasmids in pure and activated sludge cultures in the presence of environmentally representative micro-contaminant concentrations. *Sci. Total Environ.* **2014**, *468–469*, 813–820. [[CrossRef](#)] [[PubMed](#)]
300. Lopatkin, A.J.; Huang, S.; Smith, R.P.; Srimani, J.K.; Sysoeva, T.A.; Bewick, S.; Karig, D.K.; You, L. Antibiotics as a selective driver for conjugation dynamics. *Nat. Microbiol.* **2016**, *1*, 16044. [[CrossRef](#)]
301. Li, B.; Qiu, Y.; Zhang, J.; Huang, X.; Shi, H.; Yin, H. Real-Time study of rapid spread of antibiotic resistance plasmid in biofilm using microfluidics. *Environ. Sci. Technol.* **2018**, *52*, 11132–11141. [[CrossRef](#)]

302. Qiu, Y.; Zhang, J.; Li, B.; Wen, X.; Liang, P.; Huang, X. A novel microfluidic system enables visualization and analysis of antibiotic resistance gene transfer to activated sludge bacteria in biofilm. *Sci. Total Environ.* **2018**, *642*, 582–590. [[CrossRef](#)]

Publisher's Note: MDPI stays neutral with regard to jurisdictional claims in published maps and institutional affiliations.



© 2020 by the authors. Licensee MDPI, Basel, Switzerland. This article is an open access article distributed under the terms and conditions of the Creative Commons Attribution (CC BY) license (<http://creativecommons.org/licenses/by/4.0/>).

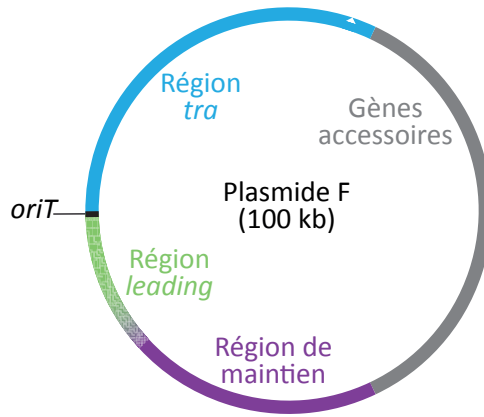
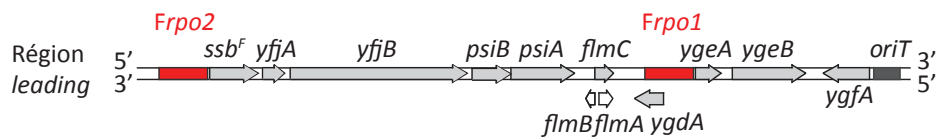


Figure 3. Carte génétique simplifiée du plasmide F.

D'une taille d'environ 100kb, le plasmide F est composé des régions *leading* (vert), région de maintien (violet) et région *tra* (bleu). La région grise comporte les gènes accessoires. D'après Couturier et al. (2023).

1.



2.

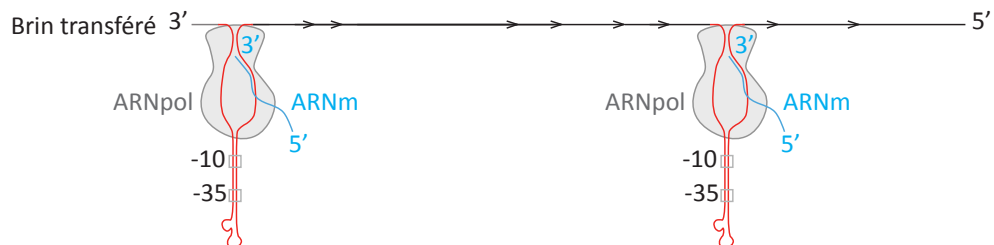


Figure 4. Carte génétique de la région leading sous forme d'ADN double-brin.

1. Position et orientation des gènes correspondants (flèches) et des promoteurs *Frpo1* et *Frpo2* (rouge).
2. Schéma de la structure secondaire en tige-boucle formée par la forme simple-brin des séquences promotrices *Frpo1* et *Frpo2* (rouge). La reconnaissance des cassettes -35 et -10 dans la région double-brin des tiges par l'ARN polymérase (gris) induit l'initiation de la transcription des gènes suivants et la synthèse d'ARNm (bleu). D'après Couturier et al. (2023).

Chapitre III : Plasmide F : un paradigme pour l'étude de la conjugaison

I. Spécificités du plasmide F et classification

Appartenant aux groupes MOB_{F12A} et IncF, plus de 200 plasmides apparentés « F-like » ont été séquencés depuis sa découverte et partagent une machinerie de transfert et T4SS hautement conservés d'une espèce à l'autre mais également entre plasmides-même (Grohmann, Muth, and Espinosa 2003; Grohmann et al. 2018; Koraimann 2018; Virolle et al. 2020). Considérés comme un sujet d'étude important de par leur large distribution chez les *Enterobacteriaceae* issus d'isolats cliniques et échantillons environnementaux, ces plasmides F-like sont souvent associés à la dissémination de colicines, de facteurs de virulence et de résistances antibiotiques (Rosenberg and Hastings 2001; Lanza et al. 2014; Fernandez-Lopez et al. 2016; T. J. Johnson et al. 2016). Le plasmide F joue ainsi un rôle central pour la compréhension des mécanismes moléculaires et structuraux impliqués dans le transfert d'ADN par conjugaison entre bactéries.

Bien qu'étant le focus de la revue ci-dessus, différents aspects concernant l'organisation génétique du plasmide F et l'importance de la région *leading* pour son établissement sont présentés ci-dessous sous un autre angle. D'une taille de 100kb, il est composé de différentes régions génétiques caractéristiques des plasmides conjugatifs. Bien décrites dans la littérature, les régions de transfert et de maintien codent respectivement la machinerie de transfert autonome du plasmide ainsi que les facteurs essentiels au maintien stable du plasmide au cours des cycles de division cellulaire. La région *leading* quant à elle reste encore peu décrite, mais un certain degré de conservation des gènes la composant révèle son importance bien que la majorité soient de fonction inconnue (Figure 3) (Rosenberg and Hastings 2001; Arutyunov and Frost 2013).

La région *tra* code pour différentes protéines essentielles au bon déroulement du processus de transfert par conjugaison. Certaines protéines Tra vont permettre la synthèse et formation du pilus conjugatif impliqué dans l'établissement d'un contact avec une bactérie receveuse tandis que d'autres vont composer le T4SS pour le transfert de l'ADN à travers les membranes du couple de conjugaison. Enfin, les protéines constituant le relaxosome permettent la préparation et le transfert du plasmide sous forme d'ADN simple-brin (Wong, Lu, and Glover 2012; Arutyunov and Frost 2013). Chez la majorité des plasmides IncF (R100, R1, R6-5 et ColB2-K77), ce cluster de gènes *tra* est régulé par différents facteurs hôtes, plasmidiques et environnementaux afin de limiter le coût métabolique

dans le cas d'une expression constitutive (Zahrl et al. 2006; Koraimann and Wagner 2014; Virolle et al. 2020).

Une fois transféré et établi, la région de maintien va permettre la pérennité stable du plasmide au sein des populations bactériennes en limitant un bas nombre de copie à une ou deux par chromosome et ainsi limiter son impact sur la physiologie hôte (Keasling, Palsson, and Cooper 1991; Cooper and Keasling 1998; Bouet and Funnell 2019). Trois types de réplication sont décrits pour les plasmides : la réplication Thêta, similaire à la réplication chromosomique et fréquemment retrouvée chez les plasmides de type F ou RP4 chez les *Enterobacteriaceae* ; la réplication en cercle roulant RCR (*rolling circle replication*), également retrouvé chez le plasmide F lors du transfert du plasmide par conjugaison ; et le type de réplication par remplacement de brin, généralement retrouvé pour les plasmides IncQ. La réplication végétative Thêta du plasmide F est un mécanisme bidirectionnel initié par la liaison du complexe « réplisome » au niveau de l'origine de réplication *oriV* et composé d'une hélicase DnaB, d'une ATPase DnaC et d'une primase DnaG permettant la synthèse d'amorces ARN pour la synthèse du brin « retardé » (*lagging strand*) en coordination avec l'ADN polymérase III (Wu, Zechner, and Marians 1992; A. Johnson and O'Donnell 2005; Tanner et al. 2008; Lilly and Camps 2015). Pour éviter la potentielle perte du plasmide au cours des divisions, la région de maintien code également pour un système de partition actif SopABC homologue aux systèmes ParABS. Ce système permet le contrôle de la localisation de l'ADN plasmidique dans la bactérie et est médié par trois facteurs : une séquence spécifique *sopC* assimilée aux centromères eucaryotes, une protéine SopB de liaison au site *parS* et une ATPase SopA permettant la ségrégation de la copie plasmidique par mécanisme de traction (Kenn Gerdes, Howard, and Szardenings 2010; Baxter and Funnell 2014; Million-Weaver and Camps 2014). Par liaison avec *sopC*, SopB permet l'appariement de deux copies plasmidiques puis couvre l'ADN environnant. SopB en complexe avec l'ADN non-centromérique promeut la polymérisation de SopA, qui s'étend radialement sur le plasmide jusqu'à rencontrer le complexe SopB/*sopC*, stimulant son activité ATPase (Bouet et al. 2007; Ah-Seng et al. 2009). Des vagues successives d'hydrolyse de l'ATP déstabilisent le désassemblage des filaments de SopA, exerçant une tension sur SopB et tirant les copies plasmidiques aux quarts de la bactérie (Lim, Derman, and Pogliano 2005).

Enfin, la région *leading* du plasmide F située proche de l'*oriT* est définie comme étant la première région plasmidique à être transférée dans la bactérie receveuse lors de la conjugaison. Cette région très conservée est encore peu caractérisée, bien qu'elle semble jouer un rôle pour

l'établissement efficace du plasmide lors des premières étapes de transfert dans la bactérie receveuse.

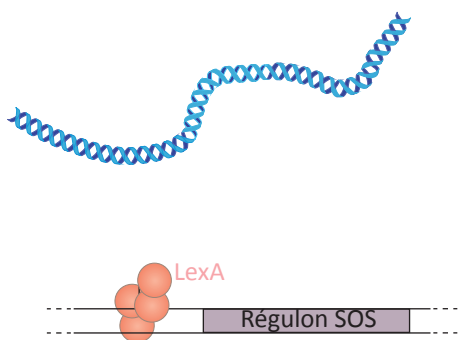
II. Région *leading*

D'une taille de 17kb chez le plasmide F, la région *leading* est retrouvée conservée chez de nombreux plasmides conjugatifs de groupes d'incompatibilité différents incluant les groupes IncF (pESBL, R1, R100, R124, pED208, pKF3), IncI (Collb-P9), IncK (R387), IncY (pIP213) ou encore IncB (R16) (Sharp, Cohen, and Davidson 1973; E. Golub, Bailone, and Devoret 1988; Bates et al. 1999; Ying et al. 2015; Benz and Hall 2022). Bien que 64% des plasmides étudiés par Wein *et al.* voient leur région *leading* conservées (270 plasmides sur 420), cette région reste très peu décrite (Wein et al. 2021). La quinzaine de gènes qu'elle code sont encore majoritairement de fonctions inconnues, excepté pour le gène *ssb* codant pour un homologue à la protéine de liaison à l'ADNsb chromosomique Ssb et le gène *psiB* codant pour un inhibiteur de la réponse SOS PsiB (*Plasmid SOS Inhibition*) (Figure 4-1) (Manwaring, Skurray, and Firth 1999). Parmi les autres gènes encore non-décrits qui composent cette région, on retrouve notamment le gène *yjjB* retrouvé conservé sous le nom *yubM* ou encore *parB2* du fait qu'il partage une homologie avec les protéines ParB.

1. Expression zygotique et *ssi*

En plus d'être les premiers transférés lors de la conjugaison, les gènes qui constituent la région *leading* sont également les premiers à être exprimés dans la bactérie transconjugante par un phénomène nommé « expression zygotique ». Ce terme proposé en 1956 par Jacob et Wollman décrit initialement l'activation transitoire de la transcription dans les cellules receveuses lors des premières étapes d'entrée d'ADN exogène viral, puis a été utilisé de façon générale dans le contexte de conjugaison lors des étapes précoces du transfert conjugal (Jacob et Wollman 1956; Bagdasarian et al. 1992; Jones, Barth, et Wilkins 1992; Miyakoshi et al. 2020). L'expression zygotique des gènes *leading* *ssb*, *psiB* et *ardA* des plasmides F et Collb-P9 a été observée et quantifiée en utilisant des fusions transcriptionnelles *lacZ*, par RT-PCR ou encore par test immunologique (Jones, Barth, and Wilkins 1992; Bagdasarian et al. 1992; Althorpe et al. 1999). Une augmentation d'expression de *psiB* est observée dans les bactéries receveuses 5 minutes à peine après l'initiation de la conjugaison, probablement même avant la fin du transfert lui-même, et se poursuit jusqu'à atteindre une augmentation 10 fois plus importante après 90 minutes de conjugaison avant de diminuer

1. Absence de cassure ADN



2. Cassure ADN

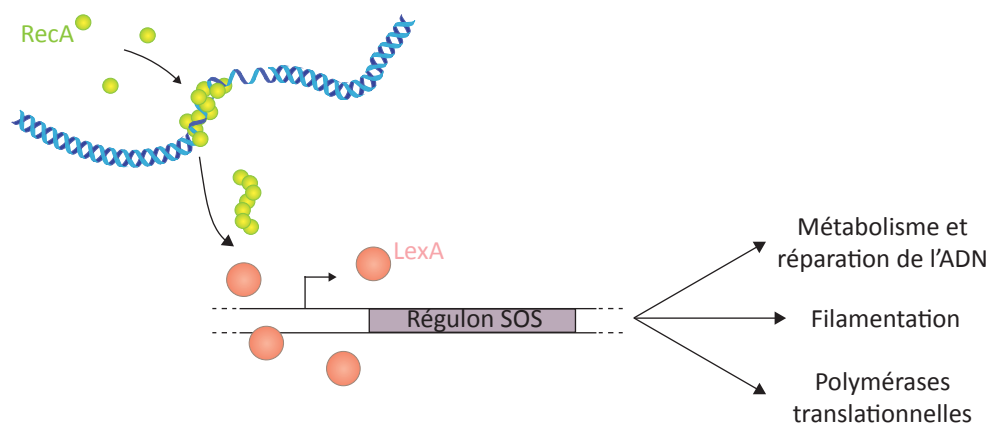


Figure 5. Réponse SOS chez *Escherichia coli*.

1. En absence de cassure ADN, le dimère de LexA réprime l'expression du régulon SOS par liaison à sa séquence promotrice.
2. La présence de cassure ADN induit la formation de nucléofilaments de RecA conduisant à l'auto-protéolyse de LexA et donc à la levée de la répression du régulon SOS. Les gènes SOS associés alors exprimés sont impliqués dans le métabolisme de l'ADN, l'arrêt de la division cellulaire ou encore la réparation de l'ADN.

progressivement dans la nouvelle bactérie transconjugante. Il a été proposé que cette expression particulière à la fois précoce et transitoire (puisque uniquement dans les nouveaux transconjugants pendant une période de temps donnée) pourrait être attribuée à la présence de promoteurs spécifiques sur la région *leading*, ou bien à la dé-répression des gènes *leading* pendant l'absence temporaire de répresseurs codés une fois le plasmide établi (Miyakoshi et al. 2020).

Il a de ce fait été démontré *in vitro* que la région *leading* du plasmide Collb porte trois séquences *ssi* (*single-stranded initiation sequence*) d'une taille de 328 pb, capables d'adopter une structure secondaire en conformation tige-boucle lorsqu'elles se retrouvent sous forme simple-brin. En reconstruisant un consensus -35 -10, ces structures permettent le recrutement de l'ARN polymérase sigma 70 pour l'initiation de la synthèse ARN (Figure 4-2) (Watanabe et al. 1992; Masai and Arai 1997). De façon similaire à la réplication de l'ADN, l'initiation de transcription à partir de ces structures est stimulée par la protéine chromosomique Ssb qui va lier la boucle et faciliter l'interaction de l'ARN polymérase avec l'ADN (Masai and Arai 1997). L'orientation de ces *ssi* au niveau de la région *leading* des plasmides F et Collb est telle que les structures promotrices sont formées sur le brin transféré, correspondant alors au brin codant et concordant avec l'induction zygotique des gènes *leading* dans la nouvelle bactérie transconjugante. Il a donc été proposé que ces régions *ssi* servent de promoteurs simple-brin lors de l'entrée du brin transféré pendant la conjugaison, permettant l'expression précoce des gènes de la région *leading*. La conversion en ADNdb va par la suite abolir la formation de ces structures, arrêtant l'expression des gènes associés. Ce profil d'expression particulier ainsi que la conservation relative de cette région mettent en avant une probable importance pour les étapes précoces du transfert. Démontré *in vitro* dans la littérature, l'importance *in vivo* de ces *ssi leading* a été étudiée au laboratoire et a abouti à une publication en 2023 dans le journal *Nature communication* présentée en première partie des résultats suivants.

2. PsiB et réponse SOS

La réponse SOS est un mécanisme bactérien induisant une cascade de réactions moléculaires en présence de concentration anormales d'ADNsb, initialement découverte lors d'études sur l'impact des radiations UV chez *Escherichia coli* (Weigle 1953; Radman 1975). En absence de cassure ADN, la protéine LexA réprime le régulon SOS ; lors de l'induction de dommage à l'ADN, la formation de nucléofilaments de RecA sur l'ADNsb va induire l'auto-protéolyse du répresseur, levant l'inhibition de plus d'une cinquantaine de gènes qui composent le régulon SOS (Simmons et al. 2008) (Figure (5)). L'activation de ce système induit entre autre l'arrêt de la division cellulaire par production des

protéines inhibitrices de division SfiA ou Sula, mais va également activer divers gènes impliqués dans les mécanismes de réparation et recombinaison de l'ADN tels que *uvrAB* (réparation par excision de nucléotides NER) ou *ruvAB* (jonctions de holliday) (Sharples, Ingleston, and Lloyd 1999; Kisker, Kuper, and Van Houten 2013). La réponse SOS peut aboutir à une augmentation de la mutagénèse ou même à la mort cellulaire dans le cas où le problème n'est pas résolu (Simmons et al. 2008; Baharoglu, Bikard, and Mazel 2010).

Majoritairement transféré sous forme d'ADNsb lors de la conjugaison, le plasmide conjugatif nouvellement acquis peut être un inducteur de la réponse SOS chez la bactérie receveuse, pouvant aboutir à la dégradation de l'ADN exogène. Il est donc logique que de nombreux plasmides conjugatifs appartenant aux groupes IncFI, IncFII, IncI1, IncK ou encore IncN codent un système anti-SOS telle que la protéine PsiB des plasmides F et Collb-P9 (E. Golub, Bailone, and Devoret 1988; Baharoglu, Bikard, and Mazel 2010; Maslowska, Makiela-Dzbenka, and Fijalkowska 2019). Une diminution de l'induction de la réponse SOS lors de la conjugaison est observée par mesure de l'expression de l'enzyme β -galactosidase dépendante de rapporteurs *lacZ* insérés dans le régulon SOS d'*Escherichia coli* (*sfiA::lacZ* et *recN::lacZ*), et confirmé par une plus forte sensibilité des cellules face aux radiations UV lors d'une surproduction de PsiB (Bailone et al. 1988; Baharoglu, Bikard, and Mazel 2010). Il est proposé que PsiB empêcherait la formation du nucléofilament de RecA sur l'ADN plasmidique en interagissant avec, inhibant alors toute activité de liaison à l'ADN, d'échanges de brins ou d'induction du clivage de LexA (Petrova et al. 2009). L'expression de *psiB* ou autre homologue permettrait donc d'inhiber temporairement la mise en place de la réponse SOS, probablement dans une stratégie visant à limiter les effets de la conjugaison-même sur la physiologie de la cellule hôte face à un stress lié à la présence d'ADNsb, tout en évitant une quelconque réponse pouvant entraver la dissémination du plasmide au sein des communautés bactériennes. On peut néanmoins noter que certains plasmides conjugatifs sont transférés efficacement sans posséder de système anti-SOS.

3. *Ssb^F*, un homologue de la protéine chromosomique *Ssb*

La protéine chromosomique de liaison à l'ADNsb *Ssb* est une protéine très conservée et essentielle puisqu'impliquée dans de nombreux mécanismes fondamentaux. *Ssb* assure la protection de l'ADNsb contre la digestion enzymatique pendant la réplication de l'ADN, la réparation ou encore la recombinaison, permettant la processivité de différentes polymérases ou la mise en place de la réponse SOS. Par interaction avec le complexe RecBCD lors de cassure double-brin d'ADN, *Ssb* va

promouvoir la liaison de RecA et permettre la prise en charge de l'ADN (Meyer and Laine 1990). De manière intéressante, des plasmides conjugatifs issus de groupes d'incompatibilité différents (IncF, IncY, Inc9, IncT et IncB/O) codent leur propre *ssb* et peuvent partiellement compléter des mutations de la copie chromosomique (Efim I. Golub and Low 1986; Porter and Black 1991). Un alignement de séquence montre une homologie entre les copies Ssb plasmidiques et chromosomiques principalement au niveau du domaine N-terminal permettant l'interaction avec l'ADNsb et le maintien d'une structure tétramérique de la protéine. Le domaine C-terminal quant à lui partage majoritairement une homologie entre copies plasmidiques plutôt que chromosomiques (Chase, Merrill, and Williams 1983). Le rôle d'une telle copie plasmidique est ainsi source de nombreux questionnements dans la littérature, et l'entièreté de la fonction de la copie Ssb^F n'est pas encore élucidée.

Malgré le profil d'expression particulier des gènes *leading*, cette région ne semble pas jouer de rôle important pour le mécanisme de transfert conjugatif lui-même. La délétion ou l'absence de certains de ces facteurs n'impacte pas l'efficacité du transfert, comme il l'a été observé en absence de *psiB*. De plus, il a été démontré que la protéine chromosomique Ssb est capable de lier spécifiquement l'ADNsb transféré, protégeant probablement l'ADN entrant contre les dégradations enzymatiques et remettant donc en question le rôle d'une telle copie plasmidique (El Golub and Low 1985). Toutefois la relative conservation de cette région parmi les plasmides suggère un rôle pour éviter ou diminuer les potentiels effets néfastes liés à l'acquisition du plasmide en agissant sur la régulation de la physiologie hôte ou de sa réponse SOS. En effet, plus l'impact métabolique lié à l'acquisition du plasmide est diminué, plus son maintien stable et sa dissémination au sein des populations bactériennes est assuré. L'importance de cette région *leading* pour le plasmide F est ainsi toujours source de nombreux questionnements auxquels nous tentons de répondre au laboratoire.

Résultats

Partie II : Dynamique de la conjugaison : production séquentielle des facteurs plasmidiques pour l'établissement dans la cellule hôte

Real-time visualisation of the intracellular dynamics of conjugative plasmid transfer

Agathe Couturier, Chloé Virolle, Kelly Goldlust, Annick Berne-Dedieu, Audrey Reuter, Sophie Nolivos,

Yoshiharu Yamaichi, Sarah Bigot & Christian Lesterlin

Article publié dans *Nature communication* (2023)

1. Contexte

Pendant ma thèse j'ai pu participer à un sujet de recherche du laboratoire concernant la quantification de la dynamique de transfert et d'expression des gènes plasmidiques lors de la conjugaison du plasmide F chez *Escherichia coli*. Ayant avant cela réalisé un stage de 6 mois au sein de l'équipe dans le cadre de ma 2^e année de Master, j'étais déjà familiarisée avec les techniques de microscopie à fluorescence et les analyses associées, désormais pratiquées en routine au laboratoire. Mes travaux et compétences ont pu alors être mis en valeurs lors de l'écriture d'un article par Couturier *et al.* publié dans le journal *Nature communication* en Janvier 2023 et pour lequel je signe en tant que deuxième auteur. Cet article traite de la visualisation en temps réel de la conjugaison et de la stratégie du plasmide F pour permettre la production séquentielle des facteurs plasmidiques lors de son établissement dans la nouvelle cellule hôte.

2. Contenu

Le processus de conjugaison est très étudié depuis des décennies, mais l'échelle cellulaire reste encore peu caractérisée. Cet article permet d'allier les outils génétiques développés au laboratoire avec notre expertise en microscopie à fluorescence en cellules vivantes afin de visualiser en temps réel l'organisation intracellulaire de la conjugaison. Pour cela, nous avons fait le choix de nous concentrer sur le transfert du plasmide F entre bactéries *Escherichia coli* souche K-12 MG1655. L'utilisation de diverses fusions protéiques fluorescentes permet de rapporter la visualisation de l'ADNsb et sa conversion en ADNdb. Nous décrivons grâce à cela une localisation et chronologie précise des étapes de transfert pour l'établissement successif du plasmide conjugatif dans la cellule

receveuse. Nos données confirment également l'efficacité du transfert du plasmide F en observant que près de 80% des transferts aboutissent directement à son établissement dans la bactérie receveuse. Nous démontrons la présence d'une séquence *Frpo2* homologue à la séquence *Frpo1* décrite *in vitro* dans la littérature comme potentielle *ssi*, et nous confirmons l'importance de ces deux séquences pour l'expression zygotique des gènes *leading*, validant *in vivo* la présence de séquences promotrices simple-brins. Nos travaux de recherches permettent également d'obtenir plus d'informations quant au rôle de la copie plasmidique de la protéine Ssb^F pour la conjugaison bactérienne. En résumé, nous mettons en avant un programme d'expression séquentielle des différents facteurs impliqués dans l'établissement, le maintien et le transfert du plasmide.

3. Ma contribution


Le rapporteur Ssb-Ypet permettant la visualisation de l'ADNsb ainsi que le système *parS*/ParB pour quantifier la conversion en ADNdb dans la receveuse sont des outils développés au laboratoire et désormais utilisés en routine pour les analyses de dynamique de la conjugaison. Les données accumulées par Agathe Couturier et moi-même ont ainsi été compilées pour obtenir un set d'évènements suffisamment robuste pour la quantification spatio-temporelle du transfert du plasmide F. En quantifiant la production des protéines *leading* YgeA, Ssb et YfjA fusionnées à la sfGFP en présence et absence des séquences *Frpo1* et *Frpo2*, mes données ont également permis d'établir l'importance de ces séquences pour l'expression des gènes correspondants au cours de la conjugaison. Nous avons de ce fait pu appuyer l'importance *in vivo* des séquences *ssi* en tant que promoteurs simple brin pour l'expression zygotique des gènes *leading*.

Real-time visualisation of the intracellular dynamics of conjugative plasmid transfer

Received: 5 October 2022

Accepted: 11 January 2023

Published online: 18 January 2023

 Check for updates

Agathe Couturier¹, Chloé Virolle¹, Kelly Goldlust¹, Annick Berne-Dedieu¹, Audrey Reuter¹, Sophie Nolivos¹, Yoshiharu Yamaichi², Sarah Bigot¹✉ & Christian Lesterlin¹✉

Conjugation is a contact-dependent mechanism for the transfer of plasmid DNA between bacterial cells, which contributes to the dissemination of antibiotic resistance. Here, we use live-cell microscopy to visualise the intracellular dynamics of conjugative transfer of F-plasmid in *E. coli*, in real time. We show that the transfer of plasmid in single-stranded form (ssDNA) and its subsequent conversion into double-stranded DNA (dsDNA) are fast and efficient processes that occur with specific timing and subcellular localisation. Notably, the ssDNA-to-dsDNA conversion determines the timing of plasmid-encoded protein production. The leading region that first enters the recipient cell carries single-stranded promoters that allow the early and transient synthesis of leading proteins immediately upon entry of the ssDNA plasmid. The subsequent conversion into dsDNA turns off leading gene expression, and activates the expression of other plasmid genes under the control of conventional double-stranded promoters. This molecular strategy allows for the timely production of factors sequentially involved in establishing, maintaining and disseminating the plasmid.

Bacterial DNA conjugation is a widespread horizontal gene transfer mechanism in which genetic information is transmitted from a donor to a recipient cell by direct contact^{1–4}. Conjugation is responsible for the intra- and inter-species dissemination of various metabolic properties and accounts for 80% of acquired resistances in bacteria⁵. The F plasmid was the first conjugative element discovered^{1,6} and is now documented as the paradigmatic representative of a large group of conjugative plasmids widespread in *Escherichia coli* and other Enterobacteriaceae species, in which they are associated with the dissemination of colicins, virulence factors and antibiotic resistance^{7–9}. Due to their fundamental and clinical importance, F-like plasmids have been the focus of extensive studies that provided a detailed understanding of the molecular reactions and factors involved in their transfer by conjugation^{3,4}.

Within the donor cell, the relaxosome components, including the integration host factor IHF, plasmid-encoded accessory proteins TraY, TraM and the multifunctional relaxase Tral, are recruited to the origin

of transfer (*oriT*) of the F plasmid^{10–12}. The relaxosome complex is then recruited to the Type IV secretion system (T4SS) by the coupling protein TraD, resulting in the formation of the pre-initiation complex^{13–17}. Tral and TraD proteins are archetype components of the core set of subunits required for the establishment of active conjugation machinery and are respectively referred to as VirD2 and VirD4 in the common nomenclature. It is proposed that the establishment of the mating pair induces a still uncharacterised signal that activates the pre-initiation complex. Then, Tral introduces a site- and strand-specific DNA cut (nick) into the plasmid's *oriT* and remains covalently bound to the 5' phosphate end. Tral also serves as a helicase that extrudes the ssDNA plasmid to be transferred, called the T-strand^{18–26}. It was initially suggested and later confirmed that two relaxases are required to carry out these functions^{27,28}. At this stage, the 3'OH of the T-strand serves to initiate the rolling-circle replication (RCR) that converts the intact circular ssDNA plasmid into dsDNA in the donor cell^{3,29,30}, while the 5' phosphate bound to Tral is transferred into the recipient cell through

¹Molecular Microbiology and Structural Biochemistry (MMSB), Université Lyon 1, CNRS, Inserm, UMR5086, 69007 Lyon, France. ²Université Paris-Saclay, CEA, CNRS, Institute for Integrative Biology of the Cell (I2BC), 91198 Gif-sur-Yvette, France. ✉ e-mail: Sarah.Bigot@ibcp.fr; Christian.lesterlin@ibcp.fr

the T4SS machinery. While the molecular structure of the T4SS has been well characterised^{31–34}, the way the T-complex (T-strand-Tral nucleoprotein) is translocated through the membrane of the donor and recipient cells' membranes remains unclear.

The first transferred segment is the ~13.5 knt leading region, carrying genes which encode the Ssb^F protein homologue to the chromosomally encoded essential single-strand-binding protein Ssb, the PsiB protein (Plasmid SOS Inhibition)^{35–38} that inhibits SOS induction during conjugation^{39,40}, and other proteins of unknown function. Remarkably, the leading region is conserved in various enterobacterial plasmids belonging to a variety of incompatibility groups^{41–46}. The adjacent and next transferred ~17 knt maintenance region carries the ParABS-like plasmid partition system (SopABC) and the origins of vegetative replication^{47–50}. The last transferred segment of the F plasmid is the large ~33.3 knt *tra* region that encodes all the protein factors required for plasmid DNA processing and transfer, including the relaxosome, the T4SS and the exclusion system against self-transfer⁴. Besides, F-like plasmids often carry cargo genes involved in various metabolic functions commonly integrated between the maintenance and the *tra* regions^{7,9}. Once both the 5' and the 3' ends of the T-strand have been internalised into the recipient cell, now called a transconjugant, the ssDNA plasmid is circularised by Tral^{26,27,51,52}. The ssDNA plasmid will also be converted into dsDNA by the complementary strand synthesis reaction. Whether this DNA synthesis reaction occurs as the plasmid enters the recipient cell or is initiated after plasmid recircularization remains unclear. Nonetheless, the completion of the ss-to-dsDNA conversion is required for plasmid replication and partition and is, therefore, critical to plasmid stability in the new host cell lineage.

The above-described mechanistic model is well-documented; however, the real-time dynamics and intracellular organisation of conjugation remain largely undescribed in the live bacterium. In particular, we know very little about the subcellular localisation and timing of the reactions in the recipient cell, including the ssDNA plasmid entry, the ss-to-dsDNA conversion and plasmid gene expression. Regarding the last-mentioned, early works reported that some leading genes (*ssb^F* and *psiB* in F plasmid, and *ssb^{Collb-P9}}*, *psiB* and *ardA* in Collb-P9 plasmid) are expressed rapidly after entry of the plasmid in the acceptor cell^{36–38,42,53,54}. In vitro work by Masai *et al.*⁵⁵ showed that the single-stranded form of the non-coding *Frpo* sequence, located in the F plasmid leading region, folds into a stem-loop structure that reconstitutes canonical –10 and –35 boxes. This promoter sequence can recruit the *E. coli* RNA polymerase that initiates RNA synthesis in in vitro assays⁵⁵. Sequences homologous to *Frpo* were also found in the leading region of Collb-P9^{56,57}. These observations led to the proposal that *Frpo*-like sequences could act as ssDNA promoters initiating the early transcription of leading genes when the plasmid is still in ssDNA form. Whether this regulation mechanism happens during in vivo conjugation remains to be demonstrated.

In this study, we use live-cell microscopy imaging to visualise the complete transfer sequence of the native F plasmid between *E. coli* K12 strains. We inspect the key steps of conjugation using specifically developed genetic reporters, including a fluorescent fusion of the chromosomally encoded single-strand-binding protein Ssb (Ssb-Ypet) to monitor the ssDNA transfer, the mCherry-ParB/*parS* system to reveal the ss-to-dsDNA conversion and subsequent plasmid duplication, and translational fluorescent fusions to quantify and time plasmid-encoded production in the new host cell^{58,59}. This approach uncovers the choreography of conjugation reactions in live bacteria and provides new insights into the interplay between plasmid processing and gene expression.

Results

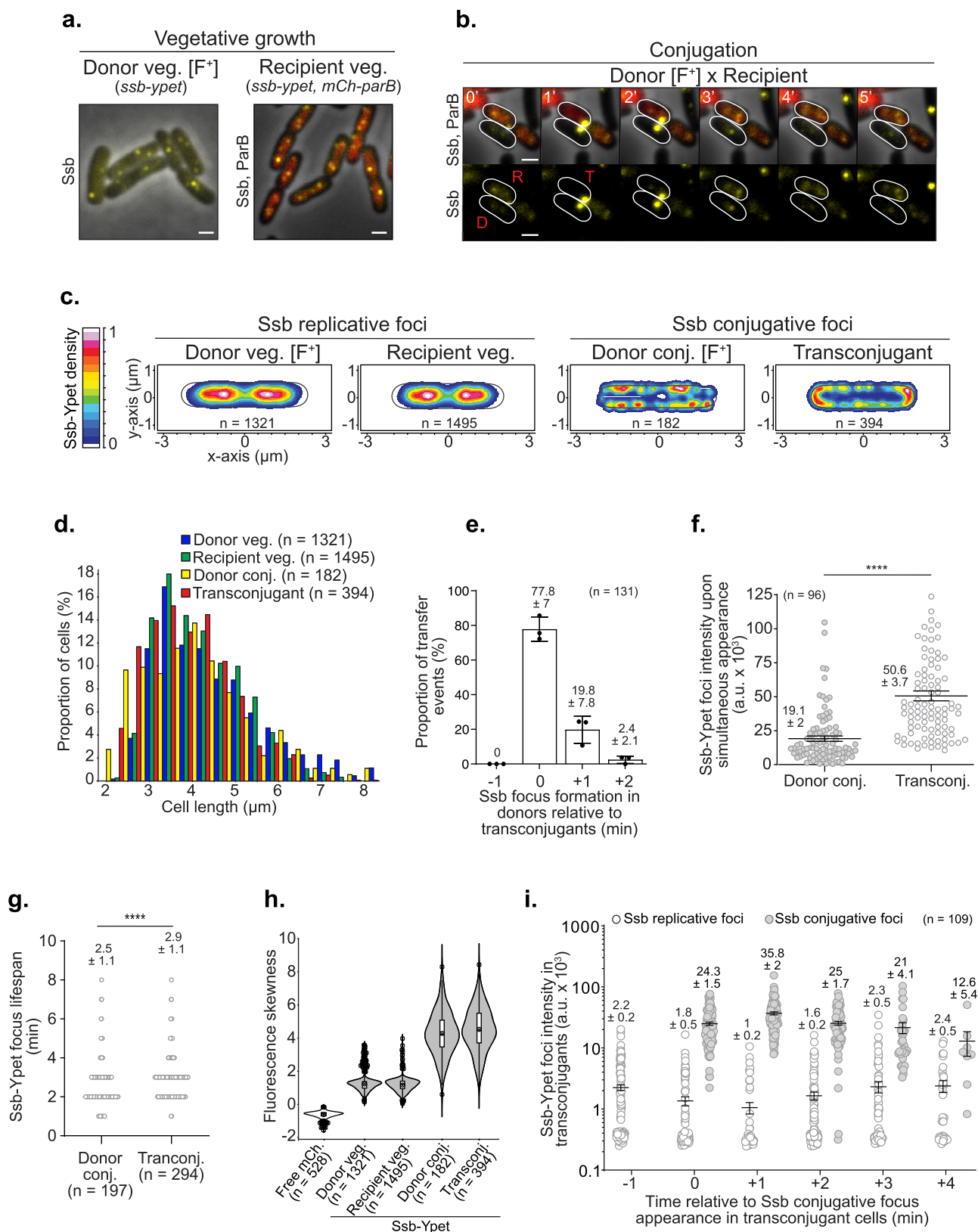
Dynamics of the ssDNA plasmid during transfer

We monitored the dynamic localisation of a fluorescent endogenous fusion of the chromosomally encoded single-strand-binding protein

Ssb (Ssb-Ypet) in donor and recipient cells, during vegetative growth and conjugation (Fig. 1a, b and Fig. S1). During vegetative growth, Ssb-Ypet forms discrete foci at midcell and quarter positions within the inner region of donors and recipient cells (Fig. 1c and Fig. S2a, b). These Ssb foci, termed Ssb replicative foci hereafter, are associated with the ssDNA that follows the replication forks onto the nucleoid DNA^{60,61}. During conjugation, the intracellular localisation of Ssb changes dramatically. As previously reported^{58,59}, the entry of the ssDNA plasmid in the recipient cell, now called a transconjugant, triggers the recruitment of Ssb molecules and the formation of bright membrane-proximal foci, we termed Ssb conjugative foci (Fig. 1b and Fig. S1). Here, we also observe the formation of Ssb conjugative foci in the donor cells, thus revealing the presence of ssDNA plasmid on each side of the conjugation pore during transfer (Fig. 1b and Fig. S1). Foci localisation analysis reveals that plasmid exit and entry occur at specific membrane positions within the mating pair cells. Ssb conjugative foci are distributed at the periphery of the donor cell and preferentially at the quarter positions (Fig. 1c and Fig. S2a, b), reflecting the preferred position for the exit of the ssDNA plasmid through active conjugation pores. By contrast, ssDNA plasmid entry predominantly occurs within the polar regions of the transconjugant cells (Fig. 1c and Fig. S2a, b). Our data also allow us to address whether conjugation occurs at a specific cell cycle stage. Analysis of cell length as a proxy of cell age reveals that donor and recipient cells engaged in plasmid transfer exhibit similar length distribution than during vegetative growth (Fig. 1d). This shows that the donors can give, and recipients can acquire the plasmid at any stage of their cell cycle, from birth to cell division.

In $77.8 \pm 7\%$ ($n = 131$) of individual plasmid transfer events visualised by time-lapse imaging (1 min/frame), Ssb conjugative foci appear in the donor and transconjugant cells on the same frame (Fig. 1e). In these cases, Ssb conjugative foci are, on average brighter in the transconjugant than in the donor cells, reflecting the relative amount of ssDNA plasmid on each side of the conjugation pore (Fig. 1f). In the remaining 22.2% of transfer events, Ssb conjugative foci first appear in the transconjugant and then in the donor one or two minutes later (Fig. 1e). The delayed accumulation of ssDNA in the donor relative to the recipient is corroborated by the quantification of a 2.9 ± 1.1 min ($n = 294$) average lifespan of Ssb-Ypet conjugative foci in the transconjugants, compared to 2.5 ± 1.1 min ($n = 197$) in the donor cells (Fig. 1g). These data indicate that the appearance of conjugative foci is asynchronous in the mating pair cells and suggest a specific sequence of ssDNA transfer. The first segment of the T-strand generated by the helicase activity of Tral in the donor cell does not dwell long enough to recruit Ssb molecules and is immediately transferred to the recipient. Only after this brief transfer stage does the ssDNA accumulates on the donor's side as well, where it can correspond to either or both the non-transferred plasmid strand or to the T-strand. This implies that the rate of ssDNA formation by Tral helicase activity is faster than that of ssDNA removal by the RCR and transfer through the T4SS (See discussion).

The internalisation of a large amount of ssDNA plasmid provokes the massive recruitment of the intracellular pool of Ssb molecules at the periphery of the donor and transconjugant cells. This change in Ssb-Ypet subcellular distribution is revealed by skewness analysis, which provides a non-biased measure of the asymmetry of fluorescence distribution within the cells without a requirement for threshold-based foci detection (Fig. 1h). Wild-type cells producing a free mCherry (mCh) exhibit a low skewness corresponding to the homogeneous pixel fluorescence distribution inside the cell's cytoplasm. During vegetative growth, Ssb-Ypet fluorescence is partly diffuse in the cytoplasm and partly locally concentrated within replicative foci, resulting in skewness of ~1.2. By comparison, Ssb-Ypet exhibits a strong skewness of ~4.1 in donors and transconjugants during plasmid transfer, reflecting the increased proportion of Ssb molecules clustered within foci. Hence,



we wondered what part of Ssb molecules are contained within conjugative foci and if their formation was associated with a depletion of Ssb within replicative foci in the transconjugant cell. To address this question, we performed Ssb-Ypet foci automatic detection and brightness quantification during plasmid transfer (Fig. 1i). We observe that one minute after the beginning of plasmid

entry Ssb-Ypet replicative foci are still present but exhibit half their initial intensity, while conjugative foci are 35 times brighter. Since the total Ssb-Ypet intracellular fluorescence is unchanged during the transfer (Fig. S2c), these variations can be attributable to the displacement of Ssb-Ypet molecules onto the incoming ssDNA plasmid rather than Ssb-Ypet de novo synthesis. This dynamic

Fig. 1 | Real-time dynamics of ssDNA plasmid transfer from donor to recipient cells. **a** Representative microscopy images of donors and recipients carrying the *ssb-yjet* fusion gene during vegetative growth. The recipients also produce the diffuse mCh-ParB fluorescent protein. Scale bars 1 μm . **b** Time-lapse microscopy images of plasmid transfer between a donor (D) and a recipient (R) that is converted into a transconjugant cell (T). Scale bars 1 μm . Additional events are presented in Figure S1. **c** 2D localisation heatmaps of Ssb-Yjet in donors, recipients and transconjugant during vegetative growth (veg.) and conjugation (conj.). Normalisation by the cell length of (n) individual cells from at least three biological replicates. The density scale bar is on the left. **d** Cell length distribution histogram of donors, recipients and transconjugants (n cells analysed from at least three independent experiments). **e** Ssb conjugative focus appearance timing in donor relative to transconjugant cells. Histograms with means and SD represent the proportion of transfer events in which the Ssb focus appears in the donors before (-1 min), simultaneously (0 min) or after ($+1$ min; $+2$ min) it appears in transconjugants. The number (n) of individual transfer events analysed from three independent experiments is indicated. **f** Jitter plot of the fluorescence intensity of Ssb-Yjet conjugative foci upon simultaneous appearance. The number of foci analysed from three independent experiments (n) is indicated with the corresponding Mean and SEM. P

value significance from Mann–Whitney two-sided statistical test is indicated by **** ($P \leq 0.0001$). **g** Jitter plots of Ssb-Yjet conjugative foci lifespan in donor and transconjugant cells. P value significance from Mann–Whitney two-sided statistical test is indicated by **** ($P = 0.0001$). The number (n) of cells analysed from at least five independent experiments is indicated. **h** Violin plots of the fluorescence skewness of a free mCherry and of the Ssb-Yjet in donors, recipients and transconjugant cells. The median, quartile 1 and quartile 3 are indicated by the boxes' bounds, the mean by a black dot, and the minima and maxima by the whiskers' limits. Black dots above and below the max and min values correspond to outliers. Free mCherry data correspond to one representative experiment. Other plots correspond to the same data set as in panel (c) from at least three biological replicates. The number of cells analysed (n) is indicated. **i** Jitter plot of Ssb-Yjet replicative and conjugative foci intensity in transconjugant cells during conjugation. Time 0 min corresponds to the appearance of the Ssb-Yjet conjugative focus in recipients. The number of cells analysed (n) from three independent experiments is indicated with the corresponding Mean and SEM. Donor (LY1007), recipient (LY358), transconjugant (LY358 after *Fwt* acquisition from LY1007); the free mCherry is produced from the chromosome in MS388 *wt* background (LY1737). Source data are provided as a Source Data file.

reflects that the incoming ssDNA plasmid recruits most Ssb-Yjet molecules in the acceptor cell during transfer.

It has been estimated that Ssb is present at about -1320 ± 420 monomers per *E. coli* cell and that a dimer of tetramers covers about 170 nt in vivo⁶¹. Consequently, there are not enough Ssb copies per cell to accommodate the 108,000 nucleotides of ssDNA F plasmid, plus the few hundreds of nucleotides of ssDNA associated with replication forks (~ 650 nt at 22°C ⁶²). In fact, it is not known whether the F plasmid is ever fully present in ssDNA form in the recipient, as it is not known if the complementary strand synthesis reaction occurs concomitantly with or after the completion of the T-strand transfer. Still, the observed massive recruitment of Ssb molecules onto the incoming ssDNA could reduce Ssb availability and provoke a transitory disturbance of the host chromosome DNA replication. One way to address this question in vivo is to monitor a fluorescent fusion of the β_2 -clamp replisome component (mCh-DnaN), which is diffused in the cytoplasm of non-replicating cells and forms discrete replisome-associated foci during DNA replication progression^{60,61,63}. Microscopy imaging and skewness analysis showed no change in DnaN localisation pattern before, during or after Ssb conjugative foci formation (Fig. S2d). This indicates that Ssb recruitment onto the incoming ssDNA plasmid does not result in the collapse of the replication fork. Whether the rate of DNA replication is affected during this transient and short process remains a possibility.

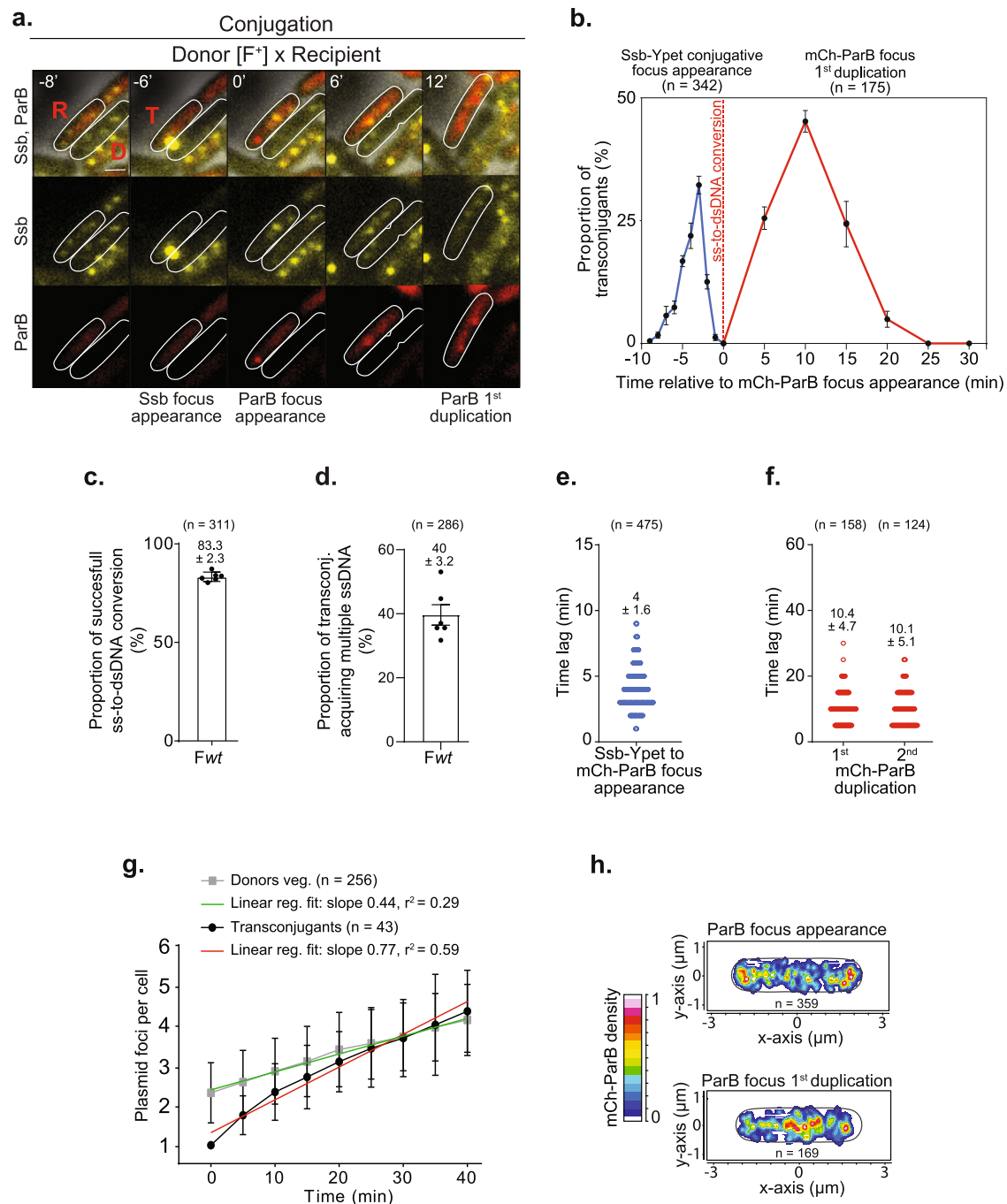
ss-to-dsDNA conversion and subsequent plasmid replication in the transconjugant cells

The conversion of the newly acquired ssDNA plasmid into dsDNA by the complementary strand synthesis reaction and the subsequent plasmid duplication events were analysed using the *parS*/ParB DNA labelling system^{58,59}. The *parS* binding site is inserted in the F plasmid, while the ParB binding protein fluorescently labelled with the mCherry (mCh-ParB) is produced from a plasmid in recipient cells only. Under the microscope, the ss-to-dsDNA conversion is reported by the disappearance of the Ssb-Yjet conjugative focus and the formation of an mCh-ParB focus in the transconjugant cells (Fig. 2a). We first performed time-lapse imaging (1 min/frame) to visualise the success rate and timing of ss-to-dsDNA conversion after ssDNA entry (Fig. 2b). Analysis shows that the appearance of the Ssb-Yjet conjugative focus is followed by the formation of the mCh-ParB focus in $83.3 \pm 2.3\%$ ($n = 311$) individual transconjugant cells analysed, indicating that the vast majority of internalised ssDNA plasmids are successfully converted into dsDNA plasmids (Fig. 2c). Notably, we observe that $40 \pm 3.2\%$ ($n = 286$) of transconjugant cells where the newly acquired ssDNA plasmid has already been converted into dsDNA subsequently

receive additional ssDNA (Fig. 2d and Fig. S3a). We quantify that $92 \pm 3.1\%$ of these multiple ssDNA acquisition events originate from the same donor, among which $79 \pm 5.3\%$ appear to take place at the same membrane position, suggesting that they occur through the same conjugation pore (Fig. S3a). The evidence for multiple transfers within an established mating pair demonstrates that a single donor can successively give several copies of the T-strand and that transconjugants in which the ss-to-dsDNA conversion has already been achieved do not become instantly refractory to de novo plasmid acquisition. Accordingly, establishing immunity to conjugation by transconjugant cells is expected to require the production of the plasmid-encoded exclusion proteins TraS and TraT.

Considering successful ss-to-dsDNA events only, we calculate an average 4 ± 1.6 min ($n = 475$) time lag between the appearance of the Ssb-Yjet conjugative focus and the formation of the mCh-ParB focus (Fig. 2e). This period reflects the time required for the completion of a reaction cascade that comprises the internalisation of the ssDNA plasmid, the initiation of the complementary strand synthesis replication, and the recruitment of ParB molecules on the *parS* site in dsDNA form. Though our system does not allow evaluating each step's contribution, results show that the complete sequence of reactions is achieved within a relatively short and consistent period.

Next, we first performed time-lapse imaging (5 min/frame) to examine the timing of plasmid duplication in transconjugant cells (i.e., replication and visual separation of the plasmid copies) (Fig. 2b). We estimate an average of 10.4 ± 4.7 min ($n = 158$) period between the ssDNA-to-dsDNA conversion and the first plasmid duplication event (from one to two mCh-ParB foci) and similar 10.1 ± 5.1 min ($n = 124$) between the first and the second duplication event (from two to three or four mCh-ParB foci) (Fig. 2f). We then decided to compare the rate of plasmid duplication in transconjugants to the rate of plasmid duplication in a vegetatively growing F-carrying donor strain. To do so, we plotted the number of plasmid foci per cell from the ss-to-dsDNA conversion (mCh focus appearance) to cell division in transconjugants and from cell birth to cell division in F-carrying donor cells (Fig. 2g). Results show that the number of F per cell increases significantly faster in transconjugant cells than in vegetatively growing F-carrying cells (75% increase of the fit curve slope), yet to reach a similar final number of $\sim 4 \pm 1$ copies per cell before division (Fig. 2g). F copy number, like chromosome replication, is known to be controlled by the cell cycle progression, where initiation occurs when a constant mass per origin is achieved⁶⁴. Therefore, our observations are consistent with the interpretation that when a single plasmid copy arrives in a recipient cell that can be at any cell cycle stage, plasmid replication initiation is unrepressed until the specific number of plasmid copies per cell mass is



restored. This accelerated plasmid replication allows for the rapid increase in F copy number before the division of the transconjugant cells, thus facilitating the segregation of plasmid copies to daughter cells.

Localisation analysis reveals that the ss-to-dsDNA conversion and the first duplication event occur at distinct subcellular positions. The initial mCh-ParB focus preferentially appears in the polar region of the transconjugant cell, comparable to the ssDNA's entry location (compare Fig. 2h to Fig. 1c and Fig. S3b to Fig. S2a). A noticeable difference is that mCh-ParB foci appear less peripheral, indicating that they are not as close to the cell membrane as Ssb-Ypet conjugation foci (compare Fig. 2h to Fig. 1c and Fig. S3c to Fig. S2b). We observe that the mCh-ParB focus subsequently migrates to the midcell position before duplication (Fig. 2h and Fig. S3b, c). These data show that the two DNA synthesis reactions involved in plasmid processing (i.e. ss-to-dsDNA conversion and plasmid replication) are separated in time and space in

the new host cell. The recruitment of the complementary strand synthesis machinery and the ss-to-dsDNA replication reaction occurs in the vicinity of the polar position of the entry of the ssDNA plasmid, while plasmid replication occurs in the midcell region. Altogether, these analyses reveal that plasmid processing steps (ssDNA entry, ss-to-dsDNA conversion and plasmid replication) occur at specific intracellular positions within the new host cell and follow a precise chronology.

Programme of plasmid-encoded protein production in transconjugant cells

We constructed *superfolder gfp (sfGFP)* translational fusions to the 3' end of several genes located in the different functional regions of the F plasmid to examine the production timing of plasmid-encoded proteins in transconjugant cells, which we use to get insights into the timing of plasmid gene expression (Fig. 3a and Fig. S4a). The *ygfA*,

Fig. 2 | Timing and spatial localisation of the ss-to-dsDNA conversion and plasmid duplication in transconjugant cells. **a** Time-lapse images showing ssDNA plasmid transfer reported by the formation of the Ssb-Ypet conjugative foci in both donor (D) and recipient (R) cells, followed by the ss-to-dsDNA conversion reflected by the appearance of an mCh-ParB focus in transconjugant (T) cells. Scale bar 1 μ m. **b** Single-cell time-lapse quantification of Ssb-Ypet focus appearance (blue line) and mCh-ParB focus first duplication (red line) with respect to the ss-to-dsDNA conversion revealed by mCh-ParB focus formation in transconjugant cells (0 min). Ssb-Ypet focus appearance was analysed using 1 min/frame time-lapses, while mCh-ParB first and second duplication were analysed using 5 min/frame time-lapses. The mean and SD calculated from the indicated number of conjugation events analysed (n) from seven independent experiments is indicated. **c** Histogram of successful ss-to-dsDNA conversion reflected by the conversion of the Ssb-Ypet conjugative foci into an mCh-ParB focus. The mean and SD are calculated from (n) individual transfer events from six biological replicates (black dots). **d** Histogram showing the percentage of transconjugants with an mCh-ParB focus that acquires multiple ssDNA plasmids as revealed by the successive appearance of Ssb-Ypet conjugative focus. The mean and SD are calculated from (n) individual transconjugant cells from six biological replicates (black dots). **e** Scatter plot showing the time lag between Ssb-Ypet and mCh-ParB foci appearance in transconjugants. The mean

and SD calculated from (n) individual events (blue circles) from seven biological replicates are indicated. **f** Scatter plot showing the time lag between the apparition of the mCh-ParB focus and its visual duplication in two foci (first duplication), and in three or four foci (second duplication). The mean and SD calculated from (n) individual duplication events (red circles) from at least six biological replicates are indicated. **g** Single-cell time-lapse quantification of the number of F foci per cell in F-carrying donor strain during vegetative growth and in transconjugants after F plasmid acquisition. For donors, the number of F foci per cell (number of SopB-sfGFP foci) with respect to cell birth ($t = 0$ min) is shown (grey curve). For transconjugants, the number of F foci per cell (number of mCh-ParB foci) with respect to mCh-ParB focus appearance ($t = 0$ min) is shown (black curve). Mean and SD calculated from (n) individual cells from four biological replicates are indicated, together with curves' linear fitting lines (green and red). F-carrying donor strain (LY834), Transconjugant (LY358 after *Fwt* acquisition). **h** 2D localisation heatmaps of mCh-ParB foci at the time of its appearance (top) and just before its duplication (bottom). Heatmaps are normalisation by the cell length of (n) individual transconjugant cells from seven biological replicates. **a–f, h** *Fwt* donor (LY1007), recipient (LY358) and transconjugant (LY358 after *Fwt* acquisition). Source data are provided as a Source Data file.

ygeA, *psiB*, *yjfb*, *yjfa* and *ssb^f* genes are located in the leading region and are transferred in order after the origin of transfer *oriT*. The *sopB* gene is part of the SopABC partition system and is located in the maintenance region. The *traM*, *traC*, *traS* and *traT* genes are located in the *tra* region that encodes factors involved in plasmid transfer. TraM is the accessory protein of the relaxosome complex that is recruited to the *oriT*⁶⁵; TraC is the traffic ATPase organised as a hexamer of dimers docked to the cytoplasmic faces of the T4SS⁶⁶; TraS and TraT correspond to the F plasmid exclusion (immunity) system that protects against self-transfer^{67–69}.

We first performed time-course experiments where microscopy snapshot images of the conjugating population were acquired 1, 2, 4 and 6 h after mixing donors and recipient cells. For each time point, the frequency of transconjugants (T/R + T) was directly measured at the single-cell level from the proportion of recipient cells exhibiting diffuse mCh-ParB fluorescence (R) or transconjugant cells harbouring mCh-ParB foci (T), and the intracellular green fluorescence signal to noise ratio (SNR) was automatically measured (Fig. S4b–d). This snapshot analysis shows that all F plasmid derivatives carrying sfGFP fusions retained their transfer ability and yielded frequencies of transconjugants between 57 and 95% after 6 h of mating. Also, fusion-carrying plasmid acquisition is systematically followed by an increase in sfGFP signal in transconjugant cells, with highly variable timing and levels (Fig. S4b–d).

Better resolution of the production level and timing of sfGFP fusions with respect to the ss-to-dsDNA conversion (appearance of the mCh-ParB focus) in individual transconjugant cells was obtained using time-lapse imaging of conjugation performed in the microfluidic chamber (Movies S1, S2). We performed transconjugant cell detection and quantification of the intracellular sfGFP SNR cells over time (Fig. S5a–d). When the transconjugant cell divided, we continued fluorescence quantification in the resulting daughter cells to monitor sfGFP production over a longer period. From this raw data, we calculated the fold-increase in SNR per 10-min interval, where a fold-increase superior to one reveals that the fusions are being produced in the transconjugants (Fig. S5a–d). These data were finally translated into a comprehensive diagram presenting the production time windows for each fusion in transconjugant cells relative to the ss-to-dsDNA conversion event (Fig. 3b). This analysis reveals that fusions belonging to the different plasmid regions exhibit specific production timings with respect to plasmid processing steps.

Remarkably, we detect the synchronous production of the leading YgeA, PsiB, Yjfb, Yjfa and Ssb^f fusion proteins even before the appearance of the mCh-ParB focus (Fig. 3b and Fig. S5a). Furthermore,

the production of these fusions is only transient as it peaks at ~5 min and stops 25–35 min after the ss-to-dsDNA conversion event. This unexpected observation indicates that leading fusions start being produced when the plasmid is still in ssDNA form and stops rapidly after the plasmid is converted into dsDNA form. An interesting exception is YgfA-sfGFP, for which production is only detected in the 10–20 min interval after mCh-ParB focus appearance. The *ygfA* gene is the closest to the *oriT* and is, therefore, the first gene to be transferred to the recipient (Fig. 3a and Fig. S4a). However, *ygfA* gene orientation is opposite to other tested leading genes, meaning that the T-strand does not correspond to the template strand for *ygfA* transcription. Consequently, and consistent with our observations, *ygfA* expression can only occur after synthesising the complementary template strand by the ss-to-dsDNA conversion.

The ss-to-dsDNA conversion is followed by the production of maintenance and Tra proteins, starting with SopB and TraM, then TraC, and eventually TraS and TraT fusions (Fig. 3b and Fig. S5b, c). The production of these fusions is expected to require the presence of the plasmid in dsDNA form since the corresponding genes are known to be controlled by dsDNA promoters (P_{SopAB} for *sopB*, P_M for *traM* and P_Y for *traC* and *traT*). However, what could explain the observed differences in the production timings? We addressed whether timing discrepancies could simply account for the fusions' position on the genetic map of the F plasmid. This possibility was excluded by the observation that insertion of the constitutive fluorescent reporter P_{lacIQ1} sfGFP (*sfGfp* gene under the control of the P_{lacIQ1} constitutive promoter) in the *repE-sopA*, *tnpA-ybaA* and *traM-traJ* intergenic regions resulted in similar sfGFP production timings, within the 0–10 min interval after the appearance of the mCh-ParB focus (Fig. 3b and Fig. S5d). Instead, we propose that the differential production timings of maintenance and *tra* genes reflect the activity and regulation of the promoters of the corresponding genes. The *sopAB* operon is under the control of the P_{SopAB} promoter, which is repressed by SopA binding. Therefore, the P_{SopAB} promoter is expected to be fully unrepressed and active in transconjugant cells devoid of SopA, thus allowing the rapid production of the SopAB partition complex required for plasmid stability and inheritance over cell divisions. The *traM* gene is controlled by the P_M promoter, which is weakly but constitutively active, even before its full activation by binding the TraY protein⁷⁰. By contrast, the P_Y promoter that controls the expression of *traC*, *traS* and *traT* genes needs to be activated by the TraJ protein, encoded by the *traJ* gene under the control of its own promoter P_J and located upstream of P_Y ⁴. The requirement for this activation cascade probably explains

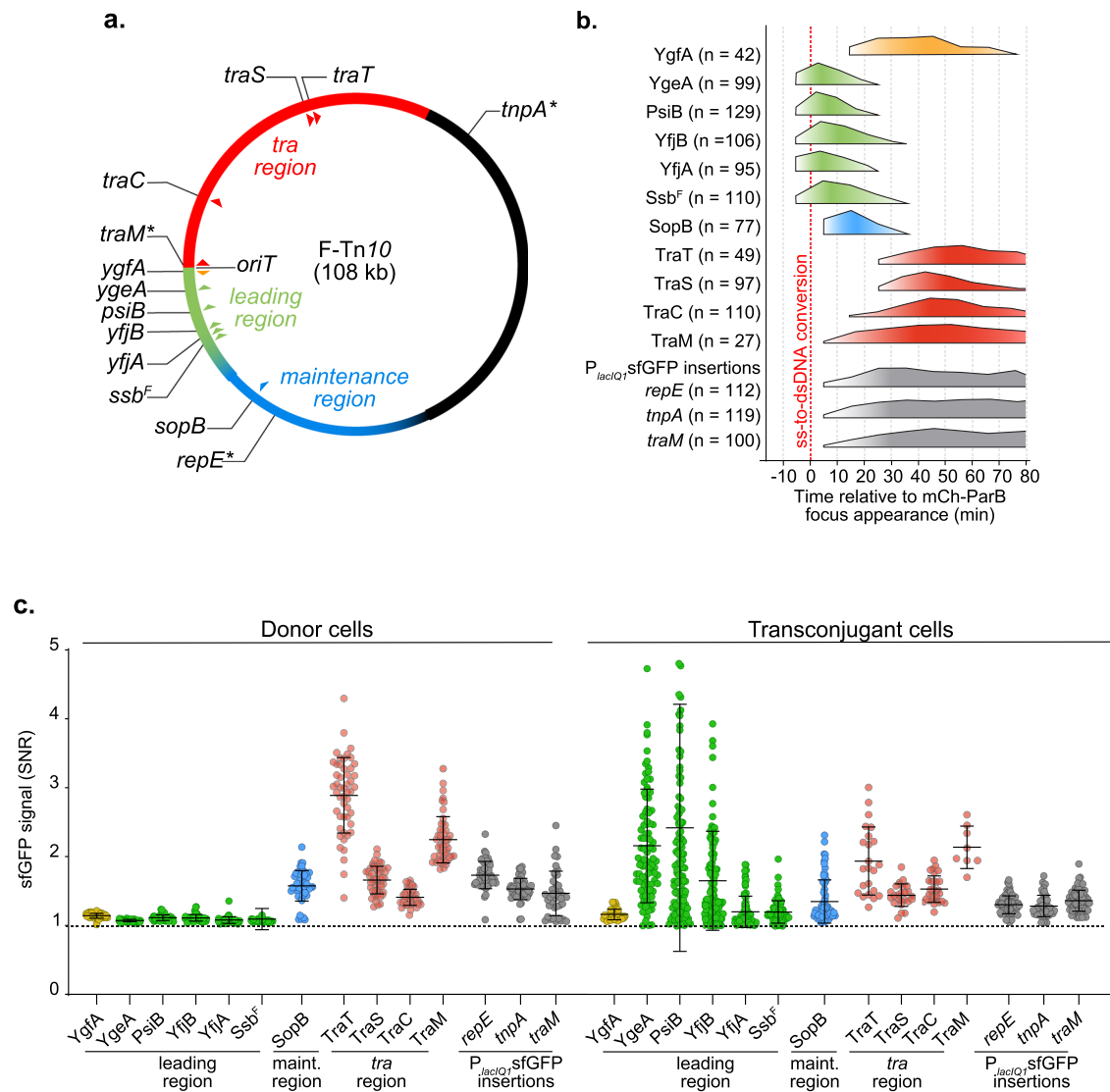


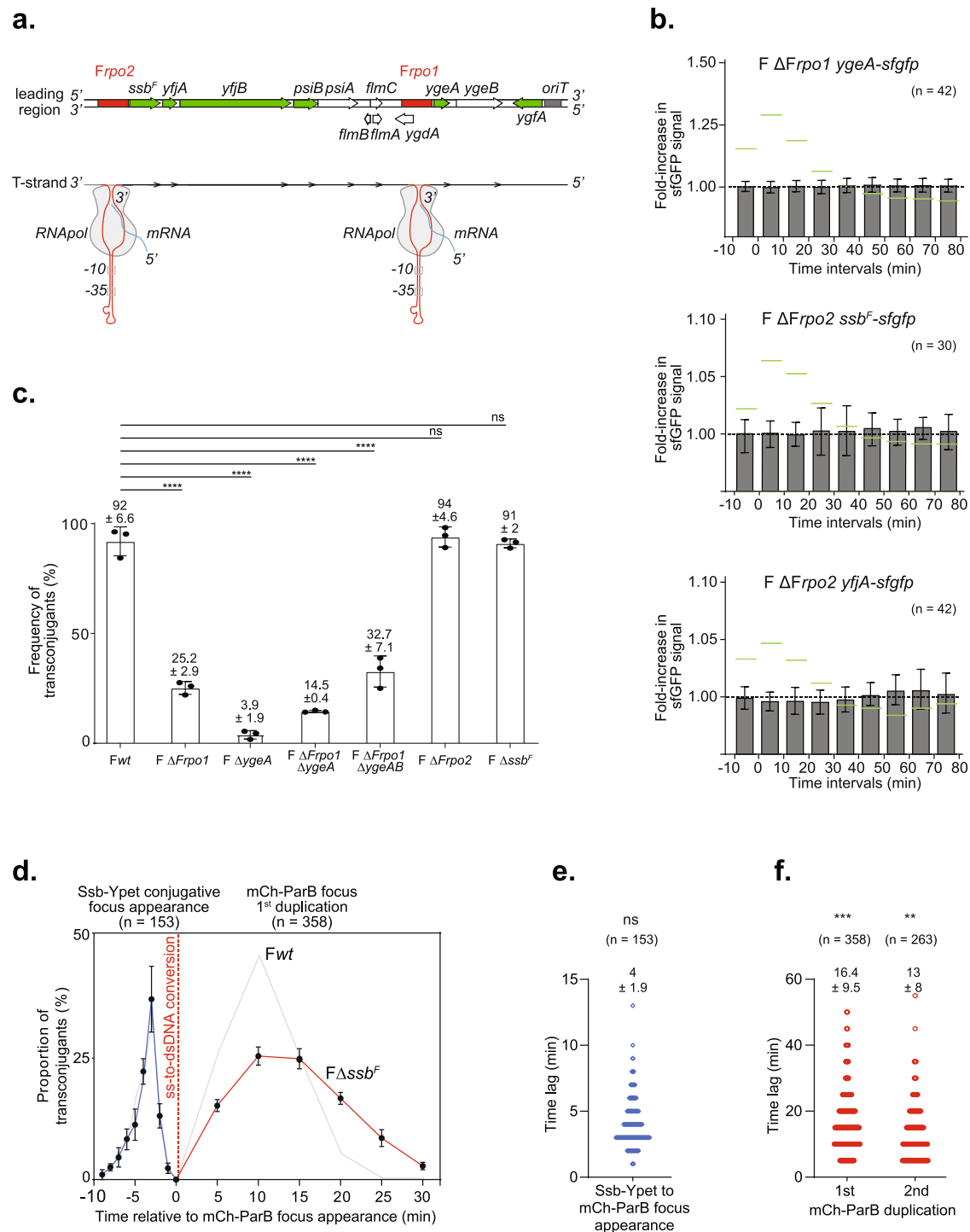
Fig. 3 | Timing of plasmid-encoded proteins production in transconjugant cells. **a** Genetic map of the 108 kb F plasmid indicating the leading (green), *Tra* (red) and maintenance (blue) regions, and the positions of the studied genes (triangles). Stars represent the genetic location of the P_{lacIQ1} ::*sfGFP* insertions. **b** Summary diagram of the production timing of each plasmid-encoded protein fusions in transconjugant cells with respect to the timing of ss-to-dsDNA conversion reflected by mCh-ParB focus appearance (0 min). The diagram represents data from the foldchange increase in sfGFP signal from Fig. S5. Orange/green, blue and red colours correspond to production of proteins from the leading, maintenance and transfer region, respectively. Timings of the cytoplasmic sfGFP production

from the P_{lacIQ1} promoter inserted in the *repE-sopA* (*repE*), *tnpA-ybaA* (*tnpA*) and *traM-traJ* (*traM*) intergenic regions are represented in grey. The number (*n*) of individual transconjugant cells from at least three biological replicates analysed is indicated. **c** Jitter plots showing the intracellular green fluorescence (SNR) for each sfGFP fusions and reporters within vegetatively growing donor (left) and transconjugant cells (right) at the maximum SNR value from Fig. S5. Each dot represents data of individual cells. Means and SD are calculated from the indicated (*n*) number of transconjugant cells from at least three independent biological replicates. Donors of F derivatives (see Table S1), Recipient (LY358). Source data are provided as a Source Data file.

the delayed production of TraC, TraS and TraT. The additional delay between TraC and TraS/TraT fusions production could potentially reflect the relative distance of these genes to the P_Y promoter (5.9 kb for *traC* and 20.4 kb for *traS*). It is important to stress that the F plasmid carries a naturally occurring insertion of the IS3 insertion sequence into the *finO* gene of the FinOP fertility inhibition system, which results in the upregulation and constitutive expression of *tra* genes⁷¹. Therefore, other IncF plasmids in which the FinOP regulatory system is still active are expected to exhibit different timings and production levels of the Tra proteins than reported here.

Notably, the intracellular levels of Tra proteins within transconjugant cells reach a plateau between 60 to 90 min after the ss-to-dsDNA conversion and remain stable throughout our observations

(Fig. 3b and Fig. S5c). This involves that, at that point, transconjugant cells have produced the transfer machinery and the exclusion system and have most likely been converted into proficient plasmid donors. In support of this interpretation, TraM, TraC, TraS, TraT and SopB are detected at similar levels in vegetatively growing F-carrying donor cells (Fig. 3c and Figs. S4c, d, S5b, c). This is not the case for YgeA, PsiB, YfjB, YfjA and Ssb^F leading proteins, which intracellular levels start decreasing 25–35 min after the ss-to-dsDNA conversion in the transconjugants, and which are not detected in vegetatively growing donor cells (Fig. 3c and Figs. S4b, S5a). These results are consistent with the interpretation that leading proteins are produced rapidly and only transiently upon entry of the ssDNA plasmid in the recipient cells and not when the plasmid is maintained in dsDNA form during vegetative replication.



Single-stranded promoters allow the early expression of the leading genes in the transconjugant cell

Together with previous works^{37,38,54,56}, the early and transient expression of leading genes in transconjugant cells supports the existence of specific sequences that would act as single-stranded promoters to initiate the transcription of leading genes from the internalised ssDNA plasmid. Using bioinformatics analysis, we identified a region upstream of the *ssbF*, *yjfA*, *yjfB*, *psiA* and *psiB* genes, which we named *Frp2*, that shares 92% identity with the previously reported *Frp1* region (renamed *Frp1*) located upstream *ygeA* and *ygeB* and previously characterised in vitro⁵⁵ (Fig. 4a). DNA folding prediction using mFold (<http://www.unafold.org>) indicates that the single-stranded form of *Frp2* can fold into a highly stable stem-loop structure that also

carries canonical -10 and -35 boxes, similar to the *Frp1* region (Fig. S6a)⁵⁵. We addressed the effect of *Frp1* or *Frp2* deletions on the expression of the downstream genes in transconjugant cells using live-cell microscopy. Microscopy analysis of transconjugant cells receiving the *F ΔFrp1 ygeA-sfgfp*, the *F ΔFrp2 ssbF-sfgfp*, or the *F ΔFrp2 yjfA-sfgfp* revealed no significant fold-increase in sGFP fluorescence before or after the ss-to-dsDNA conversion in the transconjugant cells (Fig. 4b).

We then addressed the impact of *Frp1* and *Frp2* deletions on the efficiency of conjugation after three hours of mating, as estimated by plating assays (Fig. 4c). *F ΔFrp1* exhibits a significantly reduced frequency of transconjugants of $25.2 \pm 2.9\%$ compared to $92.6 \pm 6.6\%$ for the *Fwt*. Comparable results were obtained for *F ΔFrp1 ΔygeAB*

Fig. 4 | Role of leading region factors *Frpo1*, *Frpo2* and *ssb^f* in conjugation. **a** Genetic map of the leading region showing the position of the genes (green for studied sfGFP fusions and white for the other genes) and *Frpo1* and *Frpo2* promoters (red) (top). The bottom diagram shows the stem-loop structure formed by the ssDNA forms of *Frpo1* and *Frpo2* sequences (detailed in Fig. S6). **b** Histograms of intracellular sfGFP fold-increase in transconjugants after the acquisition of F Δ *Frpo1 ygeA-sfgfp*, F Δ *Frpo2 ssb-sfgfp* and F Δ *Frpo2 yjiA-sfgfp*. Mean and SD are calculated from the indicated (*n*) individual transconjugant cells analysed from at least three independent experiments. Levels obtained with the *Fwt* plasmid from Fig. S5a are *wt* reported in green as a reference. Donor of F Δ *Frpo1 ygeA-sfgfp* (LY1368), F Δ *Frpo2 ssb-sfgfp* (LY1365), F Δ *Frpo2 yjiA-sfgfp* (LY1364) and the recipient (LY318). **c** Histograms of *Fwt*, deletion mutants F Δ *Frpo1*, F Δ *ygeA*, F Δ *Frpo1 \Delta ygeA*, F Δ *Frpo1 \Delta ygeAB*, F Δ *Frpo2* and F Δ *ssb^f* frequency of transconjugant (T/R + T) estimated by plating assays. Mean and SD are calculated from three independent experiments (shown as individual black dots). *P* value significance ns and *****P* ≤ 0.0001 were obtained from one-way ANOVA with Dunnett's multiple comparisons test. Donor of *Fwt* (LY875), F Δ *Frpo1* (LY824), F Δ *ygeA* (LY160), F Δ *Frpo1 \Delta ygeA* (LY1424), F Δ *Frpo1 \Delta ygeAB* (LY1425), F Δ *Frpo2* (LY823), F Δ *ssb^f* (LY755), recipient (MS428). **d** Single-cell time-lapse quantification of Ssb-Ypet focus appearance (blue line) and mCh-ParB

focus first duplication (red line) with respect to mCh-ParB focus formation in transconjugant cells (0 min) that receive the F Δ *ssb^f* plasmid. The number of conjugation events analysed (*n*) from five independent biological replicates is indicated. Results obtained in Fig. 2b with *Fwt* plasmid are reported in grey for comparison. **e** Scatter plot showing the time lag between the appearance of the Ssb-Ypet focus and the appearance of the mCh-ParB focus in transconjugant cells after the acquisition of the F Δ *ssb^f* plasmid. The mean and SD calculated from (*n*) individual ss-to-dsDNA conversion event (blue circles) from five biological replicates are indicated. *P* value significance ns (>0.05 non-significant) was obtained from Mann-Whitney two-sided statistical test against results obtained with the *Fwt* plasmid (Fig. 2e). **f** Scatter plot showing the time lag between the apparition of the mCh-ParB focus and its visual duplication in two foci (first duplication), and in three or four foci (second duplication) in transconjugant cells after acquisition of the F Δ *ssb^f* plasmid. The mean and SD calculated from (*n*) individual duplication events (red circles) from eight biological replicates are indicated. *P* value significance ***P* = 0.0023 and ****P* = 0.0007 were obtained from Mann-Whitney two-sided statistical test against results obtained with the *Fwt* plasmid (Fig. 2f). Donor F Δ *ssb^f* (LY1068), recipient (LY358). Source data are provided as a Source Data file.

(32.7 ± 7.1) and F Δ *Frpo1 \Delta ygeA* (14.5 ± 0.4). Surprisingly, the single deletion of *ygeA* decreases the conjugation efficiency even further ($3.9 \pm 1.9\%$), and despite our multiple attempts, the deletion of *ygeB* alone could never be constructed. By contrast, the deletions of *Frpo2* or *ssb^f* have no significant impact on the conjugation efficiency. These results show that *Frpo1* and *Frpo2* are required for the early expression of the downstream genes upon plasmid entry in recipient cells during conjugation in vivo. However, genes under the control of *Frpo1* appear to have a more critical role in conjugation than those under the control of *Frpo2*.

Role of the plasmid-encoded Ssb^f leading protein in plasmid establishment

The rapid and transient expression of leading genes upon plasmid entry strongly suggests that leading proteins have an essential role during the early steps of plasmid establishment in the new host cell. The leading region conserved in various enterobacterial plasmids encodes a homologue of the single-strand-binding protein Ssb encoded on the *E. coli* chromosome^{41,43,54,72–74}. The chromosomally encoded *ssb* gene is conserved and essential in all bacterial organisms, raising the question of the *raison d'être* of plasmid-born *ssb* homologues. Early study shows that the Ssb^f encoded by the F plasmid can partially complement conditional mutations of the chromosomal *ssb* gene^{73,75}. Consistently, we performed simultaneous visualisation of Ssb^f-mCh produced from a pTrc99a-*ssb^f-mch* plasmid and the chromosomally encoded Ssb-Ypet (Fig. S7a) and observed similar intracellular positioning (Fig. S7b) confirmed by colocalisation analysis (Fig. S7c). This indicates that both the plasmid Ssb^f and the host Ssb are recruited to the ssDNA that follows the replication forks in vegetatively growing cells. Similarly, Ssb^f-sfGFP also forms foci in transconjugant cells that have acquired the F *ssb^f-sfgfp* plasmid, mainly during the first and second plasmid duplication events (Fig. S7d, e). Nonetheless, the role of Ssb^f during conjugation is still unclear, and its deletion from the F plasmid has no significant impact on conjugation efficiency (Fig. 4c).

To get further insight into the role of Ssb^f during conjugation, we revisited the dynamics of ssDNA entry, ss-to-dsDNA conversion and duplication of the F Δ *ssb^f* plasmid. Time-lapse microscopy image analysis reveals that Ssb^f deletion has no impact on the dynamics of Ssb-Ypet conjugative foci (Fig. 4d) or the timing of the ss-to-dsDNA conversion (compare Fig. 4e to Fig. 2e). However, Ssb^f deletion dramatically delays the timing of plasmid duplication in transconjugant cells (compare Fig. 4f to Fig. 2f). The time lag between mCh-ParB appearance and the first duplication is increased by -58% (from 10.4 ± 4.7 for *Fwt* to 16.4 ± 9.5 for F Δ *ssb^f*), and the time between the first and second plasmid replication event is increased by -29% (from

10.1 ± 4.7 for *Fwt* to 13 ± 8 for F Δ *ssb^f*). This indicates that Ssb^f has a role in facilitating the first rounds of plasmid duplication in the new transconjugant cell, possibly by increasing the cellular pool of single-strand binding protein available for DNA replication. This function appears dispensable since the absence of Ssb^f delays plasmid duplication but does not affect the final efficiency of conjugation, at least when conjugation is performed in optimal conditions between *E. coli* MG1655 strains.

Discussion

Our current knowledge of conjugation mainly emerges from experimental genetic, biochemical and structural studies that provided a well-documented understanding of the molecular reactions and factors involved in DNA transfer, while genomic and computational studies uncovered the diversity of conjugative plasmids and their importance in the epidemiology of antibiotics resistance dissemination. It is only recently that the application of optical microscopy has started to provide insights into the organisation of conjugation at the cellular scale^{58,59,76–82}. In this study, live-cell microscopy combined with specifically developed fluorescent reporters offers a unique view of the cellular dynamics of conjugation while providing insights into the timing and localisation of each key step.

We report the presence of ssDNA plasmid on both the donor's and the recipient's side during plasmid transfer. Noticeably, the ssDNA plasmid is not randomly positioned but instead allocated to specific subcellular locations within the mating pair cells. The exit point of the ssDNA F plasmid is preferentially located on the side of the donor cell and preferentially at quarter positions. This pattern could reflect the intracellular position of the T4SS machinery of the F plasmid, which to our knowledge, remains to be described. This possibility would be weakened if the F plasmid T4SS machinery is homogeneously located throughout the periphery of the cells as in the case of the pTi and R388 plasmids^{79,81}. Alternatively, the lateral localisation of active conjugation pores may reflect the facilitated access to F plasmid molecules, which are also positioned at quarter positions and excluded from the cell poles^{83,84}. By contrast, the ssDNA mainly enters the polar region of the recipient cells. This could suggest that the pole of the recipients' surface is the preferred location for the donor's F pilus, attachment or the stabilisation of the mating pair. The latter possibility is reinforced by the fact that mating pair stabilisation during F conjugation involves interaction between the plasmid protein TraN exposed at the surface of the donor cells and the host outer membrane protein OmpA of the recipient cells^{82,85}. OmpA was shown to be enriched and less mobile in the polar regions of *E. coli* cells⁸⁶, possibly favouring the stabilisation of the mating pair and the conjugation pore at this location.

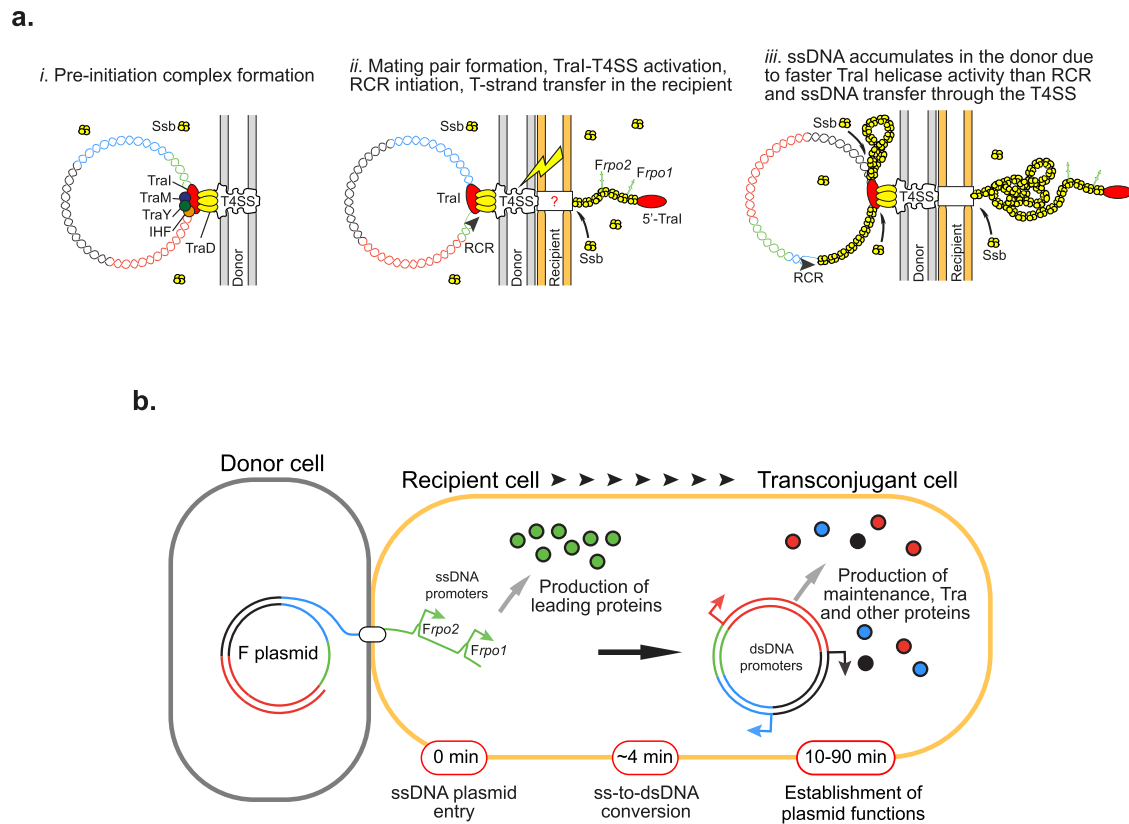


Fig. 5 | Model for conjugation initiation and intracellular dynamics. **a**(i) Before the initiation of conjugation, the pre-initiation complex bound to the plasmid's origin of transfer is docked to the Type IV secretion system (T4SS). (ii) The establishment of the mating pair transduces a signal that activates the pre-initiation complex. The unwinding of the dsDNA plasmid by the helicase activity of TraI produces the first segment of the T-strand, which is immediately transferred into the recipient cell where it recruits Ssb molecules, while the non-transferred strand is complemented by rolling-circle replication (RCR) in the donor cell. (iii) The helicase activity of TraI generates ssDNA at a higher rate than the T-strand is transferred through the T4SS or the non-transferred strand is complemented by

RCR, thus resulting in the accumulation of ssDNA plasmid coated by Ssb molecules in the donor cell. **b** Upon entry of the ssDNA plasmid in the recipient cell, *Frpo1* and *Frpo2* leading sequences form stem-loop structures that serve as promoters initiating the transcription of the downstream leading genes, rapidly resulting in the production of leading proteins. The subsequent ss-to-dsDNA conversion inactivates *Frpo1* and *Frpo2* and licences the expression of other plasmid genes under the control of conventional dsDNA promoters. The production of maintenance, transfer and other plasmid-encoded proteins eventually results in the development of new functions by the transconjugant cell.

The unexpected finding that the ssDNA first appears in the recipient cell, and later accumulates in the donor during conjugation also provides insights into the activity of TraI and its coordination with the transfer of the T-strand through the T4SS or the RCR of the non-transferred strand. Before DNA transfer initiation, the relaxosome bound to the plasmid's *oriT* is docked to the T4SS by the TraD coupling protein, thus forming the pre-initiation complex (Fig. 5a(i)). Contact with the recipient cell is proposed to induce a signal that activates the pre-initiation complex. We uncover the existence of a brief period where part of the T-strand has already been transferred into the recipient cell while no ssDNA is present within the donor (Fig. 5a(ii)). At this stage, the absence of ssDNA in the donor implicates that all the ssDNA generated by TraI has been removed, both by transfer of the T-strand through the T4SS and by complementation of the non-transferred ssDNA strand by the RCR. After this transient step, the ssDNA also accumulates in the donor, suggesting that the ssDNA is generated by TraI helicase activity in the donor faster than it is removed by transfer and RCR synthesis (Fig. 5a(iii)).

Assuming the 2.9 ± 1.1 min lifespan of the Ssb-Ypet foci in transconjugants reflects the time required to complete the internalisation of the 108,000 nt ssDNA F plasmid, we calculated a 620 ± 164 nt s^{-1} transfer rate. This is in reasonable agreement with the historical 770 nt s^{-1} rate estimated from the 100 min required to transfer the whole 4.6 Mb *E. coli* chromosome⁸⁷. Besides, the rate of DNA synthesis by the DNA polymerase III holoenzyme during RCR was estimated at 650–750

nuc s^{-1} ⁸⁸. By comparison, the rate of TraI helicase activity was measured at 1120 ± 160 bp s^{-1} ⁸⁹. These estimates support the view that ssDNA accumulation in the donor accounts for the faster rate of TraI helicase activity than the rate of T-strand plasmid transfer or RCR. Therefore, it is possible that, contrasting with the previously suggested but never demonstrated proposal, the helicase activity of the relaxase is not strictly coupled with the activity of DNA translocation through the T4SS.

Live-cell microscopy uncovers the global chronology conjugation steps, as summarised in Fig. 5b. The plasmid processing in the transconjugant cell is a relatively rapid process, as the entry of the ssDNA plasmid and its conversion into dsDNA is completed in about 4 min on average. Most importantly, the ss-to-dsDNA conversion event is the pivotal event that determines the programme of plasmid gene expression. Leading genes are the first to enter the recipient cell and also the first to be expressed from the F plasmid in ssDNA form. Consistently with previous proposals^{55–57}, we show that the early expression of leading genes depends on sequences that act as single-stranded promoters when the plasmid is still in ssDNA form. As previously described for *Frpo1*, we propose that the highly homologous *Frpo2* sequences identified here folds into a stable stem-loop structures that reconstruct –35 and –10 consensus boxes, resulting in transcription initiation.

Leading gene expression is also transient as the ss-to-dsDNA conversion turns off leading protein production by inactivating *Frpo1*

and *Frpo2* promoters while licencing the expression of maintenance, transfer and other plasmid genes under the control of conventional dsDNA promoters, often subject to their own regulation specificities. Maintenance and transfer protein levels within transconjugants reach a steady-state equivalent to that of vegetatively growing F-containing cells in about 30 to 90 min, depending on the protein. Interestingly, our previous work showed that tetracycline resistance factors encoded by the *TnI/O* transposon inserted in the intergenic region *ybdB-ybfA* of the F plasmid are also produced immediately after the ss-to-dsDNA conversion and reach the resistant cell's level within ~90 min⁵⁸. These findings consistently indicate that this time scale corresponds to the period needed for the transconjugant cells to gain plasmid-encoded functions, including plasmid maintenance, conjugation ability, immunity against self-transfer and additional resistance potentially carried by the plasmid.

The regulation of plasmid gene expression by plasmid processing is an elegant way to ensure the sequential and timely production of plasmid proteins in the transconjugant cell, and particularly to restrict the production of leading factors to a narrow time window following the entry of the ssDNA plasmid. However, de novo protein synthesis might not be the only way to provide the transconjugant cell with plasmid-encoded proteins. Recent work by Al Mamun et al. reports that the transfer of the F-like plasmid pED208 (IncFV) is concomitant with the translocation of several plasmid-encoded proteins, including *Tral*, *ParA*, *ParB1*, *Ssb* homologue *Ssb*^{ED208}, *ParB2*, *PsiB* and *PsiA*⁹⁰. Protein translocation was detected at low frequency (10⁻⁵ recombinants per donor cell between one and five hours of mating) using a highly sensitive Cre recombinase assay. Protein translocation might also occur during the transfer of the native F plasmid but could not solely explain our observations. Indeed, our microscopy analysis shows that *YgeA*, *PsiB*, *YfjB*, *YfjA* and *Ssb*^F leading fusions are below the microscopy detection threshold in donor cells but are quantified at significant intracellular levels in all transconjugant cells. This implies that the amounts of leading proteins observed in the transconjugant cells cannot just originate from donor cells, but result from de novo protein synthesis, which we show depends on *Frpo1* and *Frpo2* sequences. Therefore, it appears likely that direct protein translocation and de novo synthesis are concomitant mechanisms ensuring the presence of leading factors and associated functions immediately upon entry of the ssDNA plasmid in the transconjugant cell. This further suggests the critical role of the leading region in conjugation. Several elements support this view. The leading region is conserved in a variety of conjugative plasmids⁴¹⁻⁴⁶. In addition, the leading regions of plasmids belonging to a wide range of incompatibility groups (*IncF*, *IncN*, *IncP9* and *IncW*) classified as MOBF plasmids using the *relaxase* as a phylogenetic marker were reported to be the preferential target for CRISPR-Cas systems directed against conjugation^{8,91,92}. Recently, the leading region was shown to be an important evolutionary target for the dissemination of the pESBL (*IncI*) plasmid⁹³. Concerning the F plasmid, we can stress that *Frpo1* and *Frpo2* share 92% similarity at the nucleotide level and are located only about 5 kb apart. This implies that when in dsDNA form during vegetative plasmid replication, *Frpo1* and *Frpo2* sequences would be a potential substrate for homologous recombination, resulting in the deletion of the intervening segment. However, the intervening segment carries the *flmAB* genes, functional homologues to the *hok/sok* toxin-antitoxin system from the R1 plasmid⁹⁴, which are likely to safeguard the stability of the leading region.

Despite this body of evidence, it is currently challenging to rationalise the importance of the leading region since the molecular functions of most leading proteins are still unknown. Our data indicate that genes downstream of *Frpo1* (*ygeA* et *ygeB*) have a critical function in conjugation. By contrast, genes located downstream *Frpo2* (*ssb*^F, *yfjA*, *yfjB*, *psiB*, *psiA* and *flmC*) appear to be dispensable since deletions of *Frpo2*, *ssb*^F or *psiB*⁴⁴ have no significant impact on the overall

conjugation efficiency addressed by plating assays. Yet, *Ssb*^F and *PsiB* have been shown to suppress conjugation-induced SOS induction in the transconjugant cell^{43,54,90}, which is likely important for the transconjugant's physiology and proliferation rather than for plasmid transfer per se. One potential limitation of the conjugation study is that transfer efficiency assays are generally performed between identical or closely related bacterial strains in optimal medium and temperature conditions. This likely undermines the role of genes that are not strictly essential but might facilitate or optimise conjugation, or help the proliferation of the transconjugant cell. Hence, it is possible that the importance of the leading factors would be best revealed in less favourable conditions, between phylogenetically distant bacteria, or on the evolutionary scale. Meanwhile, real-time microscopy might help uncover the potentially subtle influence of these genes on the sequence of conjugation in live cells.

Methods

Bacterial strains, plasmids and growth

Bacterial strains are listed in Table S1, plasmids in Table S2 and oligonucleotides in Table S3. Fusion of genes with fluorescent tags and gene deletion on the F plasmid used λ Red recombination^{95,96}. Modified F plasmids were transferred to the background strain K12 MG1655 by conjugation. Where multiple genetic modifications on the F plasmid were required, the *kan* and *cat* genes were removed using site-specific recombination induced by expression of the *Flp* recombinase from plasmid pCP20⁹⁵. Plasmid cloning were done by Gibson Assembly and verified by Sanger sequencing (Eurofins Genomics biotech). Strains and plasmids were verified by Sanger sequencing (Eurofins Genomics). Cells were grown at 37 °C in an M9 medium supplemented with glucose (0.2%) and casamino acid (0.4%) (M9-CASA) before imaging, and in Luria-Bertani (LB) broth for conjugation efficiency assays. When appropriate, supplements were used in the following concentrations; Ampicillin (Ap) 100 μ g/ml, Chloramphenicol (Cm) 20 μ g/ml, Kanamycin (Kn) 50 μ g/ml, Streptomycin (St) 20 μ g/ml and Tetracycline (Tc) 10 μ g/ml.

Conjugation assays

Overnight cultures in LB of recipient and donor cells were diluted to an A_{600} of 0.05 and grown until an A_{600} comprised between 0.7 and 0.9 was reached. 25 μ l of donor and 75 μ l of recipient cultures were mixed into an Eppendorf tube and incubated for 90 min at 37 °C. About 1 ml of LB was added gently and the tubes were incubated again for 90 min at 37 °C. The conjugation mix were vortexed, serially diluted, and plated on LB agar X-gal 40 μ g/ml IPTG 20 μ M supplemented with the appropriate antibiotic to select for recipient or donor populations. Recipient (R) colonies were then streaked on LB agar containing tetracycline 10 μ g/ml to select for transconjugants (T) and the frequency of transconjugant calculated from the (T/R + T) presented in Fig. 4c.

Live-cell microscopy experiments

Overnight cultures in M9-CASA were diluted to an A_{600} of 0.05 and grown until A_{600} = 0.8 was reached. Conjugation samples were obtained by mixing 25 μ l of the donor and 75 μ l of the recipient into an Eppendorf tube. For time-lapse experiments, 50 μ l of the pure culture or conjugation mix was loaded into a B04A microfluidic chamber (ONIX, CellASIC[®])⁹⁷. The nutrient supply was maintained at 1 psi and the temperature was maintained at 37 °C throughout the imaging process. Cells were imaged every 1 or 5 min for 90 to 120 min. For snapshot imaging, 10 μ l samples of clonal culture or conjugation mix were spotted onto an M9-CASA 1% agarose pad on a slide⁹⁸ and imaged directly.

Image acquisition. Conventional wide-field fluorescence microscopy imaging was carried out on an Eclipse Ti2-E microscope (Nikon), equipped with x100/1.45 oil Plan Apo Lambda phase objective, ORCA-

Fusion digital CMOS camera (Hamamatsu), and using NIS software for image acquisition. Acquisitions were performed using 50% power of a Fluo LED Spectra X light source at 488 and 560 nm excitation wavelengths. Exposure settings were 100 ms for Ypet, sfGFP and mCherry and 50 ms for phase contrast.

Image analysis. Quantitative image analysis was done using Fiji software with MicrobeJ plugin⁹⁹. For snapshot analysis, cells' outline detection was performed automatically using MicrobeJ and verified using the Manual-editing interface. For time-lapse experiments, detection of cells was done semi-automatedly using the Manual-editing interface, which allows to select the cells to be monitored and automatically detect the cell outlines. Within conjugation populations, donor (no mCh-ParB signal), recipient (diffuse mCh-ParB signal) or transconjugant (mCh-ParB foci) categories were assigned using the 'Type' option of MicrobeJ. Recipient cells were detected on the basis of the presence of red fluorescence above the cell's autofluorescence background level detected in the donors. Among these recipient cells, transconjugants were identified by running MicrobeJ automated detection of the ParB fluorescence foci (Maxima detection). This approach was used independently of the presence or the absence of the Ssb-Ypet, or sfGFP fusions within donor and recipient cells. Within the different cell types, mean intensity fluorescence (a.u.), skewness, signal/noise ratio (SNR) or cell length (μm) parameters were automatically extracted and plotted using MicrobeJ. SNR corresponds to the ratio (mean intracellular signal/mean noise signal), where the mean intracellular signal is the fluorescence signal per cell area and the noise is the signal measured outside the cells (due to the fluorescence emitted by the surrounding medium). By contrast with the total amount of fluorescence per cell, which is depending on the cell size/age and accounts for the background, SNR quantitative estimate is more appropriate for unbiased quantification of intracellular fluorescence over time. Ssb-Ypet, Ssb^F-mCh and mCh-ParB foci were detected using MicrobeJ Maxima detection function, and foci localisation and fluorescence intensity were extracted and plotted automatically. Plots presenting time-lapse data were either aligned to the first frame where the transconjugant cell exhibits a conjugative Ssb-Ypet focus (ssDNA acquisition) or an mCh-ParB focus (ss-to-dsDNA conversion) as indicated in the corresponding figure legend. Importantly, because conjugation is asynchronous in the population, time-lapse movies do not always capture the entire sequence of DNA transfer, i.e., Ssb-Ypet focus appearance/disappearance, mCh-ParB focus formation, first and second mCh-ParB duplication events. Of note, using 1 min/frame time-lapses was suitable to analyse Ssb-Ypet appearance/disappearance relative to the mCh-ParB formation (Fig. 2b–e), but provoked mCh-ParB bleaching thus hindering the analysis of mCh-ParB duplication events on the long term. We have then used 5 min/frame time-lapses to analyse mCh-ParB first and second duplication events relative to mCh-ParB focus formation (Fig. 2b, f). Also, the characterisation of the different transfer parameters was performed using specific analysis. For instance, time lags were calculated by counting the number of frames between the two considered events (Ssb-Ypet appearance and disappearance in Figs. 2e, 4e; mCh-ParB focus formation and first or second duplications in Figs. 2f, 4f). By contrast, Figs. 2b, 4b were generated by annotating the presence/absence of Ssb-Ypet or mCh-ParB foci in each time-lapse frame.

Statistical analysis

P value significance were analysed by running specific statistical tests on the GraphPad Prism software. Single-cell data from quantitative microscopy analysis were extracted from the MicrobeJ interface and transferred to GraphPad. *P* value significance of single-cell quantitative data was performed using unpaired non-parametric Mann-Whitney two-sided statistical test, which allows to compare differences between independent data groups without normal distribution

assumption. *P* value significance for the frequency of transconjugants obtained by plating assays were evaluated using One-way analysis of variance (ANOVA) with Dunnett's multiple comparisons test, which allows to determine the statistical significance of differences observed between the means of three or more independent experimental groups against a control group mean (corresponding to the *Fwt*). When required, *P* value and significance are indicated on the figure panels and within the corresponding legend.

Reporting summary

Further information on research design is available in the Nature Portfolio Reporting Summary linked to this article.

Data availability

All data to understand and assess the conclusions of this research are available in the main text and Supplementary Information. Source data are provided with this paper in the Source Data file. Raw microscopy data are available on Figshare (<https://doi.org/10.6084/m9.figshare.21206444>). Source data are provided with this paper.

References

1. Lederberg, J. & Tatum, E. L. Gene recombination in *Escherichia coli*. *Nature* **158**, 558 (1946).
2. Grohmann, E., Muth, G. & Espinosa, M. Conjugative plasmid transfer in gram-positive bacteria. *Microbiol. Mol. Biol. Rev.* **67**, 277–301 (2003). table of contents.
3. Cruz, F. D. L., Frost, L. S., Meyer, R. J. & Zechner, E. L. Conjugative DNA metabolism in Gram-negative bacteria. *FEMS Microbiol. Rev.* **34**, 18–40 (2010).
4. Virolle, C., Goldlust, K., Djermoun, S., Bigot, S. & Lesterlin, C. Plasmid transfer by conjugation in Gram-negative bacteria: from the cellular to the community level. *Genes* **11**, 1239 (2020).
5. Barlow, M. What antimicrobial resistance has taught us about horizontal gene transfer. *Methods Mol. Biol.* **532**, 397–411 (2009).
6. Tatum, E. L. & Lederberg, J. Gene recombination in the bacterium *Escherichia coli*. *J. Bacteriol.* **53**, 673–684 (1947).
7. Lanza, V. F. et al. Plasmid flux in *Escherichia coli* ST131 sublineages, analyzed by plasmid constellation network (PLACNET), a new method for plasmid reconstruction from whole genome sequences. *PLoS Genet.* **10**, e1004766 (2014).
8. Fernandez-Lopez, R., de Toro, M., Moncalian, G., Garcillan-Barcia, M. P. & de la Cruz, F. Comparative genomics of the conjugation region of F-like plasmids: five shades of F. *Front. Mol. Biosci.* **3**, 71 (2016).
9. Johnson, T. J. et al. Separate F-type plasmids have shaped the evolution of the H30 subclone of *Escherichia coli* sequence type 131. *mSphere* **1**, e00121–16 (2016).
10. Howard, M. T., Nelson, W. C. & Matson, S. W. Stepwise assembly of a relaxosome at the F plasmid origin of transfer. *J. Biol. Chem.* **270**, 28381–28386 (1995).
11. Nelson, W. C., Morton, B. S., Lahue, E. E. & Matson, S. W. Characterization of the *Escherichia coli* F factor traY gene product and its binding sites. *J. Bacteriol.* **175**, 2221–2228 (1993).
12. Schildbach, J. F., Robinson, C. R. & Sauer, R. T. Biophysical characterization of the TraY protein of *Escherichia coli* F factor. *J. Biol. Chem.* **273**, 1329–1333 (1998).
13. Llosa, M., Zunzunegui, S. & de la Cruz, F. Conjugative coupling proteins interact with cognate and heterologous VirB10-like proteins while exhibiting specificity for cognate relaxosomes. *Proc. Natl Acad. Sci. USA* **100**, 10465–10470 (2003).
14. Gomis-Rüth, F. X., Solà, M., de la Cruz, F. & Coll, M. Coupling factors in macromolecular type-IV secretion machineries. *Curr. Pharm. Des.* **10**, 1551–1565 (2004).
15. Beranek, A. et al. Thirty-eight C-terminal amino acids of the coupling protein TraD of the F-like conjugative resistance plasmid R1

- are required and sufficient to confer binding to the substrate selector protein TraM. *J. Bacteriol.* **186**, 6999–7006 (2004).
16. Schröder, G. & Lanka, E. The mating pair formation system of conjugative plasmids—A versatile secretion machinery for transfer of proteins and DNA. *Plasmid* **54**, 1–25 (2005).
 17. Lang, S. & Zechner, E. L. General requirements for protein secretion by the F-like conjugation system R1. *Plasmid* **67**, 128–138 (2012).
 18. Clewell, D. B. & Helinski, D. E. Existence of the colicinogenic factor-sex factor Coll-b-P9 as a supercoiled circular DNA-protein relaxation complex. *Biochem. Biophys. Res. Commun.* **41**, 150–156 (1970).
 19. Willetts, N. & Skurray, R. The conjugation system of F-like plasmids. *Annu. Rev. Genet.* **14**, 41–76 (1980).
 20. Everett, R. & Willetts, N. Characterisation of an in vivo system for nicking at the origin of conjugal DNA transfer of the sex factor F. *J. Mol. Biol.* **136**, 129–150 (1980).
 21. Traxler, B. A. & Minkley, E. G. Evidence that DNA helicase I and oriT site-specific nicking are both functions of the F Tral protein. *J. Mol. Biol.* **204**, 205–209 (1988).
 22. Matson, S. W. & Morton, B. S. Escherichia coli DNA helicase I catalyzes a site- and strand-specific nicking reaction at the F plasmid oriT. *J. Biol. Chem.* **266**, 16232–16237 (1991).
 23. Reygers, U., Wessel, R., Müller, H. & Hoffmann-Berling, H. Endonuclease activity of Escherichia coli DNA helicase I directed against the transfer origin of the F factor. *EMBO J.* **10**, 2689–2694 (1991).
 24. Lanka, E. & Wilkins, B. M. DNA processing reactions in bacterial conjugation. *Annu. Rev. Biochem.* **64**, 141–169 (1995).
 25. Matson, S. W. & Ragonese, H. The F-plasmid Tral protein contains three functional domains required for conjugative DNA strand transfer. *J. Bacteriol.* **187**, 697–706 (2005).
 26. Dostál, L. & Schildbach, J. F. Single-stranded DNA binding by F Tral relaxase and helicase domains is coordinately regulated. *J. Bacteriol.* **192**, 3620–3628 (2010).
 27. Dostál, L., Shao, S. & Schildbach, J. F. Tracking F plasmid Tral relaxase processing reactions provides insight into F plasmid transfer. *Nucleic Acids Res.* **39**, 2658–2670 (2011).
 28. Ilangovan, A. et al. Cryo-EM structure of a relaxase reveals the molecular basis of DNA unwinding during bacterial conjugation. *Cell* **169**, 708–721.e12 (2017).
 29. Llosa, M., Gomis-Rüth, F. X., Coll, M. & de la Cruz Fd, F. Bacterial conjugation: a two-step mechanism for DNA transport. *Mol. Microbiol.* **45**, 1–8 (2002).
 30. Wawrzyniak, P., Plucienniczak, G. & Bartosik, D. The different faces of rolling-circle replication and its multifunctional initiator proteins. *Front. Microbiol.* **8**, 2353 (2017).
 31. Fronzes, R., Christie, P. J. & Waksman, G. The structural biology of type IV secretion systems. *Nat. Rev. Microbiol.* **7**, 703–714 (2009).
 32. Christie, P. J., Whitaker, N. & González-Rivera, C. Mechanism and structure of the bacterial type IV secretion systems. *Biochim. Biophys. Acta* **1843**, 1578–91 (2014).
 33. Grohmann, E., Christie, P. J., Waksman, G. & Backert, S. Type IV secretion in Gram-negative and Gram-positive bacteria. *Mol. Microbiol.* **107**, 455–471 (2018).
 34. Macé, K. et al. Cryo-EM structure of a type IV secretion system. *Nature* **607**, 191–196 (2022).
 35. Bailone, A. et al. PsiB polypeptide prevents activation of RecA protein in Escherichia coli. *Mol. Gen. Genet.* **214**, 389–395 (1988).
 36. Dutreix, M. et al. Identification of psiB genes of plasmids F and R6-5. Molecular basis for psiB enhanced expression in plasmid R6-5. *Nucleic Acids Res.* **16**, 10669–10679 (1988).
 37. Bagdasarian, M. et al. PsiB, an anti-SOS protein, is transiently expressed by the F sex factor during its transmission to an Escherichia coli K-12 recipient. *Mol. Microbiol.* **6**, 885–893 (1992).
 38. Althorpe, N. J., Chilly, P. M., Thomas, A. T., Brammar, W. J. & Wilkins, B. M. Transient transcriptional activation of the IncI1 plasmid anti-restriction gene (ardA) and SOS inhibition gene (psiB) early in conjugating recipient bacteria. *Mol. Microbiol.* **31**, 133–142 (1999).
 39. Baharoglu, Z., Bikard, D. & Mazel, D. Conjugative DNA transfer induces the bacterial SOS response and promotes antibiotic resistance development through integron activation. *PLoS Genet.* **6**, e1001165 (2010).
 40. Baharoglu, Z. & Mazel, D. SOS, the formidable strategy of bacteria against aggressions. *FEMS Microbiol. Rev.* **38**, 1126–1145 (2014).
 41. Golub, E. I. & Low, K. B. Conjugative plasmids of enteric bacteria from many different incompatibility groups have similar genes for single-stranded DNA-binding proteins. *J. Bacteriol.* **162**, 235–241 (1985).
 42. Golub, E. I. & Low, K. B. Unrelated conjugative plasmids have sequences which are homologous to the leading region of the F factor. *J. Bacteriol.* **166**, 670–672 (1986).
 43. Golub, E., Bailone, A. & Devoret, R. A gene encoding an SOS inhibitor is present in different conjugative plasmids. *J. Bacteriol.* **170**, 4392–4394 (1988).
 44. Loh, S., Cram, D. & Skurray, R. Nucleotide sequence of the leading region adjacent to the origin of transfer on plasmid F and its conservation among conjugative plasmids. *Mol. Gen. Genet.* **219**, 177–186 (1989).
 45. Loh, S. et al. Nucleotide sequence of the psiA (plasmid SOS inhibition) gene located on the leading region of plasmids F and R6-5. *Nucleic Acids Res.* **18**, 4597 (1990).
 46. Cox, K. E. L. & Schildbach, J. F. Sequence of the R1 plasmid and comparison to F and R100. *Plasmid* **91**, 53–60 (2017).
 47. Kline, B. C. A review of mini-F plasmid maintenance. *Plasmid* **14**, 1–16 (1985).
 48. Keasling, J. D., Palsson, B. O. & Cooper, S. Replication of mini-F plasmids during the bacterial division cycle. *Res. Microbiol.* **143**, 541–548 (1992).
 49. Thomas, C. M. Paradigms of plasmid organization. *Mol. Microbiol.* **37**, 485–491 (2000).
 50. Bouet, J.-Y. & Funnell, B. E. Plasmid Localization and Partition in Enterobacteriaceae. *EcoSal Plus* **8**, (2019).
 51. Draper, O., César, C. E., Machón, C., de la Cruz, F. & Llosa, M. Site-specific recombinase and integrase activities of a conjugative relaxase in recipient cells. *Proc. Natl Acad. Sci. USA* **102**, 16385–16390 (2005).
 52. Chandler, M. et al. Breaking and joining single-stranded DNA: the HUH endonuclease superfamily. *Nat. Rev. Microbiol.* **11**, 525–538 (2013).
 53. Cram, D., Ray, A., O’Gorman, L. & Skurray, R. Transcriptional analysis of the leading region in F plasmid DNA transfer. *Plasmid* **11**, 221–233 (1984).
 54. Jones, A. L., Barth, P. T. & Wilkins, B. M. Zygotic induction of plasmid ssb and psiB genes following conjugative transfer of IncI1 plasmid Collb-P9. *Mol. Microbiol.* **6**, 605–613 (1992).
 55. Masai, H. & Arai, K. Frp: a novel single-stranded DNA promoter for transcription and for primer RNA synthesis of DNA replication. *Cell* **89**, 897–907 (1997).
 56. Bates, S., Roscoe, R. A., Althorpe, N. J., Brammar, W. J. & Wilkins, B. M. Expression of leading region genes on IncI1 plasmid Collb-P9: genetic evidence for single-stranded DNA transcription. *Microbiology* **145**, 2655–2662 (1999).
 57. Nasim, M. T., Eperon, I. C., Wilkins, B. M. & Brammar, W. J. The activity of a single-stranded promoter of plasmid Collb-P9 depends on its secondary structure. *Mol. Microbiol.* **53**, 405–417 (2004).
 58. Nolivos, S. et al. Role of AcrAB-TolC multidrug efflux pump in drug-resistance acquisition by plasmid transfer. *Science* **364**, 778–782 (2019).

59. Goldlust, K., Couturier, A., Terradot, L. & Lesterlin, C. Live-cell visualization of DNA transfer and pilus dynamics during bacterial conjugation. *Methods Mol. Biol.* **2476**, 63–74 (2022).
60. Reyes-Lamothe, R., Possoz, C., Danilova, O. & Sherratt, D. J. Independent positioning and action of *Escherichia coli* replisomes in live cells. *Cell* **133**, 90–102 (2008).
61. Reyes-Lamothe, R., Sherratt, D. J. & Leake, M. C. Stoichiometry and architecture of active DNA replication machinery in *Escherichia coli*. *Science* **328**, 498–501 (2010).
62. Lohman, T. M. & Ferrari, M. E. *Escherichia coli* single-stranded DNA-binding protein: multiple DNA-binding modes and cooperativities. *Annu Rev. Biochem.* **63**, 527–570 (1994).
63. Moolman, M. C. et al. Slow unloading leads to DNA-bound β -sliding clamp accumulation in live *Escherichia coli* cells. *Nat. Commun.* **5**, 5820 (2014).
64. Keasling, J. D., Palsson, B. O. & Cooper, S. Cell-cycle-specific F plasmid replication: regulation by cell size control of initiation. *J. Bacteriol.* **173**, 2673–2680 (1991).
65. Di Lorenzo, L., Frost, L. S. & Paranchych, W. The TraM protein of the conjugative plasmid F binds to the origin of transfer of the F and ColE1 plasmids. *Mol. Microbiol.* **6**, 2951–2959 (1992).
66. Hu, B., Khara, P. & Christie, P. J. Structural bases for F plasmid conjugation and F pilus biogenesis in *Escherichia coli*. *Proc. Natl Acad. Sci. USA* **116**, 14222–14227 (2019).
67. Achtman, M., Kennedy, N. & Skurray, R. Cell–cell interactions in conjugating *Escherichia coli*: role of traT protein in surface exclusion. *Proc. Natl Acad. Sci. USA* **74**, 5104–5108 (1977).
68. Manning, P. A., Beutin, L. & Achtman, M. Outer membrane of *Escherichia coli*: properties of the F sex factor traT protein which is involved in surface exclusion. *J. Bacteriol.* **142**, 285–294 (1980).
69. Jalajakumari, M. B. et al. Surface exclusion genes traS and traT of the F sex factor of *Escherichia coli* K-12. Determination of the nucleotide sequence and promoter and terminator activities. *J. Mol. Biol.* **198**, 1–11 (1987).
70. Penfold, S. S., Simon, J. & Frost, L. S. Regulation of the expression of the traM gene of the F sex factor of *Escherichia coli*. *Mol. Microbiol.* **20**, 549–558 (1996).
71. Cheah, K. C. & Skurray, R. The F plasmid carries an IS3 insertion within finO. *J. Gen. Microbiol.* **132**, 3269–3275 (1986).
72. Kolodkin, A. L., Capage, M. A., Golub, E. I. & Low, K. B. F sex factor of *Escherichia coli* K-12 codes for a single-stranded DNA binding protein. *Proc. Natl Acad. Sci. USA* **80**, 4422–4426 (1983).
73. Golub, E. I. & Low, K. B. Derepression of single-stranded DNA-binding protein genes on plasmids derepressed for conjugation, and complementation of an *E. coli* ssb- mutation by these genes. *Mol. Gen. Genet.* **204**, 410–416 (1986).
74. Howland, C. J., Rees, C. E., Barth, P. T. & Wilkins, B. M. The ssb gene of plasmid ColIb-P9. *J. Bacteriol.* **171**, 2466–2473 (1989).
75. Porter, R. D. & Black, S. The single-stranded-DNA-binding protein encoded by the *Escherichia coli* F factor can complement a deletion of the chromosomal ssb gene. *J. Bacteriol.* **173**, 2720–2723 (1991).
76. Lawley, T. D., Gordon, G. S., Wright, A. & Taylor, D. E. Bacterial conjugative transfer: visualization of successful mating pairs and plasmid establishment in live *Escherichia coli*. *Mol. Microbiol.* **44**, 947–956 (2002).
77. Babić, A., Lindner, A. B., Vulić, M., Stewart, E. J. & Radman, M. Direct visualization of horizontal gene transfer. *Science* **319**, 1533–1536 (2008).
78. Clarke, M., Maddera, L., Harris, R. L. & Silverman, P. M. F-pili dynamics by live-cell imaging. *Proc. Natl Acad. Sci. USA* **105**, 17978–17981 (2008).
79. Aguilar, J., Cameron, T. A., Zupan, J. & Zambryski, P. Membrane and core periplasmic *Agrobacterium tumefaciens* virulence type IV secretion system components localize to multiple sites around the bacterial perimeter during lateral attachment to plant cells. *mBio* **2**, e00218–00211 (2011).
80. Babic, A., Berkmen, M. B., Lee, C. A. & Grossman, A. D. Efficient gene transfer in bacterial cell chains. *mBio* **2**, e00027–11 (2011).
81. Carranza, G. et al. Monitoring bacterial conjugation by optical microscopy. *Front. Microbiol.* **12**, 750200 (2021).
82. Low, W. W. et al. Mating pair stabilization mediates bacterial conjugation species specificity. *Nat. Microbiol.* **7**, 1016–1027 (2022).
83. Niki, H. & Hiraga, S. Subcellular distribution of actively partitioning F plasmid during the cell division cycle in *E. coli*. *Cell* **90**, 951–957 (1997).
84. Gordon, S., Rech, J., Lane, D. & Wright, A. Kinetics of plasmid segregation in *Escherichia coli*. *Mol. Microbiol.* **51**, 461–469 (2004).
85. Klimke, W. A. & Frost, L. S. Genetic analysis of the role of the transfer gene, traN, of the F and R100-1 plasmids in mating pair stabilization during conjugation. *J. Bacteriol.* **180**, 4036–4043 (1998).
86. Verhoeven, G. S., Dogterom, M. & den Blaauwen, T. Absence of long-range diffusion of OmpA in *E. coli* is not caused by its peptidoglycan binding domain. *BMC Microbiol.* **13**, 66 (2013).
87. Jacob, F. & Wollman, E. L. Genetic and physical determinations of chromosomal segments in *Escherichia coli*. *Symp. Soc. Exp. Biol.* **12**, 75–92 (1958).
88. Stephens, K. M. & McMacken, R. Functional properties of replication fork assemblies established by the bacteriophage lambda O and P replication proteins. *J. Biol. Chem.* **272**, 28800–28813 (1997).
89. Sikora, B., Eoff, R. L., Matson, S. W. & Raney, K. D. DNA unwinding by *Escherichia coli* DNA helicase I (TraI) provides evidence for a processive monomeric molecular motor. *J. Biol. Chem.* **281**, 36110–36116 (2006).
90. Al Mamun, A. A. M., Kishida, K. & Christie, P. J. Protein transfer through an F plasmid-encoded type IV secretion system suppresses the mating-induced SOS response. *mBio* **12**, e0162921 (2021).
91. Garcillán-Barcia, M. P., Francia, M. V. & de La Cruz, F. The diversity of conjugative relaxases and its application in plasmid classification. *FEMS Microbiol. Rev.* **33**, 657–687 (2009).
92. Westra, E. R. et al. CRISPR-Cas systems preferentially target the leading regions of MOBF conjugative plasmids. *RNA Biol.* **10**, 749–761 (2013).
93. Benz, F. & Hall, A. R. Host-specific plasmid evolution explains the variable spread of clinical antibiotic-resistance plasmids. Preprint at *bioRxiv* <https://doi.org/10.1101/2022.07.06.498992> (2022).
94. Loh, S. M., Cram, D. S. & Skurray, R. A. Nucleotide sequence and transcriptional analysis of a third function (Flm) involved in F-plasmid maintenance. *Gene* **66**, 259–268 (1988).
95. Datsenko, K. A. & Wanner, B. L. One-step inactivation of chromosomal genes in *Escherichia coli* K-12 using PCR products. *Proc. Natl Acad. Sci. USA* **97**, 6640–6645 (2000).
96. Yu, D. et al. An efficient recombination system for chromosome engineering in *Escherichia coli*. *Proc. Natl Acad. Sci. USA* **97**, 5978–5983 (2000).
97. Cayron, J. & Lesterlin, C. Multi-scale analysis of bacterial growth under stress treatments. *J. Vis. Exp.* <https://doi.org/10.3791/60576> (2019).
98. Lesterlin, C. & Duabry, N. in *Chromosome Architecture* (ed. Leake, M. C.) Ch. 6, pp. 61–72 (Springer, 2016).
99. Ducret, A., Quardokus, E. M. & Brun, Y. V. MicrobeJ, a tool for high throughput bacterial cell detection and quantitative analysis. *Nat. Microbiol.* **1**, 16077 (2016).

Acknowledgements

The authors thank the National BioResource Project and Coli Genetic Stock Center for providing strains, A. Ducret for valuable help with

MicrobeJ and N. Fraikin for helpful discussion. This research was funded by the Foundation for Medical Research, grant number FRM-EQU202103012587 to C.L. and A.C.; the French National Research Agency, grant number ANR-18-CE35-0008 to C.L., Y.Y., and K. G.; and the University of Lyon through funding to C.V. C.L. also acknowledges the Schlumberger Foundation for Education and Research (FSER 2019).

Author contributions

C.L. and S.B. conceived, designed and supervised the execution of the study; A.C., C.V., K.G., A.B.-D., A.R., S.N. and S.B. performed the experiments and analysed the data. C.L. and S.B. wrote the paper and C.L. prepared the figures. C.L. and Y.Y. provided funding.

Competing interests

The authors declare no competing interests.

Additional information

Supplementary information The online version contains supplementary material available at <https://doi.org/10.1038/s41467-023-35978-3>.

Correspondence and requests for materials should be addressed to Sarah Bigot or Christian Lesterlin.

Peer review information *Nature Communications* thanks the anonymous reviewers for their contribution to the peer review of this work. Peer reviewer reports are available.

Reprints and permissions information is available at <http://www.nature.com/reprints>

Publisher's note Springer Nature remains neutral with regard to jurisdictional claims in published maps and institutional affiliations.

Open Access This article is licensed under a Creative Commons Attribution 4.0 International License, which permits use, sharing, adaptation, distribution and reproduction in any medium or format, as long as you give appropriate credit to the original author(s) and the source, provide a link to the Creative Commons license, and indicate if changes were made. The images or other third party material in this article are included in the article's Creative Commons license, unless indicated otherwise in a credit line to the material. If material is not included in the article's Creative Commons license and your intended use is not permitted by statutory regulation or exceeds the permitted use, you will need to obtain permission directly from the copyright holder. To view a copy of this license, visit <http://creativecommons.org/licenses/by/4.0/>.

© The Author(s) 2023

4. Discussion

Ce travail de recherche nous a permis de mettre en évidence la rapidité et l'efficacité du transfert conjugatif à l'échelle cellulaire. Seules 4 minutes sont nécessaires au transfert complet du plasmide dans la bactérie receveuse (du début du transfert d'ADNsb jusqu'à sa conversion en ADNdb), allant dans le sens des 100 minutes nécessaires au transfert complet du chromosome d'*Escherichia coli*. L'ensemble de nos observations nous a ainsi permis d'établir une chronologie globale des étapes de transfert, duquel ressort l'importance de la conversion en ADNdb du plasmide pour l'expression séquentielle des facteurs plasmidiques. La caractérisation du profil d'expression de la région *leading* constitue alors un pan important pour la suite de mes travaux de thèse. Nos observations par microscopie confirment que les gènes *leading* sont les premiers à être exprimés et ce de façon transitoire uniquement dans les nouvelles cellules transconjugantes. Nous confirmons ainsi *in vivo* l'importance des séquences *ssi Frpo1* et *Frpo2* comme promoteurs simples-brin pour l'expression de cette région génétique. La conversion en ADNdb du plasmide va abolir la formation des structures tiges-boucles de ces séquences, inactivant les gènes *leading* associés tout en permettant l'expression des autres facteurs plasmidiques sous le contrôle de promoteurs conventionnels.

Alors que notre approche ait permis de quantifier et confirmer le caractère précoce d'expression des gènes *leading*, la question concernant leur rôle pour la conjugaison demeure non-résolue. Bien qu'étant relativement conservés parmi les régions *leading* de plasmides appartenant à divers groupes d'incompatibilité, la majorité des mutants délétés de ces gènes n'impactent pas l'efficacité du transfert à proprement parler. Nous proposons cependant un rôle de la protéine Ssb^F pour la duplication du plasmide directement après son transfert dans la bactérie receveuse. En augmentant le réservoir général de protéines Ssb, la production d'une copie plasmidique serait ainsi une façon d'éviter à la bactérie hôte de diminuer trop drastiquement le nombre de protéines Ssb disponibles pour sa propre réplication ou réparation de son ADN. Ajouté à la fonction d'inhibition temporaire du système SOS par PsiB, nous proposons que la région *leading* constitue en réalité un cluster de gènes permettant de modérer l'impact de la conjugaison sur la physiologie de la bactérie receveuse, afin d'assurer le succès du transfert et établissement du plasmide au sein des populations bactériennes.

Enfin, la fusion fluorescente YfjB-sfGFP est la seule des protéines *leading* hormis Ssb-sfGFP à montrer une localisation précise en foci dans les bactéries transconjugantes. De fonction inconnue, YfjB partage de façon intéressante une homologie avec les protéines de la famille ParB, et les résultats observés et confirmés au laboratoire bien avant la publication de cet article nous ont amenés à nous intéresser à la protéine *leading* YfjB.

Partie III : Caractérisation de la protéine *leading* YfjB et son rôle lors du transfert du plasmide F par conjugaison bactérienne

The ParB-like protein YfjB of the leading region reprograms the gene expression profile of the cell during F plasmid conjugation

Chloé Virolle, Jérémy Guérin, Gaël Panis, Daouda A K Traore, Frédéric Delolme, Adeline Page, Rania Zenati, Annick Berne-Dedieu, Patrick Viollier, Sarah Bigot, Laurent Terradot & Christian Lesterlin

En préparation

1. Contexte

Au cours de la caractérisation de l'expression des gènes *leading* comme démontré dans l'article précédent, la localisation particulière en foci de la protéine de fusion YfjB-sfGFP a relevé notre intérêt, d'autant que cette protéine *leading* de fonction inconnue partage une homologie avec les protéines ParB. Sarah Bigot a alors entamé une première approche de caractérisation avant le début de ma thèse, notamment en réalisant diverses constructions génétiques et observations plus précises de la localisation cellulaire par microscopie à fluorescence en cellules vivantes. Ma thèse a alors débuté en octobre 2019 dans la continuité de ces travaux de recherche, aboutissant à l'écriture d'un article de thèse pour lequel je signe en tant que 1^{ère} auteur et dont une version préliminaire est présentée ci-après.

2. Contenu

Bien qu'il soit désormais acquis que la région *leading* est la première région génétique à être transférée dans la bactérie receveuse au cours de la conjugaison du plasmide F, les rôles et fonctions de gènes qui la compose sont encore très peu décrits. Nous avons déjà confirmé *in vivo* au laboratoire que les gènes *leading* sont exprimés précocement sous forme d'ADNs_b au cours du transfert conjugatif, transitoirement et uniquement dans les nouvelles cellules transconjugantes. Cette dynamique d'expression finement régulée ainsi que la conservation de cette région parmi les plasmides conjugatifs révèlent une importance de ces protéines *leading* pour l'établissement efficace du plasmide F lors de la conjugaison bactérienne. Mon projet de thèse avait ainsi pour but de répondre à certaines questions globales concernant le rôle de la région *leading* via la caractérisation de la protéine YfjB produite par le plasmide F au cours de la conjugaison chez *Escherichia coli* souche

K-12 MG1655. J'ai eu recours à une approche combinant à la fois la bio-informatique, la biochimie structurale, la génétique, la biologie moléculaire, les analyses omic et la microscopie à fluorescence en cellules vivantes. Nous démontrons que la protéine YfjB est produite rapidement après l'initiation du transfert conjugatif et est capable de lier l'ADN chromosomique et plasmidique, induisant un changement global du profil d'expression des gènes de la bactérie hôte. Cela est reflété par la formation de foci dynamiques de la protéine de fusion YfjB-sfGFP, dont la localisation dans la région du nucléoïde est dépendante d'un domaine HTH ainsi que d'un motif GxxRxxA, de façon similaire aux protéines ParB. Enfin, nous avons pu obtenir une structure partielle de la protéine par CryoEM révélant une dimérisation de la protéine via son domaine IV ainsi qu'une forte flexibilité des autres domaines.

L'article présenté ci-après rapporte les principaux résultats obtenus, mais consiste en une version préliminaire de la version qui sera soumise auprès d'un journal à comité de lecture. En effet, si les résultats présentés sont valides et significatifs, nous avons décidé d'entreprendre des expériences complémentaires qui permettront de finaliser ce travail. Principalement, nous avons encore du mal à réconcilier les changements transcriptionnels observés et les régions d'enrichissements de ChiP-seq. Il est donc prévu de répéter l'expérience de Chip-seq sur la fin de ma thèse en utilisant une étiquette HA plutôt que sfGFP pour revisiter les loci chromosomique de fixation d'YfjB *in vivo*. D'autre part, les grilles de CryoEM obtenues sont certes d'excellente qualité mais seule une partie de la protéine a pu être reconstruite au moment de l'écriture de ce manuscrit. Un affinement de la reconstruction structurale est en actuellement en cours, dans le but de couvrir plus de résidus de la protéine et espérer obtenir la structure des trois autres domaines qui jusque-là semblent être trop flexibles. L'obtention de ces derniers résultats permettra de finaliser ce projet qui aura permis de progresser sur la caractérisation de la dynamique cellulaire, l'activité de liaison à l'ADN, la structure et la fonction biologique de YfjB.

3. Ma contribution

Étant le sujet de ma thèse, j'ai ainsi effectué la majorité des travaux de recherche. D'abord abordé par Sarah Bigot concernant la construction génétique de certaines souches, analyses de bio-informatique et observations préliminaires de la localisation intracellulaire au microscope, j'ai pu reprendre la suite des analyses pour continuer la caractérisation de cette protéine à fonction inconnue. Cela a été pour moi l'opportunité d'avoir recours à des techniques variées allant des

observations de microscopie à fluorescence, la purification protéique, la biochimie structurale ou encore les quantifications de profils transcriptomiques et protéomiques. Pour cela j'ai pu être impliquée dans plusieurs collaborations, notamment avec Laurent Terradot et Jérémy Guérin (MMSB) pour la purification et analyses de biochimies, Daouda Traore (ILL) pour la CryoEM ainsi que Gaël Panis et Patrick Viollier (UNIGE) pour l'analyse de ChiP-seq.

1 **The ParB-like protein YfjB of the leading region reprograms the gene expression profile of the**
2 **new host cell during F plasmid conjugation**

3

4 Chloé Virolle^a, Jérémy Guérin^a, Gaël Panis^b, Daouda A K Traoré^{c,d,e}, Frédéric Delolme^f, Adeline
5 Page^f, Rania Zenati^a, Annick Berne-Dedieu^a, Patrick Viollier^b, Sarah Bigot^a, Laurent Terradot^a and
6 Christian Lesterlin^{a*}

7

8 ^aMolecular Microbiology and Structural Biochemistry (MMSB), Université Lyon 1, CNRS, Inserm,
9 UMR5086, 69007 Lyon, France

10 ^bDepartment of Microbiology and Molecular Medicine, Faculty of Medicine, University of Geneva,
11 Geneva, Switzerland

12 ^cFaculté des Sciences et Techniques, Université des Science Techniques et Technologiques de
13 Bamako (USTTB), Bamako, Mali

14 ^dFaculty of Natural Sciences, School of Life Sciences, Keele University, Staffordshire ST5 5BG,
15 United Kingdom

16 ^eLife Science Group, Institute Laue-Langevin, 38042 Grenoble, France

17 ^fProtein Science Facility, SFR BioScience, CNRS, University Lyon 1, ENS, 69007 Lyon

18

19 *Corresponding author: christian.lesterlin@ibcp.fr

20

21 **Abstract**

22 DNA conjugation is a contact-dependent horizontal gene transfer mechanism by which plasmids are
23 transferred between bacterial cells, thus causing the spread of antibiotics resistance. The F plasmid is
24 composed of different genetic regions including the leading, the maintenance and the transfer regions,
25 which are sequentially transferred into the recipient bacterium. Genes carried by the leading region
26 are not expressed in the donor cell but only transiently upon entry of the DNA in the new host cell,
27 thus suggesting a role in the early steps of plasmid establishment. In this study we focus on the *yffB*
28 gene, which is conserved amongst a variety of conjugative plasmids where it is generally annotated
29 *parB2* due to its homology with ParB-like family proteins. Live-cell microscopy reveals that YfjB
30 forms bright and dynamic foci associated with the nucleoid of the transconjugant cells. YfjB focus
31 formation depends on the Helix-Turn-Helix (HTH) domain and the CTP motif, as it is the case for
32 ParB proteins. We further show that YfjB is a DNA-binding protein that forms a dimer, which
33 structure has been partially resolved by Cryo-EM. Most importantly, we reveal that YfjB induces a
34 dramatic modification of chromosome gene expression in the transconjugant cell. The deletion of
35 *yffB* has no impact on the plasmid transfer efficiencies but delays the processing of the plasmid in the
36 transconjugant cell. These data lead us to propose that YfjB acts to reprogram the physiology of the
37 new host cell in a manner that facilitates the establishment of the F plasmid.

38

39

40 **Keywords**

41 Horizontal gene transfer, bacterial DNA conjugation, drug-resistance dissemination, live-cell
42 microscopy, plasmid transfer, CryoEM, transcriptomic, proteomic

43 **Introduction**

44 The F plasmid is a paradigmatic representative of a large group of conjugative plasmids associated
45 with the dissemination of colicins, virulence factors, and antibiotic resistance amongst
46 *Enterobacteriaceae* species (Lanza et al. 2014; Fernandez-Lopez et al. 2016; Johnson et al. 2016).
47 The 100 kb F plasmid is transferred into the recipient cell in single-stranded DNA (ssDNA) form
48 starting from the origin of transfer *oriT*, immediately followed by the leading region, the maintenance
49 region that carries the SopABC partition system and the origins of vegetative replication *oriV*, and
50 eventually the *tra* region that encoded all factors required for plasmid processing and transfer during
51 conjugation. By contrast with the *tra* and the maintenance regions, the function of the leading region
52 remains largely unclear. As the name indicates, the leading region was initially named after its
53 property to enter first into the recipient cell. It was later realized that leading genes are only expressed
54 transiently upon entry of the ssDNA plasmid in the recipient cell, but not during F vegetative
55 replication in the donor cell. This zygotic induction phenomenon depends on two sequences of the
56 leading region, *Frpo1* and *Frpo2* that act as single-stranded promoters before the plasmid is converted
57 into double-stranded (ds) DNA (Masai and Arai 1997; Couturier et al. 2023).

58 The difficulty to elucidate the function of the leading regions account for the fact that most
59 leading genes are unknown, except for *ssb^F* (F-encoded single-stranded-binding protein) and *psiB*
60 (Plasmid SOS Inhibition) (Chase, Merrill, and Williams 1983; Bailone et al. 1988; Bagdasarian et al.
61 1992; Althorpe et al. 1999; Baharoglu, Bikard, and Mazel 2010). The deletions of *ssb^F* and *psiB* have
62 no impact on the overall efficiency of conjugation in optimal laboratory conditions. However, Ssb^F
63 and PsiB have been respectively shown to facilitate plasmid replication (Couturier et al. 2023) and to
64 limit the induction of the SOS response in the transconjugant cell (Bagdasarian et al. 1992),
65 respectively. This led to the proposal that leading factors are not directly involved in the process of
66 DNA transfer *per se*, but rather help the establishment of the plasmid, eventually favouring its success
67 on the evolutionary scale. Consistently, the leading region is conserved in various enterobacterial

68 plasmids belonging to multiples incompatibility groups (Golub and Low 1985; Loh, Cram, and
69 Skurray 1989; Bates et al. 1999; Wein et al. 2021; Benz and Hall 2022).

70 In this study, we investigate the structure and function of the *yffB* leading gene, which is
71 conserved in 13.8 % of the 420 plasmids studied by Wein *et al.* (58 “*parB2*” for 420 plasmids). It is
72 generally annotated *parB2* as it shares homology with the protein of the ParB family. ParB proteins
73 are part of the ParABS partitioning complex encoded by low copy number plasmids and bacterial
74 chromosomes. This system ensures the efficient distribution of chromosome or plasmid copies
75 between mother and daughter cells during cell division (Bignell and Thomas 2001). ParB protein will
76 therefore specifically bind to the *parS* centromere-like sequence via an Helix-Turn-Helix (HTH)
77 domain. A CTP motif (GxxRxxA) is important for CTP hydrolysis to CDP, inducing the spreading
78 of the protein on surrounding DNA by conformational change and thus allowing new ParB molecules
79 to bind to the *parS* sequence (Soh et al. 2019; Osorio-Valeriano et al. 2021). More recently, several
80 ParB-like proteins have been reported to be involved in a variety of biological functions unrelated to
81 DNA segregation. Examples are found for the RK2 plasmid protein KorB, that binds to 12 DNA sites
82 for transcription regulation (Bingle et al. 2005), or also for the pSa plasmid whose Osa protein is a
83 fertility inhibition factor (FIN) that selectively degrades the DNA of co-resident mobilizable
84 elements, thus blocking their transfer (Maindola et al. 2014).

85 **Results**

86 ***Genetic organisation and bioinformatic sequence analysis***

87 The *yjfB* gene (1956 bp) is localised in the *leading* region of the F plasmid, as part of the *Frpo2*
88 operon alongside *ssb^F*, *yjfA*, *psiB*, *psiA* and *flmC* (Figure 1A). Bioinformatic analysis (BlastP) of the
89 653 amino-acids sequence of the YfjB protein reveals a strong homology with the ParB/RepB/Spo0J
90 protein family from residues 36 to 243 (E-value: $6.07e^{-27}$), and an even strongest homology with
91 ParB_N_like domains within the 55-135 interval (E-value of $4.27e^{-30}$) (Figure 1B). We also predicted
92 a HTH motif on position 154-175 with 90% probability score using the Helix-Turn-Helix search tool
93 from the PRABI website (<https://prabi.ibcp.fr>) and found a GxxRxxA sequence similar to ParB's
94 CTP motif from residues 91 to 97 (Figure 1B). AlphaFold2 deep learning program (Senior et al. 2020)
95 predicted that YfjB is composed of 4 domains (Figure 1B-C). The domain I (14-136) contains the
96 ParB_N_like homology as well as the CTP motif, and the domain II (137-235) contains the HTH
97 domain. Together they composed the homology to Spo0J superfamily. Structure comparison using
98 the MatchMaker tool (Chimera software) reveals that YfjB predicted domains I and II overlap with
99 the N-terminal part of ParB (residues 34 to 237) from *Bacillus subtilis* (model 6SDK taken from
100 RCSB PDB) (Soh et al. 2019) (Figure 1C). The domains III (238-417) and IV (418-632) do not share
101 any homology with known protein domains. The ProtParam tool (Gasteiger et al. 2005) of the ExPASy
102 server website predicts that YfjB has a molecular weight of 71 759.54 Da, a theoretical pI of 5.11, an
103 extinction coefficient of $80\,285\text{ M}^{-1}\text{cm}^{-1}$ and an estimated *in vivo* half-life of ~10 hours in *Escherichia*
104 *coli*.

105

106 ***YfjB localises into nucleoid-associated foci***

107 We previously developed a system allowing to monitor the intracellular levels of YfjB in the cell
108 population during conjugation of the F plasmid. In this system, the Donor transfers a F *yjfB-sfGFP*
109 plasmid that carries a *superfolder gfp* (*sfgfp*) translational fusion to the 3' end of the *yjfB* gene and a
110 *parS* site located next to the origin of transfer *oriT*. The recipient cell produces the mCh-ParB protein,

111 which is initially diffuse in the cytoplasm. Acquisition of the dsDNA F *yffB-sfGFP* plasmid triggers
112 the recruitment of mCh-ParB molecules to the *parS* site, thus resulting in the formation a red
113 fluorescent focus in the transconjugant cell. We previously reported that plasmid acquisition is
114 immediately followed by the production of YfjB-sfGFP in the new host cell (Couturier et al. 2023).
115 Here, we monitored YfjB-sfGFP intracellular levels in cell population over nine hours of conjugation
116 (Figure 1D). Results confirm that YfjB-sfGFP is produced in *de novo* transconjugants only and that
117 this production is transient since YfjB-sfGFP intracellular level peaks 2.5 hours after the initiation of
118 conjugation and subsequently decreases to reach minimal levels after 8.5 hours (Figure 1D). Most
119 importantly, YfjB-sfGFP forms bright fluorescent foci that exhibit a precise localisation pattern
120 within the transconjugant cells (Figure 1E). Small transconjugants harbour one single YfjB-sfGFP
121 focus located around the midcell position while larger cells have multiple foci located in the cell
122 quarter regions (Figure 1F). The number of foci per cell increases with the cell length (Figure 1G)
123 from 1 to 5 with an average of $1.6 \pm 0,7$ foci per cell (Figure 1H).

124 The F *yffB-sfGFP* plasmid only allows YfjB-sfGFP production in the transconjugant
125 subpopulation on the conjugation mix. We then constructed a pTrc99a *yffB-sfGFP* plasmid that
126 allows the ectopic production of YfjB-sfGFP in the entire population of vegetatively growing cells
127 (Figure S1A). The level of green fluorescence produced from the pTrc99a *yffB-sfGFP* plasmid is
128 comparable to that produced from the F *yffB-sfGFP* plasmid in transconjugant cells (Figure S1B), yet
129 the number of foci is slightly increased to 2.2 ± 1 foci per cell on average (Figure S1C). Nonetheless,
130 the localisation pattern of these foci is similar to those observed in F *yffB-sfGFP* transconjugant cells
131 (compare Figure S1D to figure 1F). We also analysed F *yffB-sfGFP* transconjugant cells that carry a
132 pTrc99a *yffB-mCh* plasmid (Figure S1E) and observed that the co-produced fluorescently tagged
133 proteins YfjB-sfGFP and YfjB-mCh exhibit similar intracellular localisation (Figure S1F). These data
134 show that YfjB-sfGFP exhibit similar localisation in the presence or the absence of the F plasmid,
135 whether it is produced from the F *yffB-sfGFP* plasmid in transconjugant cells or from the pTrc99a
136 *yffB-sfGFP* plasmid in vegetatively growing MG1655 F- cells.

137 We then continued the characterization of YfjB-sfGFP localisation using *E. coli* cells that
138 carry the pTrc99a *yfjB-sfGFP* plasmid and produce the fluorescently tagged nucleoid-associated
139 protein HU-mCherry (Fisher et al. 2013) (Figure 1I). Fluorescence distribution analysis of
140 exponentially growing cells (M9GlucoseCASA) shows that YfjB-sfGFP fluorescence overlaps with
141 Hu-mCh, consistent with the observation that YfjB-sfGFP foci are located within the nucleoid area
142 and excluded from the polar regions of the cells (Figure 1J). YfjB-sfGFP localisation on the nucleoids
143 is maintained in different growth media (M9Glucose and Rich Defined Medium), which modulate
144 the growth rate, the cell size and the number of nucleoids per cells (Figure S1G-I). These results
145 reveal that YfjB-sfGFP localisation correlates with the nucleoid DNA localisation throughout the cell
146 cycle (Figure S1H-J), suggesting that YfjB-sfGFP binds to the chromosome DNA.

147

148 ***YfjB focus formation depends on the Helix-Turn-Helix domain and CTP motif***

149 AlphaFold2 structure prediction allowed us to predict that residues R168, R172 and K175 of YfjB
150 HTH domain are likely to be involved in the interaction with the DNA double helix (Figure 2A).
151 Therefore, we performed snapshot imaging of cells producing a range of YfjB-sfGFP mutant proteins
152 from pTrc99a *yfjB-sfGFP* plasmid derivatives (Figure 2B-(i)) and analysed the fluorescence
153 skewness (Figure 2C). Skewness analysis provides a non-biased measure of asymmetry of
154 fluorescence distribution within the cells without any requirement for threshold-based foci detection.
155 Skewness values are low when the fluorescence is diffused within the cell, and increase as the
156 fluorescence is locally concentrated in foci. Cells producing a free mCherry (mCh) exhibit a low
157 skewness of -0.66 ± 0.19 reflecting the homogeneous pixel fluorescence distribution inside the
158 cytoplasm (Figures 2B-(ii) and 2C). In exponentially growing cells, the *wt* YfjB-sfGFP protein is
159 locally concentrated within bright foci resulting in a skewness of 1.86 ± 0.82 . Deletion of the entire
160 HTH domain resulted in the loss of foci, reflected by a skewness of -0.36 ± 0.41 (Figure 2C). Single
161 mutations of the HTH domain altered YfjB-sfGFP foci formation, resulting in a decreased skewness
162 of 0.37 ± 0.43 , 0.04 ± 0.29 and 0.39 ± 0.61 for the R168A, R172A and K175A mutations, respectively.

163 Besides the HTH domain, recent published work demonstrates that the CTP motif of ParB proteins
164 is important for focus formation *in vivo* as well as for its segregation function (Graham et al. 2014;
165 Soh et al. 2019; Osorio-Valeriano et al. 2021). Therefore, we tested the effect of the single R94A
166 mutation of YfjB CTP motif, and observed the loss of focus formation reflected by a skewness of -
167 0.14 ± 0.24 (Figure 2C). These experiments confirm the importance of the identified HTH and CTP
168 domains for YfjB focus formation *in vivo*, similar to what is reported for ParB-like proteins.

169

170 ***Biochemical and structural characterization of YfjB***

171 We purified the YfjB protein from a pET-Topo151 plasmid vector in *Escherichia coli* BL21 cells
172 (Figure S2A). Size exclusion chromatography (SEC) and multi-angle light scattering (MALS)
173 allowed to measure a molecular weight of 144 kDa, twice bigger than the 71.5 kDa calculated via
174 ProtParam analysis, thus revealing that the YfjB protein forms homodimers in solution (Figure S2B).
175 Next, we attempted to solve YfjB structure using cryogenic electron microscopy (CryoEM). We
176 collected a total of 8 396 images from which 7 380 496 particles were picked for 2D classes
177 construction (Figure 3A), among which 191 738 were retained to reconstruct a structural model
178 (Figure 3B(i)). A non-uniform refinement gives a 3.7Å map of “dome” of the protein consisting of a
179 dimer of the domain IV (residues 424 to 636) that fits with the AlphaFold2 predicted structure (Figure
180 3B(ii)). So far, we failed to solve the structure of domains I, II and III composing the “legs” of the
181 dimeric protein, as they appear highly flexible. Interestingly, it is also possible to observe a kind of
182 ring-shape depending on the conformation of the protein particles (Figure 3A). Nonetheless, these
183 data allow us to propose a model for the structure of the YfjB dimer (Figure 3C). These information
184 about the dimerization of the YfjB protein are essential to better understand the function of the protein
185 and explain its specific localisation observed by previous fluorescent microscopy analysis. Not only
186 YfjB shares a sequence homology with ParB-like proteins, but the dimerization of YfjB is also
187 comparable to the dimerization of the partition proteins.

188

189 ***YfjB DNA binding activity***

190 Next, we performed ChiP-seq experiments to address the *in vivo* profile of YfjB DNA-binding after
191 1.5 hours of conjugation of the F *yfjB-sfGFP* plasmid. Results reveals 19 loci of YfjB binding
192 enrichment distributed along the chromosome, without any specific location preference (Figure 4A).
193 The coverage of the binding peaks is comprised between 346 pb and 2971 pb of length, with a median
194 of about 532 pb. No consensus motif was currently associated with the corresponding DNA
195 sequences. Few enrichments are also observed onto the F plasmid DNA (data not shown), but none
196 of them are statistically conclusive based on the threshold chosen above 1 log fold change.

197 Electrophoretic mobility shift assay (EMSA) was then performed in order to confirm the
198 specificity of this binding *in vitro* (Figure 4B). Two “specific” DNA sequences of 250pb were chosen
199 based on ChiP-seq peaks observed in both conditions and correspond to the intergenic regions *dhaK*-
200 *dhaR* (DNA 1) and *glnL-glnA* (DNA 2) of the *E.coli* chromosome. Increased concentrations of YfjB
201 protein confirm a DNA binding for a ratio of 100 YfjB molecules for 1 molecule of DNA until
202 saturation of the DNA is observed above for both “specific” DNA sequences (Figure 4B(i)-(ii)). We
203 controlled that no shift was observed in the presence of BSA instead of YfjB (Figure 4B(iii)), while
204 the addition of CTP reduces the migration shift (Figure 4B(iv)). A “non-specific” DNA sequence of
205 250 pb as well (DNA 3) corresponding to a sequence not found in any ChiP-seq experiments was
206 also tested and YfjB presence also induces a shift of DNA migration (Figure 4B(i)-(ii)-(iii)).

207

208 ***In vivo phenotype: OMIC approach***

209 In order to get insight into YfjB biological function *in vivo*, we analysed the effect of YfjB
210 production on the profile of gene expression and protein level using transcriptomic and proteomic
211 analysis. These approaches require the extraction of total RNAs and proteins from the cell population.
212 However, during conjugation, transconjugant cells that produce YfjB only represent a fraction of the
213 total cell conjugation population that also includes donors and recipient cells. This rendering the
214 analysis of total RNAs and proteins extracts from conjugation mixes polluted by the material from

215 the donors and recipient cells in which YfjB is not produced. To circumvent this limitation, we
216 performed RNAseq and TMT-mass spectrometry analysis by comparing cells ectopically producing
217 YfjB from the pTrc99a *yfjB-sfGFP* plasmid to cells carrying the empty pTrc99a plasmid.

218 RNA-seq results show that a total of 2 862 genes have their expression affected when YfjB is
219 produced in the cells. Amongst them, 17.6% are significantly repressed (505 genes) and 12.6% are
220 significantly overexpressed (361) (Figure 5A). *Escherichia coli* K-12 MG1655 strain genome is
221 composed of approximately 4 268 genes, meaning that constitutive production of YfjB from the
222 pTrc99a plasmid affects between 15.4% and 20% of its host genome. This data is consistent with
223 transcriptomic studies in the literature showing that plasmids affect from 0.59% to 20% of their host
224 genome (Coulson et al. 2015; Billane et al. 2022). By looking in the functions of the genes affected,
225 we found 52 transcriptional regulators (Figure S5B), including *arcA*, *narL* or *hcaR* master regulators
226 which are known to regulate the transcription of a variety of genes. Subtraction of the genes
227 composing the regulons of these transcriptional regulators helped us to decrease the list to a total of
228 2 655 genes that are “directly” affected by the presence of YfjB. 13% of these genes are significantly
229 repressed (346 genes) and 11.7% overexpressed (313 genes) in presence of YfjB (Figure 5A). These
230 genes are involved in various functional pathways including anaerobic respiration, glycolysis and
231 gluconeogenesis, branched-chain amino acid biosynthesis, TCA cycle, glycerol catabolism and sulfur
232 metabolism, according to the DAVID bioinformatics resources website (<https://david.ncifcrf.gov/>)
233 (Table 1; Figure 5D).

234 We then performed several experiments to determine whether gene expression changes
235 revealed by the RNA-seq analysis could be validated by assays addressing the physiology and
236 metabolic activity of the cells. RNA-seq data indicated that YfjB production induces the repression
237 of 37 genes involved in the anaerobic respiration. This effect is expected to alter redox state of the
238 cells which we characterised using the AlamarBlue kit based on the reduction of resazurin to
239 resorufin. We observed a decrease in resazurin reduction in the presence of YfjB (23.7%) compared
240 to *wt* strains and ones with empty pTrc99a (33.3% and 32.2% respectively) (Figure S3A). The higher

241 change in expression concerns the *yhjX* gene, which encodes a MFS-type transporter of pyruvate.
242 That induction of the *yhjX* gene is specifically induced by the *ydpAB* two component system in the
243 presence of high concentration of extracellular pyruvate (Fried, Behr, and Jung 2013; Vilhena et al.
244 2018). This suggests that YfjB production could be associated with metabolic changes resulting in
245 increased excretion of pyruvate in the extracellular medium. To test this hypothesis, we performed
246 pyruvate assay to quantify the concentration of extracellular pyruvate in presence and absence of
247 YfjB. The ectopic production of YfjB increases extracellular pyruvate concentration to 3.92 ± 0.81
248 $\text{ng}/\mu\text{L}$ compared to $3.3 \pm 0.2 \text{ ng}/\mu\text{L}$ and $2.2 \pm 0.5 \text{ ng}/\mu\text{L}$ for the *wt* strain with or without the empty
249 pTrc99a plasmid, respectively. The deletion of the HTH domain from YfjB reduces the extracellular
250 concentration of pyruvate to $1.96 \pm 0.45 \text{ ng}/\mu\text{L}$ (Figure S3B). This phenotype of increased pyruvate
251 concentration in the extracellular medium explains the strong overexpression of the *yhjX* gene in the
252 presence of the YfjB protein. Pyruvate is directly associated with acetate biosynthesis, but genes
253 involved in this pathway are repressed in the presence of YfjB according to RNAseq data (*aceEF*).
254 An acetate assay was done to quantify the concentration of extracellular acetate in presence and
255 absence of YfjB. No significative difference is observed between a *wt* strain and a strain harbouring
256 the empty pTrc99a plasmid ($18.67 \pm 2.22 \text{ ng}/\mu\text{L}$ and $17.67 \pm 1.6 \text{ ng}/\mu\text{L}$ respectively), while a slight
257 decrease to 15.96 ± 2.09 in extracellular concentration of acetate is observed in presence of YfjB
258 (Figure S3C). These data indicate that the production of YfjB triggers metabolic changes that result
259 in a strong increase of pyruvate excretion, which is however not associated with increased acetate
260 production. Finally, genes involved in fimbriae associated adhesion are mainly found upregulated in
261 our RNA-seq data (*fimDFG*, *ydeQRST*, *smfFH* or *flgBC*) and confirmed by a 3-fold decreased motility
262 on soft agar plates (0.2%) compared to a plasmid-free bacterium (Figure S3D).

263 In parallel, the same cell samples used for RNA sequencing were used to prepare total protein
264 extract for Tandem Mass Tag (TMT) Mass spectrometry analysis, allowing the relative quantification
265 of peptides between two given samples. Compared to cells containing the empty pTrc99a plasmid,
266 ectopic production of YfjB changes the abundance of 195 proteins inside the bacteria. 13.8% of them

267 are significantly over-represented (27 genes) and 5.6% of them are under-represented (11 genes)
268 (Figure 5C). A total of 127 genes are found in both RNA sequencing (4.7% of total RNA-seq genes)
269 and TMT-Mass spectrometry experiments (65% of total TMT-Mass spectrometry genes) (Figure 5C).
270 Only 17 of them are found significantly changed in both experiments, and can be grouped into distinct
271 metabolic groups. Genes involved in leucine, isoleucine and valine biosynthesis pathways are found
272 both overexpressed and their gene product overrepresented (*leuABCD*). On the contrary, genes of the
273 glycerol metabolism (*glpFKQ*) and maltose metabolism (*malEMP lamB*) are found repressed and
274 their gene product underrepresented. To confirm a phenotype associated with these results, bacterial
275 growth was compared between cells containing the empty pTrc99a plasmid and the plasmid
276 producing YfjB in presence of glucose, glycerol or maltose as carbon source (Figure S3E). But
277 contrarily to what was expected, bacterial growth was rather increased for cells producing YfjB when
278 adding glycerol to minimal medium M9, while bacterial growth using glucose was negatively affected
279 (Figure S3E-(i)-(ii)). These results point out the complexity of metabolism pathways and phenotypes
280 associated with different genes regulations.

281

282 ***In vivo phenotype: genetic approach***

283 The conservation of *yffB* on *leading* regions of multiple conjugative plasmids as well as the
284 early and transient production of the corresponding protein inside transconjugants cells led us to
285 suggest a role of the protein for the early steps of F plasmid transfer and establishment. However,
286 deletion of the *yffB* gene doesn't seem to affect the frequency of F plasmid transfer after 1 hour, 2
287 hours or 3 hours of conjugation (Figure 6A). These results only confirm that YfjB is not essential for
288 the maintenance and dissemination of the plasmid in laboratory conditions. We therefore wanted to
289 monitor in more details the impact of *yffB* deletion at the cellular level. Using fluorescent microscopy
290 in live cells, we followed the transfer of the single-stranded DNA (ssDNA) using the Ssb-Ypet fusion
291 protein (Couturier et al. 2023). When *yffB* is deleted of the F plasmid, the ssDNA is present during
292 the same period of time as the F *wt* inside both the donor bacteria (2.5 ± 1.1 minutes and 2.6 ± 1.5

293 minutes respectively for the F *wt* and F $\Delta yffB$) and the recipient bacteria (2.9 ± 1.1 minutes and $3 \pm$
294 1.7 minutes respectively for the F *wt* and F $\Delta yffB$) (Figure 6B). Therefore, YfjB is not involved in
295 the step of transfer of the ssDNA toward the recipient bacteria. Then we followed the lag-time before
296 conversion to double-stranded DNA using the *parS*/ParB system (Goldlust et al. 2022). A *parS*
297 sequence inserted inside the F plasmid will induce the specific binding of a mCh-ParB protein
298 produced from a pSN plasmid inside the recipient bacteria, monitored by the formation of a mCherry
299 focus inside the transconjugant. Thus, we observe an increase of time lag for Ssb-Ypet to mCh-ParB
300 focus appearance between the F *wt* (4 ± 1.8 minute) and the F $\Delta yffB$ (5.3 ± 2.8) (Figure 6C). This
301 increase of 1.3-fold reveals a delay of F plasmid conversion to dsDNA in absence of YfjB, suggesting
302 a role for the establishment of the conjugative plasmid inside *de novo* transconjugants.

303 Discussion

304 In our study, we combine various technics from live cell microscopy to structural biochemistry
305 and omics to unravel the YfjB protein function during F plasmid conjugation in *Escherichia coli* cells.
306 These approaches helped us to better understand the hypothetical role of this “ParB2” plasmidic
307 protein that was still not studied and give some new insights concerning the *leading* region role for
308 rapid and successful plasmid establishment during bacteria conjugation.

309 Here we confirmed the YfjB homology with ParB proteins by the conservation of a helix-
310 turn-helix (HTH) domain and a GxxRxxA motif both important for ParB proteins dynamic and
311 function. These are also involved in YfjB intracellular localisation, as different mutations in these
312 sequences impede the bright foci formation of the protein fused to the sfGFP fluorescent marker. We
313 also confirmed a binding to at least 19 DNA sites *in vivo* by ChiP-seq experiment in a conjugation
314 context, and two of the corresponding peaks observed were confirmed to be associated with specific
315 binding of YfjB *in vitro* by EMSA experiment. This binding could explain the transcriptomic and
316 proteomic changes observed during the ectopic production of YfjB. The presence of the protein
317 affects at least 15% of the genomic transcription of the host bacteria, involving genes that are part of
318 various cellular functions for which multiples phenotypes were experimentally confirmed, such as
319 transcription regulation, secondary metabolites pathways, gluconeogenesis, mobility or even
320 respiration. It is therefore quite consistent with observations in the literature that conjugative plasmids
321 are able to affect between 0.56% and 20% of the host genetic expression (Billane et al. 2022). Like
322 so, plasmids affect similar cellular pathways in order to modulate the host physiology for their own
323 benefit. Among them, the cells’ motility is reduced in presence of YfjB; cell-to-cell contact is
324 essential for efficient and successful conjugation, and these observations could be reflected by an
325 increased time of contact between cells needed for better conditions of plasmid transfer (Luque et al.
326 2019; Billane et al. 2022). Moreover, better use of other carbon sources than glucose by the host cell
327 when YfjB is produced could provide less competition with surrounding bacteria and might be
328 involved in bacterial survival during conjugative transfer or competition (Billane et al. 2022).

329 Additionally, an increased cellular oxidation can reflect the repression of fermentation genes induced
330 by YfjB, usually associated with anaerobic respiration and a switch from exponential to stationary
331 growth phase. Favouriting respiration pathway can provide more energy for the cells although they
332 are in late exponentially growth in order to compensate the metabolic burden that is often associated
333 with plasmid acquisition and genetic expression.

334 One can wonder how a single protein can affect the expression of so much genes, but still not
335 being important for the efficacy of transfer itself? First, maybe YfjB is able to interact non-
336 specifically to the DNA, like observed for ParB proteins when they are spreading onto the
337 surrounding DNA of a *parS* sequence after CTP hydrolysis to CDP. In addition to a constant and
338 slightly increased concentration of YfjB during its ectopic production, this could explain an increase
339 in DNA sites covered by the protein (data not shown) and thus the diversity of genes affected in RNA-
340 seq experiment. Secondly, as the *leading* gene expression is inhibited during conjugation by
341 inactivation of *Frpo2* after dsDNA conversion, the YfjB protein is diluted during 9 hours of bacterial
342 division until no protein is present in late transconjugants anymore. This transient and temporary
343 production of YfjB during conjugation may regulate the binding and functionality of the protein to
344 its essential. To assess the difference compared to ectopic production of YfjB, we need to establish a
345 way to select for transconjugants producing YfjB in quantities important enough to describe a proper
346 phenotype due to its expression during the F plasmid conjugation. It therefore must be important to
347 avoid affecting the global transcription profile of the bacteria, as it can be observed during antibiotic
348 resistance selection for example. Whilst deleting *yffB* doesn't impact de final efficacy of conjugation
349 of the F plasmid in our conditions, it therefore increased up to 30% the ss-to-dsDNA delay
350 conversion. Plasmid-mediated alterations of the bacterial phenotype may have niche-adaptive
351 consequences that may be missed in simplified and optimum laboratory conditions (Vial and
352 Hommais 2020). In that way, the absence of *yffB* could be deleterious for the F plasmid transfer in
353 more stressful environment (temperature, pH) or during inter-species conjugation. The phenotypic

354 changes induced by the YfjB protein upon the initiation of transfer could be an advantage for the
355 rapidity and efficiency of plasmid transfer in competition with other mobilizable elements.

356 Finally, only the structure of the domain IV composing the “dome” of the YfjB protein was
357 obtained, and shows a stable dimer formation of the protein confirmed by Sec-MALS experiment. As
358 seen on the 2D classes images, the three other domains form the “legs” of the structure and seem to
359 be very flexible, impeding their structure reconstruction. This observation was at first surprising,
360 because we were expecting an easier reconstruction of the two first domains as they are the ones
361 sharing the ParB homology. This reflects the ability of the protein to change in conformation
362 depending on the conditions. Maybe it acts similarly to ParB proteins, whose conformation change
363 first by DNA-binding and then by CTP hydrolysis to CDP. The structure refinement is still ongoing
364 in hope to cover additional residues and therefore finalise the protein structure. If the experiment is
365 to be repeated, addition of non-hydrolysable CTP or a DNA sequence to the purified protein before
366 Cryo-EM data collection could be very interesting to test in order to stabilize the protein in at least
367 one more stable conformation.

368 In conclusion, our study provides yet another example of a ParB-family protein member that
369 does not play a role in DNA segregation but seem to be rather important for host genetic profile
370 reprogramming. The exact action mechanism of transcription changes induced in presence of YfjB is
371 still not clear, but our results constitute a considerable step toward the comprehension of *leading*
372 region role. Like so, YfjB could act similarly as the Ssb^F and PsiB *leading* proteins in order to spare
373 the host physiology and limit the metabolic burden associated with plasmid acquisition and proteins
374 production.

375

376 **Acknowledgements**

377 The authors thank the National BioResource project, the Coli Genetic Stock Center, R. Reyes-
378 Lamothe and F. Cornet for providing strains, C. Tessa for medium preparation and A. Ducret for help
379 with MicrobeJ. **Funding:** This research was funded by the Foundation for Medical Research (grant

380 number FRM-EQU202103012587 to C.L); the French National Research Agency (grant number
381 ANR-18-CE35-0008) and the University of Lyon for funding to C.V. **Author contributions:** C.V.,
382 A-BD and S.B. constructed strains and plasmids; C.V. and S.B. acquired and analysed microscopy
383 images; C.V., J.G., D.T. and L.T. achieved protein purification and structural analysis; C.V., G.P.
384 and S.B. prepared and analysed Chip-seq samples; C.V., F.D. and A.P. did the mass-spec
385 experiments. C.V. and C.L. wrote the paper and prepared the figures. L.T., P.V. and C.L. hosted the
386 research and provided funding.

387 **Competing Interests:** The authors declare no competing interests.

388 **Methods**

389 **Bacterial strains, plasmids and growth**

390 Bacterial strains are listed in Table S1, plasmids in Table S2 and primers in Table S3. Fusion of genes
391 with fluorescent tags and gene deletion on the F plasmid used λ Red recombination (Datsenko and
392 Wanner 2000; Yu et al. 2000). Modified F plasmids were transferred to the background strain K12
393 MG1655 by conjugation. When genetic modification on the F plasmid were required, the *kan* and *cat*
394 gene were removed using site-specific recombination induced by expression of the FIp recombinase
395 from plasmid pCP20 (Datsenko and Wanner 2000). Plasmid cloning were done by Gibson Assembly
396 and verified by Sanger sequencing (Eurofins Genomics biotech). Strains and plasmids were verified
397 by Sanger sequencing (Eurofins Genomics biotech). Cells were grown at 37°C in M9 medium
398 supplemented with glucose (0.2%) (M9-Glucose) and casamino acid (0.4%) (M9-CASA) before
399 imaging; Rich Defined Medium (RDM) was also used for some microscopic experiments. When
400 needed, glucose was replaced as carbon source by glycerol (0.2%) or maltose (0.2%). Cells were
401 grown at 37°C in Luria-Bertani (LB) broth for other assays (Sigma Aldrich). When appropriate,
402 supplements were used in the following concentration: Ampicillin (Ap) 100 μ g/mL, Kanamycin (Kn)
403 50 μ g/mL, Streptomycin (St) 20 μ g/mL and Tetracyclin (Tc) 10 μ g/mL.

404

405 **Conjugation assays**

406 Overnight cultures in LB of recipient and donor cells were diluted to an A_{600} of 0.05 and grown until
407 an A_{600} comprised between 0.7 and 0.9 was reached. 25 μ L of donor and 75 μ L of recipient cultures
408 were mixed into an Eppendorf tube and incubated for 90 minutes at 37°C. 1 mL of LB was added
409 gently and the tubes were incubated again for 90 minutes at 37°C. Conjugation mix were vortexed,
410 serial diluted, and plated on LB agar X-gal 40 μ g/mL IPTG 20 μ M supplemented with the appropriate
411 antibiotic to select for recipient or donor population. Recipient (R) colonies were then streaked on
412 plates of LB agar containing Tetracyclin 10 μ g/mL to select for transconjugants (T) and the frequency
413 of transconjugant calculated from the (T/R+T) ratio presented in Figure 6A.

414 **Live-cell microscopy experiments**

415 Overnight cultures in M9-CASA were diluted to an A_{600} of 0.05 and grown until A_{600} comprised
416 between 0.7 and 0.9 was reached for conjugation analysis. Conjugation samples were obtained by
417 mixing 25 μ L of donor and 75 μ L of recipient into an Eppendorf tube. For time-lapse experiments, 50
418 μ L of the pure culture of conjugation mix was loaded into a B04A microfluidic chamber (ONIX,
419 CellASIC®) (Cayron and Lesterlin 2019). Nutrient supply was maintained at 1 psi and the
420 temperature maintained at 37°C throughout the imaging process. Cells were images every 1 or 5
421 minutes for 90 to 120 minutes. For snapshot imaging, overnight cultures in M9-CASA, M9-Glucose
422 or RDM were diluted to an A_{600} and grown until A_{600} of 0.2 was reached for analysis of exponentially
423 growing cells and 10 μ L samples of clonal culture or conjugation mix were spotted onto an M9-CASA
424 1% agarose pad on a slide (Lesterlin and Duabrry 2016) and imaged directly.

425 *Image acquisition.* Conventional wide-field fluorescence microscopy imaging was carried out on an
426 Eclipse Ti2-E microscope (Nikon), equipped with x100/1.45 oil Plan Apo Lambda phase objective,
427 ORCA-Fusion digital CMOS camera (Hamamatsu), and using NIS software for image acquisition.
428 Acquisition were performed using 50% power of a Fluo LED Spectra X light source at 488 nm and
429 560 nm excitation wavelength. Exposure settings were 100 ms for Ypet, sfGFP and mCherry and 40
430 ms for phase contrast.

431 *Image analysis.* Quantitative image analysis was done using Fiji software with MicrobeJ plugin
432 (Ducret, Quardokus, and Brun 2016). For snapshot analysis, cells' outline detection was performed
433 automatically using MicrobeJ and verified using the Manual-editing interface. For time-lapse
434 experiments, detection of cells was done semi-automatedly using the Manual-editing interface, which
435 allows to select the cells to be monitored and automatically detect the cell outlines. Within
436 conjugation populations, donor (no mCh-ParB signal), recipient (diffuse mCh-ParB signal), or
437 transconjugant (mCh-ParB foci) categories were assigned using the "Type" option of MicrobeJ.
438 Recipient cells were detected on the basis of the presence of red fluorescence above the cells'
439 autofluorescence background level detected in the donors. Among these recipient cells,

440 transconjugants were identified by running MicrobeJ automated detection of the ParB fluorescence
441 foci (Maxima detection). This approach was used independently of the presence or absence of the
442 Ssb-Ypet or YfjB-sfGFP fusions within donor and recipient cells. Within the different cell types,
443 skewness, Signal/Noise Ratio (SNR) or cell length (μm) parameters were automatically extracted and
444 plotted using MicrobeJ. SNR corresponds to the ratio (mean intracellular signal / mean noise signal),
445 where the mean intracellular signal is the fluorescence signal per cell area and the noise is the signal
446 measured outside the cells (due to the fluorescence emitted by the surrounding medium). By contrast
447 with the total amount of fluorescence per cell, which is depending on the cell size/age and accounts
448 for the background, SNR quantitative estimate is more appropriate for unbiased quantification of
449 intracellular fluorescence over time. YfjB-sfGFP and YfjB-mCh foci were detected using MicrobeJ
450 Maxima detection function, and foci localisation and fluorescence intensity were extracted and
451 plotted automatically.

452

453 **Gene cloning, protein expression and purification**

454 6his-TEV-YfjB protein was constructed with a N-terminal 6 his tag and TEV enzymatic cleavage site
455 on pET-Topo151 vector plasmid using a commercial kit. Production plasmid was then transformed
456 in *Escherichia coli* BL21 Star cells (Invitrogen). Cells were grown in 1 L flasks at 37°C in LB medium
457 supplemented with Ampiciline 100 $\mu\text{g}/\text{mL}$ until an A_{600} of 0.6 was reached. Protein expression was
458 induced with 1mM of IPTG during 16 hours at 20°C. Bacterial cells were centrifuged at 6 000 g and
459 dry pellets stored at -80°C. Harvested wells were resuspended in lysis buffer (25mM NaPi pH8, 300
460 mM NaCl, 5% Glycerol) implemented with lysozyme 1 mg/mL (Sigma Aldrich), 30 U/mL DNase I
461 (Sigma-Aldrich) and anti-protease EDTA-free cocktail (Roche). The cells were lysed by sonication
462 and debris removed by centrifuged at 20 000 g for 40 minutes at 4°C. Recombinant protein was
463 purified by chromatography using a Nickel-loaded Hitrap Chelating HP column (Cytiva). Unbound
464 material was extensively washed using 25mM NaPi pH8, 300mM NaCl, 5% Glycerol. An additional
465 washing step with 2 column volumes of 1M NaCl was done before elution of YfjB over a 0 to 500

466 mM gradient of imidazole over 8 column volumes. Peak fractions were pooled and the His tag was
467 cleaved with TEV protease (500µg/20mg of eluted protein) in presence of 1 mM DTT and 0.5 mM
468 EDTA in overnight dialysis buffer 25mM NaPi pH8, 300mM NaCl, 5% Glycerol. YfjB was further
469 purified by size exclusion chromatography (Superdex S200 increase 16/600, Cytiva) equilibrated in
470 25mM NaPi pH8, 300mM NaCl, 5% Glycerol. Purity of the samples was assessed by SDS-PAGE.
471 Freshly purified YfjB was concentrated to 10 mg/mL on 30 kDa Amicon Ultra concentrators
472 (Millipore), then stored at -80°C.

473

474 **Size exclusion chromatography (SEC)-Multi-angle light scattering (MALS)**

475 Size exclusion chromatography (SEC) experiments coupled to multi-angle laser light scattering
476 (MALS) and refractometry (RI) were performed on a superdex S200 10/300 GL (GE Healthcare)
477 equilibrated in buffer 25mM NaPi pH8, 300mM NaCl, 5% Glycerol. 50 µL of proteins were injected
478 at a concentration of 10 mg/mL. On-line MALS detection was performed with a mini DAWN-
479 TREOS detector (Wyatt Technology Corp., Santa Barbara, CA) using a laser emitting at 690 nm and
480 by refractive index measurement using an Optilab T-rex system (Wyatt Technology Corp., Santa
481 Barbara, CA). Weight averaged molar mass (Mw) were calculated using the ASTRA software (Wyatt
482 Technology Corp., Santa Barbara, CA).

483

484 **AlphaFold2 structure prediction**

485 We used the ColabFold Notebook for accessing AlphaFold2 Multimer (Jumper et al. 2021; Evans et
486 al. 2021) to submit the YfjB sequence (UNIPROT Q9S4W2) to structure prediction for three model
487 of a dimer. Figures were generated with Pymol (Schrödinger) using the output PDB files.

488

489 **CryoEM data collection and processing**

490 The vitreous grids of YfjB were prepared on Quantifoil R 1.2/1.3 holey carbon grids using a Vitrobot.
491 The grids were glow-discharged for 30 s at 10 mA current with the chamber pressure set at 0.30 mBar

492 (PELCO easiGlow; Ted Pella). The glow-discharged grids were mounted in the sample chamber of
493 a Vitrobot at 8°C and 95% relative humidity, blotted, and plunge-frozen in liquid ethane at
494 temperature -172°C . The frozen grids were tested on a JEM-1400 transmission electron microscope
495 (TEM) at VUB Brussels, and the grid preparation conditions were optimized in cycles. The final
496 optimized grids were reproducibly prepared using 5 μL of YfjB sample at a concentration of
497 1.5 mg/mL spotted on Quantifoil R 1.2/1.3 holey carbon grids, incubated on the grid for 30 s, and
498 back blotted for 12 – 14 s using two pieces of Whatman® Grade 1 filter paper. High-resolution
499 dataset was collected at ESRF-Grenoble CM01 facility using a 300 kV Titan KRIOS TEM equipped
500 with a Gatan K3 Summit direct electron detector and a Gatan energy filter. The data collection was
501 automated using EPU version 2.5 (ThermoFisher). Electron movies were collected in the counting
502 mode at a nominal magnification of 165,000x. The total exposure time was 6 s with a total dose of
503 $65\text{ e}^{-}/\text{\AA}^2$ and the movies were recorded as gain corrected MRC files. Images for y-mtRNAP IC sample
504 were collected using EPU software version 2.6.1 (ThermoFisher) in the counting mode again at a
505 nominal magnification of 165,000x yielding a pixel size of 0.827 \AA . The exposure time was 5 s for
506 each movie, accumulating to a total dosage of $50\text{ e}^{-}/\text{\AA}^2$. The beam-image shift was applied during
507 data collection to increase data throughput. 8396 movies were recorded as compressed MRC files.
508 For both data collections, the energy filter was used with a slit width of 20 eV.
509 All frames in individual movies were aligned using MotionCor2 and contrast-transfer-function (CTF)
510 estimations were performed using CTFFIND-4. An initial automated picking procedure was applied
511 to a set of 500 images and particles were classified into 10 classes. These classes were used as the
512 template for picking the particles from the complete dataset in Cryosparc. 7,380,495 particles were
513 extracted with a 300-pixel box size and submitted to several rounds of 2D classification, resulting in
514 428,068 selected particles. These were used to ab initio building of 3 models that showed different
515 maps with low resolution. Heterogenous refinement was used to refined and re-classified particles
516 leading to one map with resolution of 5.7 \AA map with 191,000 particles. These were used in non-
517 uniform refinement leading a 3.65 \AA structure.

518 **Model building**

519 The 3.7 Å map was improve and the final map was sharpened using the Autosharpen tool from the
520 Phenix (Afonine et al. 2018) using the two half maps as input. The map obtained correspond
521 remarkably to the dimer of domain IV predicted by AF2 (Figure 3C). Fitting of the predicted domain
522 was performed in ChimeraX (Pettersen et al. 2021) and the Real-Space-Refine tool from the Phenix
523 package. Model validation was analysed in Coot (Casañal, Lohkamp, and Emsley 2020) and then
524 verified using the Comprehensive validation tool from the Phenix package.

525

526 **Electrophoretic mobility shift assay**

527 DNA sequences were amplified using Polymerase Chain Reaction (PCR) on *E.coli* K-12 MG1655
528 colonies and purified following the Nucleospin Gel & PCR Clean-Up kit directions (Macherey-
529 Nagel). TATTTTGCTCCAGCAATTACGGT and TCGTTGTAAAAGCGCCACTC primers were
530 used for DNA 1 sequence amplification; AAAAGATAAAGCGAAATCTGTGCC and
531 TCGCACTACAAAACAGGATCAC primers were used for DNA 2 sequence amplification;
532 GAAACTCTCTTCGGACTGTTGC and CGCACCCATGGAAGCTGAA primers were used for
533 DNA 3 sequence amplification. Concentration were measured at A₂₆₀ using a NanoDrop device
534 (Thermo Fisher Scientific) and diluted at a concentration of 100 ng/μL with MiliQ water. Purified
535 DNA sequences were then mixed in 1.5mL microtubes Eppendorf (Dutscher) with increased
536 concentration of purified protein in a 20mM Tris, 50mM NaCl, 10mM MgCl₂, 10% Glycerol buffer
537 and incubated 30 minutes at room temperature. 20μL of samples were migrated on 7.5% Native gels
538 (Tris, Borate, EDTA, Acrylamide 37.5:1, APS 10X, TEMED) submerged by 5X TBE buffer (Tris,
539 Borate, EDTA) in electrophoretic cuves. Gels were dyed 30 minutes with agitation in 0.5X TAE
540 buffer (Tris, A, EDTA) supplemented with Ethidium Bromide (BET), and revealed under UV.

541 **Chromatin immunoprecipitation sequencing ChiP-seq**

542 *Samples preparation.* Cells were grown overnight in LB at 37°C and diluted at an A₆₀₀ of 0.05 in 5
543 mL tubes, and incubated at 37°C with agitation until they reached an A₆₀₀ comprised between 0.7 and
544 0.8. Conjugation mix of 10 mL of donor and 30 mL of recipient were done in 50 mL Falcon tube pre-
545 heated at 37°C, and briefly vortexing before incubation at 37°C during 2 hours. 100 µL were taken
546 to evaluate by serial dilution the conjugation efficiency (spread 50 µl of 10⁻⁴ and 10⁻⁵ dilution on
547 LB implemented with Xgal 40µg/ml, IPTG 20µM and LB implemented with Xgal40µg/ml, IPTG2
548 0µM, Tc10µg/ml.

549 *Formaldehyde treatment.* 400µL of a 1mM Na phosphate (pH8) and 1.08 ml of 37% formaldehyde
550 were added to 40 mL of bacterial culture. Tubes were gently mixed and incubated 10 minutes at room
551 temperature, and then at 30 minutes on ice. The cells were centrifugated at 5000 rpm for 15 minutes
552 at 4°C (Bucket 3655 SORVAL ST 16R). The supernatant was discarded and the pellet washed twice
553 with 20 ml of cold 1X PBS, pH 7.4. A third wash was done 1 ml of 1x PBS transferred to an
554 Eppendorf tube before centrifugation at 8500 rpm (AcuSpin micro17R-eppendorf). The pellets were
555 stored at -80°C for maximum 4 weeks.

556

557 **Transcriptomic experiment**

558 *Samples preparation.* Cells were grown overnight in LB at 37°C and diluted at an A₆₀₀ of 0.03 in 500
559 mL flasks, and incubated at 37°C with agitation until they reached an A₆₀₀ comprised between 0.7
560 and 0.8. The equivalent number of cells as maximum 30 mg at A₆₀₀ of 1 was harvested and washed
561 in 100 µL of lysis buffer (10mM TrisHCl, 1mM EDTA pH8, 1 mg/mL lysozyme). The RNA
562 extraction was done according to the Nucleospin RNA plus kit directions (Macherey-Nagel). RNA
563 concentrations were quantified using Qubit (Thermo Fisher Scientific) and Nanodrop (Thermo Fisher
564 Scientific) devices and RNA integrity was verified by 1% agarose gel migration. Samples were sent
565 to Montpellier GenomiX (MGX).

566 *Data analysis.* Data were given by MGX in Excel tables from which a more detailed analysis was
567 performed. Significant data were selected by keeping only those with a Log₂ Fold Change ≥ 1 or \leq
568 -1 and a $-\text{Log}_{10} P\text{-Value} \geq 1.3$. Volcano plots were generated using InstantClue software (Nolte et al.
569 2018). Metabolic pathways were obtained by GOTerm analysis of their gene ID using the DAVID
570 Bioinformatic Resources website (<https://david.ncifcrf.gov/>).

571

572 **Mass spectrometry experiments**

573 *Samples preparation.* Same initial cells as the one for transcriptomic experiment were used. Cells
574 were grown overnight in LB at 37°C and diluted at an A₆₀₀ of 0.03 in 500 mL flasks, and incubated
575 at 37°C with agitation until they reached an A₆₀₀ comprised between 0.7 and 0.8. The equivalent
576 number of cells as 10mL at A₆₀₀ 0.8 was harvested and washed twice with 1 mL of cold 50mM Tris
577 pH 7.5. Pellets were kept at -80°C. After resuspension in 1 mL 50mM Tris pH 7.5, cells disruption
578 was carried out using TissueLyser II (QIAGEN) and 0.1 mm glass beads (Sigma-Aldrich). 1%
579 Foscholine was added and the samples were incubated 90 minutes at 4°C on a rotating wheel. Cell
580 debris was removed by ultracentrifugation for 1 hour at 4°C at 15 000 g. Supernatants were
581 transferred to Eppendorf Protein Low Binding tubes and proteins were quantifies using BCA Protein
582 Assay Kit (Pierce). Further analysis and data collection were done according to the same protocole
583 used by Nolivos *et al.*, 2019 (Nolivos et al. 2019). Volcano plot were generated using InstantClue
584 software (Nolte et al. 2018), and association between genes was done using the String database
585 (<https://string-db.org/>).

586

587 **Determination of extracellular pyruvate and acetate concentrations and AlamarBlue reduction**

588 Cells were grown overnight in LB at 37°C with the appropriate antibiotic and diluted at an A₆₀₀ of
589 0.05, and incubated at 37°C with agitation until they reached an A₆₀₀ of 0.5 for pyruvate and acetate
590 assays and 0.2 for AlamarBlue redox assay (Thermo Scientific). Samples were prepared according to
591 the Pyruvate Assay or Acetate Assay kit directions (Sigma Aldrich) to determine the pyruvate

592 concentration in culture supernatant. These kits are based on pyruvate oxidase, acetate oxidase or
593 alamarBlue reduction and data were measured automatically using the TECAN Spark multimode
594 plate reader.

595

596 **Growth curves**

597 Cells were grown overnight in LB or M9 medium implemented with casamino-acids and/or glucose,
598 glycerol or maltose if needed with the appropriate antibiotic, and were diluted by 100-fold and
599 cultures were incubated 8 hours at 37°C with agitation. Growth curves were performed automatically
600 using TECAN Spark multimode plate reader. Flat transparent bottom 96-wells plates were loaded
601 with 200 μ L of cultures diluted at an A_{600} of 0.05 and incubated at 37°C, with 30 seconds agitation
602 and A_{600} measurement every 10 minutes over 900 minutes. Mean growth curves with standard
603 deviation were generated using GraphPad Prism software.

604

605 **Statistical analysis**

606 *P*-value significance were analysed running specific statistical tests on the GraphPad Prism software.
607 Single-cell data from quantitative microscopy analysis were extracted from the MicrobeJ interface
608 and transferred to GraphPad. *P*-value significance of single-cell quantitative data was performed
609 using unpaired non-parametric Mann-Whitney statistical test, which allows to compare differences
610 between independent data groups without normal distribution assumption. *P*-value significance for
611 the frequency of transconjugants obtained by plating assays were evaluated using One-way analysis
612 of variance (ANOVA) with Dunnett's multiple comparisons test, which allows to determine the
613 statistical significance of differences observed between the means of three or more independent
614 experimental groups against a control group mean (corresponding to the *F wt*). When required, *P*-
615 value and significance are indicated on the figure panels and within the corresponding legend.

616 **References**

- 617 Afonine, Pavel V., Billy K. Poon, Randy J. Read, Oleg V. Sobolev, Thomas C. Terwilliger, Alexandre
618 Urzhumtsev, and Paul D. Adams. 2018. ‘Real-Space Refinement in PHENIX for Cryo-EM and
619 Crystallography’. *Acta Crystallographica. Section D, Structural Biology* 74 (Pt 6): 531–44.
620 <https://doi.org/10.1107/S2059798318006551>.
- 621
- 622 Althorpe, Nicola J., Paul M. Chilley, Angela T. Thomas, William J. Brammar, and Brian M. Wilkins.
623 1999. ‘Transient Transcriptional Activation of the IncI1 Plasmid Anti-Restriction Gene (ArdA) and
624 SOS Inhibition Gene (PsiB) Early in Conjugating Recipient Bacteria’. *Molecular Microbiology* 31
625 (1): 133–42. <https://doi.org/10.1046/j.1365-2958.1999.01153.x>.
- 626
- 627 Bagdasarian, M., A. Bailone, J. F. Angulo, P. Scholz, M. Bagdasarian, and R. Devoret. 1992. ‘PsiB,
628 and Anti-SOS Protein, Is Transiently Expressed by the F Sex Factor during Its Transmission to an
629 Escherichia Coli K-12 Recipient’. *Molecular Microbiology* 6 (7): 885–93.
630 <https://doi.org/10.1111/j.1365-2958.1992.tb01539.x>.
- 631
- 632 Baharoglu, Zeynep, David Bikard, and Didier Mazel. 2010. ‘Conjugative DNA Transfer Induces the
633 Bacterial SOS Response and Promotes Antibiotic Resistance Development through Integron
634 Activation’. *PLoS Genetics* 6 (10). <https://doi.org/10.1371/journal.pgen.1001165>.
- 635
- 636 Bailone, A., A. Bäckman, S. Sommer, J. Célérier, M. M. Bagdasarian, M. Bagdasarian, and R.
637 Devoret. 1988. ‘PsiB Polypeptide Prevents Activation of RecA Protein in Escherichia Coli’.
638 *Molecular & General Genetics: MGG* 214 (3): 389–95. <https://doi.org/10.1007/bf00330471>.
- 639
- 640 Bates, Steven, Richard A. Roscoe, Nicola J. Althorpe, William J. Brammar, and Brian M. Wilkins.
641 1999. ‘Expression of Leading Region Genes on IncI1 Plasmid ColIb-P9: Genetic Evidence for Single-
642 Stranded DNA Transcription’. *Microbiology* 145 (10): 2655–62. <https://doi.org/10.1099/00221287-145-10-2655>.
- 643
- 644
- 645 Benz, F., and A. R. Hall. 2022. ‘Host-Specific Plasmid Evolution Explains the Variable Spread of
646 Clinical Antibiotic-Resistance Plasmids’. bioRxiv. <https://doi.org/10.1101/2022.07.06.498992>.
- 647
- 648 Bignell, Colin, and Christopher M Thomas. 2001. ‘The Bacterial ParA-ParB Partitioning Proteins’.
649 *Journal of Biotechnology* 91 (1): 1–34. [https://doi.org/10.1016/S0168-1656\(01\)00293-0](https://doi.org/10.1016/S0168-1656(01)00293-0).
- 650
- 651 Billane, Kathryn, Ellie Harrison, Duncan Cameron, and Michael A. Brockhurst. 2022. ‘Why Do
652 Plasmids Manipulate the Expression of Bacterial Phenotypes?’ *Philosophical Transactions of the
653 Royal Society of London. Series B, Biological Sciences* 377 (1842): 20200461.
654 <https://doi.org/10.1098/rstb.2020.0461>.
- 655
- 656 Bingle, Lewis E. H., Donia P. Macartney, Anaïs Fantozzi, Susan E. Manzoor, and Christopher M.
657 Thomas. 2005. ‘Flexibility in Repression and Cooperativity by KorB of Broad Host Range IncP-1
658 Plasmid RK2’. *Journal of Molecular Biology* 349 (2): 302–16.
659 <https://doi.org/10.1016/j.jmb.2005.03.062>.
- 660
- 661 Casañal, Ana, Bernhard Lohkamp, and Paul Emsley. 2020. ‘Current Developments in Coot for
662 Macromolecular Model Building of Electron Cryo-Microscopy and Crystallographic Data’. *Protein
663 Science: A Publication of the Protein Society* 29 (4): 1069–78. <https://doi.org/10.1002/pro.3791>.
- 664
- 665 Cayron, Julien, and Christian Lesterlin. 2019. ‘Multi-Scale Analysis of Bacterial Growth Under
666 Stress Treatments’. *Journal of Visualized Experiments: JoVE*, no. 153 (November).
667 <https://doi.org/10.3791/60576>.

668

669 Chase, J. W., B. M. Merrill, and K. R. Williams. 1983. 'F Sex Factor Encodes a Single-Stranded
670 DNA Binding Protein (SSB) with Extensive Sequence Homology to Escherichia Coli SSB'.
671 *Proceedings of the National Academy of Sciences of the United States of America* 80 (18): 5480–84.
672 <https://doi.org/10.1073/pnas.80.18.5480>.

673

674 Coulson, Garry B., Aleksandra A. Miranda-CasoLuengo, Raúl Miranda-CasoLuengo, Xiaoguang
675 Wang, Jenna Oliver, Jennifer M. Willingham-Lane, Wim G. Meijer, and Mary K. Hondalus. 2015.
676 'Transcriptome Reprogramming by Plasmid-Encoded Transcriptional Regulators Is Required for
677 Host Niche Adaption of a Macrophage Pathogen'. *Infection and Immunity* 83 (8): 3137–45.
678 <https://doi.org/10.1128/IAI.00230-15>.

679

680 Couturier, Agathe, Chloé Virolle, Kelly Goldlust, Annick Berne-Dedieu, Audrey Reuter, Sophie
681 Nolivos, Yoshiharu Yamaichi, Sarah Bigot, and Christian Lesterlin. 2023. 'Real-Time Visualisation
682 of the Intracellular Dynamics of Conjugative Plasmid Transfer'. *Nature Communications* 14 (1): 294.
683 <https://doi.org/10.1038/s41467-023-35978-3>.

684

685 Datsenko, Kirill A., and Barry L. Wanner. 2000. 'One-Step Inactivation of Chromosomal Genes in
686 Escherichia Coli K-12 Using PCR Products'. *Proceedings of the National Academy of Sciences* 97
687 (12): 6640–45. <https://doi.org/10.1073/pnas.120163297>.

688

689 Ducret, Adrien, Ellen M. Quardokus, and Yves V. Brun. 2016. 'MicrobeJ, a Tool for High
690 Throughput Bacterial Cell Detection and Quantitative Analysis'. *Nature Microbiology* 1 (7): 16077.
691 <https://doi.org/10.1038/nmicrobiol.2016.77>.

692

693 Evans, Richard, Michael O'Neill, Alexander Pritzel, Natasha Antropova, Andrew Senior, Tim Green,
694 Augustin Židek, et al. 2021. 'Protein Complex Prediction with AlphaFold-Multimer'. Preprint.
695 Bioinformatics. <https://doi.org/10.1101/2021.10.04.463034>.

696

697 Fernandez-Lopez, Raul, Maria de Toro, Gabriel Moncalian, M. Pilar Garcillan-Barcia, and Fernando
698 de la Cruz. 2016. 'Comparative Genomics of the Conjugation Region of F-like Plasmids: Five Shades
699 of F'. *Frontiers in Molecular Biosciences* 3. <https://doi.org/10.3389/fmolb.2016.00071>.

700

701 Fisher, Jay K., Aude Bourniquel, Guillaume Witz, Beth Weiner, Mara Prentiss, and Nancy Kleckner.
702 2013. 'Four-Dimensional Imaging of E. Coli Nucleoid Organization and Dynamics in Living Cells'.
703 *Cell* 153 (4): 882–95. <https://doi.org/10.1016/j.cell.2013.04.006>.

704

705 Fried, Luitpold, Stefan Behr, and Kirsten Jung. 2013. 'Identification of a Target Gene and Activating
706 Stimulus for the YpdA/YpdB Histidine Kinase/Response Regulator System in Escherichia Coli'.
707 *Journal of Bacteriology* 195 (4): 807–15. <https://doi.org/10.1128/JB.02051-12>.

708

709 Gasteiger, E., C. Hoogland, A. Gattiker, S. Duvaud, M.R. Wilkins, R.D. Appel, and A. Bairoch. 2005.
710 'Protein Identification and Analysis Tools on the ExPASy Server'. In *The Proteomics Protocols*
711 *Handbook*, 571–607. Humana Press. <https://link.springer.com/book/10.1385/1592598900>.

712

713 Goldlust, Kelly, Agathe Couturier, Laurent Terradot, and Christian Lesterlin. 2022. 'Live-Cell
714 Visualization of DNA Transfer and Pilus Dynamics During Bacterial Conjugation'. *Methods in*
715 *Molecular Biology (Clifton, N.J.)* 2476: 63–74. https://doi.org/10.1007/978-1-0716-2221-6_6.

716

717 Golub, E I, and K B Low. 1985. 'Conjugative Plasmids of Enteric Bacteria from Many Different
718 Incompatibility Groups Have Similar Genes for Single-Stranded DNA-Binding Proteins.' *Journal of*
719 *Bacteriology* 162 (1): 235–41.

720

721 Graham, Thomas G. W., Xindan Wang, Dan Song, Candice M. Eton, Antoine M. van Oijen, David
722 Z. Rudner, and Joseph J. Loparo. 2014. 'ParB Spreading Requires DNA Bridging'. *Genes &*
723 *Development* 28 (11): 1228–38. <https://doi.org/10.1101/gad.242206.114>.

724

725 Johnson, Timothy J., Jessica L. Danzeisen, Bonnie Youmans, Kyle Case, Katharine Llop, Jeannette
726 Munoz-Aguayo, Cristian Flores-Figueroa, et al. 2016. 'Separate F-Type Plasmids Have Shaped the
727 Evolution of the H30 Subclone of Escherichia Coli Sequence Type 131'. *MSphere* 1 (4): e00121-16.
728 <https://doi.org/10.1128/mSphere.00121-16>.

729

730 Jumper, John, Richard Evans, Alexander Pritzel, Tim Green, Michael Figurnov, Olaf Ronneberger,
731 Kathryn Tunyasuvunakool, et al. 2021. 'Highly Accurate Protein Structure Prediction with
732 AlphaFold'. *Nature* 596 (7873): 583–89. <https://doi.org/10.1038/s41586-021-03819-2>.

733

734 Lanza, Val F., María de Toro, M. Pilar Garcillán-Barcia, Azucena Mora, Jorge Blanco, Teresa M.
735 Coque, and Fernando de la Cruz. 2014. 'Plasmid Flux in Escherichia Coli ST131 Sublineages,
736 Analyzed by Plasmid Constellation Network (PLACNET), a New Method for Plasmid
737 Reconstruction from Whole Genome Sequences'. *PLOS Genetics* 10 (12): e1004766.
738 <https://doi.org/10.1371/journal.pgen.1004766>.

739

740 Lesterlin, Christian, and Nelly Duabry. 2016. 'Investigating Bacterial Chromosome Architecture'.
741 *Methods in Molecular Biology (Clifton, N.J.)* 1431: 61–72. [https://doi.org/10.1007/978-1-4939-3631-](https://doi.org/10.1007/978-1-4939-3631-1_6)
742 [1_6](https://doi.org/10.1007/978-1-4939-3631-1_6).

743

744 Loh, Sue, David Cram, and Ron Skurray. 1989. 'Nucleotide Sequence of the Leading Region
745 Adjacent to the Origin of Transfer on Plasmid F and Its Conservation among Conjugative Plasmids'.
746 *Molecular and General Genetics MGG* 219 (1): 177–86. <https://doi.org/10.1007/BF00261174>.

747

748

749 Luque, Ainara, Sonia Paytubi, Javier Sánchez-Montejo, Marta Gibert, Carlos Balsalobre, and Cristina
750 Madrid. 2019. 'Crosstalk between Bacterial Conjugation and Motility Is Mediated by Plasmid-Borne
751 Regulators'. *Environmental Microbiology Reports* 11 (5): 708–17. [https://doi.org/10.1111/1758-](https://doi.org/10.1111/1758-2229.12784)
752 [2229.12784](https://doi.org/10.1111/1758-2229.12784).

753

754 Maindola, Priyank, Rahul Raina, Parveen Goyal, Krishnamohan Atmakuri, Abhishek Ojha, Sourabh
755 Gupta, Peter J. Christie, Lakshminarayan M. Iyer, L. Aravind, and Arulandu Arockiasamy. 2014.
756 'Multiple Enzymatic Activities of ParB/Srx Superfamily Mediate Sexual Conflict among
757 Conjugative Plasmids'. *Nature Communications* 5 (October): 5322.
758 <https://doi.org/10.1038/ncomms6322>.

759

760 Masai, Hisao, and Ken-ichi Arai. 1997. 'Frpo: A Novel Single-Stranded DNA Promoter for
761 Transcription and for Primer RNA Synthesis of DNA Replication'. *Cell* 89 (6): 897–907.
762 [https://doi.org/10.1016/S0092-8674\(00\)80275-5](https://doi.org/10.1016/S0092-8674(00)80275-5).

763

764 Nolivos, Sophie, Julien Cayron, Annick Dedieu, Adeline Page, Frederic Delolme, and Christian
765 Lesterlin. 2019. 'Role of AcrAB-TolC Multidrug Efflux Pump in Drug-Resistance Acquisition by
766 Plasmid Transfer'. *Science (New York, N.Y.)* 364 (6442): 778–82.
767 <https://doi.org/10.1126/science.aav6390>.

768

769 Nolte, Hendrik, Thomas D. MacVicar, Frederik Tellkamp, and Marcus Krüger. 2018. 'Instant Clue:
770 A Software Suite for Interactive Data Visualization and Analysis'. *Scientific Reports* 8 (1): 12648.
771 <https://doi.org/10.1038/s41598-018-31154-6>.

772
773 Osorio-Valeriano, Manuel, Florian Altegoer, Chandan Das, Wieland Steinchen, Gaël Panis, Lara
774 Connolley, Giacomo Giacomelli, et al. 2021. *The CTPase Activity of ParB Acts as a Timing*
775 *Mechanism to Control the Dynamics and Function of Prokaryotic DNA Partition Complexes*.
776 <https://doi.org/10.1101/2021.05.05.442810>.
777
778 Pettersen, Eric F., Thomas D. Goddard, Conrad C. Huang, Elaine C. Meng, Gregory S. Couch, Tristan
779 I. Croll, John H. Morris, and Thomas E. Ferrin. 2021. ‘UCSF ChimeraX: Structure Visualization for
780 Researchers, Educators, and Developers’. *Protein Science: A Publication of the Protein Society* 30
781 (1): 70–82. <https://doi.org/10.1002/pro.3943>.
782
783 Senior, Andrew W., Richard Evans, John Jumper, James Kirkpatrick, Laurent Sifre, Tim Green,
784 Chongli Qin, et al. 2020. ‘Improved Protein Structure Prediction Using Potentials from Deep
785 Learning’. *Nature* 577 (7792): 706–10. <https://doi.org/10.1038/s41586-019-1923-7>.
786
787 Soh, Young-Min, Iain Finley Davidson, Stefano Zamuner, Jérôme Basquin, Florian Patrick Bock,
788 Michael Taschner, Jan-Willem Veening, Paolo De Los Rios, Jan-Michael Peters, and Stephan
789 Gruber. 2019. ‘Self-Organization of ParS Centromeres by the ParB CTP Hydrolase’. *Science (New*
790 *York, N.Y.)* 366 (6469): 1129–33. <https://doi.org/10.1126/science.aay3965>.
791
792 Vial, Ludovic, and Florence Hommais. 2020. ‘Plasmid-Chromosome Cross-Talks’. *Environmental*
793 *Microbiology* 22 (2): 540–56. <https://doi.org/10.1111/1462-2920.14880>.
794
795 Vilhena, Cláudia, Eugen Kaganovitch, Jae Yen Shin, Alexander Grünberger, Stefan Behr, Ivica
796 Kristoficova, Sophie Brameyer, Dietrich Kohlheyer, and Kirsten Jung. 2018. ‘A Single-Cell View of
797 the BtsSR/YpdAB Pyruvate Sensing Network in Escherichia Coli and Its Biological Relevance’.
798 *Journal of Bacteriology* 200 (1): e00536-17. <https://doi.org/10.1128/JB.00536-17>.
799
800 Wein, Tanita, Yiqing Wang, Myriam Barz, Fenna T. Stücker, Katrin Hammerschmidt, and Tal
801 Dagan. 2021. ‘Essential Gene Acquisition Destabilizes Plasmid Inheritance’. *PLOS Genetics* 17 (7):
802 e1009656. <https://doi.org/10.1371/journal.pgen.1009656>.
803
804 Yu, Daiguan, Hilary M. Ellis, E-Chiang Lee, Nancy A. Jenkins, Neal G. Copeland, and Donald L.
805 Court. 2000. ‘An Efficient Recombination System for Chromosome Engineering in Escherichia
806 Coli’. *Proceedings of the National Academy of Sciences* 97 (11): 5978–83.
807 <https://doi.org/10.1073/pnas.100127597>.

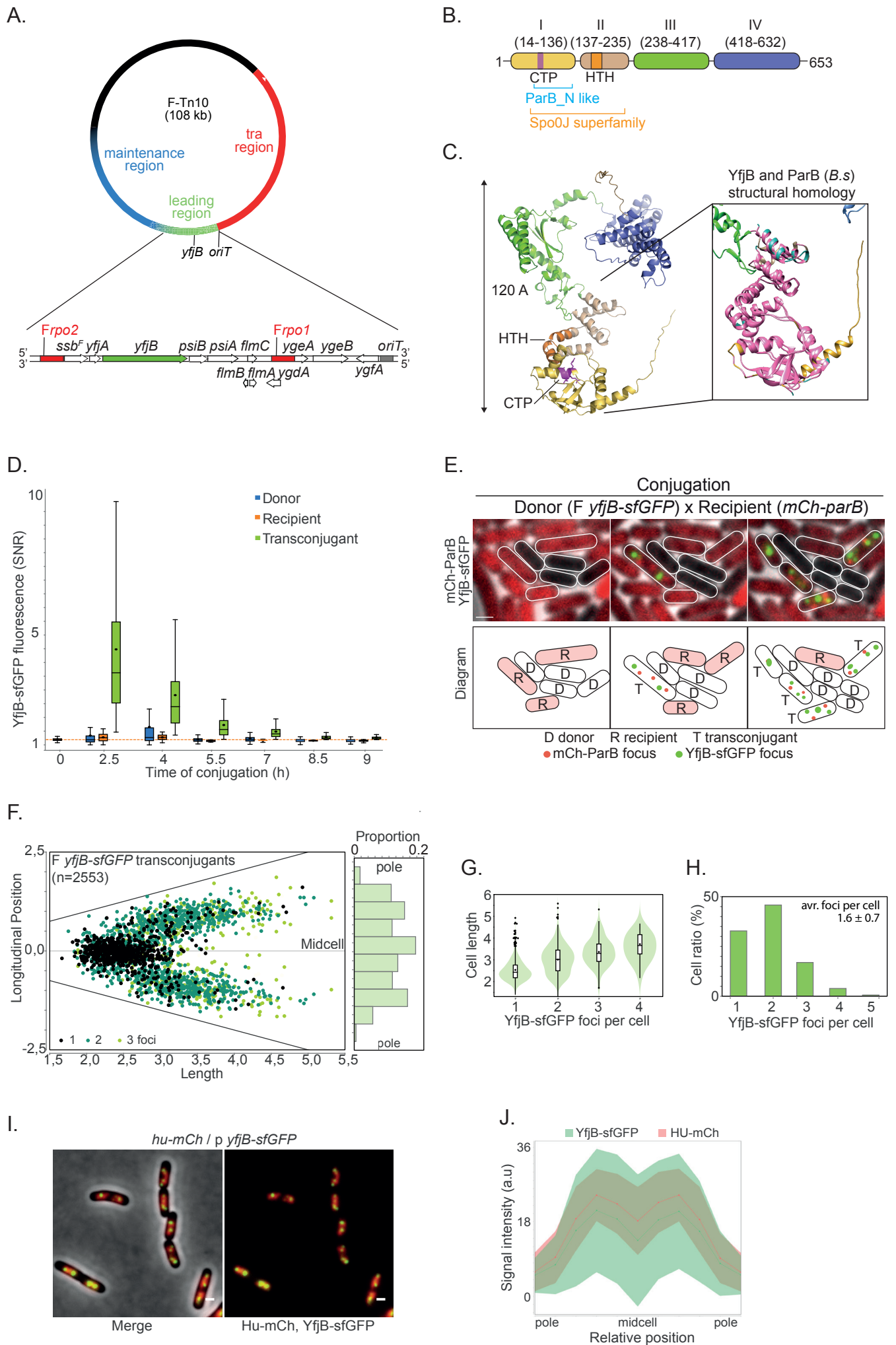


Figure 1

808 **Figure legends**

809 **Figure 1. Transient production and intracellular localisation of YfjB in transconjugant cells**

810 **(A)** Genetic map of the F plasmid showing the origin of transfer (*oriT*) as well as the leading (green),
811 maintenance (blue) and *tra* (red) regions. The map of the leading region is shown in more details
812 below. The *yffB* gene is shown in green while other genes are in white, and the *Frpo1* and *Frpo2*
813 promoters are in red. **(B)** Bioinformatic analysis predicts that YfjB is composed of four domains,
814 with domain I containing the CTP motif and domain II the HTH domain. **(C)** AlphaFold2 structure
815 prediction of YfjB. The inset shows in pink the structural homology of YfjB domains I and II with
816 ParB structure obtain from PDB model 6SDK of *Bacillus subtilis*. Colours correspond to the different
817 domains of the protein. **(D)** Box-plot for quantification of YfjB-sfGFP intracellular fluorescence
818 signal to noise ratio (SNR) in donor, recipient and transconjugant cells during conjugation over nine
819 hours. The dotted orange line corresponds to the mean of signal inside recipients before the beginning
820 of the experiment. **(E)** Time-lapse microscopy images of conjugation between the F *yffB-sfGFP*
821 plasmid donor (D) and recipient (R) cells producing the mCh-ParB protein. The transconjugant cells
822 (T) having acquired the plasmid exhibit a red fluorescence focus and foci of YfjB-sfGFP. A diagram
823 is shown below. Scale bar 1 μm . **(F)** Dot plot of YfjB-sfGFP foci localisation in transconjugant cells
824 with the histogram of foci distribution from pole to pole shown on the left. The grey line represents
825 the midcell and the black, dark green and light green the foci localization when there is 1, 2 or 3 foci
826 inside the bacteria. **(G)** Violin plot of cell length of cells with 1, 2, 3 or 4 YfjB-sfGFP foci. **(H)**
827 Histograms of the proportion of cells with 1 to 5 YfjB-sfGFP foci. **(I)** Microscopy images of the cells
828 producing HU-mCherry from the chromosome and YfjB-sfGFP from the pTrc *yffB-sfGFP* plasmid
829 Scale bar 1 μm . **(J)** Distribution of Hu-mCh and YfjB-sfGFP fluorescence along the cell length in
830 M9-CASA medium. Lines represent the mean, and the coloured area represent the SD.
831 For box plots, the median, quartile 1 and quartile 3 are indicated by the boxes' limits, the mean by a
832 black dot and the minima and maxima by the whiskers' limits. Black dots above the max values
833 correspond to outliers.

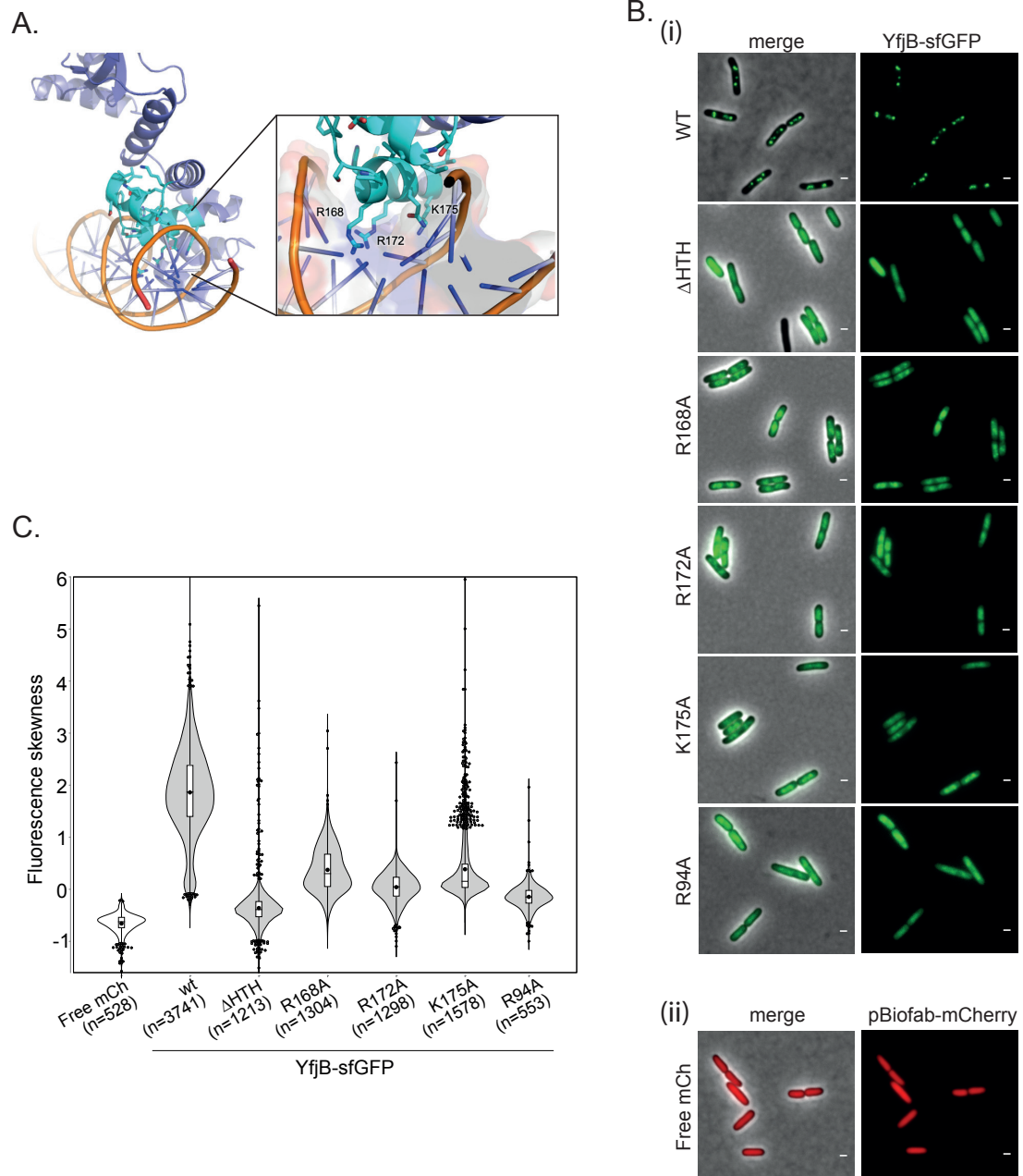
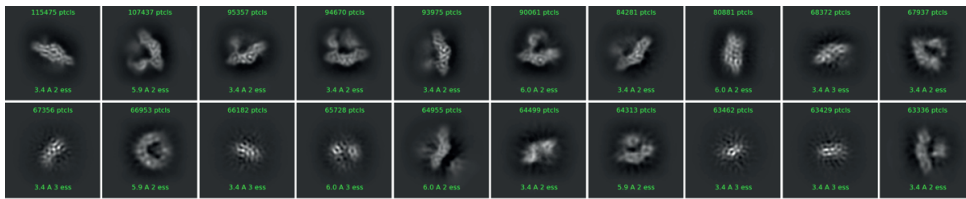


Figure 2

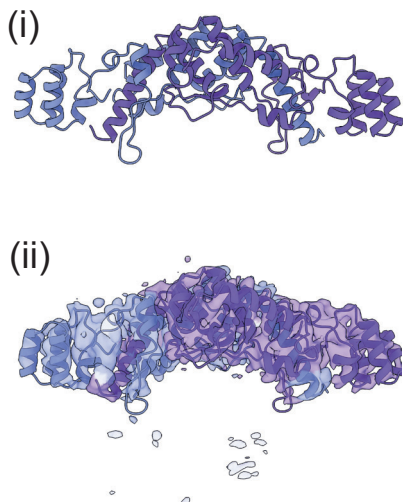
834 **Figure 2. Role of the HTH and the CTP motif in YfjB focus formation *in vivo***

835 **(A)** Structure prediction of the interaction between YfjB (dark blue) HTH domain (light blue) and the
836 DNA double helix (orange) showing the position of residues R168, R172 and K175 (right panel). **(B)**
837 Microscopy images of the cells producing different mutants of YfjB-sfGFP from the pTrc yfjB-sfGFP
838 derivatives. Scale bar 1 μ m. **(C)** Violin plots of fluorescence skewness in the strains of cells producing
839 a free mCh protein or different mutants of YfjB-sfGFP. The median, quartile 1 and quartile 3 are
840 indicated by the boxes' limits, the mean by a black dot and the minima and maxima by the whiskers'
841 limits. Free mCherry is produced from the chromosome in MS388 *wt* background, and data
842 correspond to one representative experiment. The number of cells analysed (n) is indicated.

A.



B.



C.

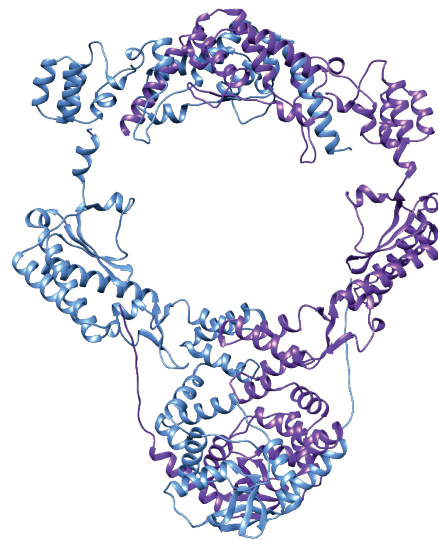


Figure 3

843 **Figure 3. YfjB structural analysis.**

844 **(A)** Images of 2D classes of YfjB particles images by CryoEM data collection and before model
845 construction. **(B)** YfjB structural model reconstructed using 191 738 particles showing (i) a dimer of
846 the domain IV (residues 424 to 636), (ii) that fits with the AlphaFold2 predicted structure. **(C)**
847 Proposed structure of YfjB dimer from AlphaFold2 and CryoEM data. Each monomer is represented
848 either in blue or purple.

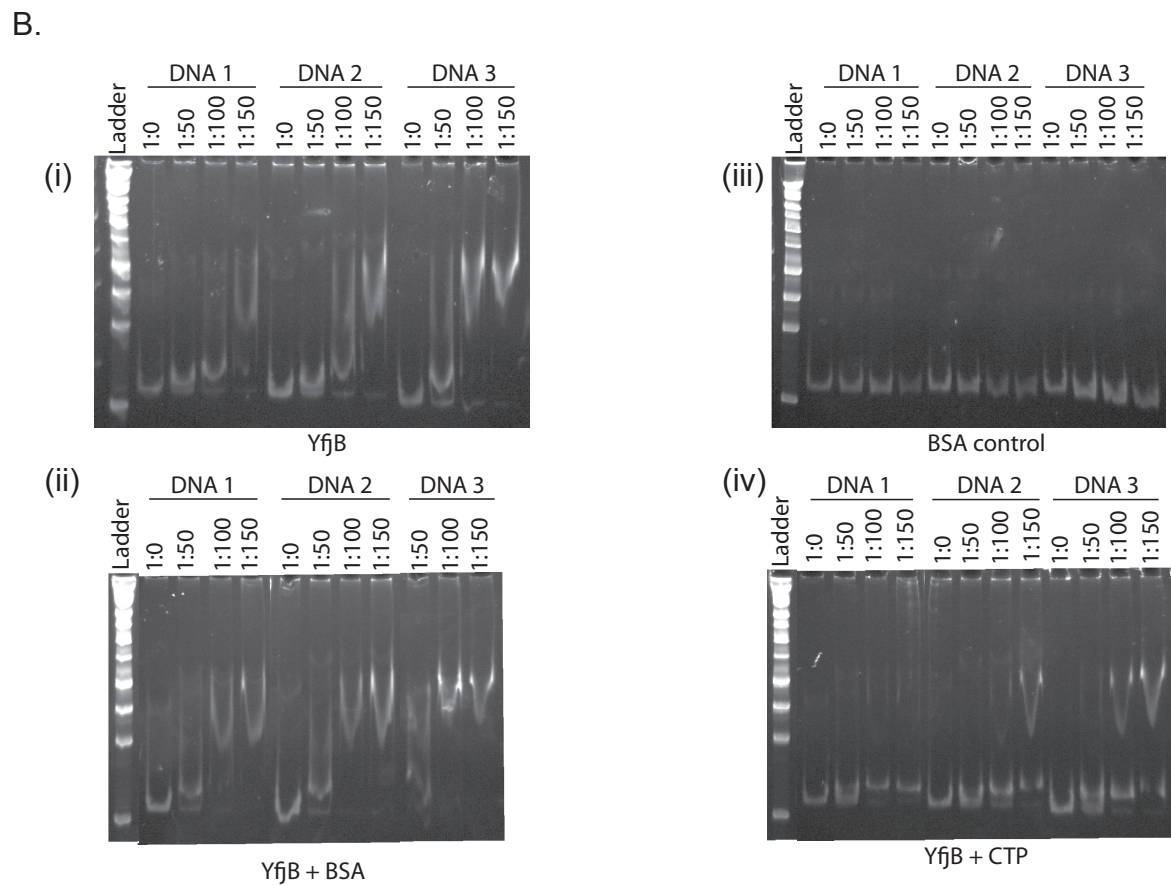
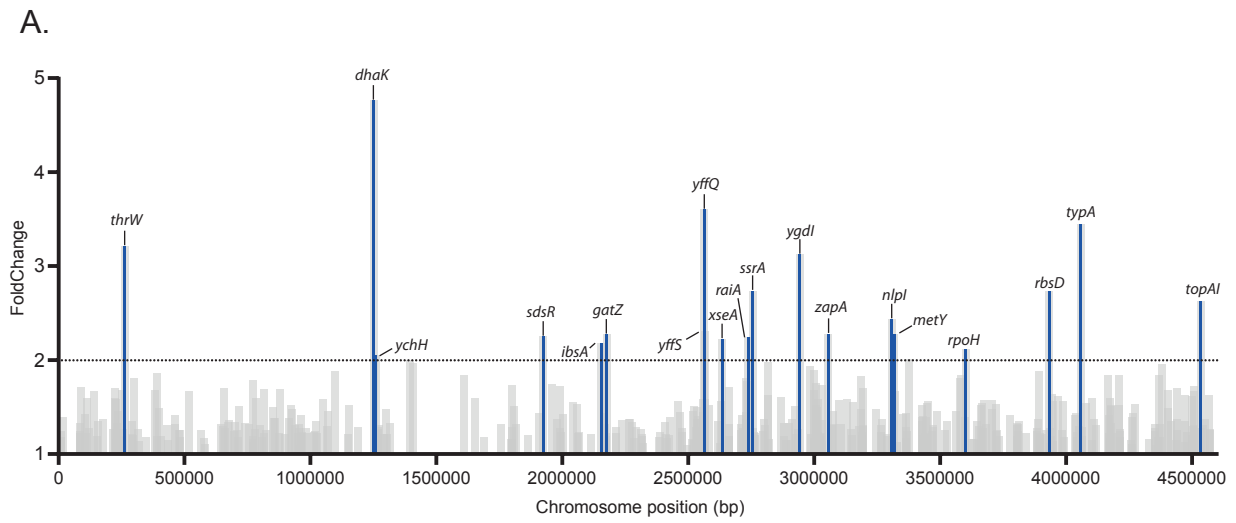


Figure 4

849 **Figure 4. YfjB DNA binding activity *in vivo* and *in vitro* analysis**

850 **(A)** Linear map of the E. coli chromosome showing the enrichment peaks of YfjB binding from Chip-
851 seq experiments in the context of conjugation. The peaks' height corresponds to their fold change.
852 Blue bars correspond to significant peaks above the chosen FoldChange threshold of 2 represented
853 by the dotted line, while grey bars represent non-significant changed genes. Significant genes'
854 names are annotated on top of each corresponding bar. **(B)** Electron mobility shift assay (EMSA) for
855 measuring the binding between YfjB protein and double-stranded DNA (i). All samples contained a
856 250 pb E.coli K12 MG 1655 DNA, incubated with an increase ratio of purified YfjB protein (ratio
857 DNA : protein). DNA 1 sequence: intergenic region dhaK-dhaR; DNA 2 sequence : intergenic region
858 glnL-glnA ; DNA 3 sequence : “non-specific” sequence. Addition of 0.1 mg/mL of BSA is tested on
859 (ii), as well as CTP on (iv). BSA is used instead of YfjB protein for binding control on (iii). 1kb
860 ladder is used on the left of each gel.

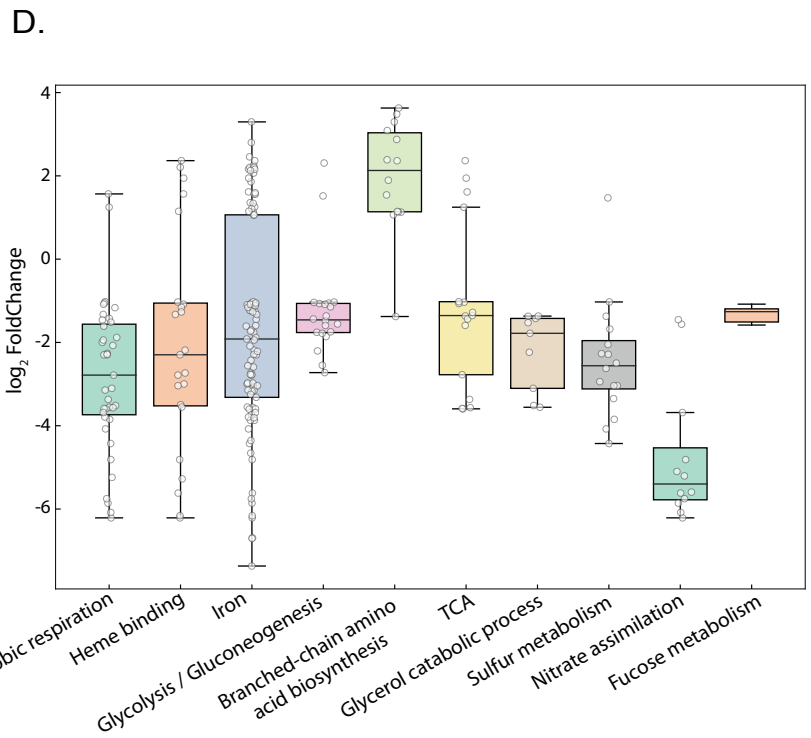
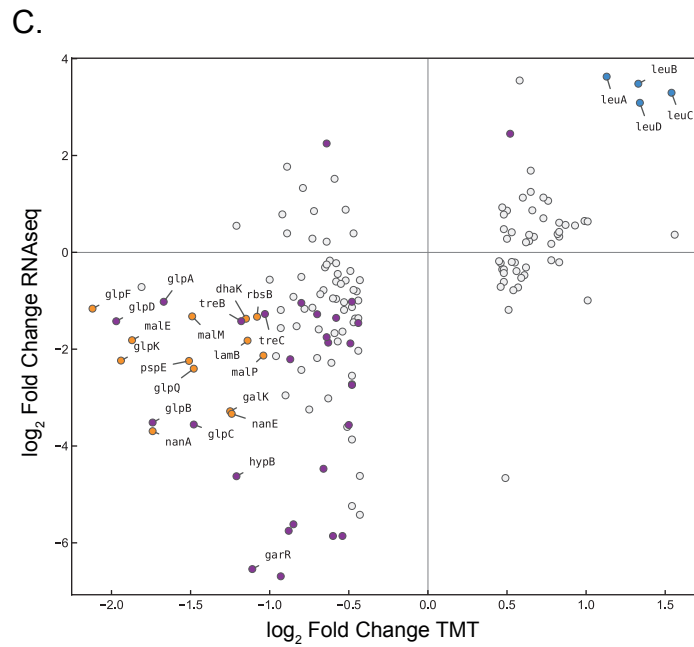
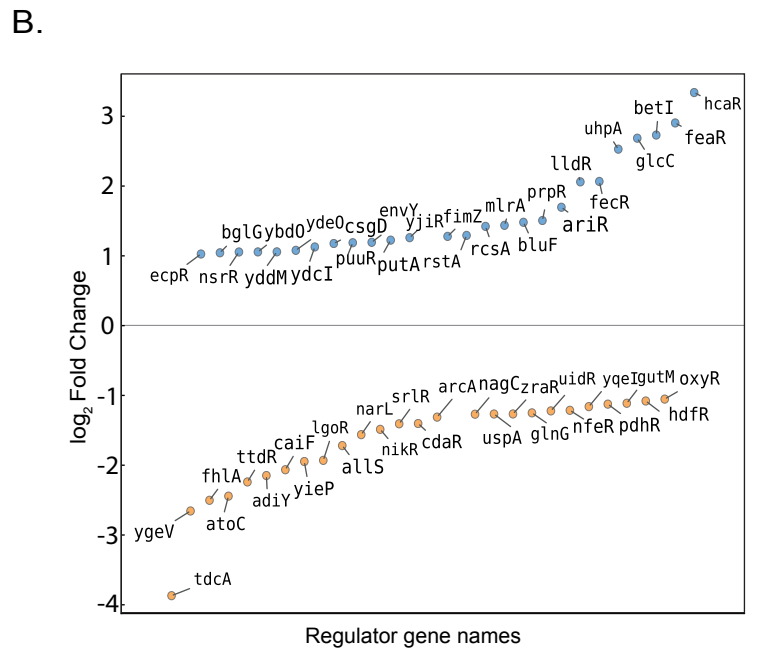
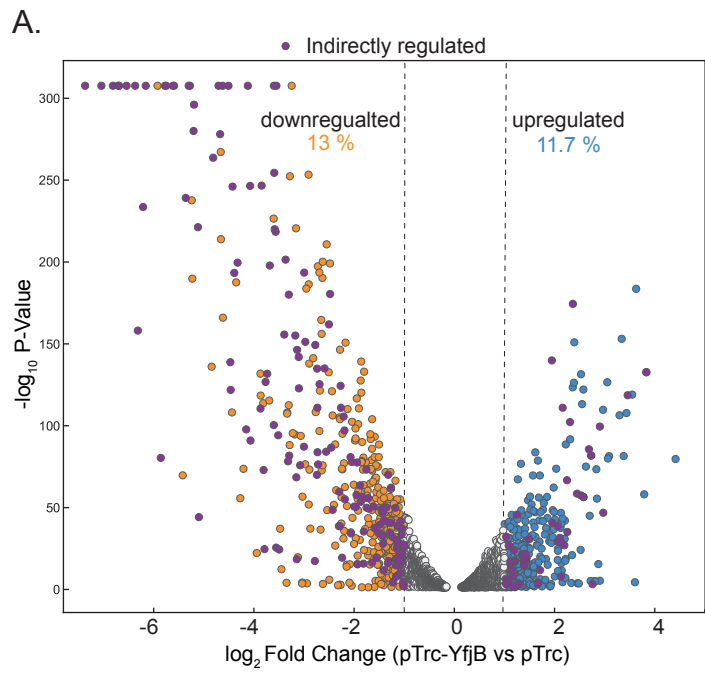


Figure 5

861 **Figure 5. Effect of YfjB on gene expression and proteins levels**

862 **(A)** Volcano plot of RNA-seq results comparing the strain containing the pTrc99a *yfjB-sfGFP*
863 plasmid to the strain containing the empty pTrc99a plasmid. Dash line indicate the significance
864 threshold for the log₂ of the Fold change (-1; 1). Upregulated genes are shown in blue, downregulated
865 genes in orange. Genes that belong to the regulons of transcription regulators that are either
866 overexpressed or under expressed are shown in purple and considered as indirectly regulated by YfjB.

867 **(B)** Plot showing the fold enrichment of transcriptional regulators that are overexpressed (blue) or
868 under expressed (orange) in RNA-seq data. Corresponding genes names are shown. **(C)** Correlation
869 plot between TMT data revealing proteins that are over- or underrepresented and RNA-seq data
870 revealing genes that are up- or downregulated in the presence of YfjB. Corresponding genes names
871 are shown. **(D)** Plot showing the different clusters of metabolic functions obtained with the DAVID
872 bioinformatics resources website (<https://david.ncifcrf.gov/>). The median, quartile 1 and quartile 3
873 are indicated by the boxes' limits, the mean by a black line and the minima and maxima by the
874 whiskers' limits. Grey dots correspond to log₂ Fold Change of the associated genes.

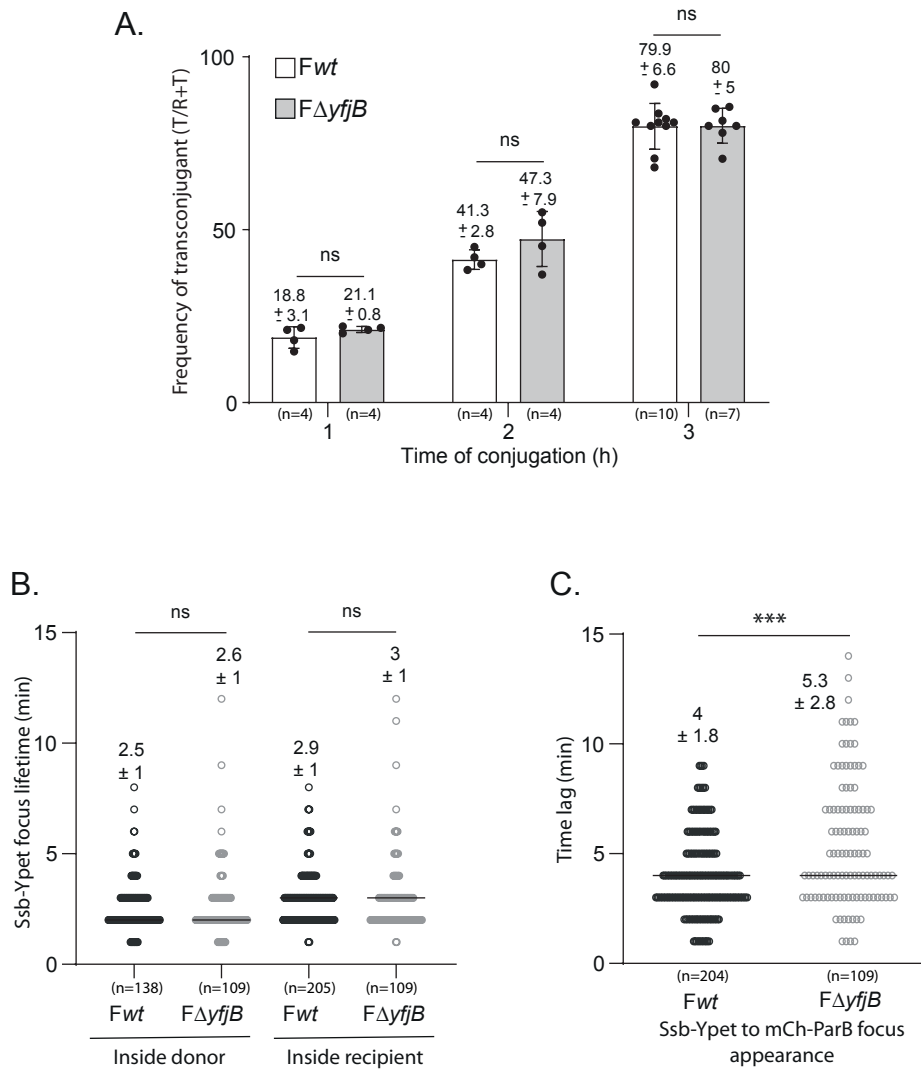


Figure 6

875 **Figure 6. In vivo phenotype of *yffB* deletion**

876 (A) Histogram of frequency of transconjugants (%) using F *wt* plasmid (white bars) or F Δ *yffB* (grey
877 bars) based on the (T/R+T) ratio after 1 hour, 2 hours and 3 hours of conjugation. The mean and SD
878 are calculated from (n) individual transfer events from at least four biological replicates (black dots).
879 (B) Jitter plot of Ssb-Ypet conjugatif foci lifespan in donor and recipient cells during conjugation of
880 the F *wt* plasmid (black dots) or the F Δ *yffB* (grey dots). Pvalue significance from Mann-Whitney
881 two-sided statistical test is indicated by ns. The mean and SD calculated from (n) individual events
882 are indicated. (C) Jitter plot showing the lag time between Ssb-Ypet and mCh-ParB foci appearing in
883 transconjugants with the F *wt* plasmid (black dots) or the F Δ *yffB* (grey dots). Pvalue significance
884 from Mann-Whitney two-sided statistical test is indicated by *** (P=). The mean and SD calculated
885 from (n) individual events are indicated.

Cluster	Gene name	Log FoldChange	Direct or indirect
Anaerobic respiration	C4-dicarboxylate transporter DcuA(dcuA)	-2,0720729	Indirect
	DUF3029 domain-containing protein YjjI(yjjI)	-5,2396175	Direct
	NADH:quinone oxidoreductase II(ndh)	-2,2618031	Direct
	aerobic glycerol 3-phosphate dehydrogenase(glpD)	-1,4229951	Indirect
	anaerobic C4-dicarboxylate transporter DcuB(dcuB)	-1,9977838	Indirect
	anaerobic glycerol-3-phosphate dehydrogenase subunit A(glpA)	-3,1022397	Indirect
	anaerobic glycerol-3-phosphate dehydrogenase subunit B(glpB)	-3,515031	Indirect
	anaerobic glycerol-3-phosphate dehydrogenase subunit C(glpC)	-3,5563176	Indirect
	cytochrome c quinol dehydrogenase TorY(torY)	1,56653205	Direct
	dimethyl sulfoxide reductase subunit A(dmsA)	-4,0757667	Indirect
	dimethyl sulfoxide reductase subunit B(dmsB)	-4,4268735	Indirect
	dimethyl sulfoxide reductase subunit C(dmsC)	-3,8466182	Indirect
	formate dehydrogenase N subunit alpha(fdnG)	-3,7896479	Indirect
	formate dehydrogenase N subunit beta(fdnH)	-3,1443164	Indirect
	formate dehydrogenase N subunit gamma(fdnI)	-2,7843313	Indirect
	fumarate reductase flavoprotein subunit(frdA)	-3,5662085	Indirect
	fumarate reductase iron-sulfur protein(frdB)	-3,5942516	Indirect
	fumarate reductase membrane protein FrdC(frdC)	-3,5851773	Indirect
	fumarate reductase membrane protein FrdD(frdD)	-3,368068	Indirect
	hydrogenase 1 cytochrome b subunit(hyaC)	-1,3280651	Indirect
	hydrogenase 1 large subunit(hyaB)	-1,5134955	Indirect
	hydrogenase 1 small subunit(hyaA)	-1,1653228	Indirect
	hydrogenase 2 iron-sulfur protein(hybA)	-1,8810018	Indirect
	hydrogenase 2 large subunit(hybC)	-1,4600473	Indirect
	hydrogenase 2 membrane subunit(hybB)	-1,6094513	Indirect
	hydrogenase 2 small subunit(hybO)	-1,9416511	Indirect
	malate dehydrogenase(mdh)	-1,0212369	Indirect
	nitrate reductase A subunit alpha(narG)	-5,8586339	Indirect
	nitrate reductase A subunit beta(narH)	-5,7518661	Indirect
	nitrate reductase A subunit gamma(narI)	-4,8131521	Indirect
	nitrite reductase (NADH) large subunit(nirB)	-6,21209	Indirect
	nitrite reductase (NADH) small subunit(nirD)	-6,0829407	Indirect
	periplasmic nitrate reductase cytochrome c protein(napC)	-2,2960669	Indirect
	periplasmic nitrate reductase cytochrome c550 protein(napB)	-2,2960669	Indirect
periplasmic nitrate reductase subunit NapA(napA)	-3,6828321	Indirect	
putative selenate reductase YnfE(ynfE)	-2,2852005	Indirect	
putative selenate reductase YnfF(ynfF)	-1,0505508	Indirect	
quinone-dependent D-lactate dehydrogenase(dld)	-1,0821734	Direct	

	succinate:quinone oxidoreductase, FAD binding protein(sdhA)	1,24766277	Indirect
Heme binding	Ni(2(+)) ABC transporter periplasmic binding protein(nikA)	-3,4948461	Indirect
	catalase/hydroperoxidase HPI(katG)	-2,7335886	Indirect
	cytochrome bd-I subunit 1(cydA)	-3,5512769	Indirect
	cytochrome bd-I subunit 2(cydB)	-2,9963951	Indirect
	cytochrome c maturation protein C(ccmC)	-1,0296154	Indirect
	cytochrome c peroxidase(ccp)	-2,1852529	Indirect
	cytochrome c quinol dehydrogenase TorY(torY)	1,56653205	Direct
	cytochrome c552 nitrite reductase(nrfA)	-5,6169492	Indirect
	formate dehydrogenase N subunit gamma(fdnI)	-2,7843313	Indirect
	heme-containing peroxidase/deferrochelataase(efeB)	2,20697548	Direct
	hydrogenase 1 cytochrome b subunit(hyaC)	-1,3280651	Indirect
	nitrate reductase A subunit gamma(narI)	-4,8131521	Indirect
	nitric oxide dioxygenase(hmp)	-1,0801114	Indirect
	nitrite reductase (NADH) large subunit(nirB)	-6,21209	Indirect
	periplasmic heme chaperone(ccmE)	-1,1588636	Indirect
	periplasmic nitrate reductase cytochrome c protein(napC)	-2,2960669	Indirect
	periplasmic nitrite reductase penta-heme c-type cytochrome(nrfB)	-6,1594598	Direct
	porphyrinogen peroxidase(yfeX)	-1,2668944	Direct
	putative cytochrome b561 YodB(yodB)	1,1493446	Direct
	putative cytochrome c-type biogenesis protein NrfE(nrfE)	-5,2760905	Direct
succinate:quinone oxidoreductase, membrane protein SdhC(sdhC)	2,36564124	Indirect	
succinate:quinone oxidoreductase, membrane protein SdhD(sdhD)	1,94540036	Indirect	
sulfite reductase, hemoprotein subunit(cysI)	-3,0384499	Direct	
Iron	3-isopropylmalate dehydratase subunit LeuC(leuC)	3,29613794	Direct
	D-altronate dehydratase(uxaA)	-1,4443948	Direct
	DNA oxidative demethylase(alkB)	1,13648934	Direct
	DNA protection during starvation protein(dps)	-1,5950711	Indirect
	DNA-binding transcriptional regulator NsrR(nsrR)	1,0553364	Direct
	Fe(2(+)) transporter FeoB(feoB)	-3,8687002	Indirect
	Fe-(CN) ₂ CO cofactor assembly scaffold protein HypD(hypD)	-3,8687002	Indirect
	GTP 3',8'-cyclase(moaA)	-1,2367957	Direct
	GarD(garD)	-6,6915491	Indirect
	L-1,2-propanediol oxidoreductase(fucO)	-1,2331572	Direct
	L-serine deaminase II(sdaB)	1,61552602	Direct
	Mn(2+)/Fe(2(+)): H(+) symporter MntH(mntH)	2,16227415	Indirect
	NADH oxidoreductase(hcr)	-3,0774502	Indirect
	PKHD-type hydroxylase YbiX(ybiX)	2,80029841	Direct
	RNA polymerase sigma factor Fecl(fecl)	2,20170874	Direct

SoxR [2Fe-2S] reducing system protein RxC(rsxC)	1,25517745	Direct
alpha-dehydro-beta-deoxy-D-glucarate aldolase(garL)	-7,3684668	Indirect
anaerobic glycerol-3-phosphate dehydrogenase subunit C(glpC)	-3,5563176	Indirect
anaerobic ribonucleoside-triphosphate reductase activating protein(nrdG)	-1,2684353	Direct
bacterioferritin-associated ferredoxin(bfd)	1,35576984	Direct
catalase/hydroperoxidase HPI(katG)	-2,7335886	Indirect
cytochrome bd-I subunit 1(cydA)	-3,5512769	Indirect
cytochrome bd-I subunit 2(cydB)	-2,9963951	Indirect
cytochrome c peroxidase(ccp)	-2,1852529	Indirect
cytochrome c quinol dehydrogenase TorY(torY)	1,56653205	Direct
cytochrome c552 nitrite reductase(nrfA)	-5,6169492	Indirect
dihydroxy-acid dehydratase(ilvD)	1,0644075	Direct
dimethyl sulfoxide reductase subunit A(dmsA)	-4,0757667	Indirect
dimethyl sulfoxide reductase subunit B(dmsB)	-4,4268735	Indirect
endonuclease III(nth)	1,56012348	Direct
ferredoxin-type protein NapG(napG)	-2,9743635	Indirect
ferredoxin-type protein NapH(napH)	-2,5911078	Indirect
ferredoxin-type protein(napF)	-3,153681	Indirect
ferric citrate regulator FecR(fecR)	2,06636781	Direct
ferric coprogen/ferric rhodotorulic acid outer membrane transporter(fhuE)	1,34177657	Direct
ferric enterobactin ABC transporter membrane subunit FebD(fepD)	1,8588863	Direct
ferric enterobactin ABC transporter membrane subunit FepG(fepG)	1,21329736	Direct
ferric enterobactin outer membrane transporter(fepA)	1,5953709	Direct
ferric-siderophore reductase FhuF(fhuF)	2,25481997	Indirect
ferrous iron transport protein A(feoA)	-3,6027459	Indirect
ferrous iron transport protein FeoC(feoC)	-3,7354846	Indirect
formate dehydrogenase H(fdhF)	-3,1745556	Indirect
formate dehydrogenase N subunit alpha(fdnG)	-3,7896479	Indirect
formate dehydrogenase N subunit beta(fdnH)	-3,1443164	Indirect
formate dehydrogenase N subunit gamma(fdnI)	-2,7843313	Indirect
fumarase B(fumB)	-2,7750302	Indirect
fumarate reductase iron-sulfur protein(frdB)	-3,5942516	Indirect
fused acetaldehyde-CoA dehydrogenase and iron-dependent alcohol dehydrogenase/aldehyde/alcohol dehydrogenase AdhE(adhE)	-1,7560232	Indirect
galactose-1-phosphate uridylyltransferase(galT)	-3,2461891	Direct
glycolate dehydrogenase, putative iron-sulfur subunit(glcF)	-1,0918935	Indirect
heme-containing peroxidase/deferrochelataase(efeB)	2,20697548	Direct
hydrogenase 1 cytochrome b subunit(hyaC)	-1,3280651	Indirect
hydrogenase 1 small subunit(hyaA)	-1,1653228	Indirect

hydrogenase 2 iron-sulfur protein(hybA)	-1,8810018	Indirect
hydrogenase 2 membrane subunit(hybB)	-1,6094513	Indirect
hydrogenase 2 small subunit(hybO)	-1,9416511	Indirect
iron catecholate outer membrane transporter Fiu(fiu)	2,45680202	Direct
iron-catecholate outer membrane transporter CirA(cirA)	2,15928023	Direct
iron-sulfur cluster repair protein YtfE(ytfE)	-1,70151	Indirect
nitrate reductase A subunit alpha(narG)	-5,8586339	Indirect
nitrate reductase A subunit beta(narH)	-5,7518661	Indirect
nitrate reductase A subunit gamma(narI)	-4,8131521	Indirect
nitric oxide dioxygenase(hmp)	-1,0801114	Indirect
nitrite reductase (NADH) large subunit(nirB)	-6,21209	Indirect
periplasmic heme chaperone(ccmE)	-1,1588636	Indirect
periplasmic nitrate reductase cytochrome c protein(napC)	-2,2960669	Indirect
periplasmic nitrate reductase cytochrome c550 protein(napB)	-2,4280497	Indirect
periplasmic nitrate reductase subunit NapA(napA)	-3,6828321	Indirect
periplasmic nitrite reductase penta-heme c-type cytochrome(nrfB)	-6,1594598	Direct
porphyrinogen peroxidase(yfeX)	-1,2668944	Direct
protein S-nitrosylase(hcp)	-2,5585095	Indirect
putative 4Fe-4S cluster-containing protein(ygcO)	-1,0594918	Direct
putative ATPase, activator of (R)-hydroxyglutaryl-CoA dehydratase(yjiL)	-1,9172129	Direct
putative amino acid dehydrogenase with NAD(P)-binding domain and ferridoxin-like domain(ykgF)	-4,3542374	Direct
putative anaerobic sulfatase maturation enzyme AslB(aslB)	2,12735574	Direct
putative anaerobic sulfatase maturation enzyme YdeM(ydeM)	-3,8072918	Indirect
putative cytochrome b561 YodB(yodB)	1,1493446	Direct
putative electron transport protein YsaA(ysaA)	-2,7677812	Direct
putative formate-dependent nitrite reductase complex subunit NrfF(nrfF)	-3,3184536	Indirect
putative glycyl-radical enzyme activating enzyme YjjW(yjjW)	-4,6576931	Direct
putative iron ABC exporter membrane subunit FetB(fetB)	-1,0222818	Direct
putative menaquinol-cytochrome c reductase 4Fe-4S subunit(nrfC)	-6,705913	Indirect
putative oxidoreductase AegA(aegA)	-2,9746288	Indirect
putative oxidoreductase YdhV(ydhV)	-1,0846048	Direct
putative oxidoreductase, Fe-S subunit(ygfK)	-1,1161208	Direct
putative pyruvate formate-lyase activating enzyme YbiY(ybiY)	-2,0858704	Direct
putative selenate reductase YnfE(ynfE)	-2,2852005	Indirect
putative selenate reductase YnfF(ynfF)	-1,0505508	Indirect
pyruvate formate-lyase activating enzyme(pflA)	-1,7279263	Direct
radical SAM family oxidoreductase YhcC(yhcC)	-2,2137696	Direct
succinate:quinone oxidoreductase, membrane protein SdhC(sdhC)	2,36564124	Indirect

	succinate:quinone oxidoreductase, membrane protein SdhD(sdhD)	1,94540036	Indirect
	sulfite reductase, hemoprotein subunit(cysI)	-3,0384499	Direct
Glycolysis / Gluconeogenesis	2,3-bisphosphoglycerate-independent phosphoglycerate mutase(gpmM)	-2,2030757	Direct
	6-phospho-beta-glucosidase A(bglA)	-1,0549789	Direct
	6-phosphofructokinase 1(pfkA)	-1,8589581	Direct
	acetyl-CoA synthetase (AMP-forming)(acs)	1,51848556	Direct
	fructose-1,6-bisphosphatase 1(fbp)	-1,478575	Direct
	fused acetaldehyde-CoA dehydrogenase and iron-dependent alcohol dehydrogenasealdehyde/alcohol dehydrogenase AdhE(adhE)	-1,7560232	Indirect
	galactose-1-epimerase(galM)	-2,7243935	Direct
	glucose-1-phosphatase(agp)	-2,5481362	Direct
	glucose-6-phosphate isomerase(pgi)	-1,5561758	Direct
	glucose-specific PTS enzyme IIBC component(ptsG)	2,3084975	Indirect
	glyceraldehyde-3-phosphate dehydrogenase A(gapA)	-1,0303632	Direct
	lipoamide dehydrogenase(lpd)	-1,0653404	Indirect
	phosphoenolpyruvate carboxykinase (ATP)(pck)	-1,5908289	Direct
	phosphoenolpyruvate synthetase(ppsA)	-1,1449331	Direct
	phosphoglycerate kinase(pgk)	-1,0841759	Direct
	putative aldose 1-epimerase YeaD(yeaD)	-1,7456705	Direct
	pyruvate dehydrogenase E1 component(aceE)	-1,3647728	Indirect
	pyruvate dehydrogenase, E2 subunit(aceF)	-1,4374437	Indirect
	pyruvate kinase 2(pykA)	-1,0381666	Direct
	triose-phosphate isomerase(tpiA)	-1,7806069	Direct
Branched-chain aa biosynthesis	2-isopropylmalate synthase(leuA)	3,62894553	Direct
	3-isopropylmalate dehydratase subunit LeuC(leuC)	3,29613794	Direct
	3-isopropylmalate dehydratase subunit LeuD(leuD)	3,08824996	Direct
	3-isopropylmalate dehydrogenase(leuB)	3,48254461	Direct
	acetohydroxy acid synthase I subunit IlvB(ilvB)	2,36351749	Direct
	acetohydroxy acid synthase I subunit IlvN(ilvN)	2,38627363	Direct
	acetolactate synthase II subunit IlvM(ilvM)	1,54219405	Direct
	branched-chain-amino-acid aminotransferase(ilvE)	1,12953551	Direct
	dihydroxy-acid dehydratase(ilvD)	1,0644075	Direct
	enamine/imine deaminase, redox-regulated chaperone(ridA)	-1,3773347	Direct
	ilvBN operon leader peptide(ivbL)	1,89550358	Direct
	ilvXGMEDA operon leader peptide(ilvL)	1,13471808	Direct
	leu operon leader peptide(leuL)	2,87413619	Direct
	threonine deaminase(ilvA)	1,14522609	Direct
TCA cycle	dihydrolipoyltranssuccinylase(sucB)	-1,0331844	Indirect
	fumarase B(fumB)	-2,7750302	Indirect

	fumarate reductase flavoprotein subunit(frdA)	-3,5662085	Indirect
	fumarate reductase iron-sulfur protein(frdB)	-3,5942516	Indirect
	fumarate reductase membrane protein FrdC(frdC)	-3,5851773	Indirect
	fumarate reductase membrane protein FrdD(frdD)	-3,368068	Indirect
	lipoamide dehydrogenase(lpd)	-1,0653404	Indirect
	malate dehydrogenase(mdh)	-1,0212369	Indirect
	malate:quinone oxidoreductase(mqo)	1,6140032	Direct
	phosphoenolpyruvate carboxykinase (ATP)(pck)	-1,5908289	Direct
	pyruvate dehydrogenase E1 component(aceE)	-1,3647728	Indirect
	pyruvate dehydrogenase, E2 subunit(aceF)	-1,4374437	Indirect
	succinate:quinone oxidoreductase, FAD binding prot	1,24766277	Direct
	succinate:quinone oxidoreductase, membrane protein	2,36564124	Direct
	succinate:quinone oxidoreductase, membrane protein	1,94540036	Direct
	succinyl-CoA synthetase subunit alpha(sucD)	-1,3541995	Indirect
	succinyl-CoA synthetase subunit beta(sucC)	-1,2782147	Indirect
Glycerol catabolic process	aerobic glycerol 3-phosphate dehydrogenase(glpD)	-1,4229951	Indirect
	anaerobic glycerol-3-phosphate dehydrogenase subunit A(glpA)	-3,1022397	Indirect
	anaerobic glycerol-3-phosphate dehydrogenase subunit B(glpB)	-3,515031	Indirect
	anaerobic glycerol-3-phosphate dehydrogenase subunit C(glpC)	-3,5563176	Indirect
	dihydroxyacetone kinase subunit K(dhaK)	-1,3717502	Direct
	dihydroxyacetone kinase subunit L(dhaL)	-1,5255	Direct
	dihydroxyacetone kinase subunit M(dhaM)	-1,3672939	Direct
	glycerol kinase(glpK)	-2,235534	Direct
	triose-phosphate isomerase(tpiA)	-1,7806069	Direct
Sulfur metabolism	3'(2'),5'-bisphosphate nucleotidase(cysQ)	-1,3715749	Direct
	3-mercaptopyruvate sulfurtransferase(sseA)	-1,6775838	Direct
	adenylyl-sulfate kinase(cysC)	-2,2858082	Direct
	cysteine synthase A(cysK)	-2,4951116	Direct
	dimethyl sulfoxide reductase subunit A(dmsA)	-4,0757667	Indirect
	dimethyl sulfoxide reductase subunit B(dmsB)	-4,4268735	Indirect
	dimethyl sulfoxide reductase subunit C(dmsC)	-3,8466182	Indirect
	homoserine O-succinyltransferase(metA)	1,47149005	Direct
	phosphoadenosine phosphosulfate reductase(cysH)	-3,3487825	Direct
	sulfate adenylyltransferase subunit 1(cysN)	-2,6238458	Direct
	sulfate adenylyltransferase subunit 2(cysD)	-3,0368194	Direct
	sulfate/thiosulfate ABC transporter ATP binding subunit(cysA)	-2,9408338	Direct
	sulfate/thiosulfate ABC transporter inner membrane subunit CysW(cysW)	-2,0486203	Direct
	sulfate/thiosulfate ABC transporter periplasmic binding protein Sbp(sbp)	-1,0275091	Direct

	sulfite reductase, flavoprotein subunit(cysJ)	-2,2691203	Direct
	sulfite reductase, hemoprotein subunit(cysI)	-3,0384499	Direct

Table 1. GoTerm classification of genes clusters

Genes affected in RNAseq experiment above or below the threshold of \log_2 FoldChange $-1 <$ and > 1 are classified depending on the GoTerm pathway they are associated to, using the DAVID Bioinformatics Resources website. Precision according to the direct or indirect effect of YfjB on these genes is made, based on the subtraction of the corresponding regulons of regulators affected.

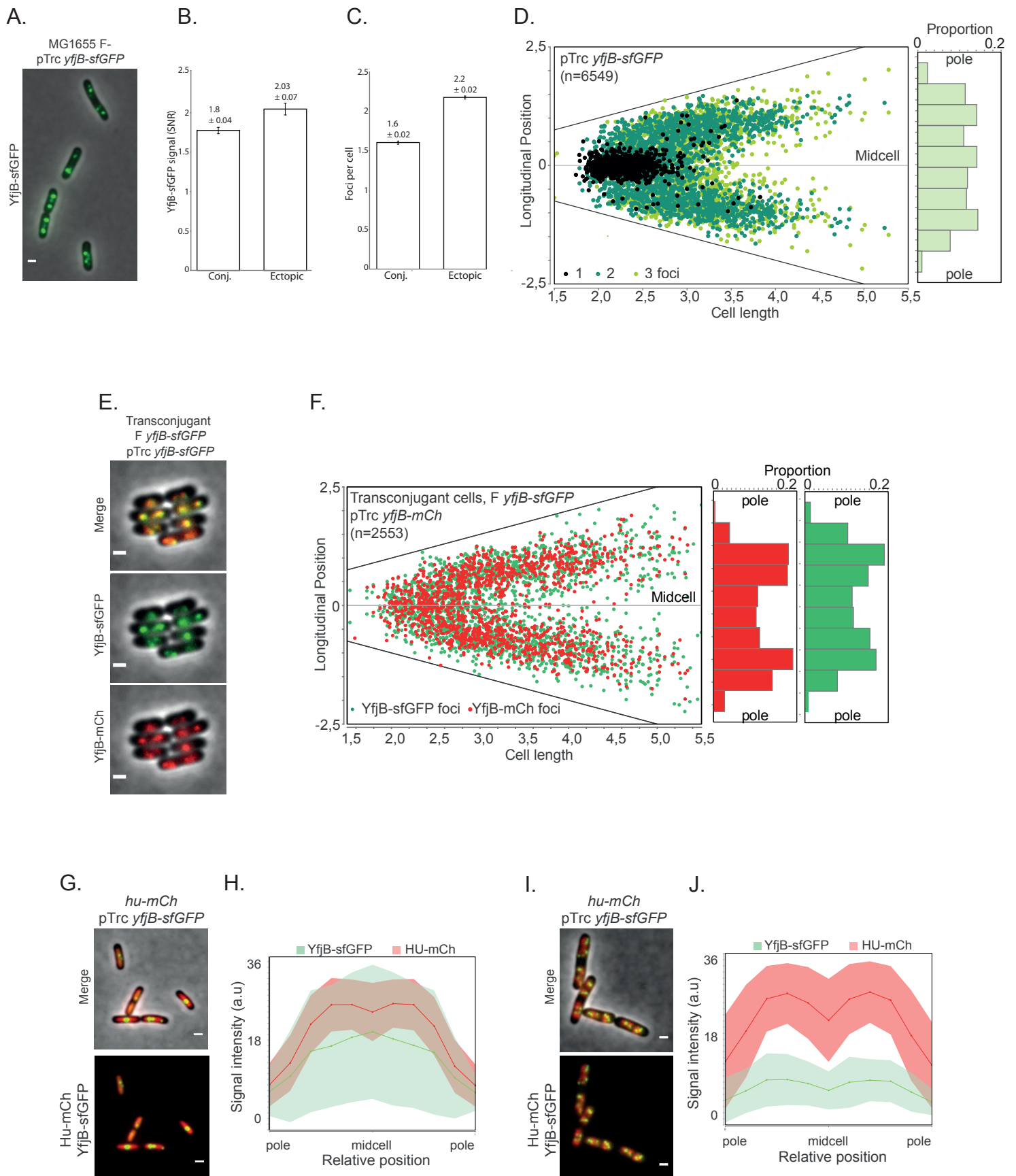


Figure S1

886 **Figure S1. Characterisation of the intracellular localization of YfjB.**

887 (A) Microscopy image of YfjB-sfGFP produced from the ectopic plasmid pTrc99a and in presence
888 of the F plasmid. Scale bar 1µm. (B) Histogram with mean and SD of signal-to-noise ratio (SNR) of
889 YfjB-sfGFP fluorescence obtained during conjugative transfer or from vegetative cells harbouring
890 the ectopic plasmid pTrc99a *yfjBsfGFP*. (C) Histogram with mean and SD of the number of YfjB-
891 sfGFP foci per cell during conjugative transfer or from vegetative cells harbouring the ectopic
892 plasmid pTrc99a *yfjBsfGFP*. (D) Dot-plot of YfjB-sfGFP foci localisation in vegetative cells
893 harbouring the ectopic plasmid pTrc99a *yfjB-sfGFP* with the histogram of foci distribution from pole
894 to pole shown on the left. The grey line represents the midcell and the black, dark green and light
895 green the foci localization when there is 1, 2 or 3 foci inside the bacteria. (E) Microscopy images of
896 YfjB localization after conjugation of the F *yfjB-sfGFP* plasmid inside cells harbouring the pTrc99a
897 *yfjBmCherry* plasmid. Scale bar 1µm. (F) Dot-plot of YfjB-sfGFP and YfjB-mCh foci localisation in
898 transconjugant cells both harbouring the F *yfjB-sfGFP* and pTrc99a *yfjB-mCherry* plasmids with the
899 histogram of foci distribution from pole to pole shown on the left. (G) Microscopy image of cells
900 expressing Hu-mCh from the chromosome and Yfjb-sfGFP from the pTrc99a plasmid in M9Glucose
901 medium. Scale bar 1µm. (H) Distribution of Hu-mCh and YfjB-sfGFP fluorescence along the cell
902 length in M9-Glucose medium. Lines represent the mean, and the coloured area represent the SD. (I)
903 Microscopy image of cells expressing Hu-mCh from the chromosome and Yfjb-sfGFP from the
904 pTrc99a plasmid in RDM medium. Scale bar 1µm. (J) Distribution of Hu-mCh and YfjB-sfGFP
905 fluorescence along the cell length in RDM medium. Lines represent the mean, and the coloured area
906 represent the SD.

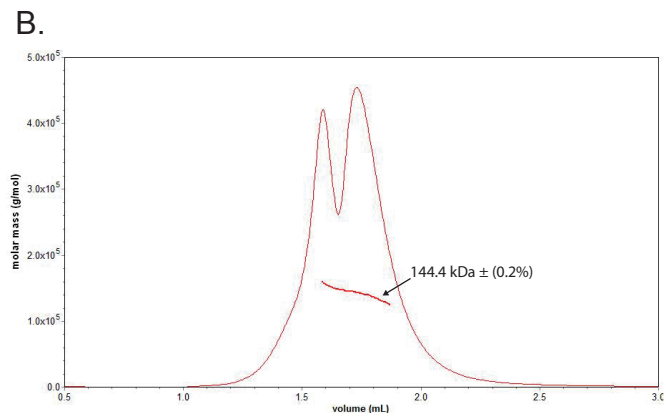
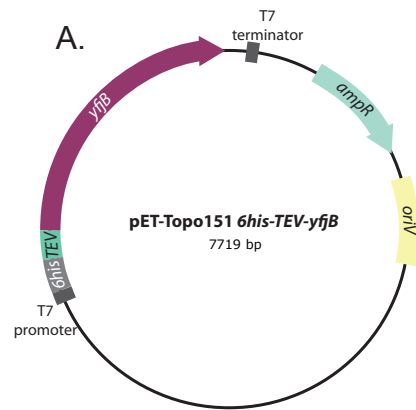


Figure S2

907 **Figure S2. Purification vector and Sec-MALS data**

908 (A) Genetic map of the 7kb pET-Topo151 vector for YfjB protein expression and production. Genes
909 are represented by the arrows. (B) Multi-angle light scattering coupled with SEC (SEC-MALS) of
910 YfjB. The YfjB protein is dimeric (Mw: 144.4 kDa). The thick line in the middle represents the molar
911 mass measured by MALS in correspondence to the SEC peaks (curve).

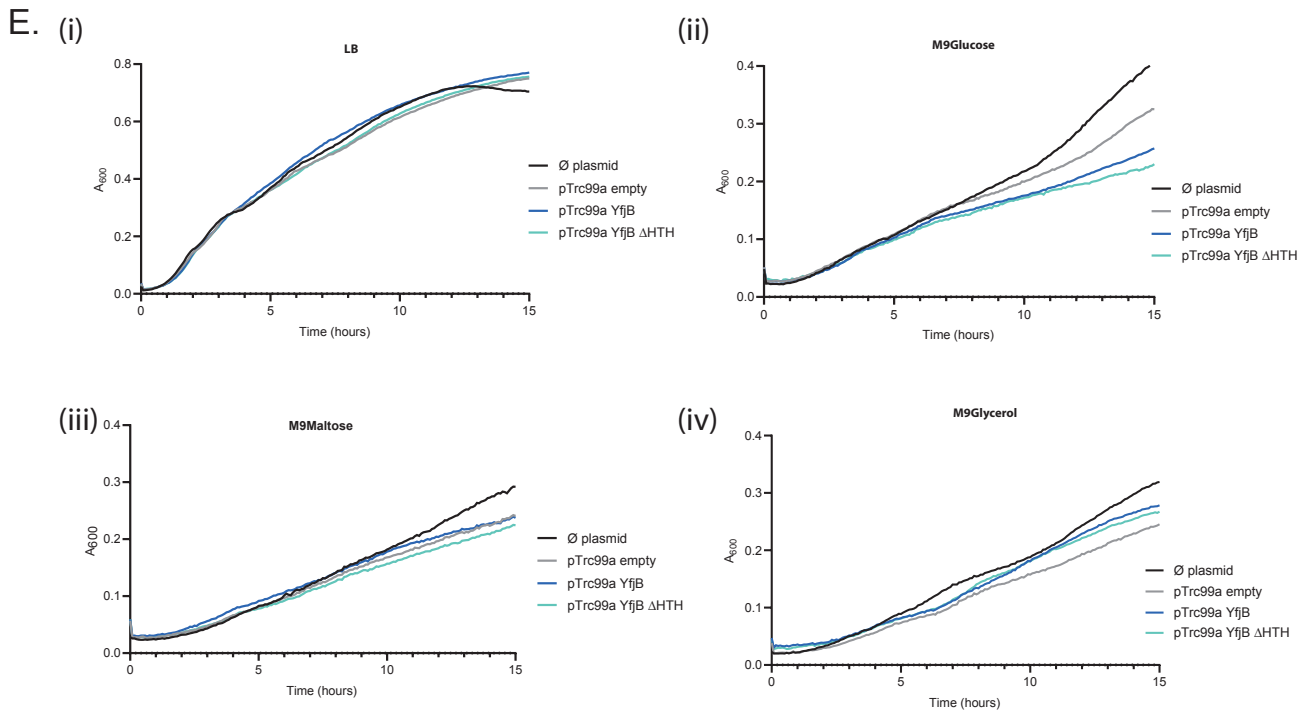
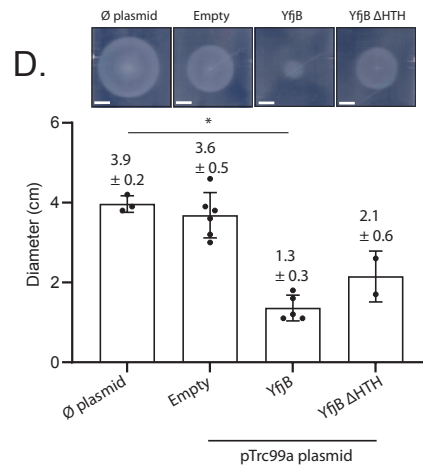
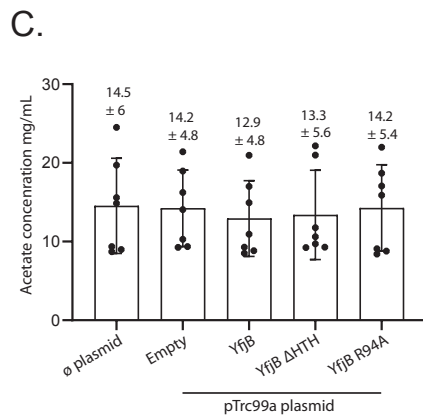
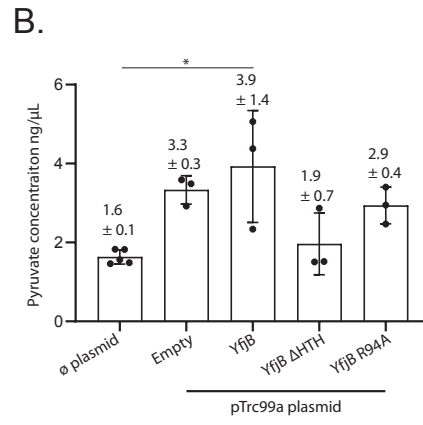
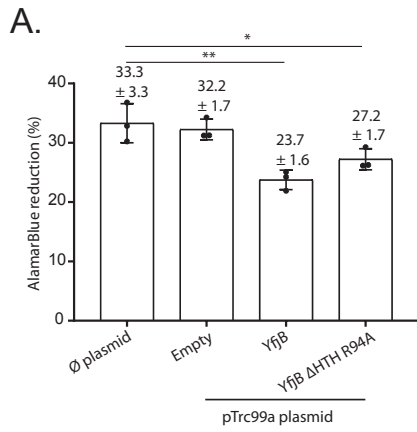


Figure S3

912 **Figure S3. Phenotypes associated with YjfB presence inside vegetative cells**

913 (A) Histogram showing the AlamarBlue reduction % of strains depending if they are plasmid free or
914 harbouring an empty pTrc99a plasmid, a pTrc99a *yjfB* plasmid or a double mutant. Mean and SD are
915 calculated based on three individual experiments (black dots). (B) Histogram showing the pyruvate
916 production by strains depending if they are plasmid free or harbouring an empty pTrc99a plasmid, a
917 pTrc99a *yjfB* plasmid, a pTrc99a *yjfB* plasmid deleted of the HTH domain or harbouring a single
918 mutation on the CTP motif. Mean and SD are calculated based on at least three individual experiments
919 (black dots). (C) Histogram showing the acetate production by strains depending if they are plasmid
920 free or harbouring an empty pTrc99a plasmid, a pTrc99a *yjfB* plasmid, a pTrc99a *yjfB* plasmid deleted
921 of the HTH domain or harbouring a single mutation on the CTP motif. Mean and SD are calculated
922 based on seven individual experiments (black dots). (D) Histogram showing the diameter of strains
923 grown on M9Casa Agar 0.2% medium and depending if they are plasmid free or harbouring an empty
924 pTrc99a plasmid, a pTrc99a *yjfB* plasmid or a pTrc99a *yjfB* plasmid deleted of the HTH domain.
925 Images examples are shown on top. Mean and SD are calculated based on at least three individual
926 experiments (black dots). Scale bar 1cm. (E) Growth curves of cells without plasmid (black), with
927 the pTrc99a empty plasmid (grey), the pTrc99a *yjfB* plasmid (blue) or deleted of the HTH (cyan),
928 measured at an A600 every 10 minutes during 15 hours. Cells were grown in triplicate in (i) LB
929 medium or M9 minimum medium implemented with (ii) Glucose, (iii) Maltose or (iv) Glycerol. Only
930 the mean of three replicates is represented here.

Strain	Relevant genotype	Source or reference
MG1655 and derivatives		
LY5	MS388 / F-Tn10	Conjugation K603 x MS388
LY110	MS388 / F-Tn10, <i>parS_{PMT1}-FRT-cat-FRT</i>	λ red <i>parS_{PMT1}-FRT-cat-FRT</i> insertion at the F plasmid intergenic <i>ygeB-ygfA locus</i> (OL1/OL2)
LY112	MS428 / F-Tn10, <i>parS_{PMT1}-FRT- cat - FRT</i>	Conjugation LY110 x MS428 to LAC ⁻ Tc ^r
LY117	MS388 <i>ssb-ypet-FRT-kan-FRT, clone 1</i>	MS388 x P1.RRL505 to Kn ^r
LY118	MS388 <i>ssb-ypet-FRT-kan-FRT, clone 2</i>	MS388 x P1.RRL505 to Kn ^r
LY119	MS388 <i>hupA-mCherry-kan</i>	MS388 x P1.Ox468 to Kn ^r
LY124	MS428 / F-Tn10, <i>parS_{PMT1}-FRT</i>	Derivative of LY112, <i>kan</i> removed via pCP20
LY128	MS388 <i>ssb-ypet-FRT</i>	Derivative of LY117, <i>kan</i> removed via pCP20
LY248	MS388 <i>hupA-mCherry-FRT</i>	Derivative of LY119, <i>kan</i> removed via pCP20
LY318	MS388 / pSN70	pSN70 x MS388 to Ap ^r
LY358	MS388 <i>ssb-ypet-FRT</i> / pSN70	pSN70 x LY128 to Ap ^r
LY735	MS388 / F-Tn10, <i>parS_{PMT1}-FRT, yjfB-sfGFP-FRT-kan-FRT</i>	Conjugation LY731 x MS388 to St ^R Tc ^r
LY792	MS388 / F-Tn10, <i>parS_{PMT1}-FRT, yjfB-sfGFP-FRT</i>	Derivative of LY735, <i>kan</i> removed via pCP20
LY1007	MS388 <i>ssb-ypet-FRT</i> / F-Tn10, <i>parS_{PMT1}-FRT</i>	Conjugation LY162 x LY128
LY1266	MS388 / F-Tn10, <i>parS_{PMT1}-FRT, ΔyjfB :: FRT-kan-FRT</i>	Conjugation LY1242 x MS388 to St ^R Tc ^R Kn ^R
LY1280	MS388 / F-Tn10, <i>parS_{PMT1}-FRT, ΔyjfB :: FRT</i>	Derivative of LY1266, <i>kan</i> removed via pCP20
LY1343	MS388 / pBG39	pBG39 x MS388 to Ap ^R
LY1344	MS388 / F-Tn10 / pBG39	pBG39 x LY5 to Ap ^R
LY1416	MS388 / pTrc99a	pTrc99a x MS388 to Ap ^R
LY1468	MS388 <i>hupA-mCherry-FRT</i> / pBG39	pBG39 x LY248 to Ap ^R
LY1476	MS388 / pBG49	pBG49 x MS388 to Ap ^R
LY1513	MS388 / F-Tn10, <i>parS_{PMT1}-FRT, ΔyjfB :: FRT, ssb-ypet-kan</i>	LY1280 x P1.LY118 to Kn ^R
LY1586	MS388, <i>ilva :: pbiofab-mCherry-FRT-kan-FRT</i>	MS388 x P1.LY1575
LY1659	MS388 / pTrc99a-yjfB	pTrc99a-yjfB x MS388 to Ap ^R
LY1737	MS388, <i>ilva :: pbiofab-mCherry-FRT</i>	Derivative of LY1586, <i>kan</i> removed via pCP20
LY1871	MS388 / pCV1	pCV1 x MS388 to Ap ^R
LY1872	MS388 / pCV2	pCV2 x MS388 to Ap ^R
LY1933	MS388 / pCV3	pCV3 x MS388 to Ap ^R
LY1934	MS388 / pCV4	pCV4 x MS388 to Ap ^R
LY1935	MS388 / pCV5	pCV5 x MS388 to Ap ^R
LY1936	MS388 / pCV6	pCV6 x MS388 to Ap ^R
LY1937	MS388 / pCV7	pCV7 x MS388 to Ap ^R
LY1938	MS388 / pCV8	pCV8 x MS388 to Ap ^R
LY2107	MS388 / pCV18	pCV18 x MS388 to Ap ^R
LY2121	MS388 / pCV19	pCV19 x MS388 to Ap ^R
LY2125	MS388 / pCV20	pCV20 x MS388 to Ap ^R
LY2209	MS388 / pCV24	pCV24 x MS388 to Ap ^R
LY2219	MS399 / pTrc99a-sfGFP	pTrc99a-sfGFP x MS388 to Ap ^R
MG1655	λ , <i>rph-1</i>	Coli Genetic Stock Center (CGSC) #6300

MS388	MG1655 <i>rpsL</i> (St ^R)	Gift from F. Cornet
Other genetic backgrounds		
BL21		
Ox468	W1485 <i>hupA-mCherry-Km</i>	Gift from F. Cornet
K603	F-Tn10	Coli Genetic Stock Center (CGSC) #6451
DH5α		
DY330	W3110 $\Delta lacU169$, <i>gal490</i> , $\lambda cl857$, $\Delta(cro-bioA)$	(Yu et al., 2000)
LY162	DY330 / F-Tn10- <i>parS_{PMT1}-FRT</i>	Conjugation LY124 × DY330 to St ^S Tc ^r
LY1242	DY330 / F-Tn10- <i>parS_{PMT1}-FRT</i> , $\Delta yjyB ::$ <i>FRT-kan-FRT</i>	$\Delta yjyB :: kan$ construct at the endogenous F plasmid <i>locus</i> (OL606/OL607)
LY1333	DH5α / pBG39	Gibson assembly <i>yjyB-sfGFP</i> construct from LY792 on pTrc99a plasmid (OL604/OL605 and OL602/ OL603)
LY1575	DY330, <i>ilva :: pbiofab-mCherry-FRT-</i> <i>kan-FRT</i>	$\Delta yjyB$ <i>pbiofam-mCherry</i> fusion (OL734/OL383)
LY1620	DY330 / pBG39	<i>sfGFP</i> deletion by PCR-ligation of LY1333 (OL602/OL776)
LY1869	DH5α / pCV1	Phosphorylation-ligation of pTrc99a- <i>yjyB</i> (OL903/OL904)
LY1870	DH5α / pCV2	Phosphorylation-ligation of pBG39 (OL903/OL904)
LY1914	DH5α / pCV3	Directed mutagenesis (OL906/OL907)
LY1915	DH5α / pCV4	Directed mutagenesis (OL908/OL909)
LY1916	DH5α / pCV5	Directed mutagenesis (OL910/911)
LY1917	DH5α / pCV6	Directed mutagenesis (OL906/OL907)
LY1918	DH5α / pCV7	Directed mutagenesis (OL908/OL909)
LY1919	DH5α / pCV8	Directed mutagenesis (OL910/OL911)
LY1983	DH5α / pCV15	PCR amplification of <i>yjyB</i> (OL932/OL933) from pTrc- <i>yjyB</i> and mix Topo151 kit
LY2035	BL21 / pCV15	pCV15 x BL21 to Ap ^R
LY2106	DH5α / pCV18	Directed mutagenesis (OL1006/OL1007)
LY2113	DH5α / pCV19	Directed mutagenesis (OL1006/OL1007)
LY2126	DH5α / pCV20	Directed mutagenesis (OL1006/OL1007)
LY2158	DH5α / pCV24	Directed mutagenesis (OL1006/OL1007)

Table S1. Strain list

The abbreviation *kan* refer to insertions conferring resistance to kanamycin (Kn^R). St^R refer to streptomycin resistance. *FRT* refers to the FLP site-specific recombination site.

Tn10 transposon is located in the intergenic region *ybdB-ybfA* on the F plasmid.

Name	Sequence	Construct
OL1	GTATTGTCACATATGATATTTTTGTGTGTG GCCTTCCAGGTCTGCTATGTGGTGCTATCT	λ red <i>parS_{PMT1}-FRT-cat-FRT</i> insertion at the F plasmid
OL2	ACAGGCATTGTCAGATACCGTTATGCCGCA AAAGCGGCAGATTGTGTAGGCTGGAGCTGC	intergenic <i>ygeB-ygfA locus</i> . PCR on pGBKD3-parS
OL383	TCTGGAAGATTTTGCCGAACCACAAATGACG TTGTGCGGCCATATGAATATCCTCCTTAG	Λ red with OL734 <i>pbiofab-</i> <i>mCherry</i> fusion at the
OL418	GGATGCCACTGAACGTACCGATAACCTGGCT GATGCCGCCAGCTCGGCTGGCTCCGCTGC	λ red <i>yjfB-sfgfp</i> fusion at the endogenous F plasmid <i>locus</i> .
OL419	TGCTGCCGCCCCGTCTCCGGCGGGGCGGTGT GGTTGTTTCATATCCTCCTTAGTTCCTATT	PCR on pR6K-sfGFP plasmid
OL602	GATCCTCTAGAGTCGACCTGCAGGC	
OL603	TCTGGAAGATTTTGCCGAACCACAAATGACG TTGTGCGGCCATATGAATATCCTCCTTAG	
OL604	AACAATTTACACAGGAAACAGACCATGTCA GTTACAGAGTCTAA	Gibson assembly <i>yjfB-sfGFP</i> insertion at the pTrc99a <i>locus</i> .
OL605	GCCTGCAGGTCGACTCTAGAGGATCTTATTT GTAGAGCTCATCCA	PCR on LY735
OL606	CGGCAGACAATCATTATTACCGTTTTGGGAG GTACTAACTGTGTAGGCTGGAGCTGCTTC	Λ red <i>kan</i> insertion at the endogenous F plasmid <i>yjfB</i>
OL607	TGCTGCCGCCCCGTCTCCGGCGGGGCGGTGT GGTTGTTTCACATATGAATATCCTCCTTAG	<i>locus</i> . PCR on pROD62 plasmid
OL675	CATGGTCTGTTTCCTGTGTG	PCR-ligation with OL775
OL734	GTCAGTCAGGAGGCCGGTCAGACCAGCCTCC GGAAGATAAGTGTAGGCTGGAGCTGCTTC	Λ red with OL383
OL775	TCTAAAGGTGAAGAACTGTTACC	PCR-ligation with OL675
OL776	TCAGGCGGCATCAGCCAGGT	<i>sfGFP</i> deletion by PCR-ligation on pBG39 plasmid
OL906	CTGGGTTATTCGCCCGCCACGTTACGCGAA TGCTGAAACTGGC	R168A mutation by directed mutagenesis. PCR on pTrc99a
OL907	GCGGGCGAATAACCCAGCAAATCACCG	YfjB plasmid
OL908	CCGCCACGTTACAGGCAATGCTGAAACTGGCA GACCTTGCGC	R172A mutation by directed mutagenesis. PCR on pTrc99a
OL909	GCCTGAACGTGGCGGGGCGAATAAC	YfjB plasmid
OL910	G TTCAGCGAATGCTGGCACTGGCAGACCTTG CGCCTGT	K175A mutation by directed mutagenesis. PCR on pTrc99a
OL911	GCCAGCATTCGCTGAACGTGGCGGG	YfjB plasmid
OL1006	GCCGCAGGTGGTCGCGCACTGGCAGCACTCA ACATGCTG	R94A mutation by directed mutagenesis. PCR on pTrc99a
OL1007	GCGCGACCACCTGCGGCGACACCGT	YfjB plasmid

Table S2. PCR primers used for strain and plasmid constructions

Name	Construct and Usage ^a	Source or reference
pCP20	Flp expression plasmid	
pmCherry- <i>parB</i> (pSN70)	IPTG inducible expression of N-terminal fusion mCherry-ParB _{PMT1}	(Yu et al., 2000) and Fig. 1D-E, Fig. 6B-C
pR6K-sfGFP	Carries <i>sfGFP-FRT-kan-FRT</i> used for several C-terminal fusion by λ red	(Yu et al., 2000)
pROD62	Carries <i>mCherry-FRT-kan-FRT</i> used for various <i>kan</i> deletions	Gift from R. Reyes-Lamothe, McGill University
pTrc99a		Fig. S3A-B-C-D-E
pTrc99a-YfjB	<i>sfGFP</i> deletion from pBG39 by PCR-ligation	Laboratory, Fig. S3A-B-C-D-E
pBG39	pTrc99a YfjB-sfGFP	Laboratory, Fig. 1I-J, Fig. 2B-C, Fig 5A-B-C, Fig. S1A-B-C-D-G-H-I-J
pBG49	pTrc99a YfjB-mCherry	Laboratory, Fig. S1E-F
pCV1	pTrc99a YfjB Δ HTH	Laboratory, Fig. S3B-C-D-E
pCV2	pTrc99a YfjB-sfGFP Δ HTH	Laboratory Fig. 2B-C
pCV6	pTrc99a YfjB-sfGFP R168A	Laboratory, Fig. 2B-C
pCV7	pTrc99a YfjB-sfGFP R172A	Laboratory, Fig. 2B-C
pCV8	pTrc99a YfjB-sfGFP K175A	Laboratory, Fig. 2B-C
pCV15	pET_Topo YfjB	Laboratory, Fig. S2A
pCV18	pTrc99a YfjB-sfGFP R94A	Laboratory, Fig. 2B-C
pCV20	pTrc99a YfjB Δ HTH R94A	Laboratory, Fig. S3A
pCV24	pTrc99a YfjB R94A	Laboratory, Fig. S3B-C
F-Tn10 conjugative plasmid (from K603) derivatives		
<i>Fwt</i>	F-Tn10 with <i>parS_{PMT1}</i> inserted at the intergenic <i>ygeB-ygfA locus</i>	(Yu et al., 2000) and Fig. 6A-B-C
<i>F ΔyfjB</i>	F-Tn10 with <i>parS_{PMT1}</i> inserted at the intergenic <i>ygeB-ygfA locus</i> ,	Laboratory, Fig. 6A-B-C
<i>F yfjB-sfGFP</i>	F-Tn10 <i>parS_{PMT1}</i> with <i>yfjB-sfgfp</i> translational fusion at the endogenous locus	Laboratory, Fig. 1D-E-F-G-H, Fig. 4A, Fig. S1B-C-E-F

Table S3. Plasmids used in this study

sfGFP gene encodes the superfolder Green Fluorescent Protein sfGFP

4. Discussion

Bien que la fonction complète de la protéine YfjB n'ait pas encore été entièrement élucidée, cet article permet d'apporter de nombreuses connaissances sur sa dynamique intracellulaire au cours de la conjugaison et son impact sur la bactérie receveuse. Le choix d'une approche multidisciplinaire nous confère une vision globale à la fois au niveau génétique, moléculaire, cellulaire et également sur la physiologie de la bactérie. Ainsi, nous démontrons que la protéine YfjB est produite immédiatement lors du transfert du plasmide F par conjugaison, et ce uniquement dans les nouvelles bactéries transconjugantes. De façon similaire aux protéines ParB, le domaine HTH ainsi que le motif GxxRxxA sont essentiels à la localisation préférentielle sous forme de foci de la protéine YfjB-sfGFP dans l'aire du nucléoïde. Cette capacité de liaison à l'ADN, confirmé *in vivo* par ChiP-seq et *in vitro* par EMSA, induit un changement global de la transcription des gènes de la bactérie hôte. La majorité des gènes dont l'expression est affectée sont retrouvés impliqués dans de multiples mécanismes cellulaires comme le métabolisme de sources carbonées, la mobilité ou encore le métabolisme du pyruvate. De façon intéressante, nos résultats sont concordants avec de récentes publications démontrant que les plasmides conjuguatifs peuvent affecter jusqu'à 20% l'expression des gènes hôte, majoritairement impliqués dans des voies métaboliques similaires à celles observées ici. Enfin, bien que partielle, l'obtention en parallèle de la structure du domaine IV sous forme de dimère constitue une avancée considérable pour la compréhension de la dynamique et de la fonction de la protéine.

En conclusion, la protéine YfjB du plasmide F partage une homologie avec les protéines ParB uniquement d'un point de vue structural de par sa capacité de dimérisation et de liaison à l'ADN. YfjB semble alors plutôt jouer un rôle dans la régulation du profil génétique hôte et affecte diverses voies métaboliques. Dans ce sens, nous observons un délai de 30% de la conversion de l'ADNsb transféré en ADNdb lorsqu'*yfjB* est déléte du plasmide F, reflétant d'autant plus un rôle pour l'établissement du plasmide. Nous proposons que cela rentre dans une stratégie établie par le plasmide F pour limiter son impact métabolique lors de l'acquisition par conjugaison, le temps que son établissement soit effectif et que d'autres facteurs plasmidiques soient exprimés plus tardivement.

Partie IV : Dynamique et mécanistique de l'acquisition de résistance antibiotique par conjugaison

Direct visualisation of drug-efflux in *Escherichia coli* cells

Audrey Reuter, Chloé Virolle, Kelly Goldlust, Annick Berne-Dedieu, Sophie Nolivos & Christian Lesterlin

Publié dans *FEMS Microbiology Reviews* (2020)

1. Contexte

Lors de ma première année de thèse, j'ai eu l'opportunité de participer à l'écriture d'un article soumis dans le journal *FEMS Microbiology Reviews* en 2020 et pour lequel je partage la position de co-1^{er} auteur avec Audrey Reuter et Kelly Goldlust. Ce travail de recherche découle directement d'une publication antécédente du laboratoire, publiée en 2019 dans le journal *Science* par le Dr. Sophie Nolivos et démontrant l'importance de pompes à efflux multi-drogues AcrAB-TolC codées par le chromosome pour l'acquisition de résistance à la tétracycline (Tc) portée par le plasmide F. Cela fut pour moi l'occasion de continuer de me familiariser avec les techniques de laboratoire et protocoles déjà mis en place tout en interagissant avec les autres doctorantes de l'équipe. Kelly Goldlust venait d'arriver au laboratoire pour débiter sa thèse, tandis qu'Audrey Reuter était à ce moment en deuxième année de thèse ; elle a ainsi pu nous partager son savoir-faire et ses connaissances concernant les outils de laboratoire. Pouvoir participer à l'écriture et la publication d'un tel article en première année de thèse a alors été très gratifiant d'un point de vue personnel et scientifique, et nous a également toutes trois permis d'assurer les conditions nécessaires auprès de l'école doctorale pour soutenir nos thèses respectives.

2. Contenu

Comme déjà présenté précédemment, notre laboratoire développe une approche d'étude entrée autour de la microscopie à fluorescence en temps réel et en cellules vivantes afin de quantifier la dynamique de la conjugaison bactérienne. Le plasmide F majoritairement utilisé lors de nos études a la particularité de porter un transposon Tn10 conférant une résistance à la tétracycline (Tc). La Tc est un antibiotique bactériostatique de la classe des cyclines et inhibant la synthèse protéique par interaction avec la sous-unité ribosomale 30S (Chopra and Roberts 2001). Ce mode d'action rend la Tc efficace contre un large spectre de bactéries Gram-positives et négative, mais son utilisation

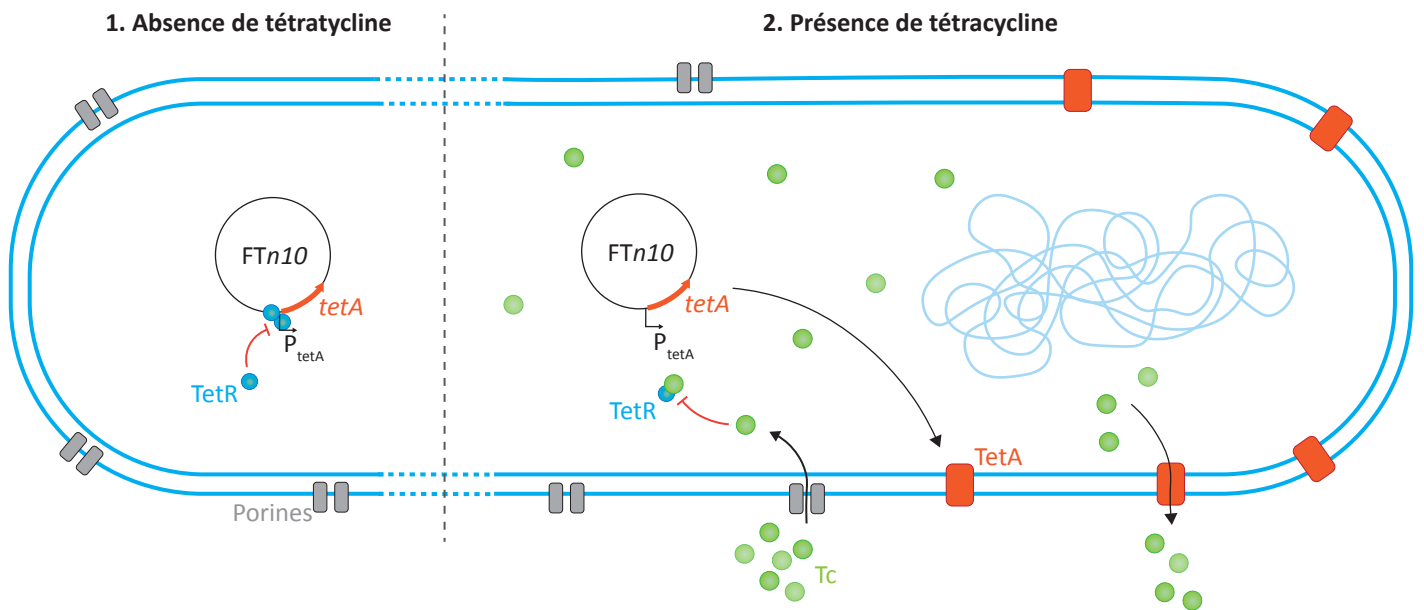


Figure 6. Schéma de la régulation du système TetA/TetR porté par le transposon Tn10.

Le transposon Tn10 inséré dans le plasmide F code les gènes *tetA* et *tetR* impliqués dans l'établissement de l'efflux spécifique de la tétracycline par les pompes TetA.

1. En absence de Tc, le répresseur TetR lie le promoteur P_{tetA} et inhibe sa transcription.
2. En présence de Tc, les molécules antibiotiques sont transportées dans le cytoplasme via des porines et pompes à efflux généralistes. Leur liaison à TetR va lever la répression du promoteur P_{tetA} . La Tc va alors être éfluée par les pompes TetA transcrites et traduites.

intense depuis son introduction en 1948 a mené au développement de nombreuses résistances (Roberts 1996; Chopra and Roberts 2001; Coenen et al. 2011). Le *Tn10* code pour le système de pompe à efflux spécifique TetA/TetR faisant parti des premières familles de pompes à efflux identifiées et le plus fréquemment retrouvées chez les bactéries Gram-négatives ayant développé une résistance à la Tc (Bryan, Shapir, and Sadowsky 2004). La répression de *tetA* par TetR est levée par inhibition de la protéine par la molécule de Tc, permettant la production des pompes TetA pour l'efflux rapide de l'antibiotique hors de la cellule et réduisant l'inhibition traductionnelle associée (Figure 6). Le fonctionnement de ce système est bien décrit dans la littérature, mais nous apportons une description de la dynamique et chronologie de production de TetA et de l'efflux de Tc associé. Nous prenons part pour cela de la propriété d'auto-fluorescence intrinsèque de la molécule de Tc et quantifions la production de la protéine TetA fusionnée au marqueur fluorescence mCherry (TetA-mCh) en réponse à l'ajout de Tc dans le milieu (Dubuy et al. 1964; Nolivos et al. 2019).

Cet article quantifie dans un premier temps l'accumulation dose-dépendante de Tc au sein de bactéries *wt* ne portant par le plasmide *FTn10* ainsi que dans un mutant *acrR* surproduisant les pompes à afflux AcrAB-TolC. L'accumulation de la Tc est ensuite mesurée dans des bactéries portant le plasmide *FTn10tetA-mCh*. En suivant la production de la protéine TetA-mCh associée, une hétérogénéité de production de la pompe TetA au sein de la population bactérienne nous a conduit à répéter les expériences en pré-induisant les bactéries avec de l'anhydrotétracycline (Atc), un analogue de la Tc sans activité antibiotique mais quand même capable de lier TetR et induire la production de TetA. Cela nous a permis d'établir une corrélation entre l'induction des pompes à efflux TetA et l'efflux de la Tc et révéler l'établissement d'une fine régulation du système TetR/TetA.

3. Ma contribution

Kelly Goldlust et moi-même avons réalisé la majorité des acquisitions d'images de microscopie lors des différents traitements à la Tc et Atc des cellules, et nous nous sommes également partagées les analyses correspondantes afin de quantifier l'accumulation de Tc et la production des pompes à efflux TetA-mCh.

RESEARCH ARTICLE

Direct visualisation of drug-efflux in live *Escherichia coli* cells

Audrey Reuter[†], Chloé Virolle[†], Kelly Goldlust[†], Annick Berne-Dedieu, Sophie Nolivos[‡] and Christian Lesterlin^{*,§}

Microbiologie Moléculaire et Biochimie Structurale (MMSB), Université Lyon 1, CNRS, Inserm, UMR5086, 69007, Lyon, France

*Corresponding author: Microbiologie Moléculaire et Biochimie Structurale CNRS-UMR5086, 7 passage du Vercors 69007, Lyon, France. E-mail: christian.lesterlin@ibcp.fr

One sentence summary: Real-time visualization of tetracycline (Tc) and the Tc-specific TetA efflux pump protein reveals the dynamics of drug accumulation and extrusion in live *Escherichia coli* cells.

Editor: Tam Mignot

[†]These authors contributed equally

[‡]Current address: Université de Pau et des Pays de l'Adour, CNRS, UMR5254, IPREM, 64000, Pau, France

[§]Christian Lesterlin, <http://orcid.org/0000-0002-9108-0848>

ABSTRACT

Drug-efflux by pump proteins is one of the major mechanisms of antibiotic resistance in bacteria. Here, we use quantitative fluorescence microscopy to investigate the real-time dynamics of drug accumulation and efflux in live *E. coli* cells. We visualize simultaneously the intrinsically fluorescent protein-synthesis inhibitor tetracycline (Tc) and the fluorescently labelled Tc-specific efflux pump, TetA. We show that Tc penetrates the cells within minutes and accumulates to stable intracellular concentration after ~20 min. The final level of drug accumulation reflects the balance between Tc-uptake by the cells and Tc-efflux by pump proteins. In wild-type Tc-sensitive cells, drug accumulation is significantly limited by the activity of the multidrug efflux pump, AcrAB-TolC. Tc-resistance wild-type cells carrying a plasmid-borne Tn10 transposon contain variable amounts of TetA protein, produced under steady-state repression by the TetR repressor. TetA content heterogeneity determines the cells' initial ability to efflux Tc. Yet, efflux remains partial until the synthesis of additional TetA pumps allows for Tc-efflux activity to surpass Tc-uptake. Cells overproducing TetA no longer accumulate Tc and become resistant to high concentrations of the drug. This work uncovers the dynamic balance between drug entry, protein-synthesis inhibition, efflux-pump production, drug-efflux activity and drug-resistance levels.

Keywords: microscopy in live bacterial cells; drug-efflux; drug-resistance; TetA efflux pump protein

INTRODUCTION

Drug-resistant microorganisms have been isolated soon after the introduction of antibiotherapy in the early 20th century. Microbiology analysis and systematic sequencing of drug-resistant bacteria from natural and clinical environments have since uncovered a vast collection of genes that confer resistance to most classes of antibiotics currently used in clinical treatments. Bacterial drug-resistance is consequently a significant

obstacle to the successful treatment of infections and is recognized as an increasingly severe threat to public health worldwide. Due to its biological importance, bacterial drug-resistance has attracted lots of attention and has been the focus of extensive research. Various mechanisms of antimicrobial resistance have been characterised, including inactivation or modification of the drug, modification of a drug target, limiting drug uptake by changing the cell membrane permeability and active efflux of the drug. Drug efflux mechanism, first described in

Received: 29 January 2020; Accepted: 22 July 2020

© The Author(s) 2020. Published by Oxford University Press on behalf of FEMS. All rights reserved. For permissions, please e-mail: journals.permissions@oup.com

1980 (McMurry, Petrucci and Levy 1980), play a prominent role in antimicrobial resistance (Nikaido 1998, 2009; Li and Nikaido 2004, 2009). Efflux of drugs from the cellular compartment to the extracellular medium can be performed by multidrug or drug-specific efflux pumps proteins.

Multidrug pumps are generally chromosome-encoded and able to extrude a wide range of toxic compounds, thus conferring a certain intrinsic level of multidrug resistance (MDR). In *E. coli*, the AcrAB-TolC tripartite complex transports a variety of antibiotics and other antimicrobials (Sulavik et al. 2001; Tal and Schuldiner 2009; Du et al. 2014; Li, Plésiat and Nikaido 2015; Bergmiller et al. 2017). AcrAB-TolC production is controlled by a complex network of transcriptional regulators (Li, Plésiat and Nikaido 2015), thus allowing for tight regulation of the efflux activity in response to environmental conditions or the presence of antimicrobials. Mutations in transcriptional repressor genes (such as *soxR*, *marR*, *acrR* or *envR*), which result in overproduction of the multidrug efflux pump, are often found in drug-resistant bacteria from natural and clinical origins.

Drug-specific pumps extrude and confer resistance to a single drug. Genes coding for drug-specific pumps are often found on mobile genetic elements such as conjugative plasmids or transposons, which acquisition is sufficient to confer resistance to minimal inhibitory concentration (MIC) of the drug. In this work we focus on the study of the paradigmatic Tetracycline-specific efflux pump TetA. Tetracycline (Tc) is a bacteriostatic protein-synthesis inhibitor that binds reversibly to the ribosome, thus preventing the association of aminoacyl-tRNA (Chopra and Roberts 2001). This fundamental mode of action renders Tc active in a broad-spectrum of both gram-positive and gram-negative bacteria. Since the introduction of Tc in 1948, resistant strains have emerged dramatically in both animal and humans (Roberts 1996; Chopra and Roberts 2001; Coenen et al. 2011). Tc-resistance dissemination together with the development of other effective antibacterial drugs led to the reduction of Tc usage in human treatments, yet Tc remains one of the most used antibiotics in livestock worldwide and is even used in plant agriculture (Eliopoulos, Eliopoulos and Roberts 2003). Notably, Tc is a substrate for the AcrAB-TolC multidrug pump. Indeed, AcrAB-TolC performs low levels of Tc-efflux activity, thus allowing *E. coli* to grow in the presence of sub-inhibitory concentration of the drug (Sulavik et al. 2001; Li, Plésiat and Nikaido 2015). However, AcrAB-TolC activity alone is not sufficient to support cell growth in the presence of minimal inhibitory concentration (MIC) of Tc (10 µg/ml). At this concentration, growth is only possible for strains carrying Tc-specific resistance genes (*tet* genes). To date, 36 *tet* genes have been identified across most bacterial genera. Ten of these genes encode ribosomal protection proteins (such as Tet(M) and Tet(O)), which prevent binding of the Tc molecule to the ribosomes (Burdett 1993; Warburton, Amodeo and Roberts 2016). However, Tc-resistance is largely mediated by efflux mechanisms as 23 of the 36 *tet* genes encode efflux pumps proteins belonging to the major facilitator superfamily (MFS). Efflux pumps of the TetA family were the first identified (Levy and McMurry 1978; McMurry, Petrucci and Levy 1980) and are among the most frequently found in resistant Gram-negative bacteria (Bryan, Shapir and Sadowsky 2004). In fact, *tetA* genes are often carried by transposons inserted in conjugative plasmids, which propagate by horizontal gene transfer between a broad-range of unrelated bacterial species. The paradigmatic Tn10 transposon carries the *tetA* gene coding for the TetA efflux pump and the *tetR* gene encoding the TetR repressor. TetA is a proton motive force-dependent metal-tetracycline/H⁺ antiporter

that selectively transports Tc through the inner membrane in exchange of a proton (Schnappinger and Hillen 1996; Thaker, Spanogiannopoulos and Wright 2010). By exporting Tc from the cytoplasm to the periplasm, TetA decreases the intracellular concentration of the drug, thus reducing protein translation inhibition. TetR is a Tc-responsive repressor protein that regulates *tetA* expression as follows. In the absence of Tc, TetR binds to the promoter region of the *tetA* gene and limits TetA production to basal steady-state levels. When present in the medium, Tc is transported into the periplasm, presumably via OmpF and OmpC porins, and then diffuses passively through the inner membrane (Mortimer and Piddock 1993; Roberts 1996; Fernández and Hancock 2012; Møller et al. 2016). Once in the cytoplasm, Tc binds to the ribosome and inhibits protein synthesis. In parallel, Tc also binds to TetR inducing a conformational change that releases the repressor from P_{tetA} promoter. This results in the induction of TetA production and Tc-efflux activity, thus helping to restore normal protein synthesis level. The level of Tc accumulation within the cells is then resulting from the balance between Tc-uptake (Tc entry) and Tc-efflux by pump proteins. Noteworthy, the non-antibiotic Tc analogue anhydrotetracycline (Atc) retains TetR binding and *tetA* induction activity, but does not inhibit protein synthesis and has no antibiotic effect.

Our current understanding of the mechanism of Tc resistance by the TetA efflux pump results from several decades of study (Roberts 1996; Chopra and Roberts 2001; Eliopoulos, Eliopoulos and Roberts 2003). Regulation of TetA production by TetR in response to the drug has been extensively investigated using genetics approaches, transcriptional analysis (Muthukrishnan et al. 2012; Møller et al. 2016) or using computational modelling (Biliouris, Daoutidis and Kaznessis 2011; Schultz, Palmer and Kishony 2017). Besides, biochemical works have provided a well-documented description of the structure and function of TetA and TetR proteins (Yamaguchi et al. 1990; Yamaguchi, Udagawa and Sawai 1990; Aldema et al. 1996; Ramos et al. 2005; Chow et al. 2012; Kumar and Varela 2012; Cuthbertson and Nodwell 2013). However, mainly due to previous technological limitations, the *in vivo* dynamics of Tc-efflux by the TetA pump in real-time at the single-cell level remains poorly understood. Here, we have developed an experimental system that enables to address this question. We use live-cell fluorescence microscopy associated with microfluidics chamber to perform the simultaneous visualization and quantification of both Tc and TetA intracellular concentrations. Tetracycline was visualized directly by taking advantage of its autofluorescence property (Dubuy et al. 1964)). In parallel, we use the fully functional carboxy-terminal fusion of TetA to the mCherry fluorescent protein (TetA-mCh) expressed from the FTn10 plasmid endogenous locus (Nolivos et al. 2019). We characterise the dynamics of entry and accumulation of Tc within the intracellular compartment and the influence of AcrAB-TolC overproduction by deletion of the *acrR* gene. We also characterise Tc accumulation in Tc-resistant strain carrying the FTn10*tetA-mCh* plasmid and we correlate the induction of TetA production with Tc-efflux activity.

RESULTS

Tc accumulation in the intracellular compartment

We performed time-lapse fluorescence microscopy imaging of live *E. coli* cells placed in microfluidic chamber during the injection of growth medium containing minimal inhibitory concentration (1MIC) of Tc (10 µg/ml) or 10MIC of Tc (100 µg/ml). Image

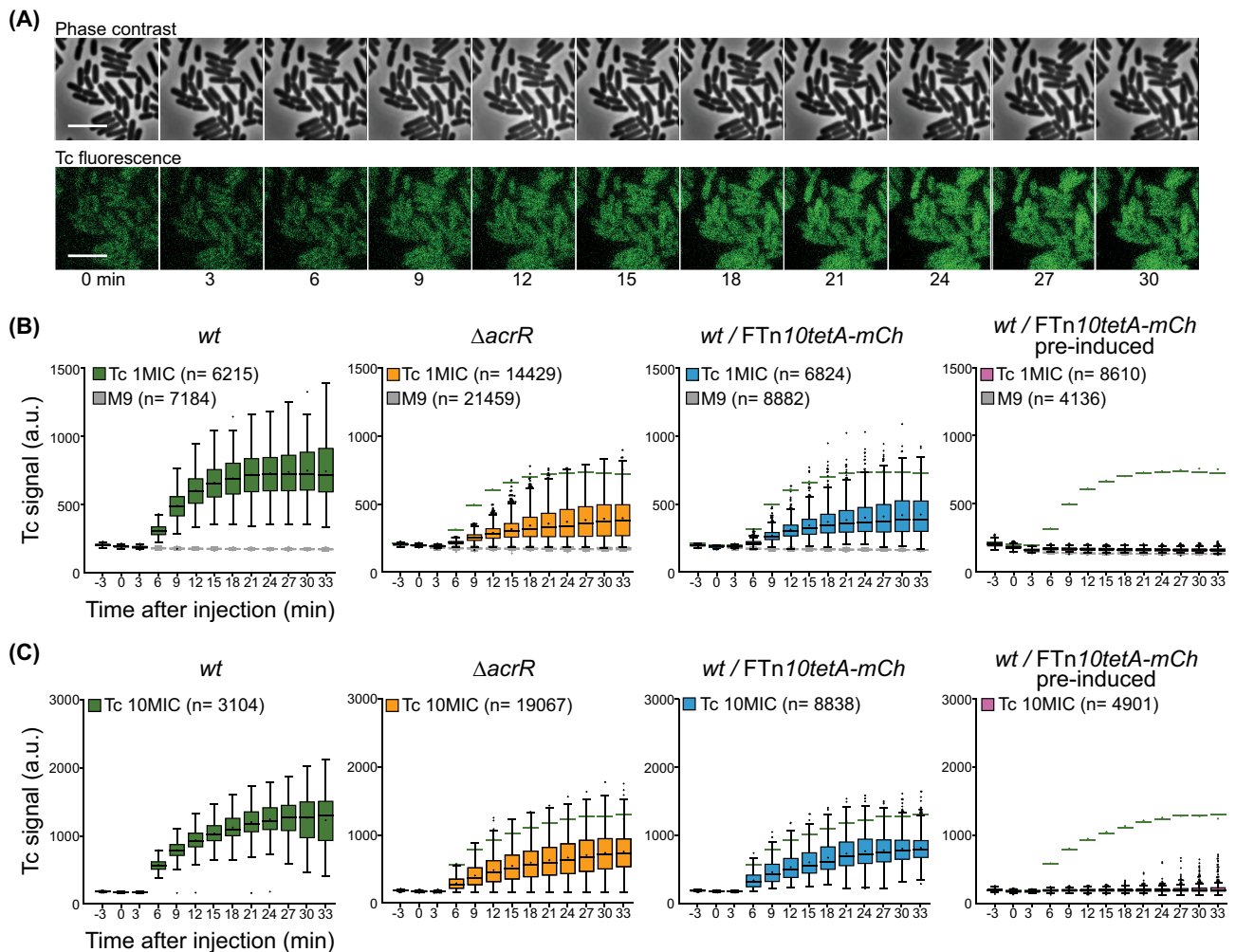


Figure 1. Dynamics of tetracycline accumulation in live *E. coli* cells. **(A)**, Time-lapse microscopy phase contrast (top) and green fluorescence channel (bottom) images of *wt E. coli* cells in microfluidics chamber during injection of Tc 1MIC (10 $\mu\text{g}/\text{ml}$). Imaging intervals 3 min. Scale bar 5 μm . **(B)**, Box plots presenting the quantification of green fluorescence intracellular signal (a.u., arbitrary unit) during time-lapse experiments after injection of M9 glucose medium with (coloured boxes) or without (grey boxes) Tc 1MIC (10 $\mu\text{g}/\text{ml}$). From left to right, results are presented for *wt*, ΔacrR , *wt/FTn10tetA-mCh* strains and for *wt/FTn10tetA-mCh* after overnight pre-induction with Atc (0.2 $\mu\text{g}/\text{ml}$). The median, quartile 1 and quartile 3 are indicated by horizontal lines and the mean by a black dot. Black dots above and below the max and min values correspond to outlier cells. The median and the mean obtained for the *wt* strain are reported on each plot by a green line and a green dot, respectively. The total number of cells analysed and plotted ($n =$) is indicated. **(C)**, Same as 1B for injection of Tc 10MIC (100 $\mu\text{g}/\text{ml}$).

analysis was achieved by running automated cell detection and quantification of Tc and TetA-mCh intracellular fluorescent signal in the course of the experiments. The early steps of Tc entry and accumulation in the cellular compartment were analysed using time-lapses with 3 min imaging intervals (Fig. 1A and Movie S1). When growth medium containing Tc at 1MIC is injected, the intracellular green fluorescence signal increases significantly, reflecting the entry of the intrinsically fluorescent Tc molecules within the cell compartment (Fig. 1A-B and Movie S1). Intracellular Tc is first detected between 3 and 6 minutes after injection, and accumulates to eventually reach a steady-state level after 21 min \pm 3. When Tc concentration is increased to 10MIC (Fig. 1C and Movie S1), we also detect the entry of the Tc between 3 and 6 minutes after injection. However, it takes a longer 27 min \pm 3 period for Tc intracellular concentration to eventually stabilize. Most importantly, the final concentration of Tc accumulated is increased by 2-fold compared to cells exposed to 1MIC. This shows that a 10-fold increase in Tc concentration in the medium only results in a 2-fold increase accumulation within the cells. These observed levels of Tc accumulation

reflect the balance between Tc-uptake by the cells (Tc entry) and the extrusion of Tc mediated by efflux pump proteins. Our observations suggest that the efficiency of Tc-uptake and Tc-efflux do not respond similarly to the increase of Tc concentration in the medium, resulting in Tc accumulation levels that are not proportionally dose-dependent (see discussion).

To better understand the contribution of Tc-efflux activity on the dynamics of accumulation within *wt* cells, we investigated the importance of the main multidrug pump in *E. coli*, the AcrAB-TolC complex. AcrAB-TolC is known to extrude Tc, thus allowing resistance and cell growth in the presence of sub-inhibitory concentrations of the drug (Sulavik et al. 2001; Li, Plésiat and Nikaido 2015). Consistently, we have previously reported that ΔacrA , ΔacrB and ΔtolC single mutants strains accumulate significantly more Tc than the isogenic *wt* strain (Nolivos et al. 2019). We then tested the effect of AcrAB-TolC overproduction induced by deletion of the *acrR* repressor gene (Nolivos et al. 2019). The entry of Tc in ΔacrR cells is detected between 3 and 6 min after injection of the drug at 1MIC, as observed for the *wt* strain (Fig. 1B). However, the final level of Tc accumulation is significantly reduced in

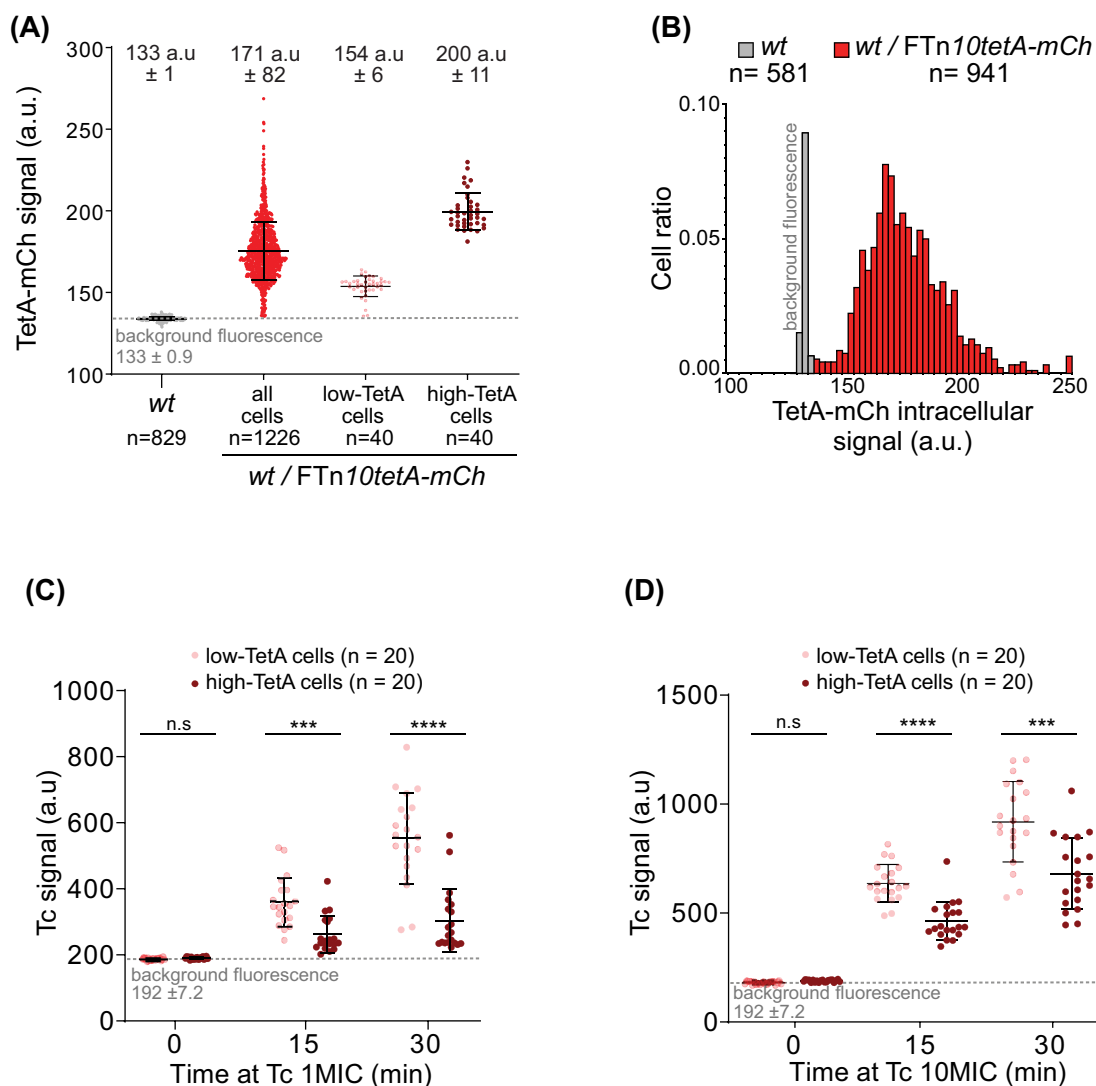


Figure 2. Influence of the initial cellular TetA-mCh content on the dynamics of Tc accumulation. (A), Jitter plots present the quantification of red fluorescence intracellular signal of single-cells (a.u., arbitrary unit). The autofluorescence background of the *wt* strain is shown by grey dots and the grey-dashed line ($133 \text{ a.u.} \pm 0.9$). Results for the *wt/FTn10tetA-mCh* cells are shown by red dots reflecting TetA-mCh signal plus the autofluorescence background. Light red and dark red dots correspond to *wt/FTn10tetA-mCh* cells selected for the low- or high-TetA initial content, respectively. Each dot corresponds to a single-cell, mean and standard deviations are shown in black lines and reported in numbers above the plots. (B), Histogram of the red fluorescence distribution in *wt* (grey) and *wt/FTn10tetA-mCh* (red) cell populations. (C and D), Jitter plots of green fluorescence intracellular signal for *wt/FTn10tetA-mCh* single-cells with initially low-TetA content (light red) or high-TetA content (dark red). Value at $t = 0 \text{ min}$ and the grey dashed line correspond to the green autofluorescence background of the cells before the injection of Tc ($192 \text{ a.u.} \pm 7.2$). Data presented for cells 15 and 30 min after injection of Tc 1MIC (C), and 10MIC (D), show a reduction of Tc accumulation in high-TetA content cells compared to low-TetA content cells. The total number of cells analysed ($n =$) is indicated in each plot. P-Value significance from unpaired statistical t-test is indicated by n.s. (>0.05 , non-significant), *** (<0.001 significant) and **** (<0.0001 significant).

ΔacrR cells compare to *wt* and is attained later ($27 \text{ min} \pm 3$ compared to $21 \text{ min} \pm 3$ for *wt*). At Tc 10MIC, Tc final accumulation was also decreased by ~ 2 -fold in the ΔacrR strain compared to *wt* strain (Fig. 1C). These observations show that the overproduction of AcrAB-TolC pump induced by *acrR* deletion enhances the cells ability to efflux Tc, consequently limiting its accumulation in the cytoplasm. Reduction of Tc intracellular accumulation is expected to attenuate the inhibition of protein synthesis. Consistently, mutations inactivating AcrR or other repressors of AcrAB-TolC (MarR, SoxR) are often found in clinical or environmental strains exhibiting partial resistance to a range of antibiotics, including Tc (Vinué, Hooper and Jacoby 2018; Hoeksema et al. 2019).

Next, we analysed Tc accumulation in *wt* cells carrying the Tc-resistant FTn10tetA-mCh plasmid (Nolivos et al. 2019). Again, Tc entry is detected between 3 and 6 min after drug injection (Fig. 1B). The final level of accumulation is attained after $21 \text{ min} \pm 3$ and is decreased by 2-fold compared to *wt* cells. Similar results are observed in the presence of Tc at 10 MIC (Fig. 1C). These results indicate that even before exposure to Tc, *wt/FTn10tetA-mCh* cells already contain TetA pump proteins readily available to perform efflux of Tc. Consistently, we quantified a significant increase of red intracellular fluorescence in *wt/FTn10tetA-mCh* cells compared to *wt* cells, reflecting the basal amounts of TetA-mCh molecules in plasmid-containing cells (Fig. 2A). These data show that even before exposure to Tc,

the steady-state repression of the *tetA* gene mediated by the TetR repressor allows for the production of a basal level of TetA molecules. This initial TetA-mCh cellular pool is immediately available to perform efflux of Tc and limit the accumulation of the drug in the cellular compartment.

Population heterogeneity in TetA initial content influences Tc accumulation levels

We noticed a certain level of heterogeneity in the initial amounts of TetA-mCh proteins contained in the *wt/FTn10tetA-mCh* cell population (Fig. 2B). We wanted to know whether this initial heterogeneity in TetA content influences the dynamics of Tc accumulation at the single-cell level. To test this possibility, we selected cells with low-TetA initial contents and cells with high-TetA initial contents (Fig. 2B). After subtraction of the red background fluorescence ($133 \text{ a.u} \pm 1$), we estimated that high-TetA content cells initially possess ~ 3.2 times more TetA molecules than low-TetA content cells (see methods). We then quantified Tc accumulation in these two cells categories, 15 and 30 minutes after Tc injection at 1MIC and 10MIC (Fig. 2C and D). Results show that high-TetA cells accumulate significantly less Tc than low-TetA cells. More specifically, the 3.2-fold increase in TetA-mCh initial content results in a 2.5-fold and 1.5-fold decrease in Tc accumulation at 1MIC and 10MIC, respectively. These findings reveal that TetR steady-state repression induces a slight heterogeneity in TetA cellular amounts, which is sufficient to translate into population phenotypic heterogeneity where cells containing more TetA pumps are predisposed to efflux Tc more efficiently. This raised the possibility that cells with very high initial amounts of TetA proteins would perform maximum Tc-efflux activity, thus reducing drug accumulation to minimal levels. To test this hypothesis, we pre-induced *wt/FTn10tetA-mCh* cells with anhydrotetracycline (Atc $0.2 \mu\text{g/ml}$), a Tc analogue that has no antibiotic activity, while retaining the ability to bind to TetR and induce the production of TetA proteins. Pre-induced cells exhibit a ~ 60 -fold increase in TetA-mCh cellular content compared to non-induced cells (Fig. S1A and B, Supporting Information). Time-lapse analysis shows that these cells accumulate virtually no Tc either at 1MIC or 10MIC concentrations (Fig. 1B and C). In these cells, Tc-efflux activity is maximized and outcompetes the constant entry of Tc within the cells.

Correlation between TetA induction and efflux of tetracycline

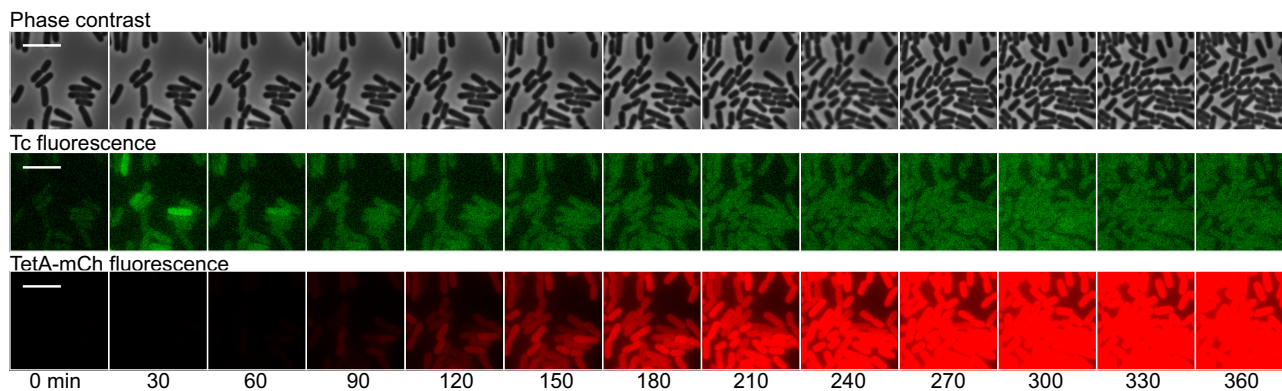
No increase of TetA-mCh fluorescence was detected during the first 30 minutes after injection of Tc (Fig. S1C, Supporting Information). We then performed time-lapses over 300 minutes periods (30 min imaging intervals) to analyse the induction of TetA-mCh production and correlate with Tc-efflux activity in *wt/FTn10tetA-mCh* cells (Fig. 3A and Movie S2). At Tc 1MIC, the accumulation of drug during the first 30 min is followed by a subtle but detectable increase of intracellular TetA-mCh signal at 60 min (Fig. 3B and C). This indicates that the internalized level of Tc is not sufficient to fully inhibit protein synthesis. The modest increase in TetA-mCh content is concomitant with the extrusion of Tc, which concentration rapidly reduces between 30 and 60 min to stabilize at low levels (Fig. 3B). Noteworthy, the low amount of Tc remaining in the cells is sufficient to maintain the induction of TetA-mCh synthesis, which ends up being produced at high levels (Fig. 3C). Importantly,

the growth of *wt/FTn10tetA-mCh* cells in the microfluidic chamber in the presence of Tc 1MIC is comparable to growth without antibiotic (Fig. S2A and Movie S2, Supporting Information). This is confirmed by OD monitoring of the *wt/FTn10tetA-mCh* strain grown in liquid culture (Fig. S2B, Supporting Information). These results indicate that the initial pool of cellular TetA reduces Tc accumulation to levels that allow protein synthesis to continue, allowing for the production of additional TetA and the continuation of cell growth and normal rate. By contrast, in the presence of Tc 10MIC, *wt/FTn10tetA-mCh* cells stop growing over the duration of time-lapse experiments (Figure S2A and Movie S2). Meanwhile, microscopy analysis reveals that high amount of Tc remain in the cells for a long period of time (Fig. 3D). At $\sim 120 \text{ min} \pm 30 \text{ min}$, we observed that TetA-mCh is produced at low rate compared to Tc 1MIC (compare Fig. 3C to E). This modest increase in TetA-mCh cellular content is nonetheless concomitant with the initiation of the efflux of Tc, which intracellular concentration reduces slowly to reach low levels at $270 \text{ min} \pm 30$ (Fig. 3D). OD monitoring consistently reveals that in the presence of Tc 10MIC, cell growth is arrested for a period of about 5 hours before restarting progressively (Fig. S2B, Supporting Information). Height hours after exposure to Tc10MIC, TetA-mCh cellular content is significantly increased (Fig. S2C, Supporting Information). These results indicate that at 10MIC concentration, the amount of Tc accumulated in the cells strongly alters the cells' ability to synthesis new TetA proteins. The cells remain in relative latency for several hours, but eventually manage to produce additional TetA-mCh proteins, which initiate the extrusion of Tc and slowly allows cells growth to restart and more TetA to be produced after 5 hours. We finally observed that pre-induced *wt/FTn10tetA-mCh* cells, which initially contain very high amount of TetA-mCh, accumulate virtually no Tc at 1MIC (Fig. S3A, Supporting Information) and very low levels of Tc at 10MIC (Fig. S3C, Supporting Information), and exhibit no growth latency at either concentration (Fig. S2B, Supporting Information). Similar results were observed for *wt/FTn10tetA-mChΔtetR* strain, in which TetA overproduction is triggered by deletion of the *tetR* gene from the *wt/FTn10tetA-mCh* plasmid (Fig. S2B, Supporting Information).

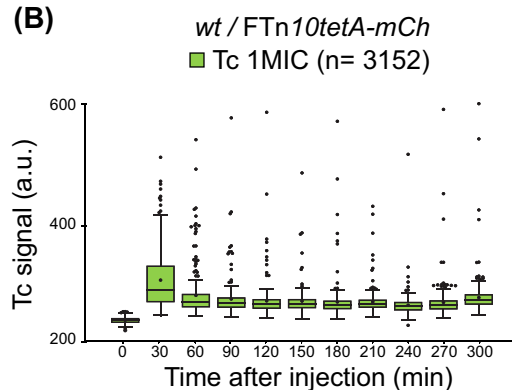
Correlation between TetA cellular content and the level of resistance to tetracycline

We next addressed the level of Tc-resistance of cells containing low or high cellular levels of TetA. To do so, we pre-induced *wt/FTn10tetA-mCh* cells with Tc 1MIC or Atc ($0.2 \mu\text{g/ml}$) for 2, 4, 8 or 24 hours. These pre-induced cell cultures were observed by snapshot microscopy to quantify TetA-mCh intracellular contents and plated on medium containing 1MIC, 10MIC, 20MIC or 40MIC of Tc in parallel (Fig. 4A-C). Snapshot analysis shows that Tc 1MIC and Atc ($0.2 \mu\text{g/ml}$) induce similar rate of TetA-mCh synthesis. In both case, the increase in TetA cellular content is clearly associated with the enhanced resistance to Tc 10MIC, 20MIC and even 40MIC to some extent. This finding reveals that cells exposed to non-lethal concentration of drug develop very high levels of acquired resistance due to the overproduction of TetA pump protein. However, we also observe that cells with high TetA contents (pre-induced *wt/FTn10tetA-mCh* cells and *wt/FTn10tetA-mChΔtetR* cells) exhibited slower growth in M9 compared to the *wt* or non-induced *wt/FTn10tetA-mCh* cells (Fig. S2B, Supporting Information). These results show that the overproduction of TetA is associated with a selective advantage in

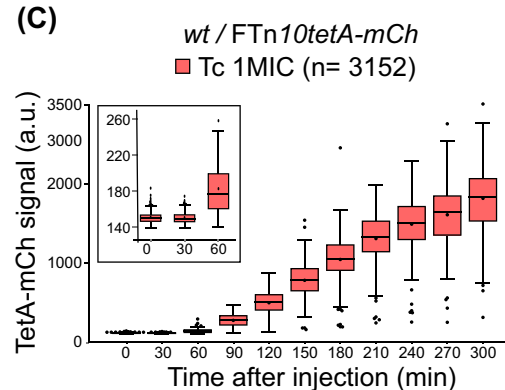
(A)



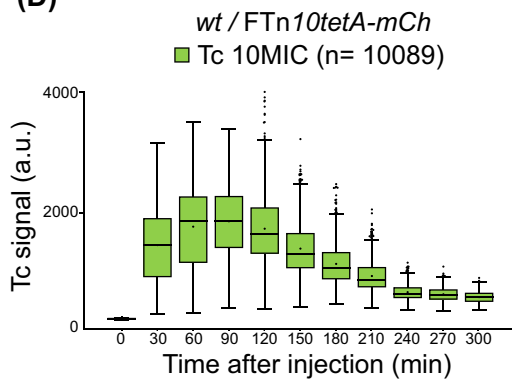
(B)



(C)



(D)



(E)

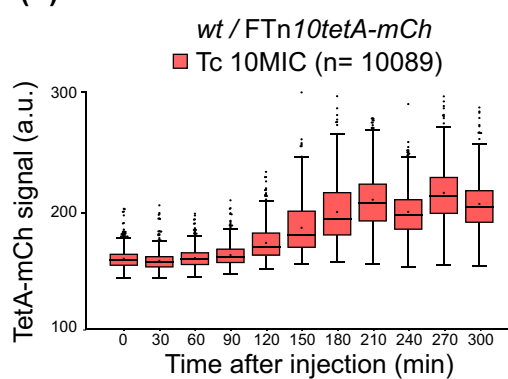


Figure 3. Dynamics of tetracycline accumulation and efflux in correlation with TetA-mCh production in live *E. coli* cells. (A), Time-lapse microscopy phase contrast (top), green fluorescence (middle) and red fluorescence (bottom) images of *wt/FTn10tetA-mCh* cells in microfluidics chamber during injection of Tc 1MIC (10 $\mu\text{g}/\text{ml}$). Imaging intervals 30 min. Scale bar 5 μm . (B and C), Box plots presenting the quantification of Tc (B) and TetA-mCh (C) during time-lapse experiments after injection of M9 glucose medium containing Tc 1MIC (10 $\mu\text{g}/\text{ml}$). (D and E), Box plots presenting the quantification of Tc (D) and TetA-mCh (E) after injection of M9 glucose medium containing Tc 10MIC (100 $\mu\text{g}/\text{ml}$). For B, C, D and E the median, quartile 1 and quartile 3 are indicated by horizontal lines, and the mean by a black dot. Black dots above and below the max and min values correspond to outlier cells. The total number of cells analysed and plotted (n =) is indicated. In these time-lapses, medium supplemented with Tc 1 or 10MIC was injected for 30 min, the injection was then stopped for the rest of the experiment.

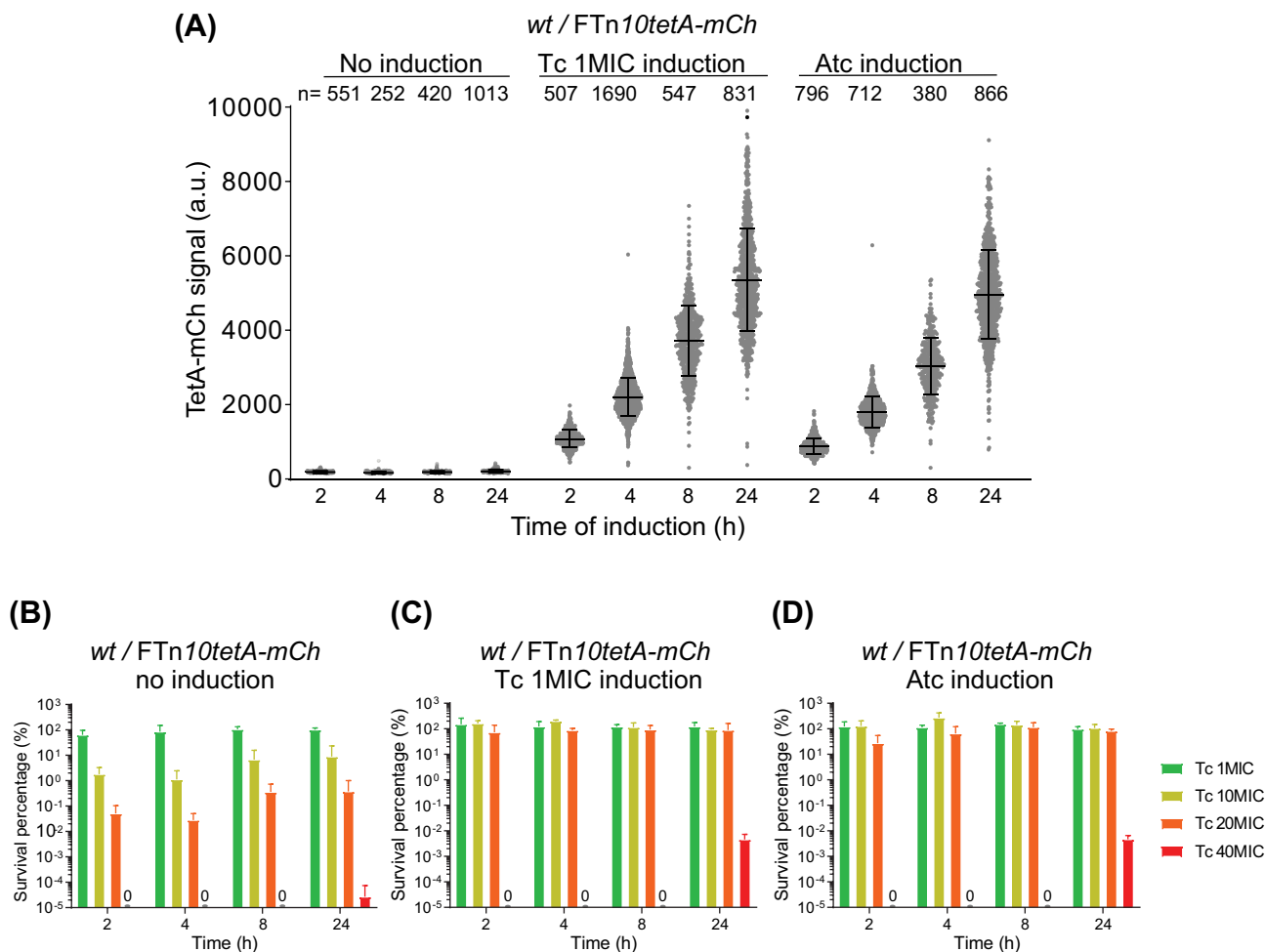


Figure 4. TetA-mCh intracellular content determines the level of Tc-resistance. (A), Jitter plots presenting the quantification of TetA-mCh intracellular signal (a.u., arbitrary unit) from snapshot microscopy imaging of the *wt/FTn10tetA-mCh* strain in the absence of induction or 2, 4, 8 and 24 hours after induction with Tc 1MIC and Atc (0.2 μ g/ml). Each dot corresponds to a single-cell, mean and standard deviations are shown in black lines. The number of cells analyzed and plotted ($n =$) is indicated. (B, C and D), Histogram presenting the survival of *wt/FTn10tetA-mCh* cells in the presence of increasing doses of Tc. Results are shown for *wt/FTn10tetA-mCh* cells corresponding to the panel (A), i.e. without induction (B), or 2, 4, 8 and 24 hours after induction with Tc 1MIC (C) or Atc (0.2 μ g/ml) (D). Survival was estimated by CFU/ml counting after plating on 1MIC, 10MIC, 20MIC or 40MIC of Tc.

the presence of Tc, but also with a loss of fitness in the absence of antibiotic (see discussion).

DISCUSSION

Live-cell fluorescent microscopy imaging represents a valuable tool to investigate bacterial responses to antibiotics in real-time. Most microscopy studies of antibiotics mode of action and interaction with bacterial cells generally requires the use of antibiotics conjugated with fluorescent moieties, such as Fluorescein or BODIPY (Stone et al. 2018). These studies are informative, yet often limited by the fact that the modification of the antibiotic might alter its biochemical properties, including the ability to penetrate the bacterial cell or to perform the inhibitory effect on the cellular machineries (Stone et al. 2018). In this work, we use the unmodified tetracycline, which is part of the few antibiotics that are intrinsically fluorescent. The simultaneous visualization of Tc and the fully functional fluorescently labelled TetA-mCh Tc-specific pump protein allowed us to characterize the real-time dynamics of drug accumulation and efflux in live bacteria.

Tc entry within the cells is observed 3 to 6 min after injection in the microfluidic chamber. Similar timing is observed for all tested strains, indicating that the rate of Tc-uptake is mostly unchanged in all tested genetic backgrounds. The observed levels of Tc accumulation reflect the balance between the two opposite effect of Tc-uptake (Tc entry) and Tc extrusion mediated by efflux pump proteins. Tc crosses the outer membrane via porins and the inner membrane by free diffusion. The internalized Tc is subsequently extruded to the extracellular medium by multidrug or drug-specific efflux pumps present in the cells. Interestingly, we observe that a 10-fold increase of Tc concentration in the medium only results in a \sim 2-fold increase of Tc accumulation levels in the cells. This absence of proportionality between Tc accumulation levels and the dose of antibiotic suggests that Tc-uptake and Tc-efflux activities do not respond similarly to the increase of Tc concentration. Tc-uptake is expected to be limited by the amount of outer membrane porins available, and Tc-efflux by the amount of efflux-pump present in the cells. Our results are compatible with a scenario where Tc 10MIC saturates Tc-uptake systems earlier than Tc-efflux systems, resulting in the relative reduction of Tc accumulation compared to Tc 1MIC condition. This proposal is consistent with the recent

reports that rate of drug-uptake is rate limited by the antibiotic's ability to diffuse through the inner membrane, which permeability properties also varies in response to conditions (pH, temperature and drug treatments) (Cama et al. 2015, 2016; Cama, Henney and Winterhalter 2019).

The ability of the cells to extrude the internalized Tc is significantly enhanced by the overproduction of the AcrAB-TolC multidrug pump in the Δ acrR strain, as well as by the presence of a basal pool of TetA produced from the FTn10tetA-mCh resistance plasmid. In both the Δ acrR and in wt/FTn10tetA-mCh cells, Tc accumulation is reduced by 2-fold compare to the wt. This reduction of Tc accumulation is not sufficient to improve the growth of the Δ acrR cells compared to the wt. However, similar reduction of Tc accumulation appears sufficient for protein synthesis to continue in wt/FTn10tetA-mCh cells, thus allowing the production of additional TetA pumps required for optimal Tc-efflux activity and subsequent cell growth. Increasing Tc concentration to 10 MIC increases Tc accumulation to levels that further inhibit protein synthesis, thus reducing significantly the rate of TetA production and delaying cell growth.

Quantitative image analysis reveals a certain level of heterogeneity of TetA-mCh initial content in the cell population. This shows that even in the absence of Tc or Atc inducers, TetR-mediated repression slightly varies at the single-cell level. Interestingly, this gene expression heterogeneity is sufficient to translate into significant phenotypic heterogeneity, where TetA initial content correlates directly with the cells initial ability to efflux Tc. Yet, Tc still accumulates in all cells, indicating that Tc-efflux activity mediated by the initial pool of TetA pumps is sub-optimal. It is only after TetA content adjustment that the equilibrium between Tc-uptake and efflux is reached, and that Tc intracellular levels become low and stable, presumably reflecting the constant entry of the drug within the cells. The low amount of Tc still detected in the cells is sufficient to induce the rapid production of TetA proteins. Using quantitative real-time PCR, it has been shown that the ratio *tetA/tetR* mRNA is increased by 4-fold in the presence of Tc 1MIC (Møller et al. 2016). This transcriptional response optimizes the synthesis rate of TetA, which accumulates to a final concentration increase by ~60-fold compare to the initial levels. We show that such cells overproducing TetA accumulate virtually no Tc and are resistant to very high doses of the drug (up to 20 MIC and 40 MIC). If the overproduction of TetA is advantageous in the presence of the drug, then why does TetR-mediated repression maintain TetA initial concentration to low levels that are sub-optimal for Tc-efflux? This is most probably explained by our observation that TetA overproduction has a deleterious effect on the cells fitness in the absence of the drug. The phenotype of fitness loss associated with TetA overproduction was previously reported and attributed to unrestricted translocation of protons and ions across the membrane, which triggers partial loss of the membrane potential (Eckert and Beck 1989). TetR-mediated repression of the *tetA* gene is then finely tuned to allow the production of sufficient TetA proteins to limit Tc-accumulation and ensure the maintenance of translation activity required for the synthesized of additional TetA pumps. On the other hand, TetR repression also avoids TetA overproduction that would be deleterious for the cells, while allowing a sensitive detection of the presence of Tc as well as a fast regulatory response.

This work emphasises that the bacterial response to tetracycline depends on the equilibrium between two opposite parameters, the ability of efflux pumps to limit drug accumulation and the ability of the accumulated drug to avoid the production of additional pumps required for the establishment

of effective resistance. The outcome of this dynamic balance primarily depends on the initial concentration of efflux pumps in the cells and the concentration of the drug in the medium.

METHODS

Bacterial strains, plasmids and growth

Bacterial strains and plasmids are listed in Table S1 (Supporting Information). Fusion of genes with fluorescent tags and gene deletion used λ Red recombination (Datsenko and Wanner 2000; Yu et al. 2000). Chromosomal gene loci were transferred by phage P1 transduction to generate the final strains. F plasmids were transferred by conjugation. Unless otherwise stated, cells were grown at 37°C in M9 medium supplemented with glucose (0.2%). When appropriate, supplements were used at the following concentrations; Streptomycin (St) 20 μ g/ml, Ampicillin (Amp) 100 μ g/ml, and Tetracycline (Tc) 10 μ g/ml. For pre-induction of TetA-mCh, wt/FTn10tetA-mCh strain was grown at 37°C in minimal medium supplemented with anhydrotetracycline (Atc) 0.2 μ g/ml.

Spot assay and growth curves

Spot assays

Cells were grown overnight in M9 minimal medium supplemented with glucose 0.2% at 37°C and serially diluted. About 10 μ l drop of each dilution was deposited on LB agar plates supplemented with Tetracycline (Tc) 10, 100, 200 or 400 μ g/ml, corresponding to 1MIC, 10MIC, 20MIC and 40MIC, respectively. Plates were incubated overnight at 37°C, and the next day the concentration of Colony Forming Unit (CFU/ml) was estimated. The survival efficiency of each strain was calculated by normalizing the CFU/ml in the presence of Tc by the CFU/ml on plates without Tc (Fig. 4B-D). Plates were scanned using a Typhoon fluo-phosphoimager GE Healthcare with standard acquisition parameters.

Growth curves

Growth curves (Fig. S2B, Supporting Information) were performed automatically using TECAN Spark multimode plate reader. Flat transparent bottom 96-wells plates were loaded with 20 μ l of exponentially growing cultures and incubated at 37°C, with 1 min agitation and A_{600} measurement every 5 min over 9 hours. Mean growth curves with standard deviation for experimental triplicates were generated using Excel and Graph-Pad Prism software.

Live-cell microscopy imaging and analysis

Cell imaging on agarose-pad

Overnight culture of cells in M9 minimal medium were diluted to an OD_{600nm} of 0.01 and grown with shaking at 37°C to an OD_{600nm} of 0.2. Treated or untreated cells cultures were collected at time points indicated and 5 μ l samples were deposited on 1% agarose-M9 medium pad (Lesterlin and Duabrry 2016) and imaged by microscopy snapshots.

Time-lapse in microfluidic chamber

Time-lapse in microfluidic chambers were performed as described previously (Nolivos et al. 2019). Here, overnight cultures of cells in M9 minimal medium were diluted to an OD_{600nm} of 0.05 and grown at 37°C to an OD_{600nm} of 0.1–0.2. Cells were immediately loaded into a B04A microfluidic chamber (ONIX,

CellASIC®) preheated at 37°C. For Tc entry time-lapses (3 min imaging intervals; Fig. 1), minimal medium supplemented or not with Tc 10 µg/ml (1MIC), Tc 100 µg/ml (10MIC), or Atc 0.2 µg/ml was injected at 3 psi into the microfluidic chamber immediately after acquisition of frame 2 and for the duration of the experiment (45 min). For Tc efflux and TetA induction experiment time-lapses (30 min imaging intervals; Fig. 3), minimal medium supplemented or not with Tc 10 µg/ml (1MIC), Tc 100 µg/ml (10MIC) or Atc 0.2 µg/ml was injected at 3 psi into the microfluidic chamber immediately after acquisition of frame 1 and stopped after 30 min. Nothing else was injected for the rest of the experiment (330 to 400 min).

Image acquisition

Conventional wide-field fluorescence microscopy imaging was carried out on an Eclipse Ti-E microscope (Nikon), equipped with x100/1.45 oil Plan Apo Lambda phase objective, FLash4 V2 CMOS camera (Hamamatsu), and using NIS software for image acquisition. Phase contrast images were also acquired at each time-point. Fluorescence signal acquisition settings were 100 ms for Tc and 100 ms for mCh for both snapshots on agarose-pad and time-lapses in microfluidic chamber, using 50% power of a Fluo LED Spectra X light source at 488 nm and 560 nm excitation wavelengths, respectively. FM 4-64 was acquired using 20 ms exposure at 50% power of a Fluo LED Spectra X light source 560 nm excitation. Structured-illumination microscopy in 3D (3D-SIM) presented in Figure 6 and in Movies was carried out on a standard Elyra PS1 Zeiss microscope. The raw 3D-SIM stacks were composed of 10 to 14 z-sections (110 nm interval for Tc signal and 126 nm interval for TetA-mCh), with 15 images per z-section with the striped illumination pattern rotated to three angles and shifted in five phase steps. Acquisition settings were 60 ms exposure with 593 nm laser (20% transmission) for TetA-mch and 40 ms exposure with 488 nm laser (10% transmission) for Tc. 3D-SIM was performed on exponentially growing cells observed cultivated in M9 minimal medium supplemented with glucose 0.2% with or without Tc.

Image analysis

Microscopy images processing was performed using the open source ImageJ/Fiji (download at [6]) and quantitative image analysis was performed using the free MicrobeJ plugin (download at <http://microbej.com>) (Ducret, Quardokus and Brun 2016). Cells outlines were detected automatically based on the segmentation of phase contrast image. When required, cell outlines were corrected using the Manual-editing interface of MicrobeJ plugin. Mean intracellular fluorescence values were extracted automatically using MicrobeJ plugin. Boxplots, fluorescence histograms, and split histograms were plotted using MicrobeJ interface. Jitter plots, growth curves with mean and standard deviation were generated using Excel and GraphPad Prism software. Imaris analysis software (Bitplane) was used to generate 3D-renderings of 3D-SIM stacks fluorescence signal presented in the Movies.

Consideration of the cells background autofluorescence

Wilt-type *E. coli* cells (without fluorescent marker) exhibit low fluorescence signal in both red and green fluorescence channels (shown in Figs 1B, 2 and Fig. S1, Supporting Information). Background red fluorescence (Brf) was 133 a.u. ± 0.9 (calculated on $n = 829$ wt cells) and background green fluorescence (Bgf) was 192 a.u. ± 7.2 (calculated on $n = 474$ wt cells). During time-lapse

imaging where fresh medium (without Tc or Atc) was injected, these signals gradually decrease (Fig. 1B-C; Fig. S1C, Supporting Information), reflecting the bleaching of the cells autofluorescence. Figures showing the variation of Tc, Atc and TetA-mCh intracellular present the raw fluorescence values (Rf), which then reflect the combination of Tc, Atc or TetA-mCh specific fluorescence (Sf), plus the Background fluorescence (Bf) of the cells. However, these background fluorescence (Bf) values were subtracted from the Raw fluorescence (Rf) value to estimate the specific fluorescence (Sf) attributable to Tc or Atc $Sf(Tc) = Rf(Tc) - Bgf$ and $Sf(TetA) = Rf(TetA) - Brf$. The ratio of two specific fluorescence valued allowed calculating the fold-change in TetA-mCh, Tc or Atc intracellular content (Fold-change = $Sf2/Sf1$). For instance the fold-change in Tc accumulation between high-tetA content cells and low-tetA content cells was:

$$\text{Fold - change in Tc intracellular content} \\ = Sf_{\text{high-tetA content cells}} / Sf_{\text{low-tetA content cells}}$$

where

$$Sf(Tc)_{\text{high-tetA content cells}} = Rf(Tc)_{\text{high-tetA content cells}} - Bgf_{wt \text{ cells}}$$

and

$$Sf(Tc)_{\text{low-tetA content cells}} = Rf(Tc)_{\text{low-tetA content cells}} - Bgf_{wt \text{ cells}}$$

SUPPLEMENTARY DATA

Supplementary data are available at [FEMSRE](https://femsres.onlinelibrary.wiley.com/doi/10.1111/fems.14446) online.

AUTHOR CONTRIBUTIONS

AR, CV, KG, AD, SN and CL made the bacterial strains and plasmids and performed the experiments. AR, CV, KG and CL analysed the data and prepared the figures. CL conceived the project and wrote the paper.

ACKNOWLEDGEMENTS

The authors thank the National BioResource Project, the Coli Genetic Stock Center and Vickers Burdett for providing strains; Nichola Teh, M Halte and M Bancale for early involvement in the project. A Ducret for valuable help with MicrobeJ.

FUNDING

CL acknowledges the ATIP-Avenir program, the Schlumberger Foundation for Education and Research (FSER 2019), FINOVI (AO-2014), the ANR PRC program (PlasMed) for funding to KG, the FRM (Fondation pour la Recherche Médicale) for funding to AR (ECO201806006855) and SN (ARF20150934201) and the University of Lyon for funding to CV.

Conflict of interest. None declared.

REFERENCES

Aldema ML, McMurry LM, Walmsley AR et al. Purification of the Tn 10-specified tetracycline efflux antiporter TetA in a

- native state as a polyhistidine fusion protein. *Mol Microbiol* 1996;**19**:187–95.
- Bergmiller T, Andersson AMC, Tomasek K et al. Biased partitioning of the multidrug efflux pump AcrAB-TolC underlies long-lived phenotypic heterogeneity. *Science* 2017;**356**:311–5.
- Biliouris K, Daoutidis P, Kaznessis YN. Stochastic simulations of the tetracycline operon. *BMC Syst Biol* 2011;**5**:9.
- Bryan A, Shapir N, Sadowsky MJ. Frequency and distribution of tetracycline resistance genes in genetically diverse, nonselected, and nonclinical *Escherichia coli* strains isolated from diverse human and animal sources. *Appl Environ Microbiol* 2004;**70**:2503–7.
- Burdett V. tRNA modification activity is necessary for Tet(M)-mediated tetracycline resistance. *J Bacteriol* 1993;**175**:7209–15.
- Cama J, Bajaj H, Pagliara S et al. Quantification of Fluoroquinolone Uptake through the Outer Membrane Channel OmpF of *Escherichia coli*. *J Am Chem Soc* 2015;**137**:13836–43.
- Cama J, Henney AM, Winterhalter M. Breaching the Barrier: Quantifying Antibiotic Permeability across Gram-negative Bacterial Membranes. *J Mol Biol* 2019;**431**:3531–46.
- Cama J, Schaich M, Al Nahas K et al. Direct Optofluidic Measurement of the Lipid Permeability of Fluoroquinolones. *Sci Rep* 2016;**6**:32824.
- Chopra I, Roberts M. Tetracycline antibiotics: mode of action, applications, molecular biology, and epidemiology of bacterial resistance. *Microbiol Mol Biol Rev* 2001;**65**:232–60; second page, table of contents.
- Chow D, Guo L, Gai F et al. Fluorescence Correlation Spectroscopy Measurements of the Membrane Protein TetA in *Escherichia coli* Suggest Rapid Diffusion at Short Length Scales. *PLoS One* 2012;**7**, DOI: 10.1371/journal.pone.0048600.
- Coenen S, Adriaenssens N, Versporten A et al. European Surveillance of Antimicrobial Consumption (ESAC): outpatient use of tetracyclines, sulphonamides and trimethoprim, and other antibacterials in Europe (1997-2009). *J Antimicrob Chemother* 2011;**66 Suppl 6**:vi57–70.
- Cuthbertson L, Nodwell JR. The TetR Family of Regulators. *Microbiol Mol Biol Rev* 2013;**77**:440–75.
- Datsenko KA, Wanner BL. One-step inactivation of chromosomal genes in *Escherichia coli* K-12 using PCR products. *Proc Natl Acad Sci USA* 2000;**97**:6640–5.
- Dubuy HG, Dubuy HG, Riley F et al. Tetracycline fluorescence in permeability studies of membranes around intracellular parasites. *Science* 1964;**145**:163–5.
- Ducret A, Quardokus EM, Brun YV. MicrobeJ, a tool for high throughput bacterial cell detection and quantitative analysis. *Nat Microbiol* 2016;**1**:16077.
- Du D, Wang Z, James NR et al. Structure of the AcrAB-TolC multidrug efflux pump. *Nature* 2014;**509**:512–5.
- Eckert B, Beck CF. Overproduction of transposon Tn10-encoded tetracycline resistance protein results in cell death and loss of membrane potential. *J Bacteriol* 1989;**171**:3557–9.
- Eliopoulos GM, Eliopoulos GM, Roberts MC. Tetracycline Therapy: Update. *Clin Infect Dis* 2003;**36**:462–7.
- Fernández L, Hancock REW. Adaptive and Mutational Resistance: Role of Porins and Efflux Pumps in Drug Resistance. *Clin Microbiol Rev* 2012;**25**:661–81.
- Hoeksema M, Jonker MJ, Brul S et al. Effects of a previously selected antibiotic resistance on mutations acquired during development of a second resistance in *Escherichia coli*. *BMC Genomics* 2019;**20**:284.
- Kumar S, Varela MF. Biochemistry of Bacterial Multidrug Efflux Pumps. *Int J Mol Sci* 2012;**13**:4484–95.
- Lesterlin C, Duabrry N. Investigating bacterial chromosome architecture. In: Leake MC (ed). *Chromosome Architecture*. Vol 1431. New York, NY: Springer New York, 2016, 61–72.
- Levy SB, McMurry L. Plasmid-determined tetracycline resistance involves new transport systems for tetracycline. *Nature* 1978;**276**:90–2.
- Li X-Z, Nikaido H. Efflux-Mediated Drug Resistance in Bacteria. *Drugs* 2004;**64**:159–204.
- Li X-Z, Nikaido H. Efflux-Mediated Drug Resistance in Bacteria: an Update. *Drugs* 2009;**69**:1555–623.
- Li X-Z, Plésiat P, Nikaido H. The Challenge of Efflux-Mediated Antibiotic Resistance in Gram-Negative Bacteria. *Clin Microbiol Rev* 2015;**28**:337–418.
- McMurry L, Petrucci RE, Levy SB. Active efflux of tetracycline encoded by four genetically different tetracycline resistance determinants in *Escherichia coli*. *Proc Natl Acad Sci USA* 1980;**77**:3974–7.
- Mortimer PG, Piddock LJ. The accumulation of five antibacterial agents in porin-deficient mutants of *Escherichia coli*. *J Antimicrob Chemother* 1993;**32**:195–213.
- Muthukrishnan A-B, Kandhavelu M, Lloyd-Price J et al. Dynamics of transcription driven by the tetA promoter, one event at a time, in live *Escherichia coli* cells. *Nucleic Acids Res* 2012;**40**:8472–83.
- Møller TSB, Overgaard M, Nielsen SS et al. Relation between tetR and tetA expression in tetracycline resistant *Escherichia coli*. *BMC Microbiol* 2016;**16**:39.
- Nikaido H. Multidrug Resistance in Bacteria. *Annu Rev Biochem* 2009;**78**:119–46.
- Nikaido H. Multiple antibiotic resistance and efflux. *Curr Opin Microbiol* 1998;**1**:516–23.
- Nolivos S, Cayron J, Dedieu A et al. Role of AcrAB-TolC multidrug efflux pump in drug-resistance acquisition by plasmid transfer. *Science* 2019;**364**:778–82.
- Ramos JL, Martínez-Bueno M, Molina-Henares AJ et al. The TetR Family of Transcriptional Repressors. *Microbiol Mol Biol Rev* 2005;**69**:326–56.
- Roberts MC. Tetracycline resistance determinants: mechanisms of action, regulation of expression, genetic mobility, and distribution. *FEMS Microbiol Rev* 1996;**19**:1–24.
- Schnappinger D, Hillen W. Tetracyclines: antibiotic action, uptake, and resistance mechanisms. *Arch Microbiol* 1996;**165**:359–69.
- Schultz D, Palmer AC, Kishony R. Regulatory Dynamics Determine Cell Fate following Abrupt Antibiotic Exposure. *Cell Syst* 2017;**5**:509–17.e3.
- Stone MRL, Butler MS, Phetsang W et al. Fluorescent Antibiotics: New Research Tools to Fight Antibiotic Resistance. *Trends Biotechnol* 2018;**36**:523–36.
- Sulavik MC, Houseweart C, Cramer C et al. Antibiotic susceptibility profiles of *Escherichia coli* strains lacking multidrug efflux pump genes. *Antimicrob Agents Chemother* 2001;**45**:1126–36.
- Tal N, Schuldiner S. A coordinated network of transporters with overlapping specificities provides a robust survival strategy. *Proc Natl Acad Sci USA* 2009;**106**:9051–6.
- Thaker M, Spanogiannopoulos P, Wright GD. The tetracycline resistome. *Cell Mol Life Sci* 2010;**67**:419–31.
- Vinué L, Hooper DC, Jacoby GA. Chromosomal mutations that accompany qnr in clinical isolates of *Escherichia coli*. *Int J Antimicrob Agents* 2018;**51**:479–83.

- Warburton PJ, Amodeo N, Roberts AP. Mosaic tetracycline resistance genes encoding ribosomal protection proteins. *J Antimicrob Chemother* 2016;**71**:3333–9.
- Yamaguchi A, Ono N, Akasaka T et al. Metal-tetracycline/H⁺ antiporter of *Escherichia coli* encoded by a transposon, Tn10. The role of the conserved dipeptide, Ser65-Asp66, in tetracycline transport. *J Biol Chem* 1990;**265**:15525–30.
- Yamaguchi A, Udagawa T, Sawai T. Transport of divalent cations with tetracycline as mediated by the transposon Tn10-encoded tetracycline resistance protein. *J Biol Chem* 1990;**265**:4809–13.
- Yu D, Ellis HM, Lee E-C et al. An efficient recombination system for chromosome engineering in *Escherichia coli*. *Proc Natl Acad Sci* 2000;**97**:5978–83.

4. Discussion

En prenant part des propriétés d'auto-fluorescence de la molécule de Tc, nous avons pu nous affranchir de l'utilisation de molécules antibiotiques conjuguées à des fluorophores. Bien qu'informatrice, une telle modification peut altérer les propriétés biochimiques et fonctionnelles de l'antibiotique donné (Stone et al. 2018). En combinaison avec l'utilisation de la protéine fluorescente TetA-mCh fonctionnelle, notre approche a permis de proprement caractériser la dynamique en temps réel de l'accumulation de Tc et la dynamique de son efflux dans les bactéries.

Nous démontrons une balance entre l'entrée et l'efflux de la Tc médiée par les pompes à efflux, permettant un niveau basal d'efflux de l'antibiotique. Nous proposons que cette accumulation est limitée par le nombre de porines et pompes à efflux disponibles à la membrane bactérienne, saturant le système dans le cas d'une concentration trop élevée de Tc. Nous observons également des différences du niveau basal de pompes à efflux TetA en absence de Tc parmi les bactéries portant le plasmide FTn10*tetAmCh*, révélant une hétérogénéité phénotypique au sein-même de la population bactérienne. Également observé par Sophie Nolivos lors de la publication antécédente, cela démontre que la conjugaison permet la mise en place d'une population de cellules avec différents niveaux de pompes à efflux. La production de pompes additionnelles en absence de Tc est certes coûteux énergétiquement parlant, pouvant aller jusqu'à perturber le potentiel de membrane si trop important (Eckert and Beck 1989), mais cela prépare également au mieux la bactérie pour face à un traitement antibiotique. A l'inverse, maintenir au minimum la production de ces pompes à efflux permet aux bactéries de mieux croître en absence de Tc mais peut être délétère en cas de traitement soudain et important. La présence de sous-populations différentes permet la répartition de fonction métabolique coûteuse au sein de la population bactérienne, minimisant l'impact négatif individuel tout en permettant à certains génotypes de persister face à un environnement fluctuant (Ackermann 2015; Spratt and Lane 2022).

Au travers de cet article, nous avons donc pu établir que la répression de *tetA* est finement régulée par TetR de sorte à permettre une production suffisante de pompes à efflux TetA pour anticiper et limiter l'accumulation de Tc. Une balance dynamique est alors instaurée, dépendante de la concentration initiale de pompes à efflux codées par le chromosome et par le plasmide mais dépendant aussi de la concentration de Tc dans le milieu. La conjugaison bactérienne pourrait alors permettre d'établir intrinsèquement un niveau d'hétérogénéité d'expression de facteurs plasmidiques, dont les pompes à efflux TetA, et ce dans un but favorable à la population bactérienne globale.

Partie V : Discussion générale

Les travaux de recherche présentés dans ce manuscrit de thèse s'intéressent à la compréhension des mécanismes impliqués dans le transfert horizontal du plasmide F au cours de la conjugaison chez *Escherichia coli*. Les études des dernières décennies sur le sujet se concentrent principalement sur la caractérisation génétique des différents plasmides conjugatifs. Ces études ont notamment démontré l'importance du transfert horizontal par conjugaison à la fois pour la plasticité et l'adaptabilité bactérienne mais également l'impact sociétal associé à la dissémination de résistances aux métaux lourds et antibiotiques (Frost et al. 2005; Keeling and Palmer 2008; Baharoglu, Garriss, and Mazel 2013; Koraimann 2018; Virolle et al. 2020). L'approche présentée dans ce manuscrit est ainsi pertinente et innovante puisqu'elle associe des techniques de microscopie à fluorescence en cellules vivantes complémentaire aux approches intrinsèques de biochimie structurale, de microbiologie classique ou encore de génétique. Par cela, nous décrivons avec précision la dynamique moléculaire du transfert conjugatif et l'impact du plasmide F sur la bactérie receveuse à l'échelle cellulaire, là où la majorité des études traitent de la conjugaison au sens large après son établissement dans les populations bactériennes.

Nos outils génétiques permettent ainsi la visualisation en temps réel des différentes étapes du transfert conjugatif par microscopie à fluorescence, révélant une organisation intracellulaire spécifique des différentes protéines plasmidiques. La conversion de l'ADN transféré en double-brin constitue le pivot de l'expression des différentes régions, organisé en un réel découplage chronologique de la production et régulation des divers facteurs plasmidiques. Nous apportons notamment plus de précisions quant au rôle joué par la région *leading* du plasmide F, sujet central de ce manuscrit de thèse. Majoritairement inconnus, les gènes associés ne semblent cependant pas jouer de rôle direct pour l'efficacité du transfert conjugatif. Nous proposons que la production d'une copie plasmidique de la protéine Ssb permette d'augmenter la concentration intracellulaire en protéine Ssb tout en permettant plus spécifiquement la duplication du plasmide directement après son transfert. En produisant sa propre copie plasmidique, le plasmide F empêche ainsi la bactérie hôte de manquer en protéines Ssb essentielles aux mécanismes de réplication de l'ADN. Ajouté au rôle d'inhibition de la réponse SOS associée à la protéine PsiB, ces deux protéines *leading* semblent ménager la physiologie de la bactérie receveuse au moment de l'acquisition du plasmide plutôt que pour l'efficacité du transfert en lui-même (Bagdasarian et al. 1992; Petrova et al. 2009; Couturier et

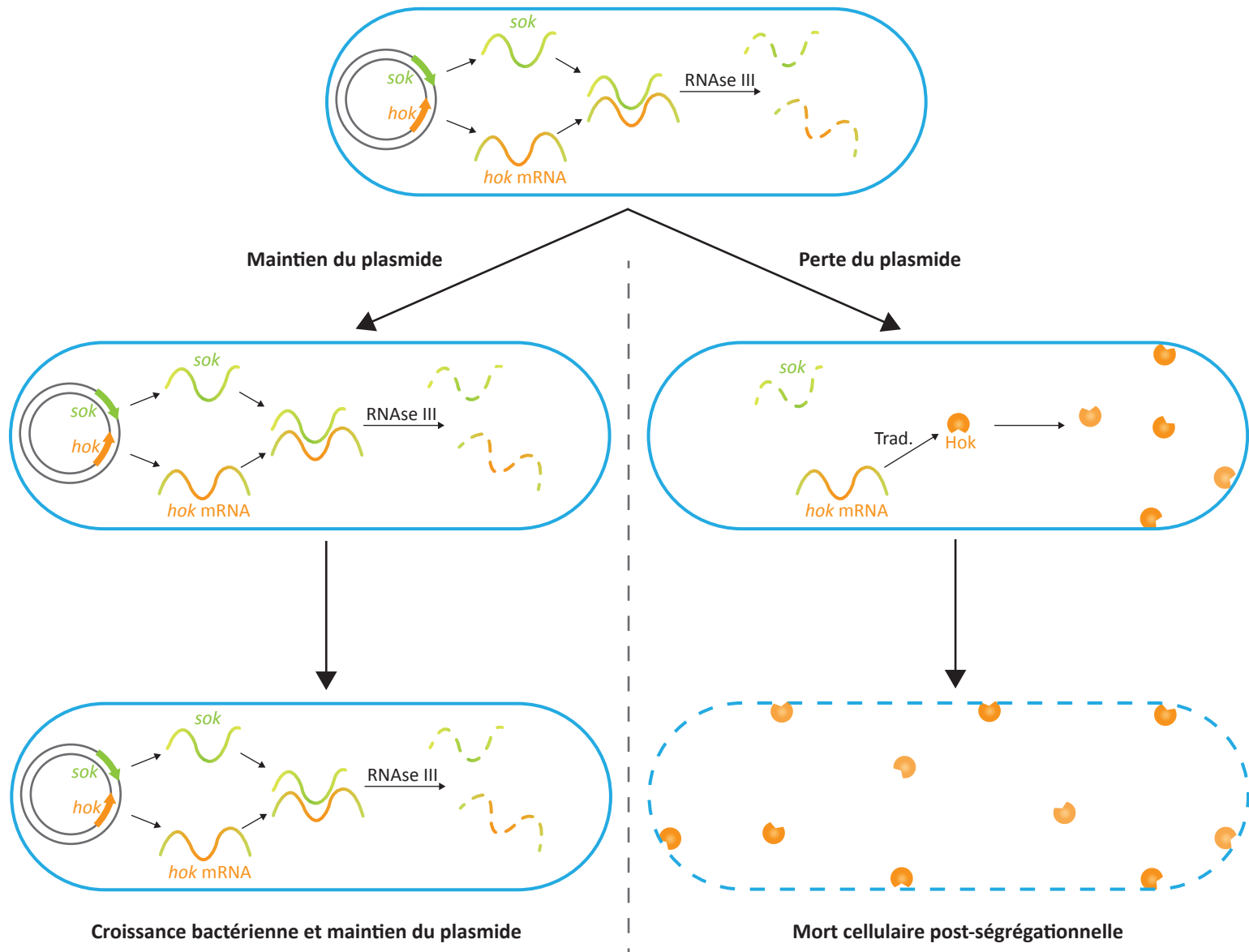


Figure 7. Système toxine-antitoxine Hok/Stok.

Le plasmide conjugatif porte des gènes codant pour la toxine Hok (orange) à longue durée de vie et l'antitoxine *sok* associée (vert) à courte durée de vie. L'ARN anti-sens *sok* lie l'ARNm *hok* par complémentarité, puis le complexe est la cible de dégradation par la RNase III. La perte du plasmide au cours des divisions cellulaires ne permet plus une production suffisante d'antitoxine pour inhiber *hok*. La dégradation de *sok* va permettre la traduction de la protéine Hok, induisant alors la mort cellulaire post-ségrégationnelle. Le maintien du plasmide au cours des divisions permet quant à lui la croissance bactérienne par production de l'antitoxine correspondante. Basé d'après Fraikin, Goormaghtigh et Van Melderen (2020).

al. 2023). Il serait alors probable que les autres protéines *leading* jouent un rôle similaire dans le but de limiter l'impact négatif sur la bactérie hôte dû à l'acquisition du plasmide et l'expression des nombreux facteurs associés, modérant alors la notion d'élément égoïste souvent utilisé pour qualifier les éléments extra-chromosomiques dont les plasmides.

Nous démontrons également la présence d'une deuxième séquence *ssi* sur la région *leading* du plasmide F, que nous avons nommé *Frpo2* du fait de sa forte homologie avec la séquence *Frpo1* déjà décrite *in vitro* dans la littérature (Masai and Arai 1997; Couturier et al. 2023). Nous confirmons *in vivo* le rôle de promoteur simple-brin de ces deux séquences pour l'expression précoce et transitoire des gènes *leading*. Toutefois, l'homologie à 92% de ces deux cassettes *Frpo1* et *Frpo2* peut facilement être à l'origine d'évènements de recombinaisons homologues qui aboutiraient à la délétion des gènes *ssb^f*, *yjjA*, *yjjB*, *psiB*, *psiA*, *flmA*, *flmB*, *flmC* et *ygdA*. La présence d'un système toxine-antitoxine (TA) semblable au système *hok/sok* porté par *flmAB* permet sans doutes d'éviter qu'un tel évènement ne se produise, en induisant la mort post-ségrégationnelle de la bactérie si elle vient à perdre cette région (Figure 4) (Hiraga et al. 1986; Loh, Cram, and Skurray 1988; Harrison and Brockhurst 2012; Carroll and Wong 2018). Très décrit depuis sa découverte chez le plasmide R1, le système TA *hok/sok* code pour un ARN messager (ARNm) *hok* (*host killing*) codant une protéine ciblant la membrane interne ainsi qu'un ARN anti-sens non traduit *sok* (*suppression of killing*) à courte durée de vie et inhibant *hok* au niveau post-transcriptionnel (Thisted and Gerdes 1992). Par la perte du plasmide après division cellulaire, la dégradation rapide de *sok* va lever l'inhibition de l'ARNm *hok* et permettre la traduction de la protéine correspondante, toxique pour la bactérie. Hok est responsable de la mort bactérienne par perturbation de divers procédés métaboliques essentiels tels que la respiration cellulaire ou l'intégrité membranaire (Figure 7) (K. Gerdes et al. 1986).

La région *leading* des plasmides conjugatifs du groupe MOB-F constitue également une région préférentiellement ciblée par certains systèmes CRISPR-Cas spécifiquement dirigés contre la conjugaison (Westra et al. 2013). Cela peut être en partie expliqué par le fait qu'en étant la première région transférée dans la receveuse, c'est également la portion génétique la plus fréquemment retrouvé dans la bactérie receveuse après un transfert abortif, et donc avec laquelle elle peut plus facilement développer un système de défense spécifique. On peut également penser que cibler plus particulièrement la région *leading* permettrait une meilleure inhibition de la conjugaison par le système CRISPR plutôt qu'en ciblant une autre région plasmidique. La région *leading* constitue également une cible évolutive des plasmides pESBL (Benz and Hall 2022). Après une quinzaine de générations sans pression de sélection, des mutations spontanées intégrant des codons stop sont

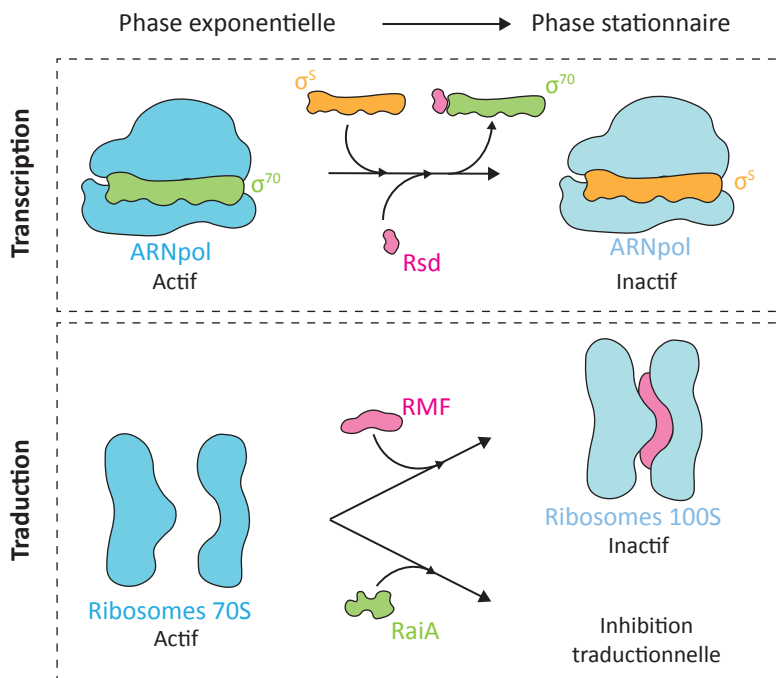


Figure 8. Régulations transcriptionnelles et traductionnelles lors de la transition de phase exponentielle à stationnaire.

Le facteur anti-sigma Rsd va séquestrer le facteur σ^{70} de l'ARN polymérase pour favoriser la liaison du facteur σ^5 , inactivant l'ARN polymérase et inhibant alors la transcription des gènes nécessaires à la croissance exponentielle. En parallèle, le facteur RMF inhibe l'activité traductionnelle des ribosomes 70S en participant à leur dimérisation en sous-unité 100S inactives. RaiA participe à l'inhibition traductionnelle en bloquant la liaison des ARNt aux ribosomes. D'après Yoshida et al. (2019).

retrouvés dans cette région. Certaines se retrouvent spécifiquement sur le gène *parB2* homologue à *yfjB*, allant même jusqu'à améliorer l'efficacité de transfert du plasmide dans quelques cas isolés. Ensembles, ces différents arguments appuient d'autant plus l'importance de la région *leading* pour le plasmide F mais mettent également en avant la complexité de compréhension des fonctions associées, puisqu'elles semblent varier d'un plasmide à l'autre.

La caractérisation de la protéine *leading* YfjB constitue également une part importante de ce manuscrit de thèse. Très peu décrite dans la littérature, on peut tout de même noter la publication d'une poignée de récents articles faisant référence à ses homologues « ParB2 » chez les autres plasmides conjugatifs et mettant d'autant plus en avant l'intérêt d'étude de cette protéine (Al Mamun, Kishida, and Christie 2021; Al Mamun et al. 2022; Benz and Hall 2022). Ici je confirme donc l'homologie avec les protéines ParB via la conservation d'un domaine HTH et d'un motif GxxRxxA, importants pour sa fonction de liaison à l'ADN chromosomique. Par cela YfjB va toucher à l'expression génétique global de la cellule en affectant jusqu'à 15% de son génome total. Cela est concordant avec l'observation réalisée par Billane *et al.* démontrant que les plasmides conjugatifs peuvent affecter jusqu'à 20% de l'expression génomique de la bactérie hôte, dans le but de manipuler sa physiologie pour leur propre bénéfice (Billane et al. 2022). Parmi les gènes affectés en présence de ces plasmides, nombreux sont associés à de multiples fonctions cellulaires comme le métabolisme du glucose, le cycle TCA, la transcription de gènes ou encore la mobilité bactérienne. Il est intéressant d'observer des modifications similaires en présence d'YfjB, probablement dans le but de préparer au mieux la physiologie hôte pour l'acquisition du plasmide conjugatif tout en limitant l'impact négatif lié au transfert. De tous les gènes dont l'expression est affectée en présence d'YfjB on retrouve *raiA* et *rmf*, codant pour des facteurs de modulation des ribosomes. RMF inhibe l'activité traductionnelle des ribosomes 70S (actifs) en participant à leur dimérisation en sous-unités ribosomiques 100S (inactifs) (Maki, Yoshida, and Wada 2000; Yoshida et al. 2019). Le facteur RaiA quant à lui stabilise les ribosomes 70S dans un état de dormance tout en inhibant la traduction en phase stationnaire de croissance en bloquant la liaison des ARNt sur le site ribosomique A, modulant ainsi l'activité ribosomique en fonction des conditions environnementales (Agafonov, Kolb, and Spirin 2001). En parallèle, le gène *rsd* est également réprimé en présence d'YfjB, dont la protéine associée est un facteur anti-sigma inhibant la transcription lors de la transition vers la phase stationnaire de croissance. Rsd séquestre le facteur sigma 70 (RpoD) lié à l'ARN polymérase, facilitant la liaison du facteur sigma S (RpoS) et donc l'inactivation de la transcription des gènes impliqués pour la

croissance exponentielle de la bactérie (Figure 8) (Hengge-Aronis 1993; Hofmann, Wurm, and Wagner 2011; Yoshida et al. 2019). Ainsi nous proposons que la présence d'YfjB renforce la diminution de transcription génétique hôte associée au passage en phase stationnaire de croissance, tout en prévenant l'inhibition des ribosomes 70S par RMF et permettant la réactivation des réserves de ribosomes mis en dormance par RaiA. Par cette stratégie, le plasmide F assure qu'assez de ribosomes soient actifs pour la traduction rapide et efficace des facteurs plasmidiques sans détourner pour autant la totalité des ribosomes de la bactérie hôte, et ce jusqu'à ce que les protéines plasmidiques prennent le relai pour réguler leur propre production.

Nous sommes toutefois à même de nous demander comment une seule protéine peut affecter autant de fonctions métaboliques différentes ? Tout d'abord, nous avons pu voir que la présence d'YfjB induit un changement d'expression d'une cinquantaine de régulateurs de transcription, induisant indirectement une cascade de régulations et de changements d'expression des régulons associés. Il est aussi nécessaire de rappeler que nous observons de tels changements en condition de production ectopique et constante d'YfjB. Peut-être qu'une production plus importante et continue de protéines YfjB permet une liaison non-spécifique à l'ADN, comme le sont capables les protéines ParB, expliquant alors l'étendue des gènes affectés ? Il est également possible qu'en condition de conjugaison, d'autres facteurs plasmidiques permettent une modulation plus précise de la fonction de la protéine YfjB.

Lors de la conjugaison, le gène *yfjB* va rapidement cesser d'être exprimé suite à la conversion en ADNdb du promoteur *F_{rho2}*. La dilution progressive de la protéine YfjB au cours des générations bactériennes indique qu'elle ne joue pas de rôle pour le maintien du plasmide au cours des générations, mais semblerait plutôt affecter la dissémination du plasmide F au sein des populations bactériennes. Nous observons également que la délétion d'*yfjB* augmente de 30% le délai de conversion de l'ADNsb transféré en ADNdb, mais ne change pas l'efficacité *in fine* de la conjugaison dans nos conditions de cultures optimales entre bactéries isogéniques. Il est cependant certain que ce délai peut être délétère pour le transfert dans des conditions plus stressantes, entre souches bactériennes différentes ou alors dans le cas d'un transfert vers une bactérie receveuse possédant déjà d'autres éléments mobilisables. En effet, tout élément génétique transféré horizontalement est particulièrement vulnérable en début de transfert, car typiquement retrouvé en une seule copie ou alors aucun facteur de défense n'a encore pu être synthétisé. Il peut également être confronté à la compétition d'autres éléments mobilisables déjà présents et établis. Les plasmides conjugatifs ne font pas exception, et même si le transfert a bien été réalisé, cela n'assure pas pour autant leur

établissement stable au sein des populations bactériennes. Il est donc fort probable que les premières protéines *leading* produites après l'initiation du transfert conjugatives permettent l'amélioration des conditions d'établissement du plasmide.

Ainsi, bien que la protéine *leading* YfjB possède une homologie avec les protéines ParB, nous démontrons qu'elle ne partage pas leur fonction de ségrégation de l'ADN et fait donc partie de la large variété de protéines polyvalentes ParB-like (Iyer et al. 2017). Les fonctions de ces protéines peuvent être multiples et éloignées de la fonction initiale de ségrégation de l'ADN, comme c'est le cas de l'activité DNase de la protéine Osa. Produite à partir du plasmide pSa, elle constitue un facteur d'inhibition de fertilité en bloquant de façon sélective le transfert d'ADN de plasmides co-résidents compétiteurs par dégradation spécifique de leur matériel génétique (Maindola et al. 2014). De façon plus similaire à ce qu'on observe pour YfjB, la protéine KorB du plasmide RK2 possède également une homologie avec les protéines ParB et est capable de se lier à plus d'une douzaine de sites ADN et réguler l'activité des promoteurs associés (Jagura-Burdzy et al. 1999; Bingle et al. 2005). Des expériences de ChiP-seq chez *Pseudomonas aeruginosa* démontrent que la protéine ParB peut fixer une centaine de séquences ADN possédant un demi motif *parS* (Kawalek et al. 2018). Cela pourrait expliquer une évolution des protéines ParB au sein des populations bactériennes et plasmidiques vers des fonctions métaboliques différentes, tout en conservant la capacité de fixation et de diffusion sur de multiples séquences ADN.

Comme dit précédemment, la poursuite de la reconstruction de la structure protéique d'YfjB est en cours au moment de l'écriture de ce manuscrit, et permettra d'apporter d'avantages informations quant à l'implication des différents domaines de la protéine pour sa fonction. Une répétition des expériences de ChiP-seq permettra également de confirmer les profils observés et ainsi établir une meilleure corrélation entre la liaison à l'ADN et les changements de transcription observés. Nos résultats constituent toutefois une avancée considérable dans la compréhension du rôle de la protéine YfjB ainsi que sur le rôle joué par la région *leading* pour le processus conjugatif. Nous proposons donc que par la production rapide et précoce des protéines *leading*, le plasmide F aurait établi une stratégie visant à préparer au mieux la physiologie de la bactérie receveuse pour son propre établissement rapide et son maintien efficace au cours des divisions. La protéine YfjB permettrait ainsi la reprogrammation globale du profil d'expression des gènes de la bactérie hôte de façon temporaire, le temps d'assurer l'établissement du plasmide et la mise en place de ses propres régulations. En affectant diverses voies moléculaires du métabolisme bactérien, YfjB permet de

préparer la bactérie receveuse à porter des informations génétiques supplémentaires tout en limitant la diminution de fitness qui peut être associée. De façon similaire aux protéines *leading Ssb^F* et PsiB, la protéine YfjB n'impacte pas l'efficacité-même du transfert conjugatif. Il est possible de penser que la région *leading* confère un avantage au plasmide F par rapport aux autres plasmides conjugatifs, pouvant expliquer l'efficacité de son transfert et sa large répartition parmi les espèces bactériennes *Enterobacteriaceae*.

Bibliographie

- Ackermann, Martin. 2015. 'A Functional Perspective on Phenotypic Heterogeneity in Microorganisms'. *Nature Reviews. Microbiology* 13 (8): 497–508. <https://doi.org/10.1038/nrmicro3491>.
- Agafonov, D. E., V. A. Kolb, and A. S. Spirin. 2001. 'Ribosome-Associated Protein That Inhibits Translation at the Aminoacyl-TRNA Binding Stage'. *EMBO Reports* 2 (5): 399–402. <https://doi.org/10.1093/embo-reports/kve091>.
- Ah-Seng, Yoan, Frederic Lopez, Franck Pasta, David Lane, and Jean-Yves Bouet. 2009. 'Dual Role of DNA in Regulating ATP Hydrolysis by the SopA Partition Protein *'. *Journal of Biological Chemistry* 284 (44): 30067–75. <https://doi.org/10.1074/jbc.M109.044800>.
- Al Mamun, Abu Amar M., Kouhei Kishida, and Peter J. Christie. 2021. 'Protein Transfer through an F Plasmid-Encoded Type IV Secretion System Suppresses the Mating-Induced SOS Response'. *MBio* 12 (4): e01629-21. <https://doi.org/10.1128/mBio.01629-21>.
- Al Mamun, Abu Amar M., Kimberly Kissoon, Kouhei Kishida, William C. Shropshire, Blake Hanson, and Peter J. Christie. 2022. 'IncFV Plasmid PED208: Sequence Analysis and Evidence for Translocation of Maintenance/Leading Region Proteins through Diverse Type IV Secretion Systems'. *Plasmid* 123–124 (September): 102652. <https://doi.org/10.1016/j.plasmid.2022.102652>.
- Althorpe, N. J., P. M. Chilley, A. T. Thomas, W. J. Brammar, and B. M. Wilkins. 1999. 'Transient Transcriptional Activation of the Inc11 Plasmid Anti-Restriction Gene (ArdA) and SOS Inhibition Gene (PsiB) Early in Conjugating Recipient Bacteria'. *Molecular Microbiology* 31 (1): 133–42. <https://doi.org/10.1046/j.1365-2958.1999.01153.x>.
- Aminov, Rustam I. 2011. 'Horizontal Gene Exchange in Environmental Microbiota'. *Frontiers in Microbiology* 2: 158. <https://doi.org/10.3389/fmicb.2011.00158>.
- Anthony, K. G., C. Sherburne, R. Sherburne, and L. S. Frost. 1994. 'The Role of the Pilus in Recipient Cell Recognition during Bacterial Conjugation Mediated by F-like Plasmids'. *Molecular Microbiology* 13 (6): 939–53. <https://doi.org/10.1111/j.1365-2958.1994.tb00486.x>.
- Arutyunov, Denis, and Laura S. Frost. 2013. 'F Conjugation: Back to the Beginning'. *Plasmid* 70 (1): 18–32. <https://doi.org/10.1016/j.plasmid.2013.03.010>.
- Averhoff, Beate, Lennart Kirchner, Katharina Pfefferle, and Deniz Yaman. 2021. 'Natural Transformation in Gram-Negative Bacteria Thriving in Extreme Environments: From Genes and Genomes to Proteins, Structures and Regulation'. *Extremophiles* 25 (5): 425–36. <https://doi.org/10.1007/s00792-021-01242-z>.
- Bagdasarian, M., A. Bailone, J. F. Angulo, P. Scholz, M. Bagdasarian, and R. Devoret. 1992. 'PsiB, and Anti-SOS Protein, Is Transiently Expressed by the F Sex Factor during Its Transmission to an Escherichia Coli K-12 Recipient'. *Molecular Microbiology* 6 (7): 885–93. <https://doi.org/10.1111/j.1365-2958.1992.tb01539.x>.
- Baharoglu, Zeynep, David Bikard, and Didier Mazel. 2010. 'Conjugative DNA Transfer Induces the Bacterial SOS Response and Promotes Antibiotic Resistance Development through Integron

Activation'. *PLoS Genetics* 6 (10). <https://doi.org/10.1371/journal.pgen.1001165>.

Baharoglu, Zeynep, Geneviève Garriss, and Didier Mazel. 2013. 'Multiple Pathways of Genome Plasticity Leading to Development of Antibiotic Resistance'. *Antibiotics* 2 (2): 288–315. <https://doi.org/10.3390/antibiotics2020288>.

Bailone, A., A. Bäckman, S. Sommer, J. Célérier, M. M. Bagdasarian, M. Bagdasarian, and R. Devoret. 1988. 'PsiB Polypeptide Prevents Activation of RecA Protein in Escherichia Coli'. *Molecular & General Genetics: MGG* 214 (3): 389–95. <https://doi.org/10.1007/bf00330471>.

Barlow, Miriam. 2009. 'What Antimicrobial Resistance Has Taught Us about Horizontal Gene Transfer'. *Methods in Molecular Biology (Clifton, N.J.)* 532: 397–411. https://doi.org/10.1007/978-1-60327-853-9_23.

Bates, Steven, Richard A. Roscoe, Nicola J. Althorpe, William J. Brammar, and Brian M. Wilkins. 1999. 'Expression of Leading Region Genes on IncII Plasmid Collb-P9: Genetic Evidence for Single-Stranded DNA Transcription'. *Microbiology* 145 (10): 2655–62. <https://doi.org/10.1099/00221287-145-10-2655>.

Baxter, Jamie C., and Barbara E. Funnell. 2014. 'Plasmid Partition Mechanisms'. *Microbiology Spectrum* 2 (6). <https://doi.org/10.1128/microbiolspec.PLAS-0023-2014>.

Benz, F., and A. R. Hall. 2022. 'Host-Specific Plasmid Evolution Explains the Variable Spread of Clinical Antibiotic-Resistance Plasmids'. *bioRxiv*. <https://doi.org/10.1101/2022.07.06.498992>.

Billane, Kathryn, Ellie Harrison, Duncan Cameron, and Michael A. Brockhurst. 2022. 'Why Do Plasmids Manipulate the Expression of Bacterial Phenotypes?' *Philosophical Transactions of the Royal Society of London. Series B, Biological Sciences* 377 (1842): 20200461. <https://doi.org/10.1098/rstb.2020.0461>.

Billman-Jacobe, Helen, Yuhong Liu, Ruth Haites, Tom Weaver, Lily Robinson, Marc Marends, and Mike Dyal-Smith. 2018. 'PSTM6-275, a Conjugative IncHI2 Plasmid of Salmonella Enterica That Confers Antibiotic and Heavy-Metal Resistance under Changing Physiological Conditions'. *Antimicrobial Agents and Chemotherapy* 62 (5): e02357-17. <https://doi.org/10.1128/AAC.02357-17>.

Bingle, Lewis E. H., Donia P. Macartney, Anaïs Fantozzi, Susan E. Manzoor, and Christopher M. Thomas. 2005. 'Flexibility in Repression and Cooperativity by KorB of Broad Host Range IncP-1 Plasmid RK2'. *Journal of Molecular Biology* 349 (2): 302–16. <https://doi.org/10.1016/j.jmb.2005.03.062>.

Bobay, Louis-Marie, Eduardo P. C. Rocha, and Marie Touchon. 2013. 'The Adaptation of Temperate Bacteriophages to Their Host Genomes'. *Molecular Biology and Evolution* 30 (4): 737–51. <https://doi.org/10.1093/molbev/mss279>.

Bouet, Jean-Yves, Yoan Ah-Seng, Nacer Benmeradi, and David Lane. 2007. 'Polymerization of SopA Partition ATPase: Regulation by DNA Binding and SopB'. *Molecular Microbiology* 63 (2): 468–81. <https://doi.org/10.1111/j.1365-2958.2006.05537.x>.

Bouet, Jean-Yves, and Barbara E. Funnell. 2019. 'Plasmid Localization and Partition in Enterobacteriaceae'. *EcoSal Plus* 8 (2). <https://doi.org/10.1128/ecosalplus.ESP-0003-2019>.

- Boyd, E. Fidelma. 2012. ‘Bacteriophage-Encoded Bacterial Virulence Factors and Phage-Pathogenicity Island Interactions’. *Advances in Virus Research* 82: 91–118. <https://doi.org/10.1016/B978-0-12-394621-8.00014-5>.
- Brito, Patrícia H., Bastien Chevreux, Cláudia R. Serra, Ghislain Schyns, Adriano O. Henriques, and José B. Pereira-Leal. 2018. ‘Genetic Competence Drives Genome Diversity in *Bacillus Subtilis*’. *Genome Biology and Evolution* 10 (1): 108–24. <https://doi.org/10.1093/gbe/evx270>.
- Bruins, M. R., S. Kapil, and F. W. Oehme. 2000. ‘Microbial Resistance to Metals in the Environment’. *Ecotoxicology and Environmental Safety* 45 (3): 198–207. <https://doi.org/10.1006/eesa.1999.1860>.
- Bryan, Andrew, Nir Shapir, and Michael J. Sadowsky. 2004. ‘Frequency and Distribution of Tetracycline Resistance Genes in Genetically Diverse, Nonselected, and Nonclinical *Escherichia Coli* Strains Isolated from Diverse Human and Animal Sources’. *Applied and Environmental Microbiology* 70 (4): 2503–7. <https://doi.org/10.1128/AEM.70.4.2503-2507.2004>.
- Bukowski, Michal, Rafal Piwowarczyk, Anna Madry, Rafal Zagorski-Przybylo, Marcin Hydzik, and Benedykt Wladyka. 2019. ‘Prevalence of Antibiotic and Heavy Metal Resistance Determinants and Virulence-Related Genetic Elements in Plasmids of *Staphylococcus Aureus*’. *Frontiers in Microbiology* 10 (April). <https://doi.org/10.3389/fmicb.2019.00805>.
- Cabezón, Elena, Fernando de la Cruz, and Ignacio Arechaga. 2017. ‘Conjugation Inhibitors and Their Potential Use to Prevent Dissemination of Antibiotic Resistance Genes in Bacteria’. *Frontiers in Microbiology* 8. <https://www.frontiersin.org/articles/10.3389/fmicb.2017.02329>.
- Carroll, Amanda C., and Alex Wong. 2018. ‘Plasmid Persistence: Costs, Benefits, and the Plasmid Paradox’. *Canadian Journal of Microbiology* 64 (5): 293–304. <https://doi.org/10.1139/cjm-2017-0609>.
- Carvalho, Gabriel, David Fouchet, Gonché Danesh, Anne-Sophie Godeux, Maria-Halima Laaberki, Dominique Pontier, Xavier Charpentier, and Samuel Venner. 2020. ‘Bacterial Transformation Buffers Environmental Fluctuations through the Reversible Integration of Mobile Genetic Elements’. *MBio* 11 (2): e02443-19. <https://doi.org/10.1128/mBio.02443-19>.
- Chase, J. W., B. M. Merrill, and K. R. Williams. 1983. ‘F Sex Factor Encodes a Single-Stranded DNA Binding Protein (SSB) with Extensive Sequence Homology to *Escherichia Coli* SSB’. *Proceedings of the National Academy of Sciences of the United States of America* 80 (18): 5480–84. <https://doi.org/10.1073/pnas.80.18.5480>.
- Chen, Wen-Ming, Lionel Moulin, Cyril Bontemps, Peter Vandamme, Gilles Béna, and Catherine Boivin-Masson. 2003. ‘Legume Symbiotic Nitrogen Fixation By β -Proteobacteria Is Widespread In Nature’. *Journal of Bacteriology* 185 (24): 7266–72. <https://doi.org/10.1128/JB.185.24.7266-7272.2003>.
- Chiang, Yin Ning, José R. Penadés, and John Chen. 2019. ‘Genetic Transduction by Phages and Chromosomal Islands: The New and Noncanonical’. *PLoS Pathogens* 15 (8): e1007878. <https://doi.org/10.1371/journal.ppat.1007878>.
- Chopra, I., and M. Roberts. 2001. ‘Tetracycline Antibiotics: Mode of Action, Applications, Molecular

Biology, and Epidemiology of Bacterial Resistance'. *Microbiology and Molecular Biology Reviews: MMBR* 65 (2): 232-260 ; second page, table of contents. <https://doi.org/10.1128/MMBR.65.2.232-260.2001>.

Coenen, Samuel, Niels Adriaenssens, Ann Versporten, Arno Muller, Girma Minalu, Christel Faes, Vanessa Vankerckhoven, et al. 2011. 'European Surveillance of Antimicrobial Consumption (ESAC): Outpatient Use of Tetracyclines, Sulphonamides and Trimethoprim, and Other Antibacterials in Europe (1997-2009)'. *The Journal of Antimicrobial Chemotherapy* 66 Suppl 6 (December): vi57-70. <https://doi.org/10.1093/jac/dkr458>.

Coluzzi, Charles, Maria Pilar Garcillán-Barcia, Fernando de la Cruz, and Eduardo P.C. Rocha. 2022. 'Evolution of Plasmid Mobility: Origin and Fate of Conjugative and Nonconjugative Plasmids'. *Molecular Biology and Evolution* 39 (6): msac115. <https://doi.org/10.1093/molbev/msac115>.

Cooper, Stephen, and Jay D. Keasling. 1998. 'Cycle-Specific Replication of Chromosomal and F-Plasmid Origins'. *FEMS Microbiology Letters* 163 (2): 217–22. <https://doi.org/10.1111/j.1574-6968.1998.tb13048.x>.

Couturier, Agathe, Chloé Virolle, Kelly Goldlust, Annick Berne-Dedieu, Audrey Reuter, Sophie Nolivos, Yoshiharu Yamaichi, Sarah Bigot, and Christian Lesterlin. 2023. 'Real-Time Visualisation of the Intracellular Dynamics of Conjugative Plasmid Transfer'. *Nature Communications* 14 (1): 294. <https://doi.org/10.1038/s41467-023-35978-3>.

Cruz, Fernando de la, Laura S. Frost, Richard J. Meyer, and Ellen L. Zechner. 2010. 'Conjugative DNA Metabolism in Gram-Negative Bacteria'. *FEMS Microbiology Reviews* 34 (1): 18–40. <https://doi.org/10.1111/j.1574-6976.2009.00195.x>.

Daubin, Vincent, and Gergely J. Szöllösi. 2016. 'Horizontal Gene Transfer and the History of Life'. *Cold Spring Harbor Perspectives in Biology* 8 (4): a018036. <https://doi.org/10.1101/cshperspect.a018036>.

Deshpande, L. M., and B. A. Chopade. 1994. 'Plasmid Mediated Silver Resistance in *Acinetobacter Baumannii*'. *Biometals: An International Journal on the Role of Metal Ions in Biology, Biochemistry, and Medicine* 7 (1): 49–56. <https://doi.org/10.1007/BF00205194>.

Dodsworth, Jeremy A., Lei Li, Shiping Wei, Brian P. Hedlund, John A. Leigh, and Paul de Figueiredo. 2010. 'Interdomain Conjugal Transfer of DNA from Bacteria to Archaea'. *Applied and Environmental Microbiology* 76 (16): 5644–47. <https://doi.org/10.1128/AEM.00967-10>.

Dostál, Lubomír, and Joel F. Schildbach. 2010. 'Single-Stranded DNA Binding by F TraI Relaxase and Helicase Domains Is Coordinately Regulated'. *Journal of Bacteriology* 192 (14): 3620–28. <https://doi.org/10.1128/JB.00154-10>.

Dubuy, H. G., H. G. Dubuy, F. Riley, and J. L. Showacre. 1964. 'Tetracycline Fluorescence in Permeability Studies of Membranes around Intracellular Parasites'. *Science (New York, N.Y.)* 145 (3628): 163–65. <https://doi.org/10.1126/science.145.3628.163>.

Eberhard, W. G. 1989. 'Why Do Bacterial Plasmids Carry Some Genes and Not Others?' *Plasmid* 21 (3): 167–74. [https://doi.org/10.1016/0147-619x\(89\)90040-1](https://doi.org/10.1016/0147-619x(89)90040-1).

- Eckert, B., and C. F. Beck. 1989. 'Overproduction of Transposon Tn10-Encoded Tetracycline Resistance Protein Results in Cell Death and Loss of Membrane Potential'. *Journal of Bacteriology* 171 (6): 3557–59. <https://doi.org/10.1128/jb.171.6.3557-3559.1989>.
- Fang, Liangxing, Xingping Li, Liang Li, Shumin Li, Xiaoping Liao, Jian Sun, and Yahong Liu. 2016. 'Co-Spread of Metal and Antibiotic Resistance within ST3-IncHI2 Plasmids from E. Coli Isolates of Food-Producing Animals'. *Scientific Reports* 6 (May): 25312. <https://doi.org/10.1038/srep25312>.
- Fernandez-Lopez, Raul, Maria de Toro, Gabriel Moncalian, M. Pilar Garcillan-Barcia, and Fernando de la Cruz. 2016. 'Comparative Genomics of the Conjugation Region of F-like Plasmids: Five Shades of F'. *Frontiers in Molecular Biosciences* 3. <https://www.frontiersin.org/articles/10.3389/fmolb.2016.00071>.
- Feschotte, Cédric, and Clément Gilbert. 2012. 'Endogenous Viruses: Insights into Viral Evolution and Impact on Host Biology'. *Nature Reviews. Genetics* 13 (4): 283–96. <https://doi.org/10.1038/nrg3199>.
- Frost, Laura S., Raphael Leplae, Anne O. Summers, and Ariane Toussaint. 2005. 'Mobile Genetic Elements: The Agents of Open Source Evolution'. *Nature Reviews. Microbiology* 3 (9): 722–32. <https://doi.org/10.1038/nrmicro1235>.
- Garcillán-Barcia, Maria Pilar, Andrés Alvarado, and Fernando de la Cruz. 2011. 'Identification of Bacterial Plasmids Based on Mobility and Plasmid Population Biology'. *FEMS Microbiology Reviews* 35 (5): 936–56. <https://doi.org/10.1111/j.1574-6976.2011.00291.x>.
- Garcillán-Barcia, María Pilar, María Victoria Francia, and Fernando de la Cruz. 2009. 'The Diversity of Conjugative Relaxases and Its Application in Plasmid Classification'. *FEMS Microbiology Reviews* 33 (3): 657–87. <https://doi.org/10.1111/j.1574-6976.2009.00168.x>.
- Gerdes, K., F. W. Bech, S. T. Jørgensen, A. Løbner-Olesen, P. B. Rasmussen, T. Atlung, L. Boe, O. Karlstrom, S. Molin, and K. von Meyenburg. 1986. 'Mechanism of Postsegregational Killing by the Hok Gene Product of the ParB System of Plasmid R1 and Its Homology with the RelF Gene Product of the E. Coli RelB Operon'. *The EMBO Journal* 5 (8): 2023–29. <https://doi.org/10.1002/j.1460-2075.1986.tb04459.x>.
- Gerdes, Kenn, Martin Howard, and Florian Szardenings. 2010. 'Pushing and Pulling in Prokaryotic DNA Segregation'. *Cell* 141 (6): 927–42. <https://doi.org/10.1016/j.cell.2010.05.033>.
- Goessweiner-Mohr, Nikolaus, Karsten Arends, Walter Keller, and Elisabeth Grohmann. 2013. 'Conjugative Type IV Secretion Systems in Gram-Positive Bacteria'. *Plasmid* 70 (3): 289–302. <https://doi.org/10.1016/j.plasmid.2013.09.005>.
- Goldlust, Kelly, Agathe Couturier, Laurent Terradot, and Christian Lesterlin. 2022. 'Live-Cell Visualization of DNA Transfer and Pilus Dynamics During Bacterial Conjugation'. *Methods in Molecular Biology (Clifton, N.J.)* 2476: 63–74. https://doi.org/10.1007/978-1-0716-2221-6_6.
- Golub, E, A Bailone, and R Devoret. 1988. 'A Gene Encoding an SOS Inhibitor Is Present in Different Conjugative Plasmids'. *Journal of Bacteriology* 170 (9): 4392–94. <https://doi.org/10.1128/jb.170.9.4392-4394.1988>.
- Golub, E I, and K B Low. 1985. 'Conjugative Plasmids of Enteric Bacteria from Many Different

Incompatibility Groups Have Similar Genes for Single-Stranded DNA-Binding Proteins.’ *Journal of Bacteriology* 162 (1): 235–41.

Golub, Efim I., and K. Brooks Low. 1986. ‘Derepression of Single-Stranded DNA-Binding Protein Genes on Plasmids Derepressed for Conjugation, and Complementation of an E. Coli Ssb-Mutation by These Genes’. *Molecular and General Genetics MGG* 204 (3): 410–16. <https://doi.org/10.1007/BF00331017>.

Gordon, Jay E., and Peter J. Christie. 2014. ‘The Agrobacterium Ti Plasmids’. *Microbiology Spectrum* 2 (6). <https://doi.org/10.1128/microbiolspec.PLAS-0010-2013>.

Griffith, Fred. 1928. ‘The Significance of Pneumococcal Types’, January, 48.

Grohmann, Elisabeth, Peter J. Christie, Gabriel Waksman, and Steffen Backert. 2018. ‘Type IV Secretion in Gram-Negative and Gram-Positive Bacteria’. *Molecular Microbiology* 107 (4): 455–71. <https://doi.org/10.1111/mmi.13896>.

Grohmann, Elisabeth, Günther Muth, and Manuel Espinosa. 2003. ‘Conjugative Plasmid Transfer in Gram-Positive Bacteria’. *Microbiology and Molecular Biology Reviews: MMBR* 67 (2): 277–301, table of contents. <https://doi.org/10.1128/MMBR.67.2.277-301.2003>.

Guiney, Donald G., and Joshua Fierer. 2011. ‘The Role of the Spv Genes in Salmonella Pathogenesis’. *Frontiers in Microbiology* 2: 129. <https://doi.org/10.3389/fmicb.2011.00129>.

Hall-Stoodley, Luanne, J. William Costerton, and Paul Stoodley. 2004. ‘Bacterial Biofilms: From the Natural Environment to Infectious Diseases’. *Nature Reviews. Microbiology* 2 (2): 95–108. <https://doi.org/10.1038/nrmicro821>.

Hamprecht, Axel, Julian Sommer, Matthias Willmann, Christina Brender, Yvonne Stelzer, Felix F. Krause, Tsvetan Tsvetkov, et al. 2019. ‘Pathogenicity of Clinical OXA-48 Isolates and Impact of the OXA-48 IncL Plasmid on Virulence and Bacterial Fitness’. *Frontiers in Microbiology* 10. <https://www.frontiersin.org/articles/10.3389/fmicb.2019.02509>.

Harrison, Ellie, and Michael A. Brockhurst. 2012. ‘Plasmid-Mediated Horizontal Gene Transfer Is a Coevolutionary Process’. *Trends in Microbiology* 20 (6): 262–67. <https://doi.org/10.1016/j.tim.2012.04.003>.

Hawkey, Jane, Hugh Cottingham, Alex Tokolyi, Ryan R. Wick, Louise M. Judd, Louise Cerdeira, Doroti de Oliveira Garcia, Kelly L. Wyres, and Kathryn E. Holt. 2022. ‘Linear Plasmids in Klebsiella and Other Enterobacteriaceae’. *Microbial Genomics* 8 (4): 000807. <https://doi.org/10.1099/mgen.0.000807>.

Hengge-Aronis, R. 1993. ‘Survival of Hunger and Stress: The Role of RpoS in Early Stationary Phase Gene Regulation in E. Coli’. *Cell* 72 (2): 165–68. [https://doi.org/10.1016/0092-8674\(93\)90655-a](https://doi.org/10.1016/0092-8674(93)90655-a).

Hiraga, S., A. Jaffé, T. Ogura, H. Mori, and H. Takahashi. 1986. ‘F Plasmid Ccd Mechanism in Escherichia Coli’. *Journal of Bacteriology* 166 (1): 100–104. <https://doi.org/10.1128/jb.166.1.100-104.1986>.

Hobman, Jon L., and Lisa C.YR 2015 Crossman. 2015. ‘Bacterial Antimicrobial Metal Ion

Resistance'. *Journal of Medical Microbiology* 64 (5): 471–97. <https://doi.org/10.1099/jmm.0.023036-0>.

Hofmann, Nina, Reinhild Wurm, and Rolf Wagner. 2011. 'The E. Coli Anti-Sigma Factor Rsd: Studies on the Specificity and Regulation of Its Expression'. *PloS One* 6 (5): e19235. <https://doi.org/10.1371/journal.pone.0019235>.

Huang, Tzu-Wen, Tsai-Ling Lauderdale, Tsai-Lien Liao, Ming-Chia Hsu, Feng-Yee Chang, Shan-Chwen Chang, Wei Xin Khong, et al. 2015. 'Effective Transfer of a 47 Kb NDM-1-Positive Plasmid among Acinetobacter Species'. *The Journal of Antimicrobial Chemotherapy* 70 (10): 2734–38. <https://doi.org/10.1093/jac/dkv191>.

Ibáñez, Fernando, Herminda Reinoso, and Adriana Fabra. 2010. 'Experimental Evidences of PSym Transfer in a Native Peanut-Associated Rhizobia'. *Microbiological Research* 165 (6): 505–15. <https://doi.org/10.1016/j.micres.2009.08.004>.

Ilangovan, Aravindan, Christopher W. M. Kay, Sandro Roier, Hassane El Mkami, Enrico Salvadori, Ellen L. Zechner, Giulia Zanetti, and Gabriel Waksman. 2017. 'Cryo-EM Structure of a Relaxase Reveals the Molecular Basis of DNA Unwinding during Bacterial Conjugation'. *Cell* 169 (4): 708-721.e12. <https://doi.org/10.1016/j.cell.2017.04.010>.

Iyer, Lakshminarayan M., A. Maxwell Burroughs, Swadha Anand, Robson F. de Souza, and L. Aravind. 2017. 'Polyvalent Proteins, a Pervasive Theme in the Intergenomic Biological Conflicts of Bacteriophages and Conjugative Elements'. *Journal of Bacteriology* 199 (15): e00245-17. <https://doi.org/10.1128/JB.00245-17>.

Jagura-Burdzy, Grazyna, Kalliope Kostelidou, Jessica Pole, Dheeraj Khare, Anthony Jones, D. Ross Williams, and Christopher M. Thomas. 1999. 'IncC of Broad-Host-Range Plasmid RK2 Modulates KorB Transcriptional Repressor Activity In Vivo and Operator Binding In Vitro'. *Journal of Bacteriology* 181 (9): 2807–15. <https://doi.org/10.1128/JB.181.9.2807-2815.1999>.

Johnson, Aaron, and Mike O'Donnell. 2005. 'Cellular DNA Replicases: Components and Dynamics at the Replication Fork'. *Annual Review of Biochemistry* 74: 283–315. <https://doi.org/10.1146/annurev.biochem.73.011303.073859>.

Johnson, Timothy J., Jessica L. Danzeisen, Bonnie Youmans, Kyle Case, Katharine Llop, Jeannette Munoz-Aguayo, Cristian Flores-Figueroa, et al. 2016. 'Separate F-Type Plasmids Have Shaped the Evolution of the H30 Subclone of Escherichia Coli Sequence Type 131'. *MSphere* 1 (4): e00121-16. <https://doi.org/10.1128/mSphere.00121-16>.

Johnston, Calum, Nathalie Campo, Matthieu J. Bergé, Patrice Polard, and Jean-Pierre Claverys. 2014. 'Streptococcus Pneumoniae, Le Transformiste'. *Trends in Microbiology* 22 (3): 113–19. <https://doi.org/10.1016/j.tim.2014.01.002>.

Johnston, Calum, Bernard Martin, Gwennaele Fichant, Patrice Polard, and Jean-Pierre Claverys. 2014. 'Bacterial Transformation: Distribution, Shared Mechanisms and Divergent Control'. *Nature Reviews Microbiology* 12 (3): 181–96. <https://doi.org/10.1038/nrmicro3199>.

Jones, A. L., P. T. Barth, and B. M. Wilkins. 1992. 'Zygotic Induction of Plasmid Ssb and PsiB Genes Following Conjugative Transfer of IncI1 Plasmid Collb-P9'. *Molecular Microbiology* 6 (5): 605–13.

- Kawalek, Adam, Aneta A. Bartosik, Krzysztof Glabski, and Grazyna Jagura-Burdzy. 2018. 'Pseudomonas Aeruginosa Partitioning Protein ParB Acts as a Nucleoid-Associated Protein Binding to Multiple Copies of a ParS-Related Motif'. *Nucleic Acids Research* 46 (9): 4592–4606. <https://doi.org/10.1093/nar/gky257>.
- Keasling, J D, B O Palsson, and S Cooper. 1991. 'Cell-Cycle-Specific F Plasmid Replication: Regulation by Cell Size Control of Initiation.' *Journal of Bacteriology* 173 (8): 2673–80.
- Keeling, Patrick J., and Jeffrey D. Palmer. 2008. 'Horizontal Gene Transfer in Eukaryotic Evolution'. *Nature Reviews. Genetics* 9 (8): 605–18. <https://doi.org/10.1038/nrg2386>.
- Kisker, Caroline, Jochen Kuper, and Bennett Van Houten. 2013. 'Prokaryotic Nucleotide Excision Repair'. *Cold Spring Harbor Perspectives in Biology* 5 (3): a012591. <https://doi.org/10.1101/cshperspect.a012591>.
- Kohler, Verena, Walter Keller, and Elisabeth Grohmann. 2019. 'Regulation of Gram-Positive Conjugation'. *Frontiers in Microbiology* 10 (May): 1134. <https://doi.org/10.3389/fmicb.2019.01134>.
- Koraimann, Günther. 2018. 'Spread and Persistence of Virulence and Antibiotic Resistance Genes: A Ride on the F Plasmid Conjugation Module'. *EcoSal Plus* 8 (1). <https://doi.org/10.1128/ecosalplus.ESP-0003-2018>.
- Koraimann, Günther, and Maria A. Wagner. 2014. 'Social Behavior and Decision Making in Bacterial Conjugation'. *Frontiers in Cellular and Infection Microbiology* 4 (April). <https://doi.org/10.3389/fcimb.2014.00054>.
- Lanka, Erich, and Brian M Wilkins. 1995. 'DNA Processing Reactions in Bacterial Conjugation', 31.
- Lanza, Val F., María de Toro, M. Pilar Garcillán-Barcia, Azucena Mora, Jorge Blanco, Teresa M. Coque, and Fernando de la Cruz. 2014. 'Plasmid Flux in Escherichia Coli ST131 Sublineages, Analyzed by Plasmid Constellation Network (PLACNET), a New Method for Plasmid Reconstruction from Whole Genome Sequences'. *PLOS Genetics* 10 (12): e1004766. <https://doi.org/10.1371/journal.pgen.1004766>.
- Lawrence, Jeffrey G., and Howard Ochman. 1998. 'Molecular Archaeology of the Escherichia Coli Genome'. *Proceedings of the National Academy of Sciences* 95 (16): 9413–17. <https://doi.org/10.1073/pnas.95.16.9413>.
- Lederberg, Joshua. 1952. 'Cell Genetics and Hereditary Symbiosis'. *Physiological Reviews* 32 (4): 403–30. <https://doi.org/10.1152/physrev.1952.32.4.403>.
- Lederberg, Joshua, and E. L. Tatum. 1946. 'Gene Recombination in Escherichia Coli'. *Nature* 158 (4016): 558–558. <https://doi.org/10.1038/158558a0>.
- Lee, Isaiah Paolo A., Omar Tonsi Eldakar, J. Peter Gogarten, and Cheryl P. Andam. 2022. 'Bacterial Cooperation through Horizontal Gene Transfer'. *Trends in Ecology & Evolution* 37 (3): 223–32. <https://doi.org/10.1016/j.tree.2021.11.006>.
- Lerminiaux, Nicole A., and Andrew D.S. Cameron. 2019. 'Horizontal Transfer of Antibiotic

- Resistance Genes in Clinical Environments'. *Canadian Journal of Microbiology* 65 (1): 34–44. <https://doi.org/10.1139/cjm-2018-0275>.
- Li, Li-Guan, Yu Xia, and Tong Zhang. 2017. 'Co-Occurrence of Antibiotic and Metal Resistance Genes Revealed in Complete Genome Collection'. *The ISME Journal* 11 (3): 651–62. <https://doi.org/10.1038/ismej.2016.155>.
- Lilly, Joshua, and Manel Camps. 2015. 'Mechanisms of Theta Plasmid Replication'. *Microbiology Spectrum* 3 (1): PLAS-0029-2014.
- Lim, Grace E., Alan I. Derman, and Joe Pogliano. 2005. 'Bacterial DNA Segregation by Dynamic SopA Polymers'. *Proceedings of the National Academy of Sciences* 102 (49): 17658–63. <https://doi.org/10.1073/pnas.0507222102>.
- Lindström, Kristina, and Seyed Abdollah Mousavi. 2020. 'Effectiveness of Nitrogen Fixation in Rhizobia'. *Microbial Biotechnology* 13 (5): 1314–35. <https://doi.org/10.1111/1751-7915.13517>.
- Livermore, D. M. 1995. 'Beta-Lactamases in Laboratory and Clinical Resistance'. *Clinical Microbiology Reviews* 8 (4): 557–84. <https://doi.org/10.1128/CMR.8.4.557>.
- Loh, S. M., D. S. Cram, and R. A. Skurray. 1988. 'Nucleotide Sequence and Transcriptional Analysis of a Third Function (Flm) Involved in F-Plasmid Maintenance'. *Gene* 66 (2): 259–68. [https://doi.org/10.1016/0378-1119\(88\)90362-9](https://doi.org/10.1016/0378-1119(88)90362-9).
- Lopatkin, Allison J, Hanna R Meredith, Jaydeep K Srimani, Connor Pfeiffer, Rick Durrett, and Lingchong You. 2017. 'Persistence and Reversal of Plasmid-Mediated Antibiotic Resistance - PMC'. 22 November 2017. <https://www.ncbi.nlm.nih.gov/insb.bib.cnrs.fr/pmc/articles/PMC5698434/>.
- Low, Wen Wen, Joshua L. C. Wong, Leticia C. Beltran, Chloe Seddon, Sophia David, Hok-Sau Kwong, Tatiana Bizeau, et al. 2022. 'Mating Pair Stabilization Mediates Bacterial Conjugation Species Specificity'. *Nature Microbiology* 7 (7): 1016–27. <https://doi.org/10.1038/s41564-022-01146-4>.
- Maindola, Priyank, Rahul Raina, Parveen Goyal, Krishnamohan Atmakuri, Abhishek Ojha, Sourabh Gupta, Peter J. Christie, Lakshminarayan M. Iyer, L. Aravind, and Arulandu Arockiasamy. 2014. 'Multiple Enzymatic Activities of ParB/Srx Superfamily Mediate Sexual Conflict among Conjugative Plasmids'. *Nature Communications* 5 (October): 5322. <https://doi.org/10.1038/ncomms6322>.
- Maki, Y., H. Yoshida, and A. Wada. 2000. 'Two Proteins, YfiA and YhbH, Associated with Resting Ribosomes in Stationary Phase Escherichia Coli'. *Genes to Cells: Devoted to Molecular & Cellular Mechanisms* 5 (12): 965–74. <https://doi.org/10.1046/j.1365-2443.2000.00389.x>.
- Manoil, Colin, and Jürg P. Rosenbusch. 1982. 'Conjugation-Deficient Mutants of Escherichia Coli Distinguish Classes of Functions of the Outer Membrane OmpA Protein'. *Molecular and General Genetics MGG* 187 (1): 148–56. <https://doi.org/10.1007/BF00384398>.
- Manwaring, N. P., R. A. Skurray, and N. Firth. 1999. 'Nucleotide Sequence of the F Plasmid Leading Region'. *Plasmid* 41 (3): 219–25. <https://doi.org/10.1006/plas.1999.1390>.
- Masai, Hisao, and Ken-ichi Arai. 1997. 'Frpo: A Novel Single-Stranded DNA Promoter for Transcription and for Primer RNA Synthesis of DNA Replication'. *Cell* 89 (6): 897–907.

[https://doi.org/10.1016/S0092-8674\(00\)80275-5](https://doi.org/10.1016/S0092-8674(00)80275-5).

Maslowska, Katarzyna H., Karolina Makiela-Dzvenska, and Iwona J. Fijalkowska. 2019. 'The SOS System: A Complex and Tightly Regulated Response to DNA Damage'. *Environmental and Molecular Mutagenesis* 60 (4): 368–84. <https://doi.org/10.1002/em.22267>.

Mathers, Amy J., Heather L. Cox, Brandon Kitchel, Hugo Bonatti, Ann Karen C. Brassinga, Joanne Carroll, W. Michael Scheld, Kevin C. Hazen, and Costi D. Sifri. 2011. 'Molecular Dissection of an Outbreak of Carbapenem-Resistant Enterobacteriaceae Reveals Intergenous KPC Carbapenemase Transmission through a Promiscuous Plasmid'. *MBio* 2 (6): e00204-00211. <https://doi.org/10.1128/mBio.00204-11>.

Mehdizadeh Gohari, Iman, Mauricio A. Navarro, Jihong Li, Archana Shrestha, Francisco Uzal, and Bruce A. McClane. 2021. 'Pathogenicity and Virulence of Clostridium Perfringens'. *Virulence* 12 (1): 723–53. <https://doi.org/10.1080/21505594.2021.1886777>.

Meinhardt, F., R. Schaffrath, and M. Larsen. 1997. 'Microbial Linear Plasmids'. *Applied Microbiology and Biotechnology* 47 (4): 329–36. <https://doi.org/10.1007/s002530050936>.

Menouni, Rachid, Geoffrey Hutinet, Marie-Agnès Petit, and Mireille Ansaldi. 2015. 'Bacterial Genome Remodeling through Bacteriophage Recombination'. *FEMS Microbiology Letters* 362 (1): 1–10. <https://doi.org/10.1093/femsle/fnu022>.

Meyer, R R, and P S Laine. 1990. 'The Single-Stranded DNA-Binding Protein of Escherichia Coli'. *Microbiological Reviews* 54 (4): 342–80. <https://doi.org/10.1128/mr.54.4.342-380.1990>.

Million-Weaver, Samuel, and Manel Camps. 2014. 'Mechanisms of Plasmid Segregation: Have Multicopy Plasmids Been Overlooked?' *Plasmid* 0 (September): 27–36. <https://doi.org/10.1016/j.plasmid.2014.07.002>.

Miyakoshi, Masatoshi, Yoshiyuki Ohtsubo, Yuji Nagata, and Masataka Tsuda. 2020. 'Transcriptome Analysis of Zygotic Induction During Conjugative Transfer of Plasmid RP4'. *Frontiers in Microbiology* 11. <https://www.frontiersin.org/articles/10.3389/fmicb.2020.01125>.

Nikaido, Hiroshi. 2009. 'Multidrug Resistance in Bacteria'. *Annual Review of Biochemistry* 78: 119–46. <https://doi.org/10.1146/annurev.biochem.78.082907.145923>.

Nolivos, Sophie, Julien Cayron, Annick Dedieu, Adeline Page, Frederic Delolme, and Christian Lesterlin. 2019. 'Role of AcrAB-TolC Multidrug Efflux Pump in Drug-Resistance Acquisition by Plasmid Transfer'. *Science (New York, N.Y.)* 364 (6442): 778–82. <https://doi.org/10.1126/science.aav6390>.

Nordmann, Patrice, Thierry Naas, and Laurent Poirel. 2011. 'Global Spread of Carbapenemase-Producing Enterobacteriaceae'. *Emerging Infectious Diseases* 17 (10): 1791–98. <https://doi.org/10.3201/eid1710.110655>.

OMS. 2020. 'Résistance aux antibiotiques'. 30 July 2020. <https://www.who.int/fr/news-room/fact-sheets/detail/antibiotic-resistance>.

O'Neill. 2014. 'MR Review'. 2014. <https://amr-review.org/>.

- Palm, Martin, Alfred Fransson, Julia Hultén, Karolina Búcaro Stenman, Amina Allouche, Oscar E. Chiang, Mirthe L. Constandse, et al. 2022. 'The Effect of Heavy Metals on Conjugation Efficiency of an F-Plasmid in Escherichia Coli'. *Antibiotics (Basel, Switzerland)* 11 (8): 1123. <https://doi.org/10.3390/antibiotics11081123>.
- Pang, Tin Yau, and Martin J. Lercher. 2019. 'Each of 3,323 Metabolic Innovations in the Evolution of E. Coli Arose through the Horizontal Transfer of a Single DNA Segment'. *Proceedings of the National Academy of Sciences of the United States of America* 116 (1): 187–92. <https://doi.org/10.1073/pnas.1718997115>.
- Paterson, David L., and Robert A. Bonomo. 2005. 'Extended-Spectrum Beta-Lactamases: A Clinical Update'. *Clinical Microbiology Reviews* 18 (4): 657–86. <https://doi.org/10.1128/CMR.18.4.657-686.2005>.
- Petrova, Vessela, Sindhu Chitteni-Pattu, Julia C. Drees, Ross B. Inman, and Michael M. Cox. 2009. 'An SOS Inhibitor That Binds to Free RecA Protein: The PsiB Protein'. *Molecular Cell* 36 (1): 121–30. <https://doi.org/10.1016/j.molcel.2009.07.026>.
- Poirel, Laurent, Jose-Manuel Rodriguez-Martinez, Hedi Mammeri, Alain Liard, and Patrice Nordmann. 2005. 'Origin of Plasmid-Mediated Quinolone Resistance Determinant QnrA'. *Antimicrobial Agents and Chemotherapy* 49 (8): 3523–25. <https://doi.org/10.1128/AAC.49.8.3523-3525.2005>.
- Porter, R.D., and S. Black. 1991. 'The Single-Stranded-DNA-Binding Protein Encoded by the Escherichia Coli F Factor Can Complement a Deletion of the Chromosomal Ssb Gene - PubMed'. 1 April 1991. <https://pubmed-ncbi-nlm-nih-gov.insb.bib.cnrs.fr/2013585/>.
- Radman, M. 1975. 'SOS Repair Hypothesis: Phenomenology of an Inducible DNA Repair Which Is Accompanied by Mutagenesis'. *Basic Life Sciences* 5A: 355–67. https://doi.org/10.1007/978-1-4684-2895-7_48.
- Rankin, D. J., E. P. C. Rocha, and S. P. Brown. 2011. 'What Traits Are Carried on Mobile Genetic Elements, and Why?' *Heredity* 106 (1): 1–10. <https://doi.org/10.1038/hdy.2010.24>.
- Reuter, Audrey, Cécile Hilpert, Annick Dedieu-Berne, Sophie Lematre, Erwan Gueguen, Guillaume Launay, Sarah Bigot, and Christian Lesterlin. 2021. 'Targeted-Antibacterial-Plasmids (TAPs) Combining Conjugation and CRISPR/Cas Systems Achieve Strain-Specific Antibacterial Activity'. *Nucleic Acids Research* 49 (6): 3584–98. <https://doi.org/10.1093/nar/gkab126>.
- Riley, Margaret A., and John E. Wertz. 2002. 'Bacteriocins: Evolution, Ecology, and Application'. *Annual Review of Microbiology* 56 (1): 117–37. <https://doi.org/10.1146/annurev.micro.56.012302.161024>.
- Roberts, M. C. 1996. 'Tetracycline Resistance Determinants: Mechanisms of Action, Regulation of Expression, Genetic Mobility, and Distribution'. *FEMS Microbiology Reviews* 19 (1): 1–24. <https://doi.org/10.1111/j.1574-6976.1996.tb00251.x>.
- Rosenberg, S. M., and P. J. Hastings. 2001. 'F Factor'. In *Encyclopedia of Genetics*, edited by Sydney Brenner and Jefferey H. Miller, 677–80. New York: Academic Press.

<https://doi.org/10.1006/rwgn.2001.0454>.

Sabharwal, Vishakha, Abbie Stevenson, Marisol Figueira, George Orthopoulos, Krzysztof Trzcinski, and Stephen I. Pelton. 2014. 'Capsular Switching as a Strategy to Increase Pneumococcal Virulence in Experimental Otitis Media Model'. *Microbes and Infection* 16 (4): 292–99. <https://doi.org/10.1016/j.micinf.2013.12.002>.

Sharp, Phillip A., Stanley N. Cohen, and Norman Davidson. 1973. 'Electron Microscope Heteroduplex Studies of Sequence Relations among Plasmids of Escherichia Coli: II. Structure of Drug Resistance (R) Factors and f Factors'. *Journal of Molecular Biology* 75 (2): 235–55. [https://doi.org/10.1016/0022-2836\(73\)90018-1](https://doi.org/10.1016/0022-2836(73)90018-1).

Sharples, Gary J., Stuart M. Ingleston, and Robert G. Lloyd. 1999. 'Holliday Junction Processing in Bacteria: Insights from the Evolutionary Conservation of RuvABC, RecG, and RusA'. *Journal of Bacteriology* 181 (18): 5543–50. <https://doi.org/10.1128/JB.181.18.5543-5550.1999>.

Shintani, Masaki, Zoe K. Sanchez, and Kazuhide Kimbara. 2015. 'Genomics of Microbial Plasmids: Classification and Identification Based on Replication and Transfer Systems and Host Taxonomy'. *Frontiers in Microbiology* 6 (March): 242. <https://doi.org/10.3389/fmicb.2015.00242>.

Simmons, Lyle A., James J. Foti, Susan E. Cohen, and Graham C. Walker. 2008. 'The SOS Regulatory Network'. *EcoSal Plus* 2008 (July): 10.1128/ecosalplus.5.4.3. <https://doi.org/10.1128/ecosalplus.5.4.3>.

Smillie, Chris, M. Pilar Garcillán-Barcia, M. Victoria Francia, Eduardo P. C. Rocha, and Fernando de la Cruz. 2010. 'Mobility of Plasmids'. *Microbiology and Molecular Biology Reviews: MMBR* 74 (3): 434–52. <https://doi.org/10.1128/MMBR.00020-10>.

Spratt, Madison R., and Keara Lane. 2022. 'Navigating Environmental Transitions: The Role of Phenotypic Variation in Bacterial Responses'. *MBio* 13 (6): e02212-22. <https://doi.org/10.1128/mbio.02212-22>.

Stone, M. Rhia L., Mark S. Butler, Wanida Phetsang, Matthew A. Cooper, and Mark A. T. Blaskovich. 2018. 'Fluorescent Antibiotics: New Research Tools to Fight Antibiotic Resistance'. *Trends in Biotechnology* 36 (5): 523–36. <https://doi.org/10.1016/j.tibtech.2018.01.004>.

Tanner, Nathan A., Samir M. Hamdan, Slobodan Jergic, Karin V. Loscha, Patrick M. Schaeffer, Nicholas E. Dixon, and Antoine M. van Oijen. 2008. 'Single-Molecule Studies of Fork Dynamics in Escherichia Coli DNA Replication'. *Nature Structural & Molecular Biology* 15 (9): 998. <https://doi.org/10.1038/nsmb0908-998a>.

Tetaz, T. J., and R. K. Luke. 1983. 'Plasmid-Controlled Resistance to Copper in Escherichia Coli'. *Journal of Bacteriology* 154 (3): 1263–68. <https://doi.org/10.1128/jb.154.3.1263-1268.1983>.

Thisted, Thomas, and Kenn Gerdes. 1992. 'Mechanism of Post-Segregational Killing by the Hok/Sok System of Plasmid R1: Sok Antisense RNA Regulates Hok Gene Expression Indirectly through the Overlapping Mok Gene'. *Journal of Molecular Biology* 223 (1): 41–54. [https://doi.org/10.1016/0022-2836\(92\)90714-U](https://doi.org/10.1016/0022-2836(92)90714-U).

Thoma, L., and G. Muth. 2016. 'Conjugative DNA-Transfer in Streptomyces, a Mycelial Organism'.

Plasmid 87–88 (September): 1–9. <https://doi.org/10.1016/j.plasmid.2016.09.004>.

Tozzoli, R, L Grande, Michelacci, P Ranieri, A Maugliani, A Caprioli, and S Morabito. 2014. ‘Shiga Toxin-Converting Phages and the Emergence of New Pathogenic Escherichia Coli: A World in Motion’. *Frontiers in Cellular and Infection Microbiology* 4 (June). <https://doi.org/10.3389/fcimb.2014.00080>.

Virolle, Chloé, Kelly Goldlust, Sarah Djermoun, Sarah Bigot, and Christian Lesterlin. 2020. ‘Bacteria DNA Conjugation: From The Cellular to The Community Level’, September. <https://doi.org/10.20944/preprints202009.0405.v1>.

Watanabe, E., M. Wachi, M. Yamasaki, and K. Nagai. 1992. ‘ATPase Activity of SopA, a Protein Essential for Active Partitioning of F Plasmid’. *Molecular & General Genetics: MGG* 234 (3): 346–52. <https://doi.org/10.1007/BF00538693>.

Weigle, J. J. 1953. ‘Induction of Mutations in a Bacterial Virus’. *Proceedings of the National Academy of Sciences of the United States of America* 39 (7): 628–36.

Wein, Tanita, Yiqing Wang, Myriam Barz, Fenna T. Stücker, Katrin Hammerschmidt, and Tal Dagan. 2021. ‘Essential Gene Acquisition Destabilizes Plasmid Inheritance’. *PLOS Genetics* 17 (7): e1009656. <https://doi.org/10.1371/journal.pgen.1009656>.

Weingarten, Rebecca A., Ryan C. Johnson, Sean Conlan, Amanda M. Ramsburg, John P. Dekker, Anna F. Lau, Pavel Khil, et al. 2018. ‘Genomic Analysis of Hospital Plumbing Reveals Diverse Reservoir of Bacterial Plasmids Conferring Carbapenem Resistance’. *MBio* 9 (1): e02011-17. <https://doi.org/10.1128/mBio.02011-17>.

Westra, Edze R., Raymond H.J. Staals, Gerrit Gort, Søren Høgh, Sarah Neumann, Fernando de la Cruz, Peter C. Fineran, and Stan J.J. Brouns. 2013. ‘CRISPR-Cas Systems Preferentially Target the Leading Regions of MOBF Conjugative Plasmids’. *RNA Biology* 10 (5): 749–61. <https://doi.org/10.4161/rna.24202>.

Wong, Joyce J. W., Jun Lu, and J. N. Mark Glover. 2012. ‘Relaxosome Function and Conjugation Regulation in F-like Plasmids – a Structural Biology Perspective’. *Molecular Microbiology* 85 (4): 602–17. <https://doi.org/10.1111/j.1365-2958.2012.08131.x>.

Wu, C. A., E. L. Zechner, and K. J. Marians. 1992. ‘Coordinated Leading- and Lagging-Strand Synthesis at the Escherichia Coli DNA Replication Fork. I. Multiple Effectors Act to Modulate Okazaki Fragment Size’. *The Journal of Biological Chemistry* 267 (6): 4030–44.

Ying, Jianchao, Songquan Wu, Kaibo Zhang, Ziqiang Wang, Wen Zhu, Mei Zhu, Ying Zhang, et al. 2015. ‘Comparative Genomics Analysis of PKF3-94 in Klebsiella Pneumoniae Reveals Plasmid Compatibility and Horizontal Gene Transfer’. *Frontiers in Microbiology* 6 (September): 831. <https://doi.org/10.3389/fmicb.2015.00831>.

Yoon, Young Geol, and Michael D. Koob. 2005. ‘Transformation of Isolated Mammalian Mitochondria by Bacterial Conjugation’. *Nucleic Acids Research* 33 (16): e139. <https://doi.org/10.1093/nar/gni140>.

Yoshida, Hideji, Akira Wada, Tomohiro Shimada, Yasushi Maki, and Akira Ishihama. 2019.

‘Coordinated Regulation of Rsd and RMF for Simultaneous Hibernation of Transcription Apparatus and Translation Machinery in Stationary-Phase *Escherichia Coli*’. *Frontiers in Genetics* 10 (December): 1153. <https://doi.org/10.3389/fgene.2019.01153>.

Zahrl, Doris, Maria Wagner, Karin Bischof, and Günther Koraimann. 2006. ‘Expression and Assembly of a Functional Type IV Secretion System Elicit Extracytoplasmic and Cytoplasmic Stress Responses in *Escherichia Coli*’. *Journal of Bacteriology* 188 (18): 6611–21. <https://doi.org/10.1128/JB.00632-06>.

Résumé

L'incroyable capacité d'adaptation des bactéries face à leur environnement leur permet de coloniser diverses niches écologiques, allant des sols et eaux jusqu'aux tissus vivants et surfaces inertes. Il est désormais acquis que le transfert horizontal de gènes joue un rôle prépondérant dans la plasticité des génomes bactériens, permettant un bond évolutif associé à la dissémination rapide et efficace de nouveaux traits phénotypiques. La conjugaison bactérienne est ainsi un mécanisme de transfert horizontal de gènes d'intérêt majeur puisque responsable de 80% des disséminations de résistances aux antibiotiques acquises chez les bactéries. Étant le sujet de nombreuses recherches depuis la découverte du mécanisme en 1946, le plasmide F est désormais considéré comme un modèle pour l'étude de la conjugaison bactérienne. Parmi les différentes régions génétiques le composant, la région *leading* est définie comme étant la première à être transférée dans les cellules receveuses. Retrouvée conservée chez certains plasmides conjugatifs appartenant à divers groupes d'incompatibilité, il a été montré que cette région est exprimée de manière précoce lors de l'entrée du plasmide dans la receveuse. Bien que la plupart des gènes qui la composent soient de fonctions inconnues, il est proposé que la région *leading* joue un rôle majeur dans les étapes initiales d'établissement du plasmide dans la nouvelle cellule hôte.

L'objectif principal de cette thèse est d'étudier le rôle de la région *leading* au cours de la conjugaison du plasmide F chez *Escherichia coli*, et plus précisément de caractériser le gène *yfjB*. La protéine YfjB partage une homologie avec les protéines de la famille ParB, notamment par la conservation d'un domaine de liaison à l'ADN. Afin de caractériser cette protéine *leading*, j'ai eu recours à une approche multidisciplinaire combinant la microbiologie classique, la microscopie à fluorescence en cellules vivantes, la génétique, les analyses omic ou encore la biochimie structurale. Les résultats obtenus permettent de mieux comprendre la dynamique de la protéine YfjB au niveau cellulaire, son activité moléculaire et son rôle dans l'établissement du plasmide F chez la bactérie receveuse. Mes travaux nous amènent alors à proposer un rôle de la protéine YfjB pour le bon déroulement des premières étapes de transfert du plasmide via une reprogrammation globale du profil d'expression génétique de la bactérie hôte. Cela irait dans le sens d'une stratégie développée par le plasmide F visant à limiter l'impact négatif de son acquisition sur la physiologie de la cellule receveuse, appuyant l'hypothèse d'une importance de la région *leading* pour l'établissement du plasmide.

Bien que le transfert de gènes par conjugaison ait été extensivement étudié au cours des dernières décennies, les différents projets de recherche auxquels j'ai pu participer au cours de ma thèse apportent de nouvelles connaissances par diverses approches innovantes. En couvrant l'ensemble du mécanisme de conjugaison, nous proposons alors de nouveaux modèles intégrant les différents mécanismes moléculaires régissant la conjugaison dans le contexte de la cellule vivante.